

UNIVERSITA' DEGLI STUDI DI PARMA

Dottorato di ricerca

in

Progettazione e Sintesi di Composti Biologicamente Attivi

Ciclo XXIV

MD Simulations and Conformational Sampling of Monomeric and
Dimeric GPCRs

Relatore:

Chiar.mo Prof. GABRIELE COSTANTINO

Dottorando: AGOSTINO BRUNO

Contents

ABSTRACT	6
PUBLISHED WORK	7
LIST OF FIGURES	8
LIST OF TABLES	11
PREFACE	12
CHAPTER 1 G PROTEIN-COUPLED RECEPTORS (GPCRS)	15
1.1 STRUCTURE AND CLASSIFICATION SYSTEM	15
1.1.1 CLASSIFICATION SYSTEM AND COMMON STRUCTURE	15
1.1.2 RESIDUE NUMBERING SCHEME	18
1.1.3 X-RAY CRYSTAL STRUCTURES	19
1.2 ORTHOSTERIC AND ALLOSTERIC BINDING SITES	23
1.2.1 ORTHOSTERIC BINDING SITE	23
1.2.2 ALLOSTERIC BINDING SITE	27
1.3 ACTIVATION MECHANISM	32
1.3.1 MATHEMATICAL MODELS OF GPCR PHARMACOLOGY	41
1.3.2 LIGAND-SELECTIVE RECEPTOR CONFORMATIONS	43
1.4 GPCR DIMERS AS NEW PHARMACOLOGICAL TOOLS	45
1.5 CHOLESTEROL EFFECTS ON GPCR PHARMACOLOGY	48
1.6 THE SEROTONINERGIC RECEPTOR SUBTYPE 2A	51

1.7 THE METABOTROPIC GLUTAMATE RECEPTOR SUBTYPE 2	52
1.8 5-HT_{2A} HOMO- AND HETEROMER AS PHARMACEUTICAL TARGETS	54
1.8.1 THE 5-HT _{2A} -5-HT _{2A} HOMOMER COMPLEX	54
1.8.2 THE mGLUR2-5-HT _{2A} HETEROMER COMPLEX	56
<u>CHAPTER 2 AIMS OF THE PROJECT</u>	59
<u>CHAPTER 3 EXPERIMENTAL SECTION</u>	62
3.1 HOMOLGY MODELS OF GPCRS	63
3.1.1 5-HT _{2A} HOMOLGY MODEL	64
3.1.2 mGLUR2 HOMOLGY MODEL	65
3.2 PROTEIN-PROTEIN DOCKING	67
3.2.1 PROTEIN-PROTEIN DOCKING PROCEDURE AND THE ROSETTA SUITE.	68
3.3 CONSTRUCTION OF THE MEMBRANE-RECEPTOR COMPLEXES	71
3.3.1 CONSTRUCTION OF THE MOLECULAR SYSTEMS FOR THE GPCR DIMER MD EXPERIMENTS	71
3.3.2 CONSTRUCTION OF THE MOLECULAR SYSTEMS FOR THE GPCR-CHOLESTEROL MD EXPERIMENTS	72
3.4 MOLECULAR DYNAMICS SIMULATIONS	73
3.4.1 INTRODUCTION TO MD	73
3.4.2 CPU AND GPU COMPUTER ARCHITECTURES	73
3.4.3 NAMD, ACEMD AND VMD SOFTWARE PACKAGES	74
3.4.4 MOLECULAR DYNAMICS EXPERIMENT SETTINGS	75
3.4.5 CONFORMATIONAL SAMPLING	77
3.4.6 ESSENTIAL DYNAMIC ANALYSIS	79
3.4.7 ELECTRON DENSITY PROFILE	80
3.4.8 KERNEL DENSITY FUNCTION	82
3.5 LIGAND DOCKING	83
3.5.1 ANALYSIS OF THE DIMER INTERFACE EFFECTS ON THE 5-HT _{2A} BINDING POCKET.	83
3.5.2 mGLUR2 MODEL VALIDATION	86

CHAPTER 4 RESULTS	87
4.1 DIMER INTERFACE EFFECTS ANALYSIS	87
4.1.1 ANALYSIS OF THE MD TRAJECTORIES.	87
4.1.2 ANALYSIS OF THE BINDING POCKET	89
4.1.3 CLUSTER ANALYSIS	92
4.1.4 LIGAND DOCKING EXPERIMENTS	96
4.1.5 ESSENTIAL DYNAMIC ANALYSIS	104
4.2 CHOLESTEROL EFFECTS ANALYSIS	109
4.2.1 CHOLESTEROL EFFECTS ON THE MONOMERIC 5-HT _{2A}	109
4.2.2 A SODIUM BINDING PATHWAY IN THE 5-HT _{2A} RECEPTOR	115
4.2.3 CHOLESTEROL EFFECTS ON THE MONOMERIC mGLUR2	120
CHAPTER 5 CONCLUSIONS	133
5.1 GENERAL OVERVIEW	133
5.2 DIMER INTERFACE EFFECTS	134
5.3 CHOLESTEROL EFFECTS	137
5.3.1 CHOLESTEROL EFFECTS ON 5-HT _{2A} FLEXIBILITY	137
5.3.2 CHOLESTEROL EFFECTS ON THE mGLUR2 FLEXIBILITY	139
CHAPTER 6 FUTURE PERSPECTIVES/OUTLOOK	141
6.1 FUTURE COMPUTATIONAL WORK	141
6.2 BIOLOGICAL ASSAYS	142
REFERENCES	143
APPENDIX A	169

Abstract

G protein-coupled receptors (GPCRs) constitute the largest family of membrane-bound receptors with more than 800 members encoded by 351 genes in humans. It has been estimated that more than the 50% of clinically available drugs act on GPCRs, with an amount of about 400, 50 and 25 druggable proteins for the class A, B and C, respectively. Furthermore, Class A GPCRs, with approximately 25% of marketed small drugs, represents the most attractive pharmaceutical class so far identified. The recent availability of high-resolution 3-dimensional structures of some GPCRs supports the notion that GPCRs are dynamically versatile, and their functions can be modulated by several factors. In this scenario, molecular dynamics (MD) simulations techniques appear to be crucial when studying GPCR flexibility associated to functioning and ligand recognition.

In this project we have focused on two aspects of GPCR functioning, which are gaining a considerable interest, namely dimerization and membrane composition. In particular, we have studied the effect of different dimer interfaces, and the effect of cholesterol concentration on the flexibility of two pharmaceutically relevant GPCRs, the 5-HT_{2A} and the mGluR2 receptors.

Herein I report several methodological tools useful in the study of the effects of the aforementioned issues on GPCRs flexibility, and we propose that the chosen MD simulation conditions strongly impact the results carried out by the MD toolbox. This has to be taken into account when using these models for further computational studies, such as in silico screening or docking purposes.

Published Work

1. Molecular Dynamics Simulation of the Heterodimeric mGluR2/5HT_{2A} Complex. An Atomistic Resolution Study of a Potential New Target in Psychiatric Conditions. **Bruno A.**; Guadix AE.; Costantino G. *J. Chem. Inf. and Mod.*, 49:1602-1616, **2009**.

This work has been selected for the cover picture of JCIM, Issue 6, 2009.

2. Addressing the Conformational Flexibility of Serine Racemase by Combining Targeted Molecular Dynamics, Conformational Sampling and Docking Studies. **Bruno A.**; Amori L.; Costantino G. *Mol. Inf.*, 30:317-328, **2011**.

3. Molecular Dynamics Simulations and Docking Studies on 3D models of the Heterodimeric and Homodimeric 5-HT_{2A} Receptor Subtype. **Bruno A.**; Beato C.; Costantino G. *Fut. Med. Chem.*, 3:665-681, **2011**.

4. Molecular Dynamics Simulations of G-Protein Coupled Receptors. **Bruno A.**; Costantino G. *Mol. Inf.* (accepted paper)

5. Crosstalk within GPCR heteromers in Schizophrenia and Parkinson's disease: physical or just functional? Guixa-Gonzalez R.; **Bruno A.**; Marti-Solano M. and Selent J. *Curr. Med. Chem.* (accepted paper)

List of Figures

- Figure 1.** GPCR functioning representation (16)
- Figure 2.** Phylogenetic GPCR tree (17)
- Figure 3.** GPCR numbering scheme (18)
- Figure 4.** X-ray crystal structure trend (20)
- Figure 5.** Conserved orthosteric binding site in Class A GPCRs (23)
- Figure 6.** Class C GPCR orthosteric binding site (26)
- Figure 7.** Class A GPCR allosteric binding site (29)
- Figure 8.** Allosteric vs. orthosteric binding site in Class A GPCRs (30)
- Figure 9.** Activation mechanism for rhodopsin (35)
- Figure 10.** Retinal location in active and inactive rhodopsin states (36)
- Figure 11.** TM5-6 outwards displacement in rhodopsin receptor (37)
- Figure 12.** TM5-6 outwards displacement in β_2 -adrenergic receptor (38)
- Figure 13.** Active and inactive β_2 -adrenergic binding pockets (39)
- Figure 14.** Active and inactive A_{2A} binding pockets (40)
- Figure 15.** Cubic Ternary Complex model (42)
- Figure 16.** Effect of G-protein coupling on the activation pathway (43)
- Figure 17.** Representation of the ligand functional selectivity (44)
- Figure 18.** Example of ligands effects on GPCR dimers (48)
- Figure 19.** Cholesterol Consensus Motif (CCM) (50)

Figure 20. Agonist trafficking of receptor signaling for the 5-HT_{2A} receptor (52)

Figure 21. Structural and functional representation of the mGluR2 receptor (53)

Figure 22. 5-HT_{2A}-5-HT_{2A} homomer crosstalk (55)

Figure 23. 5-HT_{2A}-mGluR2 heteromer crosstalk (57)

Figure 24. Homology modeling flow chart (63)

Figure 25. Alignment for the 5-HT_{2A} receptor (65)

Figure 26. Alignment for the mGluR2 receptor (A) (66)

Figure 27. Alignment for the mGluR2 receptor (B) (67)

Figure 28. Cluster analysis metrics (78)

Figure 29. Electron density profile (EDP) method (81)

Figure 30. Ligand docking protocol (85)

Figure 31. mGluR2 negative allosteric modulators (NAMs) (86)

Figure 32. RMSD comparison for the dimer simulations (88)

Figure 33. Average RMSD comparison (89)

Figure 34. RMSD of the 5-HT_{2A} binding pocket residues (90)

Figure 35. Average RMSD of the 5-HT_{2A} binding pocket residues (91)

Figure 36. CWxP fluctuations (91)

Figure 37. Cluster analysis (93)

Figure 38. Binding pocket displacements in representative structures (94)

Figure 39. LSD binding mode (97)

Figure 40. LSD and 5-HT binding map interactions (97)

Figure 41. ROC analysis (100)

Figure 42. Essential Dynamics subspace (104)

Figure 43. p square values (105)

Figure 44. Relevant residues (106)

Figure 45. Location of the relevant residues (107)

Figure 46. Location of the representative structures in the essential subspace (108)

Figure 47. 5-HT_{2A} RMSD comparison in cholesterol simulations (110)

Figure 48. 5-HT_{2A} CCM (111)

Figure 49. Average RMSD of the 5-HT_{2A} CCM residues (111)

Figure 50. Cholesterol interaction with the 5-HT_{2A} CCM (112)

Figure 51. Membrane thickness for the 5-HT_{2A} simulations (114)

Figure 52. Asymmetric behavior of the membrane in 5-HT_{2A} simulations (115)

Figure 53. Sodium binding pathway (116)

Figure 54. D₂-5-HT_{2A} alignment (117)

Figure 55. Na⁺ pathway against K⁺ pathway (118)

Figure 56. Na⁺ effects (119)

Figure 57. mGluR2 model (121)

Figure 58. mGluR2 validation (122)

Figure 59. mGluR2 RMSD comparison in cholesterol simulations (123)

Figure 60. Probability Density Functions for the mGluR2 receptor (125)

Figure 61. Direct cholesterol interaction with mGluR2-H8 receptor (126)

Figure 62. Average EDP for the mGluR2 receptor (A) (129)

Figure 63. Average EDP for the mGluR2 receptor (B) (130)

List of Tables

Table 1. Relevant X-ray crystal structures (22)

Table 2. List of GPCRs showing ligand functional selectivity (45)

Table 3. List of GPCRs having the CCM (50)

Table 4. Protein-protein docking score (70)

Table 5. RMSD matrix (70)

Table 6. System size (A) (71)

Table 7. System size (B) (71)

Table 8. System size (C) (72)

Table 9. MD settings (A) (76)

Table 10. MD settings (B) (77)

Table 11. Cluster analysis metrics (78)

Table 12. Selected representative structures (96)

Table 13. List of relevant residues (107)

Table 14. H-bond pattern (113)

Table 15. Membrane composition for the 5-HT_{2A} simulations (114)

Table 16. Statistical analysis results (124)

Table 17. Structural analysis prediction (132)

Preface

The ensemble of activities allowing organisms or cells phenotype adaptation to the environment conditions are usually grouped with the term plasticity. This property allows for the preservation of individuals, and can be exerted from the organisms or cells through biological macromolecules such as DNA, RNA, and proteins. In human, plasticity underlies relevant processes such as memory and learning processes, and behavioral control. In this scenario, proteins and their intrinsic flexibility play a key role in both long and short-term adaptations. Indeed, endogenous (neurotransmitter, hormones and so on) or exogenous (xenobiotic) compounds contact a protein target, inducing protein structural rearrangements. Those structural modifications promote cellular responses, such as intracellular signaling cascades, allowing long- or short-term adaptation (i.e. neuronal plasticity or fight or flight reaction, respectively), and the preservation of the individuals. As a matter of fact, proteins and their intrinsic flexibility received great interest. For the determination of the hemoglobin structure at atomic level resolution, in 1958 *Perutz* was honored with the Nobel Prize. At the same time, several attempts to explain the mechanism by which a compound interacts with its target protein were carried out, and the lock and key model was the first widely accepted representation of the drug-protein interaction mechanism. However, the limitations of the lock and key model were soon recognized, among which the lack of an explicit treatment of both protein and ligand flexibility. In 1958 *Perutz* obtained the first static picture of a protein, the hemoglobin. In subsequent studies, the relevance of hemoglobin flexibility was recognized. Indeed, hemoglobin has at least two conformational states, depending on the amount of oxygen molecules bound. Since then, increasing experimental evidence highlighted that proteins are functional versatile, dynamic and flexible. As protein flexibility plays a crucial role in protein functioning and signaling, nowadays it is a widely accepted concept that flexibility

must be taken into account in drug design strategies. Several efforts were made, and several experimental techniques were developed to study protein flexibility in both *ex vivo*, *in vitro*, and *in silico* conditions. Techniques such as Nuclear Magnetic Resonance (NMR, *in vitro*), Fluorescence Resonance Energy Transfer (FRET, *ex vivo*, *in vitro*) and computational techniques (Molecular Dynamics Simulations (MD), Monte Carlo techniques (MC), *in silico*) are devoted to the study of protein structure plasticity. Indeed, protein flexibility underlies relevant biological processes, such as ligand-binding, and signaling mechanisms. The ability to predict the binding mode, the ligand-binding mechanism of a compound to a protein, and thus inferring their mechanism of interaction, is a leading component in medicinal chemistry.

During my PhD project I have analyzed, with the aid of computational techniques, the impact of structural flexibility in the definition of protein-ligand interaction, putting particular emphasis on those structural components affected by protein flexibility. As protein prototype, the G Protein-Coupled Receptors (GPCRs) were used, and the effects of the dimerization phenomenon, and the role of the membrane composition on the definition of the conformational state of GPCRs were assessed. GPCRs are integral membrane proteins, and with approximately 50% of marketed small drugs, represent the most attractive pharmaceutical class of proteins. Moreover GPCRs are extraordinary membrane-bound receptors having versatile dynamic behavior, and their functions depend on a high degree of plasticity. As a matter of fact, GPCRs stand in equilibrium among several pharmacologically relevant conformational ensembles, and *Kenakin* named this ensemble of conformations the *conformational cafeteria*. In this *scenario*, we gave particular emphasis to the serotonergic receptor subtype 2A, and the metabotropic glutamate receptor subtype 2 (5-HT_{2A} and mGluR2 respectively). They belong to two unrelated Class GPCRs (Class A and Class C, respectively), and are implicated in the development of Central Nervous System (CNS) pathologies, such as schizophrenia and epileptic disorders. Moreover, both 5-HT_{2A} and mGluR2 receptors have been implicated in the generation of different GPCR dimers, with functional consequences in the mechanism of action of both antipsychotic and hallucinogenic drugs. Until now, the 5-HT_{2A} receptor was considered and studied as a monomeric entity mainly through homology modeling

studies, while the identification of the complexity of the 5-HT_{2A} architecture also offers new challenges for medicinal and computational chemists to build up reliable and predictive models of homo- or hetero-complexes.

In Chapter 1 a description of the GPCRs taxonomy system, structure, and functioning are provided. Furthermore, detailed descriptions of the main experimental techniques devoted to the GPCR structure definition as well as the relevant aspects affecting GPCRs functioning are discussed.

In Chapter 2 the main goals of the project are elaborated.

In Chapter 3 and 4 the computational methods employed and the main results achieved in the project are discussed, respectively.

Finally in Chapter 5 and 6 the conclusion and the future perspective/outlook are presented.

Chapter 1

G Protein-Coupled Receptors (GPCRs)

1.1 Structure and Classification System

1.1.1 Classification System and Common Structure

G protein-coupled receptors (GPCRs) constitute the largest class of membrane-bound receptors with more than 800 members encoded by 351 genes.¹⁻³ GPCRs modulate cellular responses to a variety of chemical or physical stimuli, such as hormones and neurotransmitters as well as photons. They exhibit a common structure composed by seven-membrane spanning α -helices (Heptahelical Transmembrane Domain, HTM), three extracellular (EL1-3) and three intracellular (IL1-3) loops, a N-terminal extracellular and a C-terminal intracellular domains (Figure 1).⁴⁻⁶ Despite their structural similarities, GPCRs can activate unique signal transduction pathways by coupling with different G-protein subtypes or activating G protein-independent signaling pathways,^{4,5} as well as interacting with large amount of different proteins (Figure 1).^{5,7} Depending on the nature of the endogenous ligand, structural features, and biological functions, human GPCRs are classified into six main families: Rhodopsin like (Family A), Secretin (Family B), Glutamate (Family C), Adhesion, Vomeronasal/Taste receptors (V1R, V3R & T2R); Frizzled/Smoothed family (Figure 2a,b).^{3,4,8,9} GPCRs are implicated in several physiological and pathological processes (i.e. vision, cell migration, platelet aggregation, inflammatory response, cancer, CNS diseases, etc...), and they represent the most important class of druggable proteins. As a matter of fact, it has been estimated that more than the 50% of clinically available drugs act on GPCRs,¹⁰ with an amount of 400, 50 and 25 druggable protein for class A, B and C, respectively (Hopkins and Groom data).¹¹

Furthermore, Class A GPCRs with approximately 25% of marketed small drugs represents the most attractive pharmaceutical class, so far identified.^{1,11}

Figure 1. Snake-cartoon representation of the common structure (TM1-7 and H8) of GPCRs embedded in a phospholipids bilayer (yellow circle the polar heads, gray line the hydrophobic tails). Into the colored circle examples of the chemical stimuli, which can interact with GPCRs (top part of the bilayer, extracellular side of the cells). In the bottom part of the bilayer (intracellular side of the cells) are represented the main protein partners, interacting with GPCRs. The green arrows highlight the G-protein dependent pathways (G_α ; G_i ; G_q ; G_{12} , G_β ; G_γ), the red arrows highlight the G-protein independent pathways (PDZ, GIP, β arr, JAK).

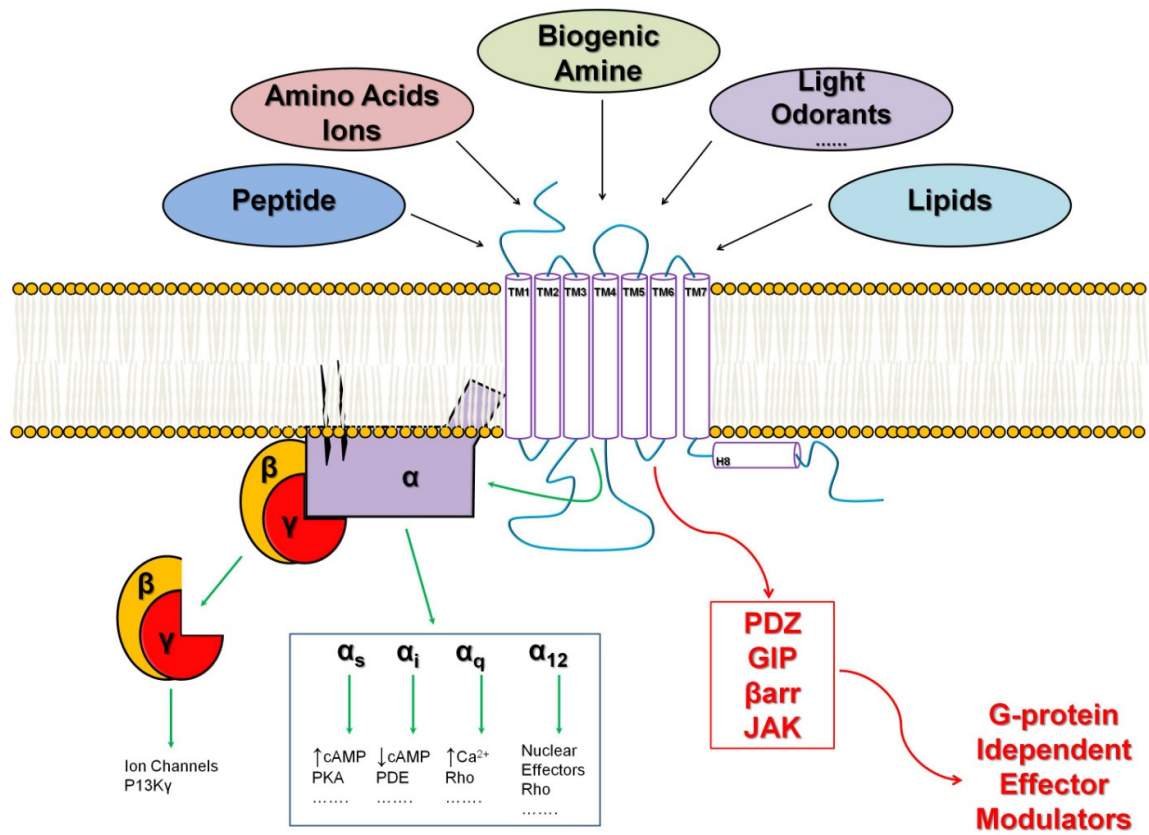
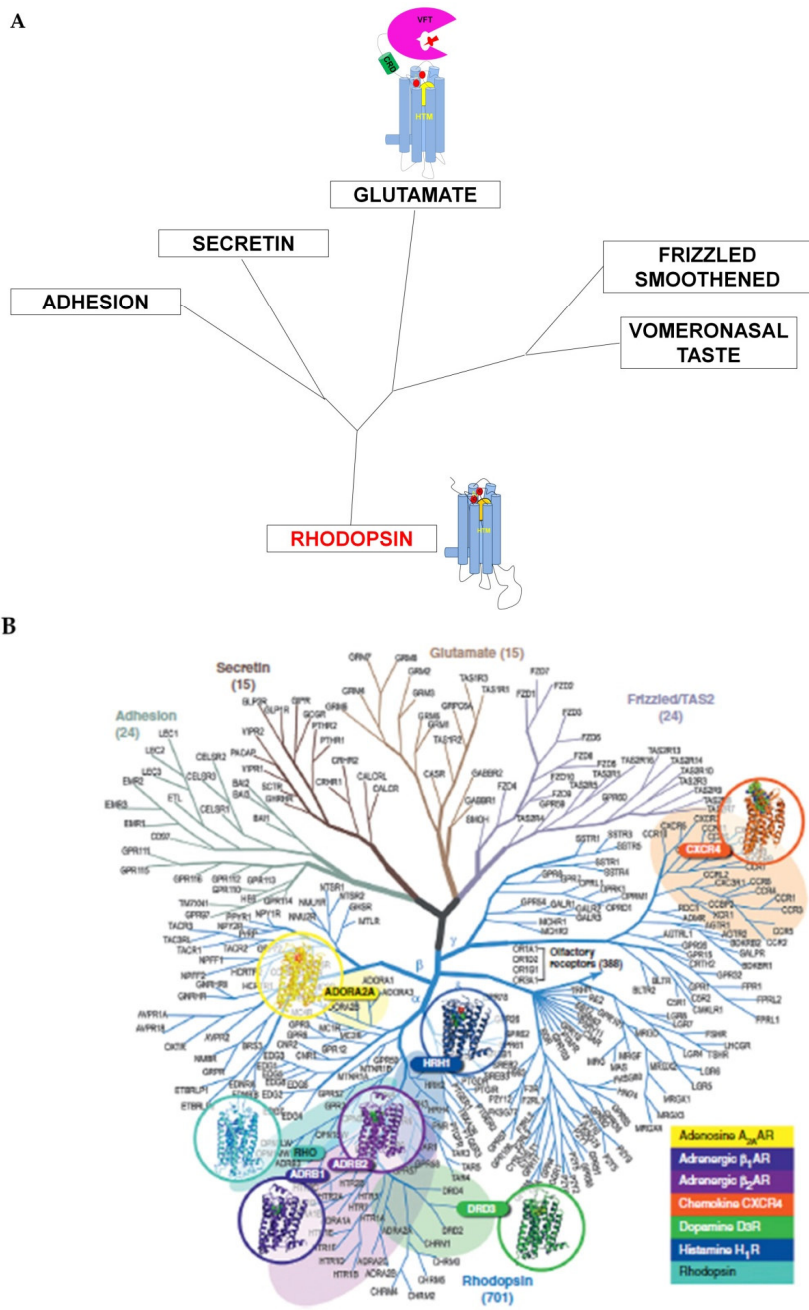


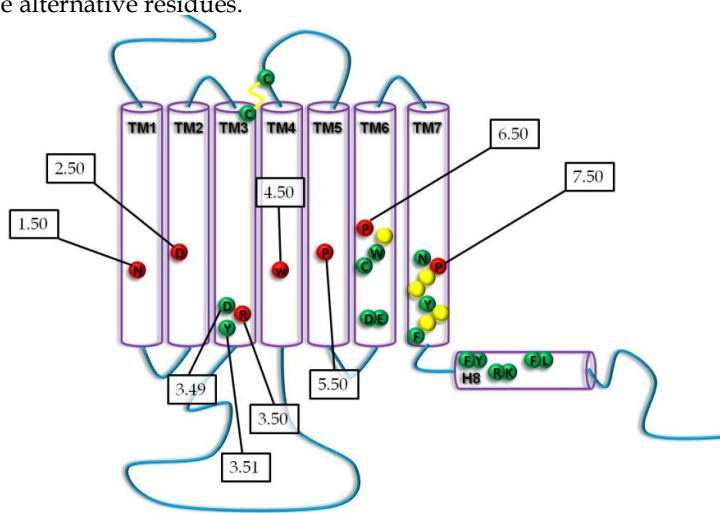
Figure 2. (A) Representation of the six human GPCRs families and their phylogenetic relationship. For Class A (Rhodopsin-like) and Class C (Glutamate-like) GPCRs a cartoon-snake representation of the structures are reported (light purple *Venus Fly Trap Domain*, VFT; green *Cysteine Rich Domain*, CRD; light blue, *Heptahelical Transmembrane Domain*, HTM; red and yellow, respectively, the orthosteric and allosteric binding cleft for Class C GPCRs; orange the orthosteric binding cleft for Class A GPCRs; red circle the conserved cysteine residues forming the conserved disulphide bond). (B) Picture adapted from ref. 53, representing the GPCR phylogenetic tree. Highlighted in the colored circle the X-ray crystal structure so far available (Opsin, β -adrenergic (β_1 , β_2), Adenosine (A_{2A}), Histamine (H_1), and Chemokine (CXCR4) subfamilies).



1.1.2 Residue Numbering Scheme

GPCRs are extraordinary biological structures, which can be activated by remarkably varied physical or chemical stimuli, and can activate disparate signal transduction pathways. Despite this extraordinary pool of differences, they share a common structure and a conserved activation mechanism.^{4,12-21} This is likely due to the great structural flexibility of these membrane-bound receptors.²²⁻²⁵ Moreover, *Nature* uses few structural motifs to reach flexibility and diversity. Indeed, there are only twenty natural amino acids available in *Nature*, but the pool of proteins and the functions exerted by proteins are limitless. Therefore, the presence of conserved amino acids motifs and similar structural features in proteins is the *leitmotiv* in *Nature*, and protein groups sharing common structural features, and functions can be defined as homologous. As aforementioned, GPCRs are not exception and in 90's *Ballesteros* and *Weinstein* comparing GPCR sequences identified super-conserved amino acids residues (SCRs) among GPCRs.²⁶ On the basis of those observations *Ballesteros* and *Weinstein* developed a numbering index scheme for which the most conserved residues into a TM domain takes the x.50 index. The x represents the number of the TM domain, so as to the most conserved residue in the TM1 is defined by the 1.50 index. The subsequent residues will be defined by the 1.51 index, while the previous one by the 1.49 index, and so for all the residues and TM domains (Figure 3).

Figure 3. Snake-cartoon representation of Class A GPCR structures. In red spheres the super-conserved residues for each TM domains, in green spheres the conserved residues in GPCRs micro-domains, in yellow spheres the non conserved residues into conserved GPCRs micro-domains. The overlapped spheres represent two possible alternative residues.

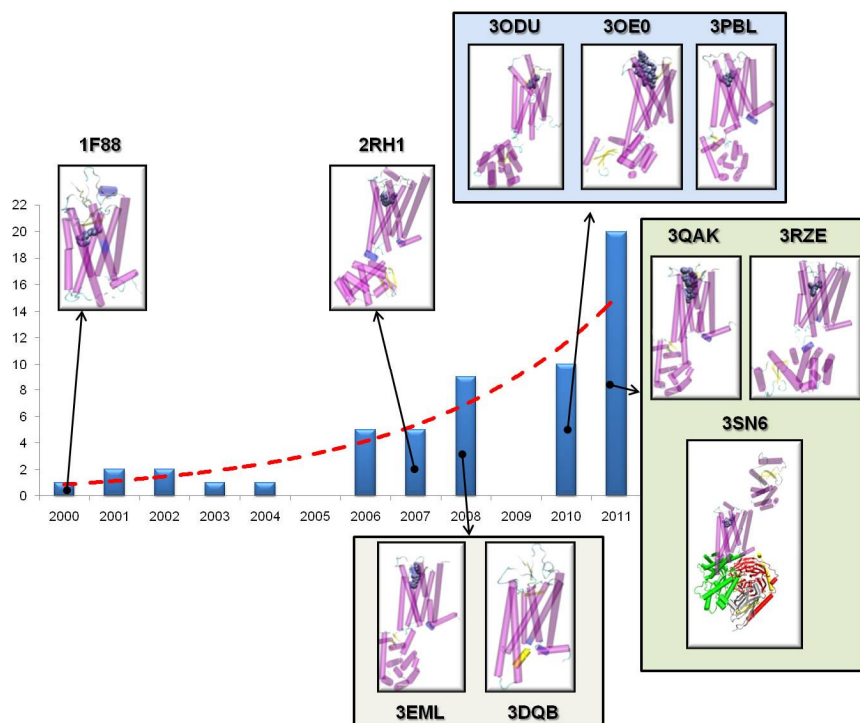


This residue numbering scheme is widely accepted from the scientific community and in this thesis I will refer to particular amino acid residues using the *Ballesteros-Weinstein numbering index*.

1.1.3 X-ray Crystal Structures

X-ray crystal structures of proteins represent one of the most important source of experimental information about the form and function of such proteins at atomic level. To grasp atomic details of a protein of interest is useful not only to understand the structural features of that protein, but also in the understanding of the thin connections binding a protein to a drug, and to pick up initial information about the mechanism underlying a physiological process (i. e. comparing different conformational states of the same protein). For long time membrane proteins represented the most challenging target in structural biology owing partially hydrophobic surface, flexibility, and poor stability.²⁷ For this reason, despite their pharmaceutical relevance, 3D structures of GPCRs were not available until 2000, when *Palczewski et al.*¹⁸ reported the crystal structure of the bovine Rhodopsin receptor, thus inaugurating a new era in the GPCRs field. From this time onwards the number of X-ray crystal structures of GPCRs in their inactive state has continuously increased (Figure 4), and the first hypothetical structure for an active state of a GPCR was also reported.^{17,28-30} The increased availability of crystallographic structures,^{17,30-36} along with other experimental data,³⁷⁻³⁹ supports the notion that GPCRs are dynamically versatile, and their functionality depends upon a high degree of plasticity.^{22,23,40} For many years this GPCR dynamic plasticity was elusive, and represented one of the greatest challenges for medicinal and computational chemists. In this section I describe the main breakthroughs made in GPCR structural biology, presenting a short description of the main crystallographic techniques used to solve GPCRs structures, and discussing the main GPCRs X-ray Crystal structures representing milestones in this field.

Figure 4. Number of X-ray crystal structures deposited in the PDB Database, per year (Blue Histograms). Representative structures are highlighted in the boxes along with their pdb code.



After the release of the first X-ray crystal structure for a GPCR, the bovine rhodopsin one,¹⁸ tremendous breakthroughs in several disciplines have been made, allowing successes in determining the structure of membrane proteins.⁴¹ As a matter of fact, in GPCR structural biology, three main techniques evinced the greatest successes. In particular, (i) the IL3-TL4 exchange in liquid cubic phase (LCP);⁴² (ii) the nanobody stabilization;⁴³ and (iii) the receptor stabilization by amino acid mutations.⁴⁴ In the IL3-TL4 exchange and liquid cubic phase (LCP) technique the combination of LCP and IL3-TL4 replacement is used to improve the structure stability of the GPCRs under study. The limiting step in membrane proteins crystallization is represented by the necessity to remove proteins from their lipid bilayer environment, exposing them to conditions drastically different with respect to their native environment. LCP provides with a more native lipid environment, allowing the stabilization of the membrane protein structure, and the growth of well-ordered 3-dimensional crystal. Moreover, the IL3-TL4 replacement facilitates the growth of diffraction-quality crystal, indeed the TL4 segment provides important crystal-packing interactions, without affecting the receptor structure.¹²

Differently, in the nanobody stabilization approach a G-protein surrogate is used to trap a GPCR under study in a particular conformational state.⁴³ A growing body of experimental evidences suggest that GPCRs are conformationally complex, and can signal through different pathways in a ligand specific manner.^{22–25,37–39,45–48} To solve a high-resolution 3-dimensional structure of a GPCR in its active state is more challenging than to solve the inactive one. Indeed, several studies showed that agonist alone is not sufficient to stabilize the full active state of GPCRs.⁴⁹ In this context, the *Kobilka Lab*⁵⁰ developed the nanobody stabilization technique.⁴³ In this approach, a series of commercially available compounds for the β_2 -adrenergic receptor were screened, in order to identify a full agonist with a long dissociation half-life from the receptor. The identification of compounds characterized by long dissociation half-life is a necessary condition to generate appropriate antibody-derived single domain proteins (nanobody). As a matter of fact, the active-state antigen is required, and compounds with low affinity or that rapidly dissociate are not good candidate for the immunization process. The high affinity and slow off-rate of the agonist increased the probability of maintaining the receptor in an active conformation facilitating the immunization process. Once identified the proper nanobody, this is used to stabilize the agonist-bound state of the receptor in the crystallization environment. Finally, in the receptor stabilization by amino acids mutations approach a conformational stabilization is reached through the identification of a pool of single point mutations able to stabilize the receptor in a specific conformation.^{33,51,52} In this case a library of mutants throughout the receptor is created, every amino acid residues is mutated in alanine, or if the residue is already alanine, to leucine. Each receptor mutant is then expressed, solubilised and its thermostability is evaluated. This, strategy can be also used to identify mutations able to stabilize the receptor in complex with a specific compounds, such as the case of the A_{2A} receptor in complex with the agonist NECA.³³ In that work, the authors identified a pool of 4 amino acid mutations able to trap the A_{2A} receptor in complex with the NECA agonist in its active state, increasing the probability to obtain high-resolution 3-dimensional structures. Table 1 lists the main GPCR X-ray crystal structures, representing milestones in the understanding of GPCRs function and flexibility.

Table 1. Representative GPCRs X-ray Crystal Structures grouped per family. The publication year refers to the release date.

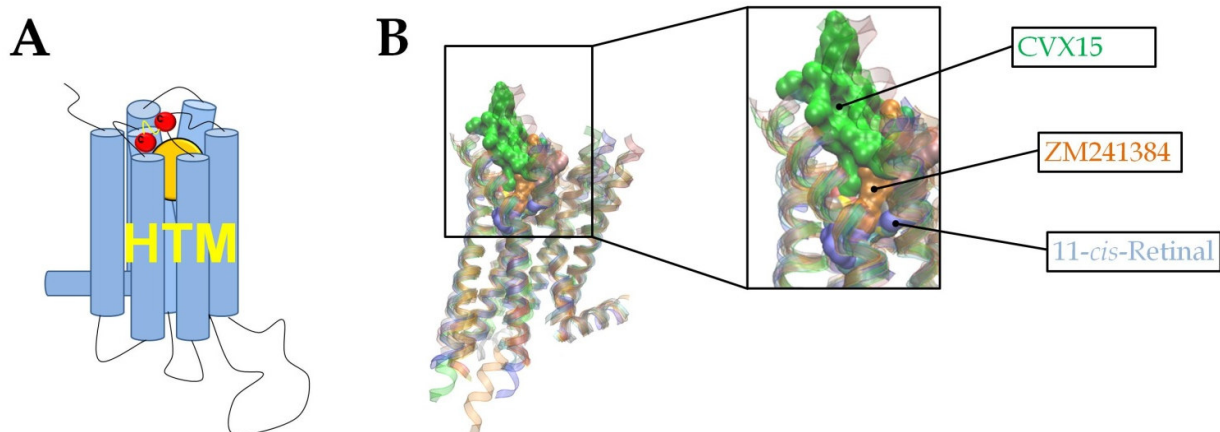
Opsin Family			
PDB Code	Resolution	Pub. Year	Comments
1F88	2.8	2000	First Experimental GPCRs Structure
3CAP	2.9	2008	Hypothetical Active Form of a GPCR
3DQB	3.2	2008	First Active GPCRs Structure in Complex with G _α Fragment
2X72	3.0	2011	First Experimental Evidence of Direct Contacts between ligand and W6.48
Adenosine Family			
PDB Code	Resolution	Pub. Year	Comments
3EML	2.6	2000	A _{2A} Antagonist State
3QAK	2.9	2011	A _{2A} Agonist State
2YD0	3.0	2011	A _{2A} Agonist State, Complexed with the Endogenous Ligand Adenosine
2YDV	2.6	2011	A _{2A} Agonist State, Complexed with NECA
3RFM	3.6	2011	A _{2A} Inverse Agonist State, Complexed with Caffeine
Histamine Family			
PDB Code	Resolution	Pub. Year	Comments
3RZE	3.1	2011	H ₁ Antagonist State
Dopamine Family			
PDB Code	Resolution	Pub. Year	Comments
3PBL	2.89	2010	D ₃ Antagonist State
β-Adrenergic Family			
β ₁ -Adrenergic Receptor			
PDB Code	Resolution	Pub. Year	Comments
2VT4	2.70	2008	β ₁ Antagonist State
2Y00 to 2Y04	2.50-3.05	2011	β ₁ Partial Agonist/ Agonist State (inactive conformations)
β ₂ -Adrenergic Receptor			
2RH1	2.40	2007	First Non Rhodopsin GPCRs Antagonist State
3D4S	2.80	2008	First Experimental Evidences of Direct GPCRs-Cholesterol Interactions
3PDS	3.50	2010	β ₂ Agonist State, Covalently Linked to an Agonist
3POG	3.50	2010	Hypothetical Ternary Complex with G _α -like protein (camelid antibody fragment)
3SN6	3.20	2011	Full Ternary Complex Agonist-β ₂ -G _α β _γ , First Hypothetical Full Active GPCRs Structure
Chemokine CXCR Family			
PDB Code	Resolution	Pub. Year	Comments
3ODU	2.5	2010	First Experimental GPCRs Dimer Structure
3OE0	2.90	2010	Monomeric CXCR4 Antagonist State, in Complex with Peptide
3OE6	3.2	2010	Monomeric CXCR4 Antagonist State, in Complex with Small Molecule

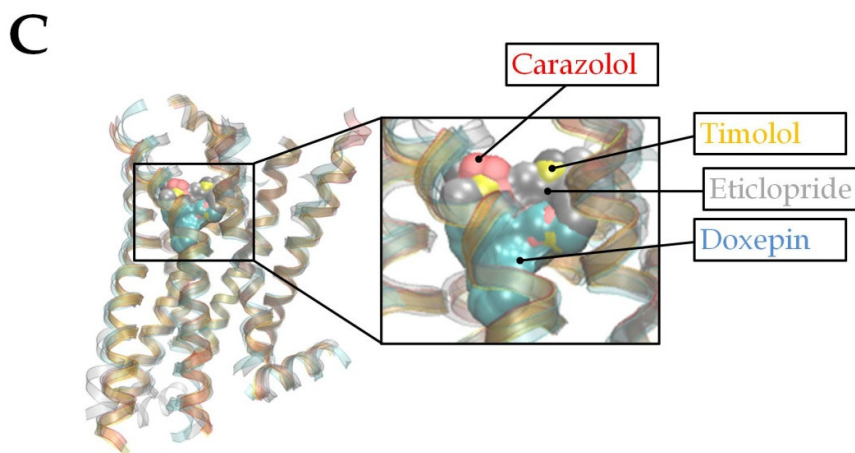
1.2 Orthosteric and Allosteric Binding Sites

1.2.1 Orthosteric Binding Site

Class A GPCRs: by comparing the disclosed X-ray crystal structures of different Class A GPCR subfamilies (Figure 4 and Table 1) it can be appreciate that this class has a conserved location of the orthosteric binding pocket, which is buried into the HTM (Figure 5a). Nevertheless, the way by which ligands can interact with the orthosteric binding site can vary quite markedly, depending on the subfamily considered (Figure 5b,c).

Figure 5. (A) General cartoon-snake representation of a Class A GPCRs, highlighted in dark yellow the location of the conserved binding cleft. (B) Comparison of the X-ray crystal structures of bovine rhodopsin (1GZM, blue); turkey β_1 -adrenergic (2VT4, silver); human β_2 -adrenergic (2RH1, red and 3D4S, yellow); human H₁ (3RZE, cyan); human D₃ (3PBL, gray), human A_{2A} (3EML, orange); and human CXCR4 (3OE0, green and 3OE6, pink) receptors, in their inactive states. Highlighted in the black box the location of each compound within its own X-ray crystal structure (represented in vdW surface mode, and color coded according to the legend of the X-ray crystal structure). (C) Comparison of the X-ray crystal structures of the aminergic subfamily, turkey β_1 -adrenergic (2VT4, silver); human β_2 -adrenergic (2RH1, red and 3D4S, yellow); human H₁ (3RZE, cyan); human D₃ (3PBL, gray). Highlighted in the black box the location of each compound within its own X-ray crystal structure (represented in surface mode, and color coded, according to the legend of the X-ray crystal structure).





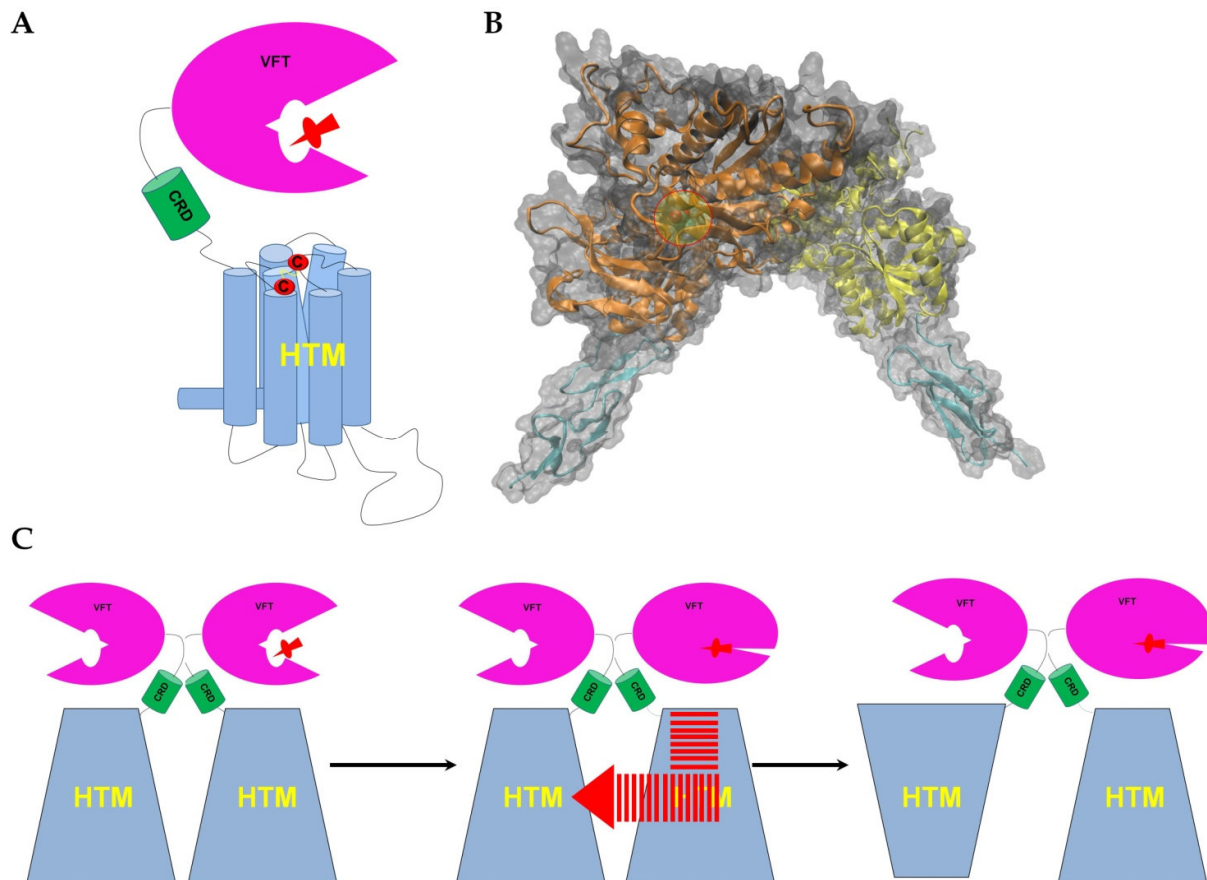
The aminergic subfamily shows a high degree of conservation of both location of the cavity (Figure 5c) and residues involved in the ligand-binding pocket, with respect to other Class A subfamilies.^{4,53,54} As a matter of fact, in the aminergic receptors the core binding site is localized fairly deeply within the HTM bundle (Figure 5c), by contrast the A_{2A} binding site is much closer to the loops, and in the CXCR4 the cavity is much larger and shallower than in other disclosed GPCR structures (Figure 5b,c). Moreover, aminergic receptors have a high degree of conservation of the residues involved in ligand recognition, in particular D^{3.32}, T^{3.37}, S^{5.43}, S^{5.46}, W^{6.48}, and Y^{7.43} seem to be a recurrent motif in aminergic receptors. The high conservation of the ligand-binding pocket likely underlies the difficulty to obtain very selective drugs. Nevertheless, subtype selective drugs for the β_1 - and β_2 -adrenergic receptors were reported.^{55,56} In this case the subtype selectivity of the reported drugs refers to the ability of the compounds to induce different conformational arrangement in different regions of the receptors, rather than the direct interactions with the residues forming the binding cleft. Differently from the ligand-binding cavity, the EL2 is the source of the most suggestive differences, at the extracellular side level.^{4,53,54} The analysis of the disclosed X-ray crystal structures highlighted that EL2 takes part in the definition of the binding pocket, and the degree of participation in the definition of the ligand-receptor contacts markedly vary in a family/subfamily related manner. Indeed, in the rhodopsin structure EL2 adopts a β -hairpin structure, which covers the 11-*cis*-retinal binding site, while the ECL2 in other GPCR families (adopting different conformations) keeps the pocket unlocked and accessible to the ligands. The β_2 -adrenergic

receptor has a 2.5 turns of α -helix, whilst the ECL2 of the D₃ and H₁ lacks any structural organization. The A_{2A} receptor contains both one turn α -helix and short β -strand. Finally, the CXCR4 receptor possesses a β -hairpin ECL2, which shows a very different spatial orientation with respect to the rhodopsin one, playing a crucial role in the ligand recognition. Indeed, the resolution of the X-ray crystal structure of the CXCR4 receptor in complex with a cyclic peptide (CVX15) and a small ligand (IT1t) has given the opportunity to catch the way through which a small ligand can reach a pocket which evolved to interact with bulky endogenous compounds (chemokines). In this case IT1t (small ligand) interacts with D187, R183, I185 (on ECL2), and with E^{7.39}, D^{2.63} (on HTM) that are also relevant for the binding of the N-terminus of the chemokines, as well as the cyclopeptide CVX15. Moreover, until the disclosure of the 3-dimensional structure of the β_2 -adrenergic receptor it was believed that a unique disulphide bond linking the ECL2 to the TM3 domain was a common conserved feature among GPCRs. The analysis of the aforementioned structures made known that more than one disulphide bond are possible at the ECL level, and that these bridges take part in the definition of the ECL conformational state, as further confirmed by the disclosure of the X-ray crystal structure of the A_{2A}, D₃, H₁ and CXCR4 receptors.

Class C GPCRs: another important class of the GPCR family is represented by the Class C or Glutamate family. The first members of the Class C to be cloned were the metabotropic glutamate receptors (mGluRs) at the beginning of 90s.^{57,58} Class C GPCRs are poorly characterized at structural level, and X-ray crystal structures of full-length Class C are still lacking. Nevertheless, the members of this family represent intriguing and attractive targets in medicinal chemistry. Indeed, in Class C we can find receptors for the major excitatory neurotransmitter into the CNS, the glutamate, which binds the metabotropic glutamate receptors (mGluRs), and receptors for the major inhibitory neurotransmitter into the CNS, the GABA, that binds GABA_B receptors.^{59,60} It has been hypothesized that Class A, and C members share common structural features at the HTM level,²⁰ but differently from the Class A, Class C members possess a huge N-terminal extracellular domain, named *Venus Fly Trap domain* (VFT). Moreover, the VFT domain is linked to the HTM domain by a communication hinge, named *Cysteine Rich Domain* (CRD) (Figure 6a).

The VFT domain contains the orthosteric binding site (Figure 6a), and given the pharmaceutical relevance of the members of Class C,⁵⁹⁻⁶⁵ several efforts to decipher the structures of the VFT domains were made (Figure 6b).⁶⁶⁻⁶⁸ Another peculiar characteristic of this class is their constitutive dimerization at the extracellular surface level.^{59,60} The homomeric receptors were covalently linked by disulphide bonds at the VFT level, while the heteromeric ones are not covalently linked, but heteromerization is a required feature to have functional dimers.^{59,60} Indeed, it has been hypothesized that in both homo- and heteromers, one of the subunits is responsible for the ligand binding at the VFT level, while the other one transmits the signal to the downstream signal machinery inside the cell (Figure 6c).^{59,60,69,70}

Figure 6. (A) General cartoon-snake representation of a Class C GPCRs, highlighted in purple the VFT domain, in green the CRD, in blue the HTM, and in red a general orthosteric ligand for Class C. (B) X-ray crystal structure of dimeric VFT of mGluR3 (2E4U), in orange and yellow the two VFTs, in cyan the CRD of each VFT, and in gray and transparent the vdW surface of the whole extracellular portion of the VFTs module for mGluRs, highlighted in the yellow transparent circle the *L*-Glu. (C) Hypothetical trans-activation mechanism for Class C GPCRs.



1.2.2 Allosteric Binding Site

As introduced in the previous sections of this paragraph endogenous ligands bind GPCRs at the orthosteric binding site level, which is located in different regions of the receptors depending on the considered family (such as Class A, and C). Moreover, it has been shown that GPCRs can bind compounds in regions that are different from the orthosteric binding site, usually, called allosteric binding sites.⁷¹ Drugs binding at the aforementioned sites are named allosteric modulators.⁷¹ As a matter of fact, GPCRs can be allosterically modulated by regulatory proteins,^{40,72} lipids and sterols,^{73,74} ions,⁷⁵ and by homo- and heteromerization.⁷⁶ Allosteric binding site for small molecules were identified in different GPCRs, for both Classes A,⁷⁷⁻⁷⁹ and C.^{80,81} Chemical entities targeting regulatory or allosteric clefts can provide relevant advantages in therapeutic applications, in terms of drug safety.⁸² As allosteric binding sites are not exposed to evolutionary pressure to accommodate endogenous ligands, they show high sequence divergence between receptor subtypes. Therefore, allosteric modulators have the possibility to reach greater selectivity than orthosteric ligands, due to the high sequence divergence in allosteric sites among receptor subtypes. Indeed, a well-known example is represented by the mGluRs family, in which all the receptor subtypes possess a VFT domain evolved to bind the endogenous ligand *L*-Glu, while each receptor subtype shows a peculiar allosteric binding site.⁹²

In the next sections I discuss about allosteric binding sites for both Classes A, and C. Moreover, implications in drug design strategies of compounds acting at these sites are elaborated.

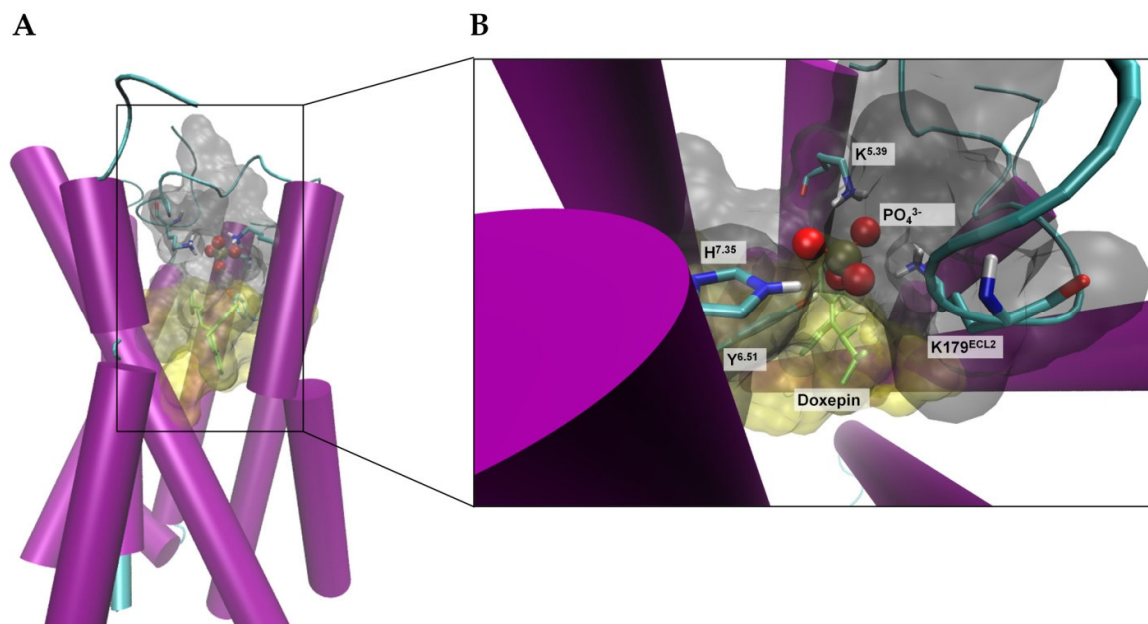
Class A GPCRs: a growing body of experimental evidence about the mechanisms through which allosteric modulators can interact, and modulate Class A GPCRs were reported.^{13,14,53,54,71,75,77-79,82-92} On the basis of the data reported we can subdivide Class A GPCR allosteric modulators into three main groups: (i) ions;^{14,75,87} (ii) bitopic compounds (compounds that bind at the same time both orthosteric and allosteric binding sites);^{53,77-79,83,84,87,89} and cell-penetrating membrane-associated compounds.^{85,90,91,93}

It has long been known that ions concentrations can modulate the ligand-binding affinity for some Class A subfamilies,^{94,95} such as the cases of the H₁,¹⁴ D₂,^{75,96,97} 5-HT_{1A},^{98,99} and

A_{1/2A}⁸⁷ receptors. Ions can alter the ligand-binding affinities for Class A GPCRs through two main mechanisms. In the first one, monovalent or bivalent ions directly interact with the conserved residues D^{2.50} and N^{7.49,75,94,96-100}. The D^{2.50} residue is located in the conserved motif, L^{2.46}xxxD^{2.50,94,95} that faces another conserved micro-domain N^{7.49}P^{7.50}xxY^{7.53}. These motives contribute to the definition of the conformational state for Class A GPCRs.^{4,101-103} Ions interacting with the D^{2.50} and N^{7.49} alter the conformational states of these two conserved motives, and therefore of the whole receptor, inducing different affinity states for the orthosteric ligands. The main structural feature for which a GPCR can become ion-sensitive is the protonation state of the D^{2.50} residue.^{75,94,96-100} As a matter of facts, D^{2.50} is fairly deeply located in the HTM bundle, and the surrounding environment affects its pKa values, and therefore its protonation state. Only GPCRs with an appropriate environment, allowing the deprotonation of the D^{2.50}, can be ion-sensitive.¹⁰⁴⁻¹⁰⁷

The second mechanism for which ions can alter the ligand-binding affinity properties for Class A GPCRs arise from the resolution of the X-ray crystal structure of the H₁ receptor.¹⁴ In this case H₁ receptor shows an anion-binding site close to the entrance of the ligand binding pocket (Figure 7a,b). Phosphate ions bind the aforementioned pocket affecting the ligand-binding affinities of certain orthosteric compounds.¹⁴ The anion-binding pocket represent an ECL subpocket, also able to allocate the carboxylic moiety of the second-generation antihistaminic drugs, characterized by improved pharmacology with fewer side effects.^{14,108} Moreover, it has been reported that sodium ions modulate antagonist binding to the H₁ receptor, in a way similar to that seen in other Class A GPCRs.^{14,75,87,109,110} Therefore, the H₁ receptor represents a borderline example, in which two allosteric ion-binding sites were identified. The first one refers to an ECL subpocket, and is devoted to the binding of anions or the carboxylic moiety of the second-generation antihistaminic drugs, while the second one corresponds to that found in other Class A GPCRs characterized by the presence of the conserved D^{2.50} residue, and is devoted to the binding of cations.^{14,75,87,109,110} Finally, the ECL subpocket is also the site of interaction of the second-generation antihistaminic drugs, joining the H₁ receptor into the GPCR class modulated by bitopic ligands.

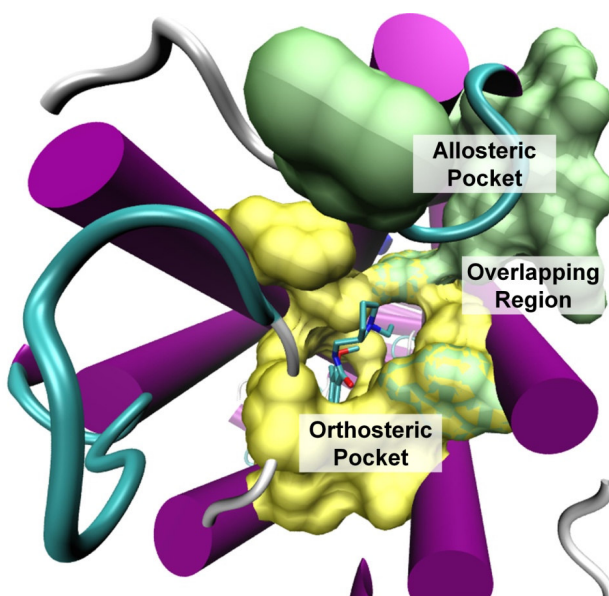
Figure 7. (A) H₁ X-ray crystal structure (purple-cyan cartoon), highlighted in gray and transparent the residues surrounding the phosphate group (dark yellow and red, and balls and sticks); in yellow and transparent the doxepin binding pocket. (B) ECL subpocket allocating the phosphate groups, in stick and color coded according to the atom types the main residues involved in the coordination of the anion (K179^{ECL2}; K^{5.39}; H^{7.35}; Y^{6.51}).



Another class of allosteric modulators for Class A GPCRs is represented by modulators that bind the receptor in proximity of the ligand binding pocket, at the ECL level.^{53,54,71,111} In literature several examples of these types of modulators targeting different Class A GPCRs were reported, such as the case of the M_{1/2/4},^{78,84} CXC_{1/2},⁸⁹ and D_{2/3}.^{13,79} receptors. These modulators can provide relevant pharmaceutical advantages, supporting the possibility to develop bitopic ligands.^{53,54,71,111,112} Differently from Class C GPCRs, Class A have N-terminal domains characterized by reduced size, and in some cases the allosteric binding site can be much closer to the orthosteric binding site. Dualistic (bitopic) compounds combining orthosteric and allosteric pharmacophores can occupy both pockets, leading to drugs with improved affinity and receptor subtypes selectivity.^{53,54,71,111,112} Well-known examples are the case of the M₂,⁸⁴ and D₃ receptors.¹³ In the case of the D₃ receptor the resolution of the X-ray crystal structure (Figure 8) provided

the necessary structural information to elucidate the bitopic behavior of the R22 compound for the D₃ receptor.^{13,53}

Figure 8. X-ray crystal structure of the D₃ receptor (purple-cyan cartoon) in complex with eticlopride (stick and color coded according to the atom types). Highlighted in yellow the vdW surface of the residues lining up the eticlopride binding pocket, in green the vdW surface of the residues forming the putative accessory binding pocket, which accommodates the bulky substituent of the R22 compound. It can be appreciate a partially overlapping region of the orthosteric and allosteric clefts (yellow-green vdW surface).



The last Class A allosteric modulators analyzed in this section refers to the cell-penetrating membrane-associated compounds.^{85,90,91,93} In this case the modulators interact with the receptor through the membrane environment. Cholesterol is the well-known example of this type of GPCR allosterism,^{85,90,91,93} and cholesterol effects on GPCRs functioning will be detailed discuss in the next sections of this Chapter. To date the only examples of cell-penetrating membrane-associated compounds reported in literature is the case of the JF5 modulator, acting on the PAR1 receptor.⁹⁰ In that work the author reported that the JF5 compound interacting with the helix 8 of the PAR1 receptor disrupts the downstream signaling cascade, selectively blocking the coupling of the receptor with G_{αq}-protein.

Class C GPCRs: allosteric modulators acting on this GPCRs class represent the most promising class of modulators.¹¹³⁻¹¹⁷ In Class C we can found the GABA_b, mGluRs and

Ca²⁺-sensing subfamilies. Among them, the mGluRs group is the most representative family of Class C GPCRs, and a huge number of allosteric modulators for the mGluRs family were reported.¹¹⁵⁻¹¹⁷ mGluRs family grouped eight receptor subtypes, and all of them bind the *L*-Glu at the VFT level. Thus, drug targeting mGluRs at their orthosteric binding site have showed important pharmaceutical limitations, such as low subtype selectivity and low ability to cross the blood brain barrier (BBB), due to their charged nature (in this case orthosteric ligands mimic the endogenous ligand *L*-Glu).¹¹⁵⁻¹¹⁷ Therefore, the discovery of allosteric modulators able to target the HTM of the mGluRs receptor (and more in general the HTM of Class C GPCRs¹¹³⁻¹¹⁷), provided new opportunities to gain in terms of drug subtype selectivity and drug bioavailability. Class C, and A share common structural features at the HTM domain level,²⁰ and also for Class C GPCRs the HTM domain hosts the binding site for allosteric modulators. Allosteric modulators were discovered for almost all the member of the Class C,^{83,113-117} and recently the cinacalcet (Sensipar/Mimpara; Amgen) a positive allosteric modulators (PAM) of the Ca²⁺-sensing receptor reached the market.^{83,118}

1.3 Activation Mechanism

The GPCR signaling mechanism has been described as the agonist's ability to induce (or to select) an 'active' conformational state, enabling the coupling of the receptor with its respective G-protein.^{22-25,46-48,119} As already discussed in previous sections of this chapter from 2007 to 2011 relevant breakthroughs in structural biology were made, and the X-ray crystal structure for hypothetical full active states, and intermediate active states for GPCRs were released. X-ray crystal structures provide with static pictures of the proteins under study. On the contrary, proteins are thought to exist in an ensemble of conformations, and each of them can be stabilized by a series of peculiar chemical interaction, defining the energy of that conformational state. The thermodynamically most favorable conformations predominate in the ensemble, and it is conceivable that these structures correspond to those grasped in the X-ray crystal structures. GPCR are not expected to be an exception. Although X-ray crystal structures represents a static frame of GPCRs, these structures together with experimental data,³⁷ such as NMR,¹²⁰ Electron cryomicroscopy density map,¹²¹ and infrared spectroscopy on azido-labeled rhodopsin,¹²² provided with a framework of structural information useful to decipher the activation mechanism pathway for GPCRs. In light of these structural information two main activation mechanisms were proposed,²³ (i) the induced-fit mechanism, that refers to GPCRs with low or null basal activity, such as rhodopsin and angiotensin AT1 receptor, in which a ligand binds the R state (ground state), to form the R-L complex and to promote the formation of the R*-L activated complex; and (ii) the conformational selection mechanism, that refers to GPCRs with high basal activity, such as the β_2 -adrenergic receptor, in which the receptor stand in equilibrium among two main states, the R one (ground state) and the R* one (active state), and agonists bind, and stabilize the R* state.

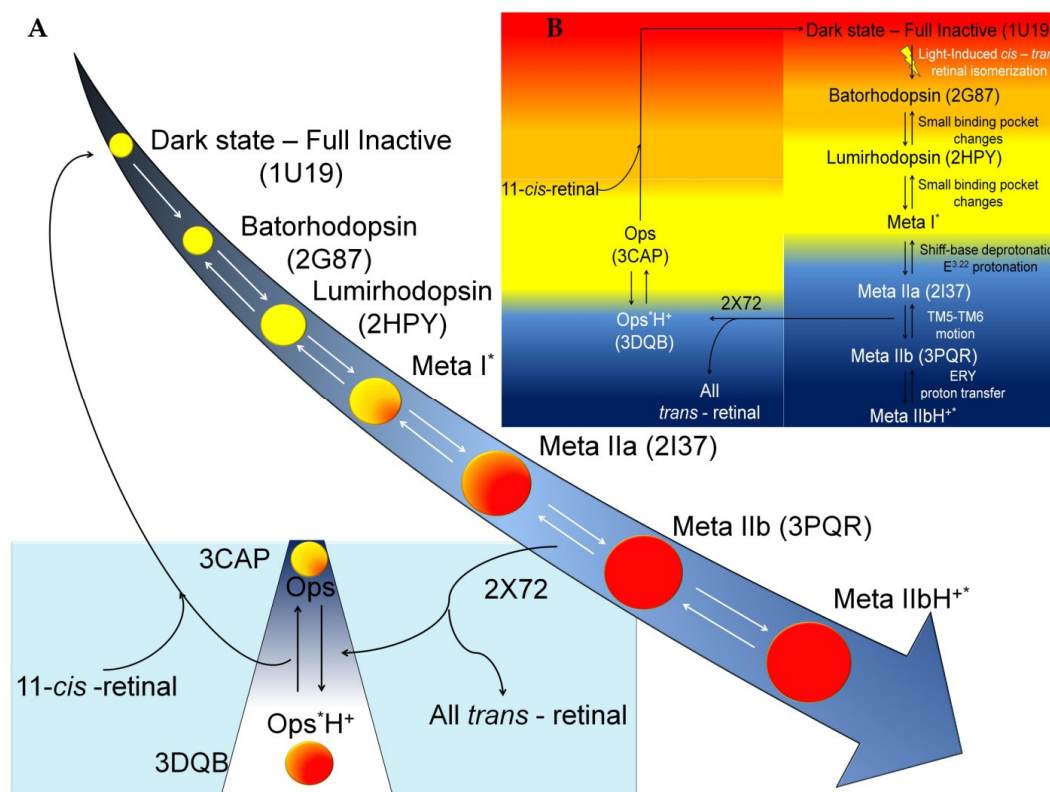
For a long time, rhodopsin was the sole GPCR for which atomic resolution details were reported. Furthermore, rhodopsin shows some methodological advantages with respect to other GPCRs. For instance, rhodopsin can be purified in large quantities from its natural source, and it is stable for weeks in detergent solution.¹²³ These technological advantages, together with the considerable amount of X-ray crystal structure reported, for different intermediate states, make rhodopsin the reference structure, providing a unique

framework in the GPCR functions understanding.¹²³ Along this section I discuss the main steps in the GPCRs activation mechanism, using the aforementioned framework as reference pathway. After that, I discuss the main structural differences occurring in the activation mechanism of each Class A subfamily, so far solved at atomic resolution. It is worth to mention that this framework refers to the conformational changes occurring at the HTM level, and it can be applicable to other GPCR classes, taking into account the recognized differences occurring at the orthosteric binding site, and in the related ligand-binding mechanism.

According to this scheme, three main conformational changes have been described as relevant for the switch between the inactive and the active GPCR states, namely: (i) a W^{6.48} toggle-switch;^{124,125} (ii) the breaking of a ionic lock;¹²⁶ (iii) the TM5-TM6 outwards displacement.^{4,127} In the rhodopsin activation mechanism the first step is represented by the isomerization of the inverse agonist 11-*cis*-retinal to the full agonist all-*trans*-retinal induced by a photon. The isomerization step causes the disruption of the salt-bridge between the protonated Schiff-base and E^{3.28}, responsible for the low basal activity of rhodopsin. Furthermore, the retinal isomerization generates a series of ligand-receptor steric clashes that increase the energy of the system (Figure 9). The ligand-receptor complex relaxes through a series of intermediate active states, named Bato, Lumi, and Meta-I (Figure 9). X-ray crystal structures are reported for each of the aforementioned state (Figure 9). The Bato and Lumi structures highlighted small additional changes occurring at the retinal binding pocket level, for which interaction between the retinal β -ionone ring and residues located on the TM5 and TM6 are changed upon retinal isomerization. In particular, three aromatic residues F^{5.47}, W^{6.48}, and Y^{6.51} are involved in the definition of the interface between retinal and the protein during the transition through the aforementioned intermediate active states. At the Meta-I intermediate state level the deprotonation of the Schiff-base and the protonation of E^{3.22} occur. Moreover, both electron cryomicroscopy density map¹²¹ and infrared spectroscopy on azido-labeled rhodopsin¹²² suggested small rotation of the cytoplasmic side of TM5 and TM6 domains. The Bato, Lumi and Meta-I states are formed in microseconds, because of the low energy barriers among them, and the main activation effects refer to retinal binding pocket

changes (Figure 9).²³ The rate-limiting step is represented by the transition from the Meta-I to Meta-II states, in which large-scale conformational rearrangements occur. In these stages Meta-II substates (Meta-IIa, Meta-IIb, and Meta-IIbH⁺) reached a G protein-dependent equilibrium in few milliseconds (Figure 9). During the Meta conversion relevant changes sequentially occur, (i) β -ionone shift and the released of the W^{6.48} from its ground state; (ii) motion of TM6, and ionic lock breaking; and (iii) proton transfer at the ionic lock level. The opsin states (Figure 9) are reached through the release of the all-*trans*-retinal. These states are characterized by lower affinity for the G protein than the Meta-II states. In summary, retinal isomerization provide the necessary energy to overcome the first activation wall from the dark state to the Bato state, activation proceeds through small structural changes at the binding pocket level, until the Meta-I state. Subsequently, changes in the protonation state beside large-scale conformational changes lead to the Meta-II states, characterized by a G protein-dependent equilibrium (Figure 9).

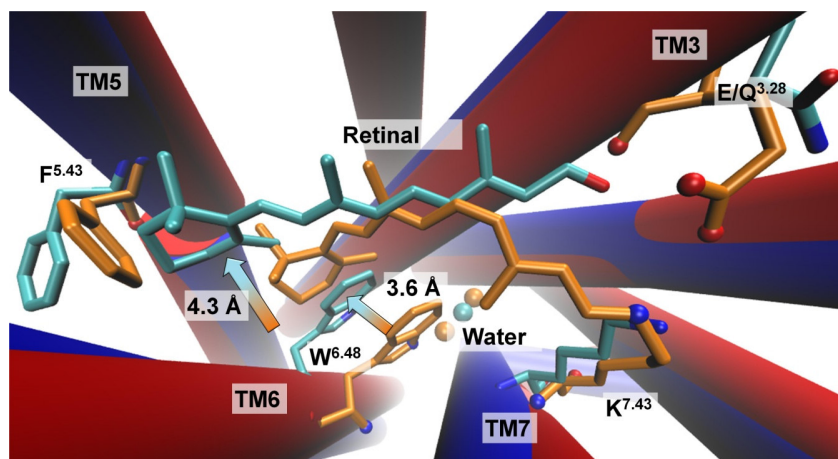
Figure 9. Schematic representation of the rhodopsin activation mechanism. **(A)** Main conformational states occurring during the activation process, beside each conformational state the pdb code of the corresponding X-ray crystal structures. The Meta-I and the Meta-IIbH⁺ states were characterized by electron cryomicroscopy density map and infrared spectroscopy on azido-labeled rhodopsin (*). The affinity of each state for the G protein is color-coded using a yellow-orange-red scale, for which red circles correspond to the highest value of affinity. **(B)** Flow-chart representing the main conformational states during the activation process and the corresponding conformational changes and the pdb codes. The energy profile of each conformational state is color-coded according to the scheme reported in (A), and using a red-yellow-blue scale, in which the blue one corresponds to the most favorable state, taking into account the G protein presence, along the activation process.



As far as the W^{6.48} toggle-switch is concerned, a milestone was placed by the resolution of the constitutively active rhodopsin mutant E113Q in complex with the carboxy terminus of the α -subunit of its cognate G-protein (2X72).¹⁰¹ Differently from the other hypothetical active states of the rhodopsin, 2X72 is trapped in an active conformation able to retain the retinal in the binding pocket after photoactivation. In the 2X72 structure the β -ionone ring is shifted by 4.3 Å with respect to the position of the retinal in the ground state of the receptors, and the indole group of the W^{6.48} residue is placed 3.6 Å away from its ground state (Figure 10). The authors proposed that the indole ring of the W^{6.48}, following the β -

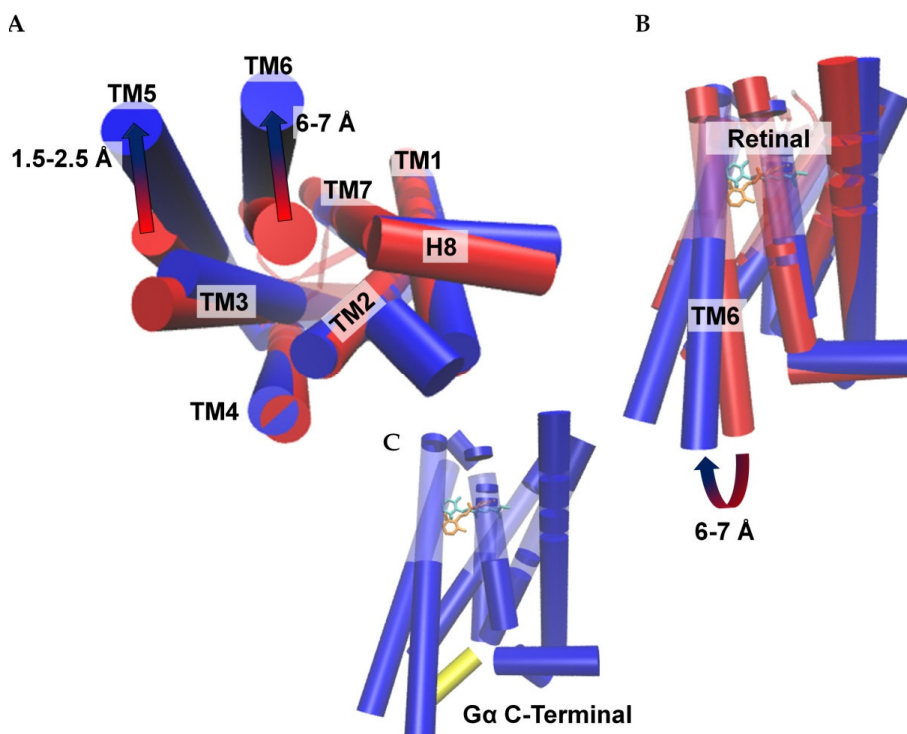
ionone ring, is released from its ground state orientation. The displacement of the indole ring enables the rotation of the TM6, and the authors proposed that the TM6 shift is not achieved by a hinge movement or rotamer changes, but by a global rearrangement of the TM6 through the rotation of the helix, in which the conformational change is accompanied by the bend described by the CW^{6.48}xP^{6.50} motif and the formation of different hydrogen bonding pattern involving conserved water molecules (Figure 10). Moreover, it has been reported that structural activation of conserved water molecules may define the rhodopsin signaling status, thus suggesting a possible allosteric communication, which could be conserved among Class A GPCRs.^{128,129}

Figure 10. Comparison of the 2X72 structure (blue) with respect to the 1GZM structure (full inactive, red). Highlighted in stick and orange the residues of the 1GZM structure in close contact with the inverse agonist 11-*cis*-retinal (stick and orange), in stick and cyan the same residues of the 2X72 structures and the full agonist all-*trans*-retinal. It can be appreciate the shift of the β -ionone ring, and the corresponding shift of the indole ring of the W^{6.48} residues. In close contact with the W^{6.48} residue two water molecules (in orange for the 1GZM structure), and one water molecule (in cyan for the 2X72 structure). In the latter case the water molecule is too far to form the H-bond with the N-H group of the indole ring of the W^{6.48} residue, this interaction is present in the 1GZM structure.



Comparing the structures reported for the rhodopsin receptor it can be appreciate that, during the activation mechanism, the largest conformational change occur at the TM5-TM6 level (Figure 11a,b). The cytoplasmic end of TM6 and TM5 are tilted outwards from the HTM bundle of 6-7 Å, and 1.5-2.5 Å, respectively (Figure 11a,b). These rearrangements allow the formation of a crevice, enabling the binding of the C-terminal domain of the G α protein (Figure 11c).

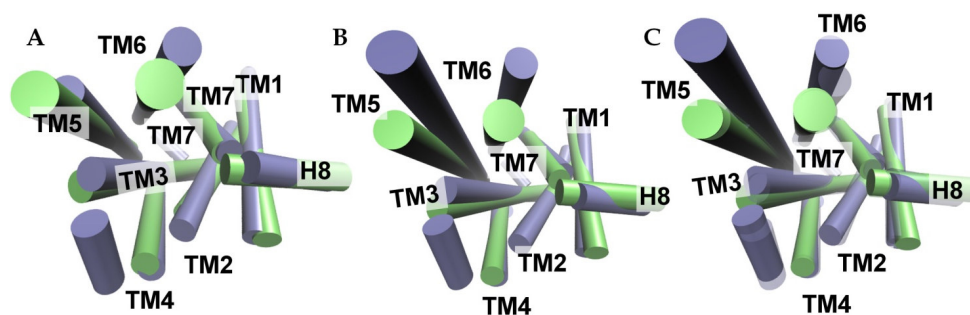
Figure 11. (A) Intracellular side view of the full inactive state (1U19, red), and the full active state (3PQR, blue) of the rhodopsin receptor. Highlighted by red and blue arrows the outward displacements of the TM5 and TM6 domains. (B) side view of the same structures of (A), in which it is possible to appreciate the different position of the retinal into the rhodopsin binding pocket, depending on the active (cyan), and inactive (orange) states. (C) The full active structure (3PQR) of the rhodopsin receptor, in complex with the C-terminal domain of the G_α protein. The different position of the retinal into the rhodopsin binding pocket is highlighted, according to the color code scheme of (B).



Several lines of experimental evidence support the notion that rhodopsin and other Class A GPCR share a common activation mechanism.^{23,102,123,130} X-ray crystal structures for hypothetical GPCRs active states were released for the turkey β_1 -adrenergic,¹⁰³ the human β_2 -adrenergic,^{17,30,31} and the human A_{2A} receptors.^{32,102,131} In the case of the turkey β_1 -adrenergic receptor the receptor was solved in complex with both full and partial agonists. In this occasion the structures were obtained using the thermostabilizing amino acids mutation technique, so as to trap the receptor in a conformation able to bind the agonist or the partial agonists.¹⁰³ These mutant showed conserved ability to activate G protein after stimulation through agonist binding with respect to the wild-type receptor. Nevertheless, those X-ray crystal structures showed conformational arrangements close to the full

inactive state of the same receptor.²¹ These findings suggest that the only agonist binding is not sufficient to trap the receptor in its full active conformational state, and it has been hypothesized that these structures resemble the Lumi state of the rhodopsin (see Figure 9).¹²³ Using the nanobody stabilizing technique the full active state of the β_2 -adrenergic receptor in complex with a G protein surrogate (the camelid Fab fragment),³⁰ and an engineered G_{cs} protein¹⁷ were released. The former one provides a structure resembling the conformational changes occurring at the Ops* stage (Figure 9 and Figure 12a), but does not provide any structural information about the mode of interaction of the receptor with its cognate G protein, and whether these are conserved with respect to those observed in the full active state of the rhodopsin. The latter one resembles the structural arrangements occurring in the Meta-IIb stage (Figure 9 and Figure 12b,c). Interestingly, the β_2 - G_{cs} complex shows larger displacement at the TM5 TM6 level than the Meta-IIb state of the rhodopsin, highlighting structural differences in the way of interaction between these two GPCRs, nevertheless the β_2 - G_{cs} complex underlies a conserved G protein binding pocket among Class A GPCRs.¹⁷ However, the authors stressed the fact that the differences observed in the β_2 - G_{cs} interaction with respect to the Meta-IIb state of the rhodopsin are likely due to the different extension of the contacts formed by the entire G protein.

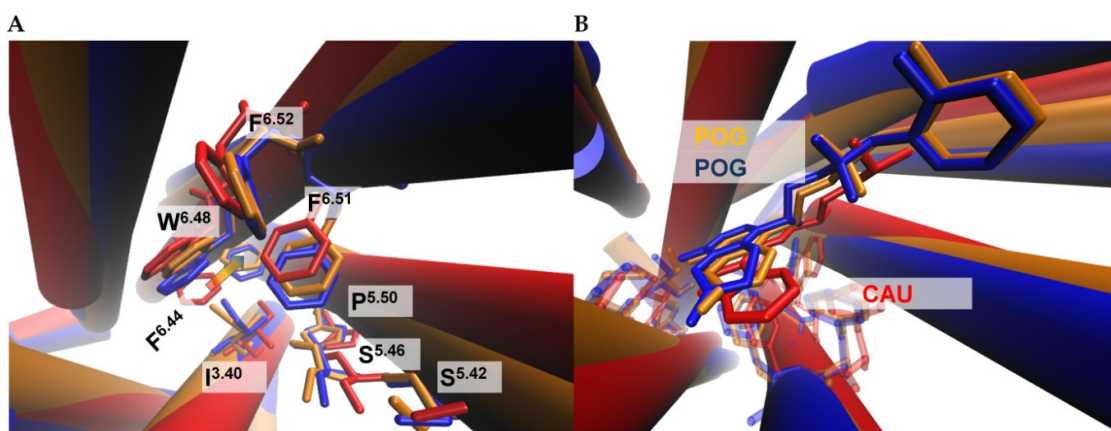
Figure 12. (A) Superposition of the 3POG (iceblue, β_2 -adrenergic receptor in complex with the nanobody), and the 3DQB (lime, Ops* state in the photoactivation mechanism of the rhodopsin receptor) structures. (B) Superposition of the 3SN6 (iceblue, β_2 -adrenergic receptor in complex with an engineered G_{cs} protein), and the 3PQR (lime, hypothetical full active state of the rhodopsin receptor). (C) Superposition of the 3POG (iceblue and transparent), 3DQB (lime and transparent), 3SN6 (iceblue), and 3PQR (lime) structures.



The analysis of the binding pocket of the β_2 -adrenergic structures in both inactive, and active states reveals agonist-induced conformational changes similar to those observed in the rhodopsin receptor (Figure 13a). In particular, the different interaction of the agonist

with the residues of S^{5.42} and S^{5.46} lead to a receptor conformation showing inward displacement of the S^{5.46} and P^{5.50} residues, with respect to the inactive conformation (Figure 13a). These binding pocket rearrangements are translated to a relocation of the I^{3.40} and F^{6.44} residues (Figure 13a). Interestingly, the displacement of the F^{6.44} highlights a rotation of the TM6 domain, when compared to the position of the same residue in the inactive state (Figure 13a). In figure 13b it can be appreciate how the inverse agonist carazolol, and the full agonist POG occupy a very similar position into the binding pocket, with the only differences related to the interaction with the residues of S^{5.42} and S^{5.46} (Figure 13a,b).

Figure 13. (A) Superposition of the binding pocket of the X-ray crystal structures 2RH1 (red, inactive state, inverse agonist-bound state), 3POG (orange, active state, agonist-bound state in complex with the nanobody), and 3SN6 (blue, active state, agonist-bound state in complex with the engineered G_{as} protein). The F^{6.44} displacement is highlighted by the arrow color-coded according to the colors of each structure (red-orange-blue). (B) Superposition of the inverse agonist and the full agonist POG in the binding pockets of each related structure, the colors are in accordance to (A).

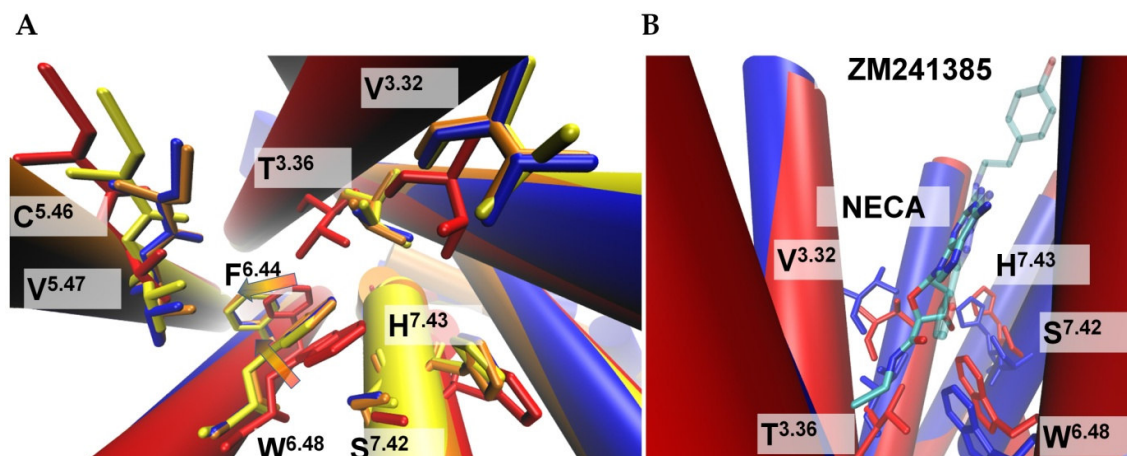


Differently from the rhodopsin receptor, the β_2 -adrenergic receptor shows basal activity,¹³² suggesting that the β_2 receptor is not trapped in a fully inactive conformation in the agonist absence, but possesses several conformational states separated by small energy barriers. In this context, a β_2 agonist would bind different conformations of the ensemble, and the agonist binding to certain conformational intermediates lead to a stabilization of the receptor-ligand complex, shifting the ensemble equilibrium towards those conformations with high affinity for the G protein.²³ These observations are not consistent

with the induced-fit mechanism, suggesting that for the β_2 -adrenergic receptor the activation mechanism occurs through the conformational selection mode.

A further proof that Class A GPCRs share a common activation mechanism was provided by the resolution of the X-ray crystal structure of the A_{2A} receptor.^{32,102} In this sense the comparison of both inactive and active state of the A_{2A} receptor (Figure 14a) highlights similar displacement of the key residues involved in the agonist binding and activation mechanism, when compared to the rhodopsin and β_2 -adrenergic receptor structures (Figure 10, 13, and 14). Moreover, the active states for the A_{2A} receptor show similar outwards displacements, with respect to the active states of both rhodopsin and β_2 -adrenergic receptors.^{32,102} The only difference refers to the dimension of the crevice that allocates the C-terminal domain of the G protein. The small G-protein pocket observed in the A_{2A} receptor in its active state is likely the results of the crystallization techniques used. As a matter of fact, those structures were obtained using the thermostabilizing amino acids mutation, and the TL4-IL3 exchange techniques without to take into account the presence of a G protein or any of its surrogates (nanobodies). G protein takes part in the stabilization of the full active state for a GPCRs, while the presence of the TL4 portion could limits the mobility of the TM5 and TM6 domains.

Figure 14. (A) Superposition of the binding pocket of the X-ray crystal structures 3EML (red, inactive state, inverse agonist-bound state, ZM241385), 3QAK (yellow, active state, agonist-bound state, UK432097), 2YDO (orange, active state, agonist-bound, Adenosine), and 2YDV (blue, active state, agonist-bound, NECA). The F^{6.44} displacement is highlighted b through the arrow color-coded according to the colors of each structure (red-yellow-orange-blue). (B) Superposition of the inverse agonist ZM241385 and the full agonist NECA in the binding pockets of each related structure, the colors are in accordance to (A).



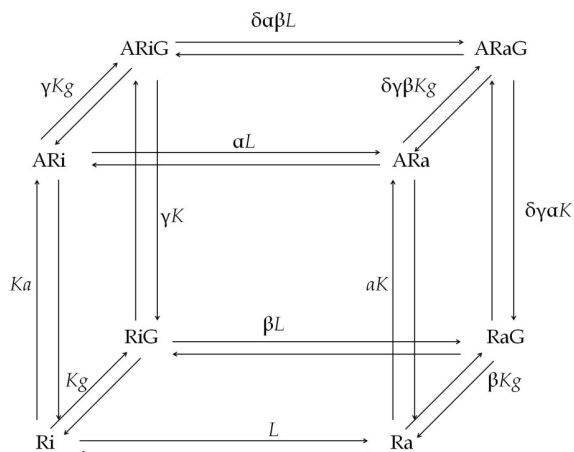
The analysis of the disclosed active states for the rhodopsin, β_1 -, β_2 -adrenergic and A_{2A} receptors clearly demonstrates that agonists bind GPCRs inducing small structural changes at the binding pocket level (in the conserved position 5.42, 5.43, 5.46, and 6.48), that are translated in large conformational arrangements to the TM5 and TM6 domains, following a common activation pathway (in the position 5.50, 6.44, 6.48). Indeed, agonists differently interact with some key residues lining up the GPCRs binding pocket, with respect to antagonists or inverse agonists, enabling the necessary conformational changes at the cytoplasmic surface of the receptors.

1.3.1 Mathematical Models of GPCR Pharmacology

Pharmacological models represent simple mechanistic methods to describe pharmacological responses to a drug. These models required assumption such as the null method, that allows the consideration of the solely interaction between a drug and an enzyme/receptor, excluding the cellular effects in the quantification of the drug-enzyme/receptor complex activity. *Clark* reported the first attempt to apply mathematical approaches to systematically describe the effects of the drug-enzyme interactions on tissues. From that time onwards multidiscipline breakthroughs were made, and several GPCR pharmacological models were proposed.¹³³ To date, the widely accepted models used to describe GPCRs pharmacology are the Cubic Ternary Complex (CTC) model,¹³⁴ and the probabilistic model of GPCR behavior.¹³⁵

In the CTC model the receptor exists in two main states, active and inactive (R_a and R_i respectively). Ligands have different affinities for the R_i and R_a states (K_a and αK_a respectively). R_a that is not bound to a ligand is characterized by certain affinity for the G protein (K_g), and the ligand-binding confers different affinity of the receptor for the G protein (γK_g). The CTC model also takes into account the interaction between the R_i state and the G protein, and β described the different affinity of the receptor active state, over the inactive one, for the G protein (Figure 15).¹³⁴

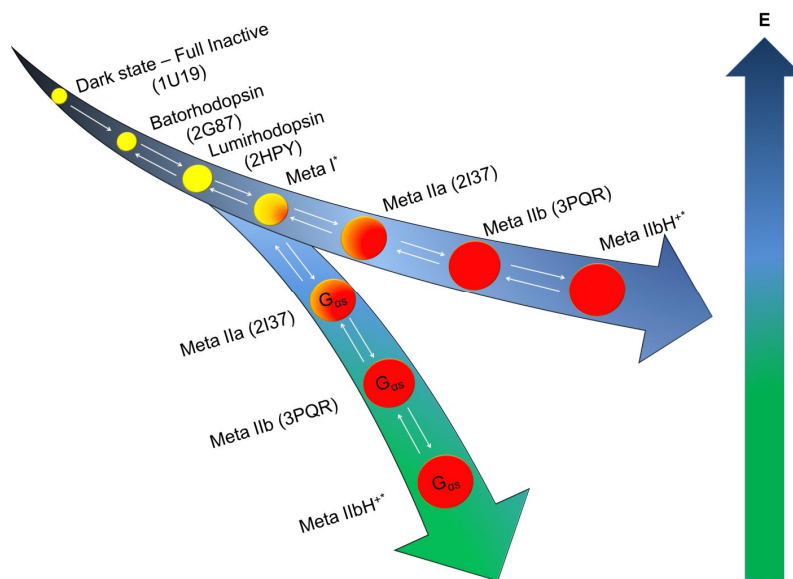
Figure 15. Schematic representation of the CTC model. The Receptor exists in two main states, inactive and active (Ri and Ra respectively), depending on their ability to activate G proteins (G). These conformations coexist according to an equilibrium constant unique for the receptor type ($L=[Ra]/[Ri]$), The term α is the differential affinity of the ligand for Ra and the term γ is the differential affinity of the ligand-bound ARa for G proteins, β refers to the differential affinity of the receptor active state, over the inactive state, for the G protein.



The CTC model is characterized by technical limitations, such as the fact that it must pre-define the species present into the thermodynamic space.¹³³ The Probabilistic Model of GPCR behaviors try to overcome the aforementioned issues. This model assumes that GPCRs have peculiar conformational distribution state in the phase space, and the distribution, characterizing the ground state, is changed upon ligand- and/or G protein-binding. Therefore, the pharmacological activity of a ligand is defined by the amount and the nature of receptor conformations stabilized into the phase space, so as to the amount of the pharmacologically relevant ligand-dependent ensembles are directly linked to the pharmacological activity of the ligand.¹³⁵

The data collected in this section support a three-fold role for G proteins: (i) initiate the intracellular signaling cascade upon ligand-binding to a GPCR; (ii) increase the ligand-binding affinity of an agonist to a GPCR; and (iii) stabilize the active state for a GPCR.^{23,130,133,134} G protein-binding takes part in the definition of the conformational distribution state for a GPCR, lowering the energy barrier of the ligand-active state complex, and displacing the equilibrium towards the active form of the receptor (Figure16).

Figure 16. Hypothetical energy landscape for the rhodopsin ternary complex (11-*cis*-retinal/all-*trans*-retinal-Rhodopsin-G_{as} protein). The presence of the G_{as} protein changes the shape of the energy landscape, stabilizing the ligand-active state complex. The energy of the system increase following the green-blue-dark blue color scheme. In this case we do not take into account the Ops and Ops*H⁺ states as in Figure 9. The affinity of each state for the G protein is color-coded using a yellow-orange-red scale, for which red circles correspond to the highest value of affinity.



1.3.2 Ligand-selective Receptor Conformations

In the previous sections of this chapter I highlighted that GPCRs stand through an ensemble of conformations, and some of them configure the pharmacologically relevant states.¹³⁶ Several lines of evidence suggest that not all agonists produce the same active state.¹³⁶⁻¹³⁸ In particular using the fluorescence lifetime spectroscopy technique it was possible to discriminate different receptor substates for the β_2 -adrenergic receptor, depending on the ligand used for the assay.¹³⁷ *Kenakin* was the first to recognize the pharmacological relevance of this phenomenon, proposing a new scheme for the GPCR signaling pathway, namely “*Agonist Trafficking of Receptor Signaling*”.^{139,140} According to the CTC model reported in Figure 15 a ligand (A) can bind a receptor (R), inducing a particular complex (ARa) characterized by a unique affinity for the G protein (γ). The new idea of *Kenakin* supports the fact that the agonist-binding induces a receptor form ARa that is different from the Ra form of the same receptor, and according to the *Agonist Trafficking of Receptor Signaling* can exist infinite states ARa, depending on the γ value of the ligand

considered. More in general, a ligand can stabilize a given receptor conformation or an ensemble of receptor conformations, exerting its own pharmacological effect. *Kenakin* defined the ensemble of conformation accessible for a given GPCRs '*conformational cafeteria*', and ligands enter the *conformational cafeteria*, and selectively stabilize those conformations for which they have the highest affinity.^{48,136} This new scheme allows to explain the behavior of the so called protean agonism, for which ligands are partial positive agonists in particular receptor systems, and inverse agonist for the same receptor in constitutively active systems, or the pleiotropic behavior of some GPCRs, for which a single receptor activates more than one G protein (Figure 17).¹³⁶

Figure 17. Schematic representation of the Agonist Trafficking of Receptor Signaling scheme. Three different ligands (A_1 , A_2 , and A_3) bind different conformational inactive states (R_i) of the same pleiotropic GPCR, selecting a particular pathway through the potential energy surface (PES) for that receptor. The selected pathway lead to the activation of a particular G protein (A_1 , and A_2), or in the case of the compound A_3 lead to the activation of both G proteins. It can be appreciate that each compound is characterized by different pharmacological parameters (αK , $\delta\gamma\beta K_g$), allowing the selection of a particular pathway through the PES. Thus, exploring different basins characterized by different amount of substates, according to the depth of such ensemble.

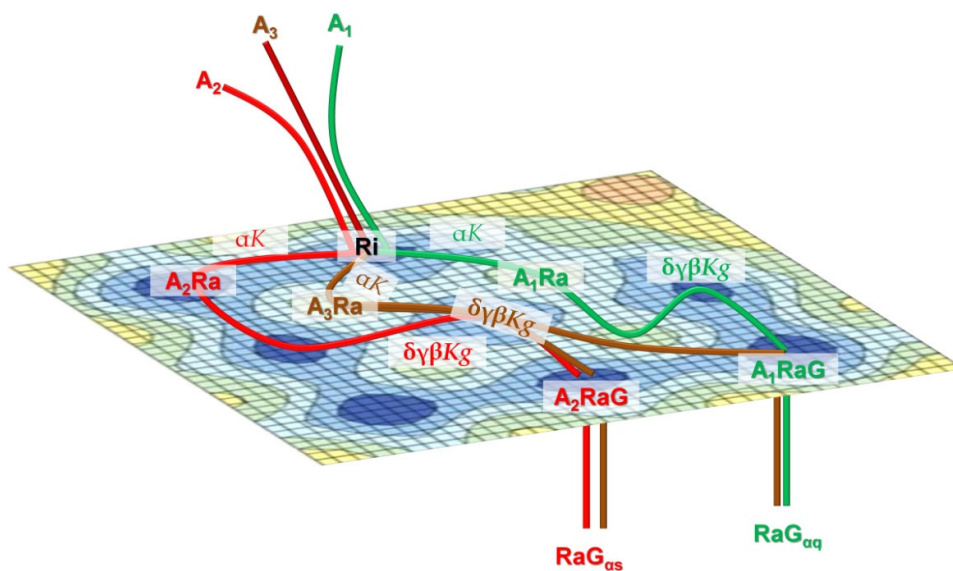


Table 2 lists GPCRs for which experimental evidences for the Agonist Trafficking of Receptor Signaling were reported, references about the data reported in the receptor listed in Table 2 can be found in ref. 49.

Table 2. List of relevant GPCRs for which the Agonist Trafficking of Receptor Signaling was experimentally reported.

Receptor
PACAP
Dopamine D ₂
β ₁ -adrenergic
β ₂ -adrenergic
α _{2A} -adrenergic
5-HT _{1A}
5-HT _{2A}
5-HT _{2C}
Chemokine CCK
Chemokine CCK2
Chemokine CCR5
Chemokine CXCR2
Muscarine Acetylcholine
Adenosine A ₁
Cannabinoid
Delta Opioid
Parathyroid
Bradykinin
NK ₁
Angiotensin II
Bombesin
Calcitonin

1.4 GPCR Dimers as New Pharmacological Tools

For a long time it was believed that GPCRs work as a single functional units, assuming that receptors participate as monomeric unit in ligand-binding, and signal transduction process. The monomeric functional unit view is today challenged by the notion that GPCRs may dimerize or even oligomerize under physiological conditions,¹⁴¹⁻¹⁴⁴ allowing a reinterpretation of some unusual or anomalous observations observed in the past years in the field of GPCR pharmacology,¹⁴⁵ and provides potentially exploitable new targets for a variety of therapeutic conditions.¹⁴¹⁻¹⁴⁴ Although it is well accepted that a monomeric GPCR can activate the downstream signaling cascade,¹⁴⁶ GPCR oligomerization is becoming a widely accepted concept in the GPCR pharmacology field.¹⁴¹⁻¹⁴⁴ The first experimental evidence supporting the GPCR oligomerization phenomenon was reported in the second half of 90s, when *Marshall et al.* reported the existence of the first GPCR heteromer for Class C GPCRs, the GABA_{B1}-GABA_{B2} one.¹⁴⁷ To date, several example of GPCR oligomers for both Class A, B and C were reported,¹⁴¹⁻¹⁴⁴ and it was also revealed that unrelated GPCR classes can oligomerize to form functional heteromer

complexes.^{142,148-150} Despite the increasing amount of reported experimental evidences indicating that GPCR oligomerization is a pharmacologically relevant aspect,¹⁴¹⁻¹⁴⁴ GPCRs aggregates have only sporadically been observed experimentally with structural details,^{15,148,149,151-154} and their existence is based upon a variety of indirect evidences.¹⁴¹⁻¹⁴⁴ In this context, *Pin et al.* proposed criteria that should be required to identify different and physiologically relevant receptor aggregates.¹⁴³ Based on these general guidelines GPCR oligomers show specific and functional properties that can be observed in both heterologous and *in vivo* conditions, such information indicate that GPCR oligomers can be considered the unique receptor functional unit. According to the criteria proposed by *Pin et al.*¹⁴³ the existence of a GPCR oligomer should be accepted by the scientific community if at least two of the following criteria should be met:

- (i) evidence for physical association in native tissue or primary cell;
- (ii) a specific functional property for the oligomeric receptors will be critical to identify such receptors in native tissue (such as positive and negative cooperative binding behaviors, and particular downstream signaling cascade).
- (iii) the use of knock-out animal models or RNAi technology may also provide key information on the existence of oligomeric GPCRs *in vivo* (such as the response mediated by the oligomeric receptor unit should be greatly modified in the absence of one of the protomer species into the complex)

As a matter of fact, it can be possible to distinguish between two different GPCR cross-talk mechanisms, in the first case the cross-talk occurs at the signaling pathway solely (functional crass-talk), in the other case the crass-talk is based on physical receptor-receptor interactions, impairing both ligand-binding and signaling behavior (physical crass-talk).¹⁴³ GPCR oligomerization phenomenon represents a particular case of GPCR allosterism,^{53,92,155,156} in which each protomer into a oligomeric complex allosterically modulate the counter-partner, inducing different pharmacological properties.^{53,92,155,156}

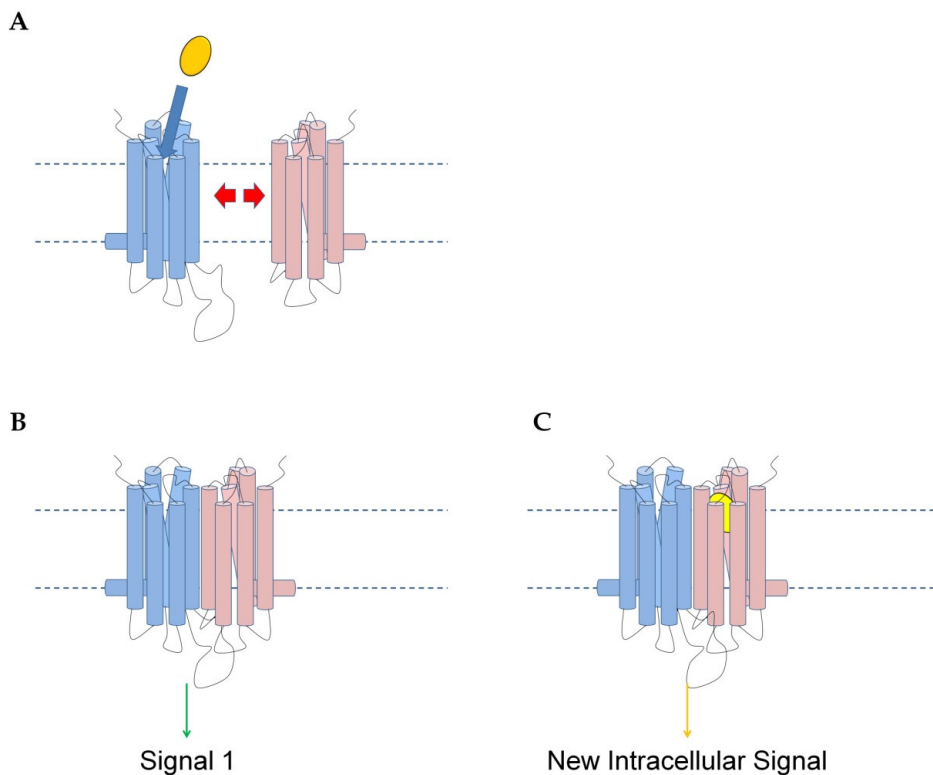
Based on these concepts several examples of pharmacologically relevant GPCR oligomers were reported,¹⁴¹⁻¹⁴⁴ and particularly interesting are the case of the Rhodopsin,¹⁵²⁻¹⁵⁴ Melatonin,^{157,158} Opioid,^{159,160} β_1 - β_2 -adrenergic,¹⁶¹⁻¹⁶⁵ mGluR2-5-HT_{2A},¹⁴⁸⁻¹⁵⁰ and 5-HT_{2A}-5-

HT_{2A}^{166,167} dimers. All the examples aforementioned are characterized by peculiar tissue distribution and structural properties, showing similar or different dimer interfaces.¹⁴¹⁻¹⁴⁴ According to the GPCRs ensemble theory proposed by *Kenakin*,¹³⁶ GPCRs possess different micro-domains that control the interaction with other membrane proteins, also mediating homo- and heterologous dimerization.¹³⁶ GPCRs adopting different micro-conformation states can expose different micro-domains, and therefore can interact with different membrane-bound partners. In this scenario *Kobayashi et al.* reported that the mutation of conserved residues on the β_1 -receptor HTM bundle results in conformational changes disrupting the β_1 -homomerization, but not the β_1 - β_2 -heteromerization.¹⁶⁵ The authors, also found that the lipophilic β -blocker alprenolol acts as a pharmacological chaperone, selecting proper conformational state of the β_1 -mutant, and restoring the basal level of β_1 -homomer.¹⁶⁵ Other examples of the ligand's ability to select different conformational state of protomers into a complex were reported for the D₁,¹⁶⁸ D₂,¹⁶⁸⁻¹⁷³ 5-HT_{2A},^{148-150,166,170-173} CCR5,¹⁷⁴ and mGluR2 receptors.¹⁴⁸⁻¹⁵⁰

Thus, a ligand with peculiar properties can affect the downstream signaling pathway of a GPCR dimer, selecting different conformational states of protomers into a dimer, and promoting or disrupting the formation of a particular GPCR complex (Figure 18).^{148,149,166,169-173}

Taken together these experimental evidences support the notion that GPCR oligomers represent new druggable targets.^{143,175,176}

Figure 18. (A) A general ligand can interact with a GPCR, selecting particular conformational state of that receptor, and promoting or disrupting the formation of a peculiar GPCR dimer, (B) A GPCR dimer have to show a particular downstream signaling cascade according to the criteria proposed by *Pin et al.*¹⁴³, that differs from the downstream signaling cascade of each protomer involved in the formation of the oligomeric complex. (C) According to the criteria proposed by *Pin et al.*,¹⁴³ and to the GPCR ensemble theory a ligand selecting particular conformational state of a protomer into a complex alters the downstream signaling cascade, originating a new signal in terms of intensity and/or nature of the signal.



1.5 Cholesterol Effects on GPCR Pharmacology

Cholesterol is an essential cellular component of biological membranes in almost all eukaryotes, not only providing structural support to the membrane maintenance, but also playing a regulatory role for several membrane-bound proteins, either indirectly through its ability to modulate physical properties of the membrane, and indirectly through specific interaction with selected protein domains.^{177,178} GPCRs constitute the largest class of membrane-bound receptors,^{1,2} and it has long been known that cholesterol takes part in the modulation of GPCR pharmacology.^{93,178-181} In this context cholesterol represents a

particular case of GPCR allosterism, which is classified in the *Allosteric Binding Site* section as cell-penetrating membrane-associated modulators.^{85,90,91,93} In 2008 the *Stevens Lab*¹⁸² released the X-ray crystal structure of the human β_2 -adrenergic receptor in complex with cholesterol molecules.⁹³ In that work the authors also analyzed the cholesterol concentration effects on the ligand-binding affinity for both beta-blockers (timolol) and beta-agonist (isoproterenol). The authors showed that high cholesterol concentration solely increased the ligand-binding affinity of the beta-blocker timolol. This was a relevant outcome of that work, because timolol is a drug currently used in the treatment of cardiac arrhythmias, and blood-pressure diseases.⁹³ Moreover, the authors found that cholesterol binds a cleft described by the TM2-4 domains, and that the residues lining up the cholesterol binding cleft are conserved among several Class A GPCRs (*Cholesterol Consensus Motif*, CCM, Figure 19).⁹³ On the basis of their findings the authors proposed a new classification system for Class A GPCRs based upon the degree of conservation of the residues forming the CCM. On the basis of this new classification system, GPCRs showing a high degree of conservation of the CCM belong to the strict-CCM class (Table 3), while GPCRs showing low percentage of conservation of the aforementioned motif belong to the CCM class (Table 3).⁹³ In another work *Pontier et al.* combining extensive biochemical and pharmacological approaches showed that cholesterol depletion in lipid raft structure increases the ability of the β_2 -adrenergic receptor to interact with its cognate G_{as} protein, while the enrichment of the membrane environment with cholesterol shifts the receptor into its inactive state,¹⁸³ according to the data reported by the *Stevens Lab*¹⁸² for which cholesterol binding to the CCM motif affects only the ligand-binding affinity of the beta-blocker, without any effects on the binding curve of the beta-agonist.⁹³

Figure 19. CCM of the β_2 -adrenergic receptor, in white and vdW surface the two cholesterol molecules (in red the oxygen atoms) binding the CCM, highlighted in red, orange, green, and cartoon the TM2, TM3, and TM4 respectively. In stick and color-coded according to the atom types the conserved residues into the CCM, in transparent and iceblue the cholesterol cleft described by the TM2-4 domains.

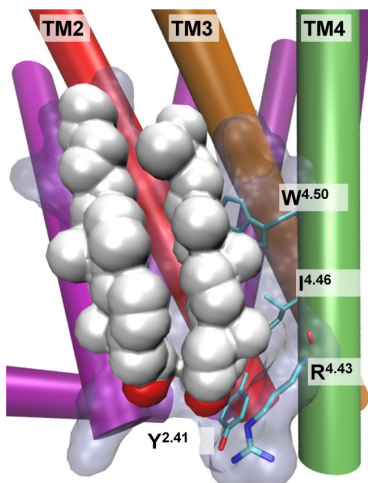


Table 3. Representative examples of Class A GPCRs belonging to the Strict-CCM or the CCM classes.

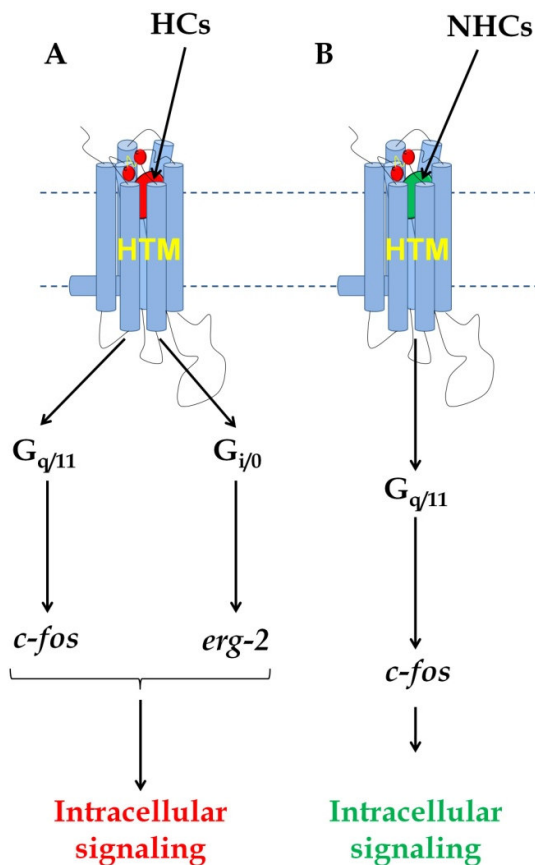
Class A GPCRs	
Strict-CCM	CCM
5-HT _{2A}	β_1
β_2	CB ₂
D ₂	D ₄
Oxytocin	H ₁

Furthermore, it has been reported that cholesterol can modulates the functions of other GPCR classes, such as the Class C.¹⁸⁴⁻¹⁸⁶ For instance, cholesterol effects on the endogenous orthosteric binding affinity for the mGluR2 receptor were reported.^{184,186} It is worth to mention that Class C GPCRs show low sequence similarity to Class A, and they do not show the conserved CCM, nevertheless the signaling status of Class C GPCRs is strongly affected by the membrane composition, such as in the case of the mGluRs receptors.¹⁸⁴⁻¹⁸⁶

1.6 The Serotonergic Receptor Subtype 2A

Serotonin (5-Hydroxytryptamine, 5-HT) system is involved in the modulation of an impressive number of physiological processes. The effects of the 5-HT are mediated by a large number of GPCR subtypes, influencing smooth muscle contraction, platelet aggregation, digestion, and cardiovascular system. Moreover, 5-HT is one of the endogenous amine involved in the neurotransmission at the Central Nervous System (CNS) level, controlling both behavior, food intake, and neuronal plasticity.^{187,188} There are seven 5-HT receptor subtypes (5-HT₁₋₇),¹⁸⁷ and with the exception of the 5-HT₃ subtype, they are all Class A GPCRs. 5-HT receptor subtypes represent relevant pharmaceutical targets,¹⁸⁸ and among them the 5-HT₂ subtypes received large attention by the scientific community.¹⁸⁹⁻¹⁹³ In particular 5-HT_{2A} receptor subtype represents a validated target in the treatment of CNS disorders, such as anxiety,¹⁹⁴ depression,¹⁹⁴ and schizophrenia.^{195,196} Schizophrenia is a chronic central nervous system (CNS) disease¹⁹⁷ which involves different neurochemical systems,¹⁹⁸ like the dopaminergic,¹⁹⁹ the serotonergic,²⁰⁰ as well as the glutamatergic.²⁰¹⁻²⁰³ The serotonergic hypothesis of schizophrenia received considerable attention and noteworthy is the observation that there are two sets of 5-HT_{2A} agonists namely Hallucinogen Compounds (HCs) and Non-Hallucinogen Compounds (NHCs).^{195,196} HCs and NHCs act at the same serotonergic receptor subtype (5-HT_{2A}) while displaying substantially different phenotypic effects on the behavior.^{195,196,204} These findings are in agreement with the so called agonist trafficking of receptor signaling theory^{46,47,119,136,140,195,205} in which HCs and NHCs can activate different intracellular pathways by selecting different active states of the 5-HT_{2A} receptor.^{195,205} In detail, HCs activate both G_{αq/11} and G_{i/o} inducing the expression of c-fos and erg-2 (Figure 20a), while NHCs solely activate G_{q/11} inducing the expression of only c-fos (Figure 20b).¹⁹⁵ Thus, erg-2 induction is a specific marker for hallucinogen signaling.¹⁹⁵ Moreover, 5-HT_{2A} subtype belonging to Class A shows an high degree of conservation of the CCM, particularly 5-HT_{2A} belongs to the strict-CCM class,⁹³ and several lines of evidence correlated low cholesterol level with behavioral disorders.^{206,207}

Figure 20. Signaling at the 5-HT_{2A} receptor induced by hallucinogenic compounds (HCs, **A**) and non-hallucinogenic compounds (NHCs, **B**);

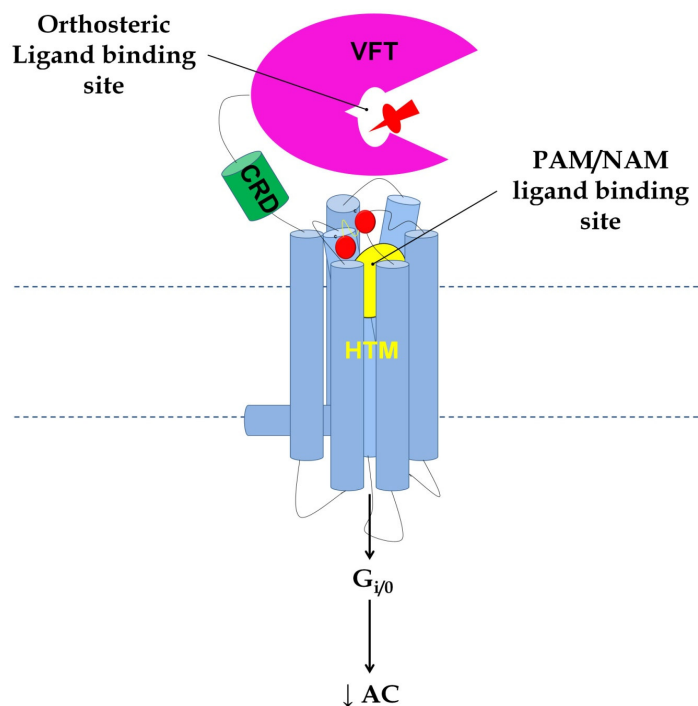


1.7 The Metabotropic Glutamate Receptor Subtype 2

Glutamate is the major excitatory neurotransmitter in the CNS, and it binds two different type of receptors, the ionotropic glutamate receptors (iGlu), and metabotropic glutamate receptors (mGluRs).^{208,209} The mGluRs belong to the Class C GPCRs, and they are grouped in three main families, mGluRI, mGluRII, and mGluRIII, for a total of eight receptor subtypes (mGluR1-8).²¹⁰ Among them the mGluR2 belonging to the mGluRII group received particular attention as pharmaceutical target for the treatment of CNS disease.²⁰¹⁻²⁰³ mGluR2 is negatively coupled to adenylate cyclase via G_{i/0} protein (Figure 21). As discussed in the Orthosteric and Allosteric Binding site section such receptors are characterized by an orthosteric binding site at the VFT domain, and an allosteric binding site at the HTM bundle level (Figure 21). Both orthosteric and allosteric sites represent

druggable targets, especially for the treatment of mental disorders.^{115,203,211-213} Potent mGluR2 orthosteric agonists were identified,^{203,214,215} but due to the high sequence homology at the VFT level with the close-related mGluR3 subtype it was difficult to reach subtype selectivity. Only with the use of mGluR2/3 knockout animal models it was possible to identify mGluR2 as the major responsible of the behavioral control.^{216,217} Based on these assumptions new pharmaceutical strategies devoted their efforts to discover selective mGluR2 allosteric modulators. In this context to reach allosteric subtype selectivity is easier than orthosteric subtype selectivity, because of the low sequence similarity at the allosteric binding site level (see Orthosteric and Allosteric Binding Sites section). As a matter of fact, based on their pharmacological effects it has been possible to identify positive or negative allosteric modulators selective for the mGluR2 (PAM and NAM respectively),^{115,211-213} and mutagenesis studies for antagonist modulators were reported.²¹³ Finally, it has been also reported that mGluR2 signaling status is strongly affected by the membrane composition, in particular by the cholesterol concentration.¹⁸⁴ As discussed in the Serotonergic Receptor Subtype 2A section, low cholesterol levels were also associated to mental disorders.^{206,207}

Figure 21. Cartoon-snake representation of mGluR2, highlighted in purple the VFT domain, in green the CRD, in blue the HTM, in red a general orthosteric ligand binding at the orthosteric cleft, in yellow the allosteric binding site.



1.8 5-HT_{2A} Homo- and Heteromer as Pharmaceutical Targets

As discussed above, the orthosteric binding site of the 5-HT_{2A} receptor represents the target site of several compounds, showing pharmacological activity at CNS level (such as the so called HCs, and NHCs).^{195,196,205} It is also well known that the 5-HT_{2A} receptor is involved in a large number of physiological processes (such as smooth muscle contraction, platelet aggregation, food intake).¹⁸⁸ Recently, it has been reported that 5-HT_{2A} participates to an intricate network of functional crosstalks,^{142,148-150,166,170-173,218} with intriguing consequences on the mechanism of action of antipsychotic drugs. Finally, the 5-HT_{2A} receptor represents a well-known example of functional selectivity, for which (i) different agonists (HCs, NHCs) activate different signaling pathways,^{148,149,195,196,205,219} and (ii) different antagonists induce different effect on the 5-HT_{2A} trafficking and signaling.^{166,220}

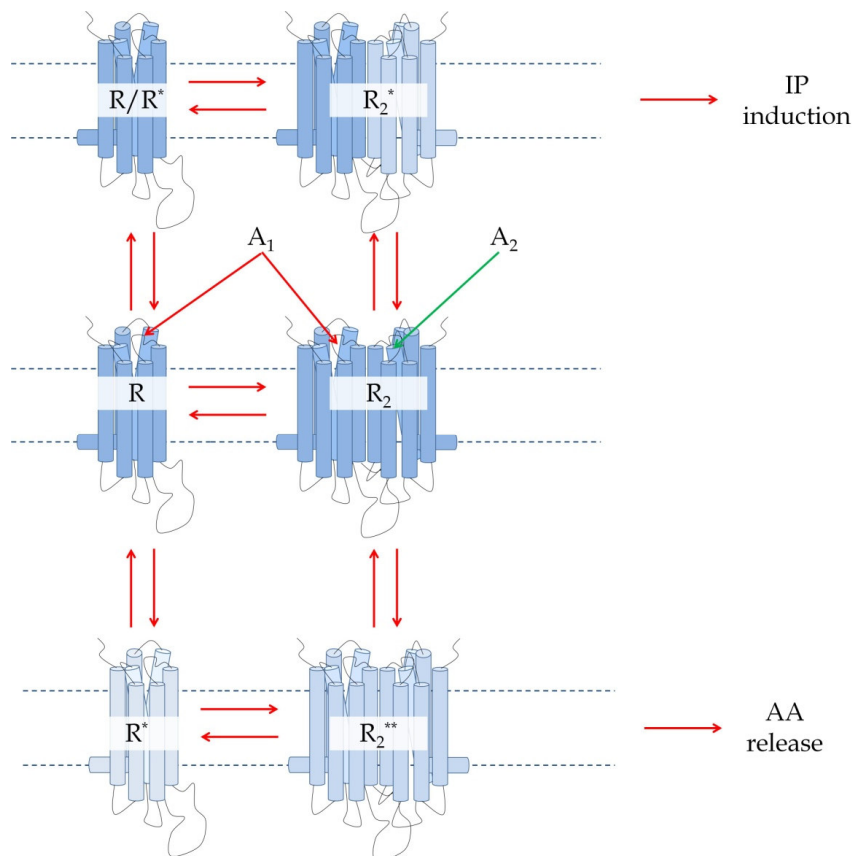
In the next sections of this chapter I introduce two GPCR dimers involving the 5-HT_{2A} receptor, namely 5-HT_{2A}-5-HT_{2A} homomer, and the 5-HT_{2A}-mGluR2 heteromer. Both dimers meet the criteria proposed by *Pin et al.*,¹⁴³ and represent key examples in which GPCR allosterism and GPCR functional selectivity concur to define the nature of the intracellular signaling. Furthermore, the 5-HT_{2A}-5-HT_{2A} homomer, and the 5-HT_{2A}-mGluR2 heteromer represent intriguing pharmaceutical targets, since disrupted functional and physical crosstalks of these two GPCR dimers has seen implicated in CNS diseases, such as schizophrenia, depression and anxiety.^{142,148,149,166}

1.8.1 The 5-HT_{2A}-5-HT_{2A} Homomer Complex

In 2009 *Brea et al.* reported that 5-HT_{2A} homomerized in cells, displaying a dynamic equilibrium between its monomeric and dimeric forms.¹⁶⁶ In this work the authors proposed that atypical and typical antipsychotic drugs, acting at the 5-HT_{2A} orthosteric binding site, antagonized the 5-HT_{2A} receptor in a pathway-specific manner.¹⁶⁶ The 5-HT_{2A} receptor activation induces inositol-phosphate (PP) accumulation through a PLC-correlated pathway, and arachidonic acid (AA) release through a PLA₂-correlated pathway. 5-HT_{2A} agonists show functional selectivity discriminating between these two

downstream signaling pathways.²²¹ The authors performed co-immunoprecipitation, and FRET experiments, showing that 5-HT_{2A} forms homomers in live cells. Furthermore, the authors were able to show that typical and atypical antipsychotic drugs differentiate themselves by blocking 5-HT_{2A} responses by two distinct mechanisms. On the basis of the aforementioned observations, *Brea et al.* proposed the Three-State Receptor Dimer Model,¹⁶⁶ which hypothesizes that the receptor exists in equilibrium between an inactive dimeric form (R_2), and two distinct active states (R_2^* , and R_2^{**}). The model explains the differential functional antagonist profiles by assuming different receptor active conformations for each pathway, for instance the R_2^* state for the IP induction, and R_2^{**} for the AA release (Figure 22). In summary, the authors proposed that 5-HT_{2A} antagonists are characterized by functional selectivity, deactivating GPCR responses in a ligand- and pathway-related manner, thus providing evidences of a functional antagonist-dependent cooperativity for both atypical and typical antipsychotic drugs.

Figure 22. Representation of the Three-State Receptor Dimer Model.



1.8.2 The mGluR2-5-HT_{2A} Heteromer Complex

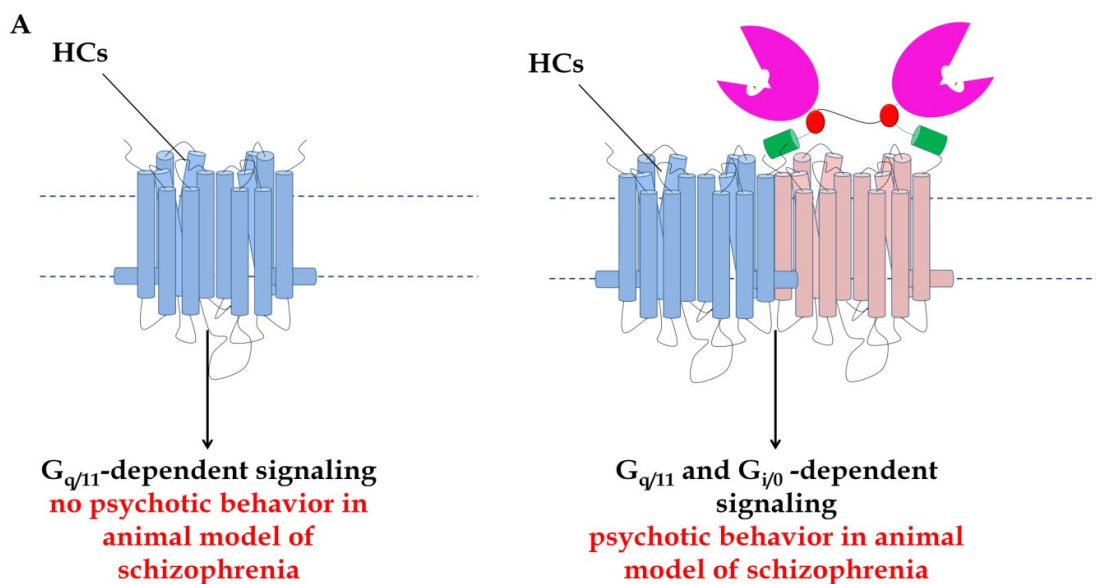
In 2008 *Gonzalez-Maeso et al.* reported that the metabotropic glutamate receptor subtype 2 and the serotonergic receptor subtype 2A physically interact, at pyramidal neurons of prefrontal cortex structures, to form functional heteromer complex.¹⁴⁹ The existence of a functional crosstalk between mGluR2 and 5-HT_{2A} receptors have long been hypothesized by different research groups,²²²⁻²²⁴ but only in 2008 a physical crosstalk was proved.¹⁴⁹ Furthermore, the existence of a functional complex between the mGluR2 and 5-HT_{2A} receptors has been associated with important functional consequences related to the mechanism of action of antipsychotic drugs, for which both receptor subtypes are considered validated targets.²⁰⁰⁻²⁰³ These findings allowed the reconciliation of the serotonergic and glutamatergic hypothesis of the schizophrenia.²⁰⁰⁻²⁰³ In a further work *Moreno et al.* showed that the mGluR2 receptor is necessary for the pharmacological and behavioral effects induced by hallucinogenic 5-HT_{2A} receptor agonist (Figure 23a).¹⁵⁰ In this context, mGluR2 behaves as an allosteric modulator of the 5-HT_{2A} intracellular signaling pathway. Finally, in 2011 *Fribourg et al.* showed that mGluR2 and 5-HT_{2A} receptors are indeed necessary for the pharmacological and behavioral effects induced by both HCs, NHCs, and antipsychotic drugs.¹⁴⁸ In this work, the authors investigated the role of the mGluR2-5-HT_{2A} heteromer complex in altering the G protein signaling. The authors measured the influence of dimerization on signaling of mGluR2 through G_{i/0} protein, and 5-HT_{2A} receptor through G_{q/11}. They reported that ligand binding to both mGluR2 and 5-HT_{2A} protomers alters the G_{q/11}- G_{i/0} balance (Figure 23b). Based on their findings, they propose a new metric, named balance index (BI), to describe the balance between the G_{i/0} and G_{q/11} signaling. This study suggests that both functional and physical mGluR2-5-HT_{2A} crosstalk induce cellular and phenotypic behavior effects different from those produced by mGluR2 and 5-HT_{2A} receptors separately. According to the BI metric, the G_{q/11}- G_{i/0} signaling balance is the dependent variable predicting the psychotic state. Thus, they proposed that 5-HT_{2A} inverse agonists, and/or mGluR2 strong agonists and/or PAM would be the most effective compounds in restoring the physiological BI balance for the treatment of schizophrenia. The observation that the close related mGluR3 receptor was not able to form heteromer complex with the 5-HT_{2A} receptor¹⁴⁹ provided an useful support to investigate which TM domains are involved in the physical interaction between

the mGluR2 and 5-HT_{2A} receptors, so as to grasp the structural bases underlying the mGluR2 and 5-HT_{2A} physical crosstalk the authors studied mGluR2/3 receptor chimera.¹⁴⁹ On the basis of that study the authors proposed a TM4-TM5 heteromer interface arrangement (Figure 23a,b).

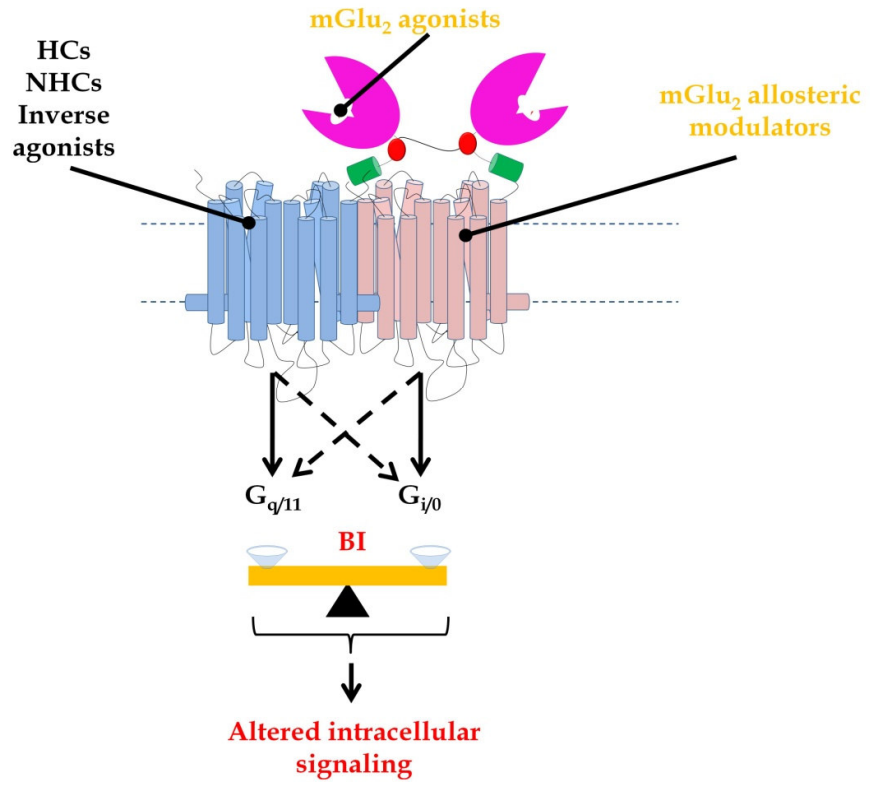
Taken together, all these observations indicate that mGluR2 behaves as an allosteric modulator of the 5-HT_{2A} receptor through direct interaction at the HTM bundle, selecting particular conformational states of the serotonergic receptor depending on the mGluR2-bound ligand (agonist, antagonist or allosteric modulators).^{142,148,149} The observations are also in agreement with the functional selectivity theory.^{46,136,139,140}

The experimental evidences about the existence of a mGluR2/5-HT_{2A} heteromer complex^{142,148,149} and its tissues specificity (pyramidal neurons of prefrontal cortex structures) provide a new and intriguing pharmaceutical target for the treatment of schizophrenia.^{142,148,149,219,225} As a consequence, compounds targeting the specific mGluR2-5-HT_{2A} heteromer complex, and restoring a physiological BI are likely to have improved specificity and reduced side effects.

Figure 23. Schematic Representation of the mGluR2-5-HT_{2A} cross-talk. (A) Different effects exerted by HCs in mGluR2 knockout mice (no psychotic effects), and in WT mice (psychotic effects). (B) Putative sites of action of antipsychotic and psychotic compounds, affecting the BI metric.



B



Chapter 2

Aims of the Project

In the previous chapter I have introduced some concepts highlighting the extraordinary pharmacological and dynamical versatility of GPCRs. Indeed, these membrane-bound proteins revealed an ensemble of complex features. On one hand, GPCRs show challenging pharmacological aspects, such as allostereism, aggregation phenomenon, multi-intracellular signaling pathways, and functional selectivity for different ligand chemotypes. On the other hand, GPCRs reach this extraordinary pool of pharmacological activities by making use of a conserved flexible structure. As a matter of fact, the increased availability of crystal structures, along with other experimental data, supports the notion that GPCRs are dynamically versatile. Their functions depend on a high degree of plasticity, which is strongly affected by a large number of environmental factors in a tissue specific manner. For instance, membrane composition, ionic strength, pH, and interacting proteins alter the pharmacological behavior of a GPCR, concurring to stabilize specific signaling-conformation. For many years this dynamic flexibility was elusive, representing one of the greatest challenges for medicinal and computational chemists. Now, in the light of experimental evidence, it is becoming apparent that computational approaches must be integral to any effort aimed at understanding GPCR functioning. Indeed, not all the 3-dimensional structures of GPCRs have been revealed, and not all the pharmacologically relevant conformation can be grasped by X-ray crystallography, because of their inherent instability.

In this context, with the aid of computational techniques we have focused our attention on the study of two aspects affecting GPCR functioning: (i) the dimerization phenomenon, and (ii) the effect of the membrane composition on GPCR flexibility.

With regard to the dimerization phenomenon, given the increasingly recognized functional importance of dimeric or oligomeric GPCR aggregates, one can ask whether explicit models of homo- or heteromers can better address issues related to ligand recognition or receptor activation. As reported in Chapter 1, the 5-HT_{2A} and mGluR2 receptors are implicated in the formation of different GPCR dimer aggregates. These new functional units have showed functional consequences on the activation mechanism of both antipsychotic and hallucinogenic drugs. Taken together, these information suggest that heuristic constructs of the mGluR2-5HT_{2A} and 5HT_{2A}-5HT_{2A} dimers can have the potential for being better models than the corresponding monomeric models, either in terms of drug discovery efforts or in supporting experiments aimed at deciphering the molecular basis of protomer crosstalk into dimer complexes. The identification of the complex 5-HT_{2A} functioning thus offers a unique possibility to revise the pharmacology of HCs and NHCs in the context of their ability to select individual, yet uncharacterized, dimeric states that in turn can activate (or repress) individual intracellular signaling pathways. Until now, the 5-HT_{2A} receptor was considered and studied as a monomeric entity mainly through homology modeling studies, while the identification of the complexity of the 5-HT_{2A} architecture also offers new challenges for medicinal and computational chemists to build up reliable and predictive models of both homo- and heteromer complexes.

Moreover, it is well-known that cholesterol affects GPCRs functioning through its ability to modulate the physical properties of the membrane environment (indirect effects), or through its ability to establish direct contact with selected domain of the GPCR structure (direct effects). Interestingly, high cholesterol concentrations are found in lipid rafts, which are high-specialized membrane domains, characterized by peculiar physical and pharmacological properties. Lipid rafts provide the structural support to facilitate physiological events, such as protein aggregation. The connection between cholesterol

effects on GPCR functioning, and the cholesterol concentration effects on protein-protein interactions, allows us to speculate about the role of cholesterol in GPCR aggregation.

With the aim to shed light on the aforementioned aspects, we set up a computational study based on the comparative analysis of the effects of each component (dimer interface, and cholesterol concentrations) on the monomeric and dimeric forms of both mGluR2 and 5-HT_{2A} receptors. The following are particularly relevant points:

1. assessment of the dimer effects on the putative 5-HT_{2A} binding pocket, comparing MD simulations of the monomeric form of the 5-HT_{2A} receptor, with respect to the MD simulations of different dimeric forms of the same receptor (5-HT_{2A}-5-HT_{2A}, and mGluR2-5-HT_{2A} dimers)
2. assessment of the cholesterol effects on the monomeric forms of both mGluR2 and 5-HT_{2A} receptors, performing MD simulations of the receptors embedded in membrane environment with different cholesterol concentrations.
3. finally, it is worth to mention that most of the so far reported MD simulations of GPCRs only considered the monomeric forms of these receptors, and did not take cholesterol as membrane component into account. Therefore, we decided to evaluate which is the impact of the MD experimental conditions on the trajectories, thus, obtained.

Chapter 3

Experimental Section

Molecular Modeling groups all those mathematical approximations underlying theoretical methods, and computational techniques. These mathematical approximations are used in computational chemistry, computational biology, and materials science to model or mimic the behavior of both small molecules, and biological systems. Molecular modeling provides useful tools to simplify the complexity within the reality. Therefore, molecular models have intrinsic limitations, which must be taken into account when studying biological system. Nevertheless, molecular models hold an indispensable role in biology, chemistry, physics, and so on. For instance, the growing availability of crystal structures of biological molecules of increasing complexity required the development of molecular modeling techniques, as an aid to their interpretations.

“A Model must be wrong, in some respects, else it would be the thing itself. The trick is to see where it is right”, *Henry A. Bent* said.

In Chapter 1, I showed how the increased availability of crystal structures, along with other experimental data, support the notion that GPCRs are dynamically versatile, and their functionality depends upon a high degree of plasticity. Nevertheless, X-ray crystal structures provide static picture of a system, while GPCRs stand in an equilibrium of pharmacologically relevant conformational ensembles, and it is conceivable that crystallography grasps the thermodynamically most favorable conformation, which predominates in just one of the ensemble. Furthermore, X-ray crystal structures of the HTM domain for the majority of Class A GPCRs, and for all the others GPCR classes are still lacking. In this context molecular modeling techniques such as *Homology Modeling*,

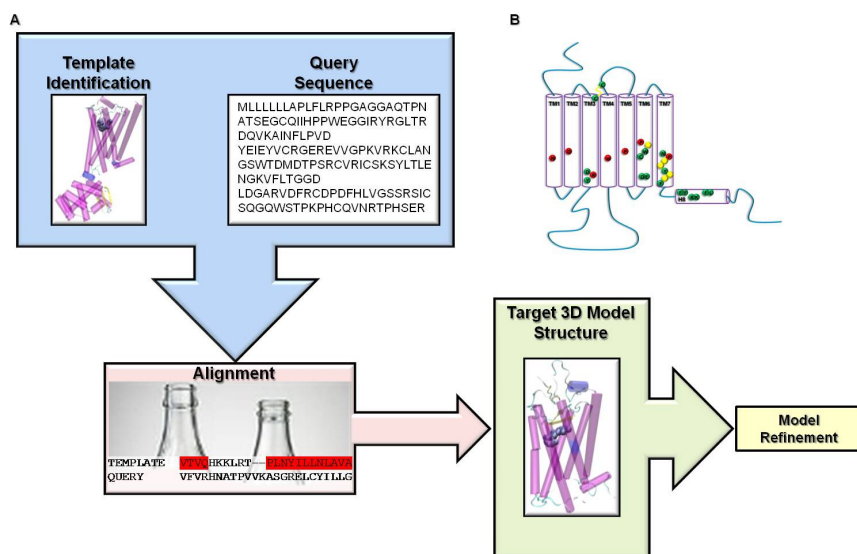
Molecular Dynamics Simulations, and Docking techniques provide with useful tools to overcome, or partially overcome the aforementioned issues.

In this Chapter the molecular modeling techniques used in the project are presented. In detail, for each employed technique I provide a short introduction, discussing both potentialities and limitations of such techniques. After that, details about the experimental settings used in this project are provided.

3.1 Homology Models of GPCRs

Structure Based Drug Design (SBDD) is a computational approach that requires the availability of a 3D structure of the target macromolecule.²²⁶ The 3D structure of the target macromolecule (usually a protein) could be obtained by X-ray crystallography, NMR or by homology modeling. Although in the last years the amount of GPCRs X-ray crystal structures is increased (Figure 4), the homology modeling technique is still a standard method in GPCR SBDD.²²⁷⁻²³¹ Homology modeling or comparative modeling is a computational technique in which the 3D structure of a protein (template) is used to construct an atomic resolution structure model of a target protein for which the 3D structure is unknown (query) (Figure 24a).

Figure 24. (A). Homology Modeling Flow Chart. (B) General snake-cartoon representation of GPCRs. Highlighted in green and red the position of conserved residues in Class A GPCRs, according to Figure 3.



This approach is based on the assumption that homologue proteins have super-conserved stretches of amino acid residues (SCRs) sharing similar 3D structures, and that, in general, 3D protein structures are more conserved than the amino acid sequences. Using the SCRs, the template and query amino acid sequences are aligned to produce a structural model of the target protein (Figure 24a,b).^{229,232}

The 3D structures of both 5-HT_{2A} and mGluR2 receptors were built using the MOE-*Homology Tool* of the suite Molecular Operating Environment (MOE).²³³

3.1.1 5-HT_{2A} Homology Model

The 5-HT_{2A} 3D structure was constructed by homology modeling, using the structure of the human β_2 -adrenergic receptor in its resting state (2RH1) as template. In particular, we chose the aforementioned structure as a template for human 5HT_{2A} due to the close evolutionary relationship between the two receptors (both belonging to Class A GPCRs and both using a biogenic amine as transmitter). Thus, the two sequences of 5HT_{2A} and β_2 were aligned using the ClustalW server,²³⁴ and the resulting alignment (Figure 25) was consistent with that reported by *Gonzalez-Maeso et al.*¹⁴⁹ The loops were built by the loop search method implemented in MOE. The resulting model showed the possibility for the conserved disulfide bond between C148 on TM3 and C227 on the EL2. The protonation state of ionizable residues was fixed by using Protonate3D tool of MOE and then checked by visual inspection. The geometry of the final model was optimized using a stepwise approach: first the internal strain of the model was manually reduced, modifying the rotamers of residues participating to steric clashes. Then, the structure was relaxed by using several cycles of Amber99 force field (available in MOE) minimization, until a gradient of 0.1 kcal/mol Å⁻¹ was reached.

Figure 25. Alignment for the 5-HT_{2A} receptor model (P28223:5-HT_{2A} sequence; P07550: sequence of β 2-adrenergic receptor)

```

sp|P28223|5HT2A_HUMAN      NRTNLSCEGCLSPSCLSLLHLQEKNSALLTAVVIIILTIAGNIIIVIMAVS 100
sp|P07550|ADRB2_HUMAN     -----VWVVGMGIVMSLIVLAIIVFGNIVLVITAIA 59

sp|P28223|5HT2A_HUMAN      LEKKLQNAATNYFLMSLAIADMLLGFLVMPVSMLTILYGYRWPLPSKLCVA 150
sp|P07550|ADRB2_HUMAN     KFERLQTVTNYFITSLACADLVMG LAVVPPFGAAHILMKM-WTFGNFWCEF 108

sp|P28223|5HT2A_HUMAN      WIYLDVLFSTASIMHLCAISLDRYVAIQNPIHHSRFNSRTKAFLKIIAVW 200
sp|P07550|ADRB2_HUMAN     WTSIDVLCVTASIE TLCVIAVDRYFAITSPFKYQSLLTKNKARV IILMVW 158

sp|P28223|5HT2A_HUMAN      TISVGISMPIPVFGL-----QDDSKVFKEGSC-LLADDNFVLIGSFVSF 243
sp|P07550|ADRB2_HUMAN     IVSGLTSFLPIQMHWRATHQEAINCYANETCCDFFTNQAYAIASSIVSF 208

sp|P28223|5HT2A_HUMAN      FIFLTIMVITYFLTIKSLQKEATLCVSDLGTRAKLASFSFLPQSSLSSEK 293
sp|P07550|ADRB2_HUMAN     YVFLVIMVVFVYSRVFQEAKRQLQKIDKSEG-RFHVQNLSQVEQDGRTG-- 255

sp|P28223|5HT2A_HUMAN      LFQRSIHREP GSYTGRRTMQSISNEQKACKVLGIVFFL FVVMWCFEFTITN 343
sp|P07550|ADRB2_HUMAN     -----HGLRRSSKFKLKEHKALKTLGIIMGTFTLCWLPEFFIVN 293

sp|P28223|5HT2A_HUMAN      IMAVICKEESCNEVDVIGALLNVFVWIGYLSSAVNPLVYTLFNKTYRSAFSRYIQ 397
sp|P07550|ADRB2_HUMAN     IVHVIQDNLIRK----EVYILLNWIGYVNSGFNPLIYCR-SPDFRIAFQELLCL 339

```

3.1.2 mGluR2 Homology Model

In the case of the Transmembrane domain of mGluR2, we used the structure of bovine rhodopsin (1GZM) as a template, since there are no clues indicating that the others GPCR X-ray crystal structures could be better templates for family C GPCRs, while 3D models built on the basis of the rhodopsin structure were already reported and partially validated.^{149,235} Differently from the technique used for the 5-HT_{2A} receptor, for the construction of the model of the transmembrane region of human mGluR2 the following approach was used. First of all, the large amino terminal domain (ATD) was manually eliminated from the primary sequence (Expasy Q14416).²³⁶ Then, the TM helices were aligned to the sequence of bovine rhodopsin (1GZM), reproducing the alignment reported by *Gonzalez-Maeso et al.*¹⁴⁹ However, the resulting model, built in MOE, lacked the disulfide bond between C632 on TM3 and C721 on EL2 (numbering from the full length sequence of human mGluR2, Expasy code Q14416). In a different approach, we reproduced the alignment between human mGluR1 and bovine rhodopsin, reported by *Vanejevs et al.*²³⁵ The resulting 3D model of the transmembrane region of mGluR1 was then used as a template for the construction of the 3D model of the highly conserved mGluR2, which, now, showed the TM3-E2 disulfide bond. The models of the

transmembrane regions of mGluR1 and mGluR2 were generated by using the same tools, procedures, and protocols described above for 5HT_{2A}.

Figure 26. Alignment for the mGluR2 receptor model (1GZM: partial sequence of the bovine rhodopsin receptor; hmGluR1/2 sequences of the metabotropic glutamate receptors subtypes 1 and 2 respectively)

```

TM1
1GZM      38 SMLAAYMFLIMLGFPIINFLTLYVTVQ
hmGluR2  565 DAWAVGPVTIACLGALATLFVLVGVFVR
hmGluR1  590 NIESIIAIAFSCLGILVTLFVTLIFVL
                                     1.50

TM2
1GZM      71 PLNYILLNLAVADLFMFVGGFTTTLY
hmGluR2  600 ASGRELCYILLGGVFLCYCMTFIFIA
hmGluR1  625 SSSRELCYIILAGIFLGYVCPPTLIA
                                     2.50

TM3
1GZM     107 TGCNLEGGFFATLGGEIALWSLVVLAIERYVVVC
hmGluR2  630 AVCTLRRLGLGTAFSVCYSALLTKTNRIARIFG
hmGluR1  655 TSCYLQRLLVGLSSAMCYSALVTKTNRIARILA
                                     3.50

TM4
1GZM     148 ENHAIMGVAFTWVMALACAEAPGT
hmGluR2  682 ICLALISQLLIVVAWLVVEAPGT
hmGluR1  709 IASILISQLTLVVTLIIMEPPMP
                                     4.50

TM5
1GZM     204 IYMFVVHFIIPLIVIFFCYQLVFTV
hmGluR2  725 DASMLGSLAYNVLLIALCTLYAFKTR
hmGluR1  750 NLGVVAPLGYNGLLIMSCTYYAFKTR
                                     5.50

TM6
1GZM     249 EVTRMVIIMVIAFLICWLPYAGVA
hmGluR2  757 NEAKFIGFTMYTTCIIWLAFLPIF
hmGluR1  782 NEAKYIAFTMYTTCIIWLAFVPIY
                                     6.50

TM7
1GZM     288 MTIPAFFAKTSAVYNPVIYIMMNKQFRNCMV
hmGluR2  788 RVQTTMCVSVLSSGSVVLGCLFAPKLHIIL
hmGluR1  811 KIITTCFAVSLSVTVALGCMFTPKMYIIAK
                                     7.50

```

For the MD experiments performed to assess the cholesterol effects on the mGluR2 we decided to use a new alignment for the construction of the 3D structure of that receptor. Respect to our previous model of the mGluR2 receptor, we used a new alignment (Figure 27a). Comparing the new alignment with the old one, the main change refers to the TM5, where we shifted the alignment of four residues. In Figure 27b, I report the comparison of the old and the new alignments for the TM5 domain. The 3D structure of the mGluR2 was generated using the MODELLER software²³⁷ which carried out 10 models. The best model was selected among these 10 structures according to the MODELLER objective function and visual inspection. We evaluated the quality of the model on the basis of structural properties such as the presence of the conserved ionic lock and the presence of the disulphide bond between C632 on TM3 and C721 on EL2.

Figure 27. Alignment for the mGluR2 receptor model (P02699: bovine rhodopsin sequence, Q14416:mGluR2 sequence, without VFT)

A

```

sp|P02699|OPSD_BOVIN      MNGTEGPNFYVPFSNKTGVVRSPEAPQYYLAEPWQFSMLAAYMFLIMLGFPINFLTLY
sp|Q14416|GRM2_HUMAN      -----IRWGDAAVAVGPVTIACLALATLFLVLG

sp|P02699|OPSD_BOVIN      VTVQHHKLRT--PLNYILLNLAVADLLFMVFGGFTTTLYTSLHGYFVFGPTGCNLEGFFFAT
sp|Q14416|GRM2_HUMAN      VVVRHNATPVVKASGRELCYILLGGVFLCYCMTFIFIA----KPST---AVCTLRRLGLG

sp|P02699|OPSD_BOVIN      LGGETALWLSLVLAIERYVVVCKPMSNFRFG-----ENHAIMGVAFTVVMALACA
sp|Q14416|GRM2_HUMAN      TAFSVCYSALLTKTNRIARIFGGAREGAQRPRFISPASQVAICLALISGQLLIVVAWLIV

sp|P02699|OPSD_BOVIN      APPLVGWSRYIPEGMQ-----CSCGIDYYTPHEETNNESSVIYMFVVFHFIIPLIVIFFC
sp|Q14416|GRM2_HUMAN      EAPGTGKE----TAPERREVVTLRCNHR-----DASMLGSLAYNVLLIALCTLYA

sp|P02699|OPSD_BOVIN      YGQLVFTV-KEAAAQQQEATTQKAEKEVTRMVIIMVIAFLICWLEEYAGVAFYIFTHQGS
sp|Q14416|GRM2_HUMAN      FKTRK-----CPENF-----NEAKFIGFTMYTTCIIWLAFLPIFYVTSSDYRVQ

sp|P02699|OPSD_BOVIN      FGPIF-MTIPAFFAKTSAVYNEVIYIMMNKQFRNCMVTTLCGKNPLGDDEASTTVSKTE
sp|Q14416|GRM2_HUMAN      TTTMCVSVSLSGSVVLGCLFAPKLHIIILFQPQKNVSHRAPT---SRFGSAAARASSSLGQ

sp|P02699|OPSD_BOVIN      TSQVAPA
sp|Q14416|GRM2_HUMAN      GSG-----

```

B

```

TM5
1GZM      197  ESFVIYMFVVFHFIEPLIVIFFCYGQLV
hmGluR2  725  DASMLGSLAYNVLLIALCTLYAFKTR
                    5.50

TM5
1GZM      204  IYMFVVFHFIEPLIVIFFCYGQLVFTV
hmGluR2  725  DASMLGSLAYNVLLIALCTLYAFKTR

```

3.2 Protein-Protein Docking

Protein-Protein interactions represent one of the most complex and critical event in biology.²³⁸ Such complexes play crucial roles in a variety of both pathological and physiological processes.²³⁸ Therefore, to catch the 3-dimensional structures of a protein complex is fundamental for drug design strategies. Despite their pharmaceutical relevance, to decipher the 3-dimensional structure of a protein complex is still a challenging task.²³⁹ Thus, in the last decades several algorithms designed to protein-protein docking were developed.^{240,241} Nevertheless, protein-protein docking algorithms show common limitations regarding the searching and scoring procedures.²⁴⁰ The former one refers to the possibility to find native protein-protein complex *vs.* misdocked

structures, the latter one refers to the possibility to discriminate among native and misdocked dimer interface on the basis of a scoring functions. For the searching problem, some algorithms seem to give encouraging results,²⁴² while none of the scoring function so far developed seem capable to robustly discriminate between native and misdocked protein complex.²⁴⁰ In order to overcome the aforementioned issues we developed a protein-protein docking method based on (i) collection of the experimental data reporting structural information about GPCR dimer interfaces, (ii) validation of the protein-protein docking procedure using the template so far available, (iii) scoring of the docking poses based on the comparison of the GPCR dimer structures reported. In the next section the experimental procedure and the software employed to build the GPCR dimer interface of interest.

3.2.1 Protein-Protein Docking Procedure and the Rosetta suite.

The dimer complex formed between the 5-HT_{2A} receptor and the mGluR2 receptor is a peculiar case of a heteromer formed by receptors belonging to different GPCR families, namely, Class A, and C, respectively. *Gonzalez-Maeso et al.* demonstrated, by using receptor chimeras and FRET techniques, that TM4 and TM5 of the mGluR2 receptor are necessary and sufficient to form the 5-HT_{2A}-mGluR2 heteromer complex.¹⁴⁹ However, no direct structural evidence of such interface exist for the 5-HT_{2A}-mGluR2 complex. In the same study, *Gonzalez-Maeso et al.* constructed a three-dimensional model with a TM4,5(5-HT_{2A})-TM4,5(mGlu2) interface¹⁴⁹ based on an atomic force microscopy study of rhodopsin in native disc membrane.^{151,243,244} In addition, different research groups implicate the TM4,5 domains in the homomerization of the related receptors 5-HT_{2C}²⁴⁵ and 5-HT₄.²⁴⁶ Taken together all these experimental information support the implication of TM4,5 (5-HT_{2A}) in both 5-HT_{2A}-mGluR2 and 5-HT_{2A}-5-HT_{2A} 's interfaces. Furthermore, *Brea et al.* performing co-immunoprecipitation, and FRET experiments showed that 5-HT_{2A} forms homomers in live cells,¹⁶⁶ based on a dynamic equilibrium between the monomeric and dimeric forms of the receptor, thus, highlighting a transient nature of the 5-HT_{2A} homomeric form, and allowing the formation of different dimers involving the 5-HT_{2A} receptor, such as in the case of the mGluR2-5-HT_{2A} heteromers.¹⁶⁶

The models of both hetero- and homomer complexes were generated using Rosetta++.^{241,242,247} Rosetta works by simultaneously optimizing the side-chain conformation and the rigid body position of the two docking partners. In this case we have used the “blind docking” tool present in Rosetta, thus performing a global random rigid-backbone docking. Before the docking was performed, the side-chain prepacking was carried out as implemented in the Rosetta side chain packing algorithm to prevent errors in docking due to irregularities. After that, a docking with a full atom, high-resolution search protocol, was carried out. A simple Coulombic potential with distance-dependent dielectric was used (only aromatic-aromatic, aromatic-charged, and charged-charged interactions are considered). Finally 50 cycles of Monte-Carlo minimization were used to optimize the resulting complexes. In a calibration study carried out on the theoretical model of rhodopsin homomer (pdb code: 1N3M) by *Pacelwski et al.*,^{151,243,244} starting from two monomers of rhodopsin, we observed that energetic scores could not correctly sort out the output models (Tables 4). Thus, the Rosetta++ outputs were scored and sorted according to visual inspection and RMSD matrix (Table 5). More in details, we visually selected only those models owing a TM4/TM5 interface, and, among them, the ranking was manually performed by using as reference parameters the distance between the monomer, the angle of interaction, and the alignment between the top and bottom edge of the receptors, in such a way as to match as much as possible those found in the 1N3M homomer structure. In Table 5 the RMSD matrix for the mGluR2-5-HT_{2A} heteromer complex is reported, however the same methodology was applied also for the 5-HT_{2A}-5-HT_{2A} homomer. The 5-HT_{2A}-5-HT_{2A} homomer was built by using a 5-HT_{2A} protomer constructed by homology modeling, as previously described. In the next sections, I refer to the protomers of the homomer complex as protomerA (ProA) and protomerB (ProB). The homomerisation interface was modeled as a TM4/TM5 interface, and constructed by selecting a Rosetta++ output structure after visual inspection of geometrical parameters, as described for the mGluR2-5-HT_{2A} heteromer complex.

Table 4. Scores for the docking poses carried out during the validation procedure. In green, the best pose selected by visual inspection.

Rhodopsin dimer					
Filename	Score	bk_tot	fa_atr	fa_rep	hbcs
aatest.ppk_0027.pdb	-726,36	-522,53	-2601,59	1054,32	180,14
aatest.ppk_0050.pdb	-719,71	-528,1	-2610,48	1047,83	180,15
aatest.ppk_0038.pdb	-719,17	-555,25	-2616,49	1012,32	181,79
aatest.ppk_0036.pdb	-718,97	-591,53	-2609,46	989,01	184,26
aatest.ppk_0011.pdb	-718,37	-599,6	-2601,56	972,61	181,14
aatest.ppk_0047.pdb	-718,33	-620,64	-2601,78	962,66	181,43
aatest.ppk_0046.pdb	-718,29	-630,27	-2608,08	947,35	182,34
aatest.ppk_0014.pdb	-716,81	-639,65	-2595,51	932,49	179,08
aatest.ppk_0040.pdb	-716,51	-665,05	-2603,75	917,57	182
aatest.ppk_0020.pdb	-714,97	-667,68	-2589,74	903,6	178,72
aatest.ppk_0007.pdb	-714,71	-671,73	-2594,12	902,51	179,07
aatest.ppk_0008.pdb	-713,57	-671,73	-2594,12	902,51	179,07
aatest.ppk_0010.pdb	-713,34	-675,72	-2595,48	903,19	179,74
aatest.ppk_0049.pdb	-711,26	-676,75	-2595,43	899,83	179,32
aatest.ppk_0021.pdb	-707,06	-677,43	-2578,35	889,24	180,51
aatest.ppk_0015.pdb	-706,77	-678,71	-2591,02	890,53	180,4
aatest.ppk_0033.pdb	-704,8	-684,72	-2600,2	893,48	180,23
aatest.ppk_0043.pdb	-702,51	-684,81	-2596,36	887,43	178,76
aatest.ppk_0012.pdb	-700,29	-691,94	-2592,82	884,35	180,42

Table 5. RMSD matrix of the several output turn out by rosetta++. 1N3M in this case represents the homomeric form of the murine rhodopsine receptor, while the others file are the output poses for the mGluR2-5-HT_{2A} docking poses. In the red circle highlighted the selected complex.

RMSD = 15.522 Å

	2	4	6	8	10	12	14	16	18	20	22	24	26	28	
2: 1N3M.C	0.00	33.3	32.5	33.5	32.9	33.3	33.3	32.4	32.4	34.6	34.5	35.0	35.4	32.4	4.0
4: aatest.ppk_0001.	33.3	0.00	7.87	4.59	2.70	3.67	3.91	9.63	12.0	8.17	6.58	7.35	7.81	7.38	3.5
6: aatest.ppk_0015.	32.5	7.87	0.00	12.0	7.48	9.80	11.2	3.45	6.41	11.0	13.5	11.7	13.1	2.94	3.0
8: aatest.ppk_0018.	33.5	4.59	12.0	0.00	5.76	3.39	1.25	13.9	16.2	11.0	6.02	8.83	8.75	11.7	3.0
10: aatest.ppk_0019.	32.9	2.70	7.48	5.76	0.00	3.94	4.71	8.70	12.0	8.82	8.25	9.41	9.74	6.53	2.5
12: aatest.ppk_0002.	33.3	3.67	9.80	3.39	3.94	0.00	2.42	11.7	14.7	11.3	8.26	9.89	10.2	9.76	2.5
14: aatest.ppk_0022.	33.3	3.91	11.2	1.25	4.71	2.42	0.00	13.0	15.6	10.8	6.56	9.21	9.19	10.8	2.0
16: aatest.ppk_0028.	32.4	9.63	3.45	13.9	8.70	11.7	13.0	0.00	5.40	10.6	14.6	13.2	14.1	2.47	2.0
18: aatest.ppk_0028.	32.4	12.0	6.41	16.2	12.0	14.7	15.6	5.40	0.00	10.8	15.7	12.8	14.0	6.36	1.5
20: aatest.ppk_0029.	34.6	8.17	11.0	11.0	8.82	11.3	10.8	10.6	10.8	0.00	7.27	6.87	5.93	9.04	1.0
22: aatest.ppk_0048.	34.5	6.58	13.5	6.02	8.25	8.28	6.56	14.6	15.7	7.27	0.00	6.16	4.40	12.4	1.0
24: aatest.ppk_0006.	35.0	7.35	11.7	8.83	9.41	9.89	9.21	13.2	12.8	6.87	6.16	0.00	2.87	11.3	0.5
26: aatest.ppk_0007.	35.4	7.81	13.1	8.75	9.74	10.2	9.19	14.1	14.0	5.93	4.40	2.87	0.00	12.2	0.5
28: aatest.ppk_0009.	32.6	7.38	2.94	11.7	6.53	9.76	10.8	2.47	6.36	9.04	12.4	11.3	12.2	0.00	0.0

3.3 Construction of the Membrane-Receptor complexes

3.3.1 Construction of the Molecular Systems for the GPCR Dimer MD Experiments

The mGluR2-5HT_{2A} heteromer and, separately, the 5-HT_{2A}-5-HT_{2A} homomer and the 5HT_{2A} monomer were embedded in explicit phospholipid bilayers resembling a cellular membrane environment. For this purpose, the Membrane Builder tool in the Charmm-gui.org server was used, by employing the ‘replacement method’ for the construction of the bilayer.²⁴⁸⁻²⁵¹ For both systems, a dimyristoyl-phosphatidyl-choline (DMPC)-based bilayer was generated in a rectangular water box in which the ionic strength was kept at 0.15 M by KCl. The overall charge of both systems was automatically neutralized by the Membrane Builder tool. Table 6 and 7 list the characteristics of both systems. Among the several output files generated by the Charmm-gui.org server, there are the topology files that we used for the subsequent molecular dynamic simulations.

Table 6. Parameters used for the embedding of the heterocomplex and of the 5HT_{2A} monomer into the phospholipid bilayer.

Membrane-Receptor complexes						
	mGluR2-5HT _{2A}			5HT _{2A}		
Box Type	rectangle			rectangle		
System Size	x	y	z	x	y	z
	118.863	96.3427	103.672	94.9372	94.9372	104.583
Crystal Angle	α	β	γ	α	β	γ
	90.0	90.0	90.0	90.0	90.0	90.0
Number of Lipids	307			257		
System Building Options	Replacement Method			Replacement Method		
Component Building Options	Water Box	Include Ions (0.15M KCl)		Water Box	Include Ions (0.15M KCl)	
Number of Atoms	123079			97004		
Number of Waters	25816			20429		
Lipids	DMPC			DMPC		

Table 7. Parameters used for the homomer complex embedding into the phospholipid bilayer.

Membrane-Receptor complexes			
5-HT _{2A} -5-HT _{2A}			
Box Type	rectangle		
System Size	x	y	z
	88.525	115.25	112.181
Crystal Angle	α	β	γ
	90.0	90.0	90.0
Number of Lipids	260		
System Building Options	Replacement Method		
Component Building Options	Water Box	Include Ions (0.15M KCl)	
Number of Atoms	114960		
Number of Waters	24526		
Lipids	DMPC		

3.3.2 Construction of the Molecular Systems for the GPCR-Cholesterol MD Experiments

Two different pre-equilibrated SDPC phospholipids bilayers were generated using the membrane-builder tool of charm-gui.org²⁴⁸⁻²⁵¹ (i) 94x94 Å (xy) 0% of cholesterol; (ii) 94x94 Å (xy) with a ratio SDPC:Chol of 3:1. In order to place the receptor into the bilayer a hole was generated, and lipids in close contact (<1 Å distance from any protein atoms) were deleted. For the membrane with cholesterol some SDPC or cholesterol molecules were manually deleted in each layer in order to retain the same ratio (3:1). The membrane-receptor complexes thus obtained were solvated and neutralized using the solvation and autoionize modules of VMD1.8.7.^{233,252} The ionic strength was kept at 0.15 M by NaCl and we used TIP3 water model. The all-atom models of each system were generated by using the CHARMM force-field parameters.²⁵³ Table 8 lists the characteristics of both systems.

Table 8. Parameters used for the embedding of the 5HT_{2A} and mGluR2 monomers into the phospholipid bilayer.

Membrane-Receptor Complex											
5-HT _{2A}						mGluR2					
0% Chol			25% Chol			0% Chol			25% Chol		
System Size (Å)			System Size (Å)			System Size (Å)			System Size (Å)		
<i>x</i>	<i>y</i>	<i>z</i>	<i>x</i>	<i>y</i>	<i>z</i>	<i>x</i>	<i>y</i>	<i>z</i>	<i>x</i>	<i>y</i>	<i>z</i>
94	94	110	94	94	110	94	94	110	94	94	110
Number of Lipids		Number of Lipids				Number of Lipids		Number of Lipids			
195 SDPC		174 SDPC / 58 Chol				200 SDPC		180 SDPC / 60 Chol			
Ions		Ions				Ions		Ions			
SOD	CLA	SOD	CLA	SOD	CLA	SOD	CLA	SOD	CLA	SOD	CLA
47	56	47	56	44	60	44	60	44	60	44	60
Waters		Waters				Waters		Waters			
18166		18207				18231		18282			
Box Type		Box Type				Box Type		Box Type			
Rectangle		Rectangle				Rectangle		Rectangle			

3.4 Molecular Dynamics Simulations

3.4.1 Introduction to MD

MD simulations are computational techniques that, by solving the Newton's equation of motion, provide atomically detailed trajectories describing the dynamic behavior of biologically relevant molecular systems.²⁵⁴⁻²⁵⁶ MD simulation techniques can be subdivided into three main groups: (i) all-atom standard MD simulations or unbiased MD simulations; (ii) enhanced MD simulations or biased MD simulations (such as Umbrella Sampling,²⁵⁷ well-tempered metadynamics²⁵⁸); and (iii) coarse-grained MD simulations.²⁵⁹ In the biased MD simulations a biased potential (external force) is added to enhance the sampling of the phase space, while the coarse-grained techniques are used to represent a system with reduced number of degrees of freedom allowing to perform very long simulations. Several examples of MD simulations of GPCRs and an historical overview of the state of the art of MD simulations applied to GPCRs can be found in *Grossfield*²⁶⁰ and *Johnston et al.*²⁶¹

In this project the dimer interface and cholesterol effects on GPCR flexibility were assessed using unbiased MD simulations techniques.

3.4.2 CPU and GPU Computer Architectures

Last years have seen considerable progresses in the understanding of GPCR structures and functions, and these knowledge have often translated into reliable models for drug discovery. These progresses have been made possible by the increasing availability of GPCR crystal structures and by the availability of new high performance computing (HPC) technologies increasingly potent.²⁶²⁻²⁶⁵ MD software packages were originally developed for serial machines, thus limiting the simulation time of the MD experiments, and the size and complexity of the systems under study. As a consequence, in the majority of the cases MD simulations were carried out in vacuum and for a very short simulation time. The more recent progresses in computing resources provided the necessary support to set up more complicated MD simulations experiments. In this section I discuss the major breakthroughs in the computer architecture field such as the use of CPU and GPU platforms.

Scientific computing requires vast computational resources, and insufficient computing power can result in impracticably long simulation-time or poor accuracy of the results. To date, two technologies enabling parallelism are widely used to overcome the aforementioned issues: (i) multi-core processing units (CPU), and (ii) streaming processor on graphics processing units (GPU). These technologies represent conceptually different methods for parallelizing simulation of physical systems. Differently from CPUs, GPUs have parallel throughput architecture so as to execute many concurrent threads slowly, rather than executing a single thread very fast.²⁶²⁻²⁶⁵ Although GPUs are slower than CPU, having a huge amount of threads may make it possible to perform better than the current multi-core CPUs. Analyzing the memory structure it is possible to differentiate between multi-threaded CPUs and GPUs programming.²⁶²⁻²⁶⁵ Indeed, in a multi-threaded CPU application, all threads have access to a common memory space, so the primary challenge is synchronizing access to shared data structure. On the other hand, GPUs involve threads that run in a separate memory space from the main application, which runs on the CPUs.²⁶²⁻²⁶⁵ This implies that the data must be transferred to the GPU memory before any processing can be started, and the results must be copied back to the main memory. This data transfer must be kept to a minimum. Thus, it is important to make sure that the time spent processing data on the GPU is long with respect to data transfer time. Furthermore, traditional CPU threads required separated resources, such as stack memory, and whose creation and management are expensive. In order to reduce the resource demanding, it is affordable to create as few CPU threads as possible and to make them run as long as possible. Whereas, GPU threads are not expensive to create and manage, so it is possible to create a large number of threads and run them for shorter duration.²⁶²⁻²⁶⁵

3.4.3 NAMD, ACEMD and VMD software packages

To perform the MD experiments reported in this thesis the software NAMD,^{266,267} and ACEMD²⁶⁸⁻²⁷⁰ were used. The trajectories were analyzed using the visual molecular software VMD.^{271,272} Along this section a brief description of the main features of each software are provided.

NAMD is a molecular dynamics code based on Charmm++ parallel object,²⁷³ and designed for HPC. NAMD works with AMBER, CHARMM, and X-PLOR force fields, parameters

and file formats. NAMD is well-known for its performance on large parallel computers. Moreover, NAMD is equipped with a Tcl scripting capability, allowing the implementation of advance phase space sampling protocols,^{266,267} and other analytical tool user-based. With the availability of GPU technologies and CUDA code NAMD become the first software package to incorporate GPU acceleration.²⁶⁵

ACEMD is a MD software package explicitly designed for execution by a single GPU workstation cluster, and as well as NAMD, ACEMD works with AMBER, and CHARMM force fields, parameters and file formats. Differently from NAMD, ACEMD uses a task parallel decomposition strategy, rather than the spatial data-parallel decomposition. To date, is the most effective GPU-based software for system size of 10000-100000 atoms.²⁶⁵

VMD is a software devoted to the visualization, and analysis of MD trajectories and large biomolecular systems. VMD is complemented by both MD software packages NAMD, and ACEMD, offering a complete modeling environment. For instance, using VMD it is possible to built AMBER, and CHARMM parameter files, which will be used in NAMD and ACEMD MD experiments, or to analyze the trajectories carried out from the aforementioned software, using a large panel of tools.

3.4.4 Molecular Dynamics Experiment Settings

MD setting for the GPCR Dimer MD Experiments

Molecular dynamic simulations were carried out using NAMD2.6^{266,267} and using Charmm22/27 as force field,²⁵³ and the results were analyzed with VMD.^{271,272} The two models were first separately equilibrated in a NVT system by following the protocols depicted in Table 9. The harmonic constraints were progressively reduced during the equilibration to achieve a smooth relaxation of the assembly. The last 250 ps were carried out with no constraints. The simulations were then carried out, separately, in a NPT system, by imposing a pressure target value of 1.01325 bar (see Table 9). Both simulations were carried out with the same nonbonded interaction parameters (van der Waals and nonbonded electrostatic interactions); a cutoff of 16 Å was imposed for nonbonded interactions, and a smooth switching function was used to truncate the van der Waals potential energy smoothly at the cutoff distance; the parameters that specifies the distance

at which the switching function should start was set to 14 Å. The nonbonded electrostatic interactions are truncated at the same cutoff value for the van der Waal interactions with the same switchdist value. Moreover, we used a nonbonded pair list with a ‘pairlistdist’ parameter set to 18 Å. The periodic boundary conditions were set by using the system size showed in Table 6 and 7 as reference. The two simulations were conducted for 40 ns each, with an integration step of 1 fs.

Table 9. Parameters used for the MD equilibration and production phases of both 5-HT_{2A}, mGluR2-5-HT_{2A}, and 5-HT_{2A}-5-HT_{2A} systems.

Equilibrations Steps									
Timestep	Numstep	Temperature	Harmonic Constraints (Kcal/mol)					Constant Temperature control	
			Backbone	Sidechains	Lipids	Waters	Ions		
Step1	1.0 fs	2500 fs	300 K	50	50	50	50	50	NVT
Step2	1.0 fs	2500 fs	300 K	10	10	10	5	5	NVT
Step3	1.0 fs	5000 fs	310 K	10	10	10	5	5	NVT
Step4	1.0 fs	5000 fs	310 K	10	5	10	5	5	NVT
Step5	1.0 fs	25000 fs	310 K	2.5	2.5	2.5	1.0	1.0	NVT
Step6	1.0 fs	25000 fs	310 K	2.5	1	2.5	1	2.5	NVT
Step7	1.0 fs	25000 fs	310 K	-	-	-	-	-	NVT
Simulation									
Step7	1.0 fs	40 ns	310 K	-	-	-	-	-	NPT P= 1.01325 bar

MD setting for the GPCR-Cholesterol MD Experiments

For the GPCR-Cholesterol MD experiments the MD software package ACEMD²⁶⁸⁻²⁷⁰ was used. Before the relaxation step each system was submitted to a minimization procedure for 1000 steps. During the relaxation phase the system were equilibrated using the NPT ensemble with a target pressure equal to 1.01325 bar, a time-step of 2 fs and using the RATTLE algorithm for the hydrogen atoms. In this stage, the harmonic constraints were progressively reduced until an elastic constant force equal to 0 kcal/mol (step2 relaxation phase Table 10) and the temperature was increased to 300K. All the simulations were conducted using the same non-bonded interaction parameters, with a cutoff of 9 Å, a smooth switching function of 7.5 Å and the non-bonded pair list set to 9.5 Å. The periodic boundary conditions were set by using the system size showed in Table 8, and for the long

range electrostatics we used the PME methodology with a grid spacing of 1 Å.²⁷⁴ Each production phase was performed using the same parameters, with a time-step of 4 fs, and a hydrogen scaling factor of 4.

Table 10. Parameters used for the MD equilibration and production phases of both 5-HT_{2A} (no Chol), mGluR2 (no Chol), 5-HT_{2A} (Chol), and mGluR2 (Chol) systems.

Relaxation Phase									
	Timestep	Numstep	Temperature	Harmonic Constraints (Kcal/mol)					Constant Temperature control
				Backbone	Sidechains	Lipids	Waters	Ions	
Step1	2.0 fs	10 ns	200 K	10	10	-	-	-	NPT
Step2	2.0 fs	10 ns	300 K	-	-	-	-	-	NPT
Production Phase									
Step3	4.0 fs	160 ns	300 K	-	-	-	-	-	NPT

3.4.5 Conformational Sampling

All the MD trajectories regarding to the GPCR Dimer MD Experiments were analyzed with VMD.^{271,272} Ideally, a long MD simulation allows the sampling of the whole conformational space for the molecular system under investigation. RMSD clustering of individual snapshots along the MD simulation allows to evaluate the degree of sampling and, thus, the goodness of the MD simulation.²⁷⁵ The representative structures of each cluster can ideally be considered models of individual conformational states for a given system. In addition, these structures can be used for docking studies,²⁷⁶⁻²⁷⁹ thus expecting to give hints on the ligand's ability to select individual conformational states. We are aware that 40 ns MD simulations certainly cannot be considered sufficient to cover the whole conformational state of a dimeric receptor embedded in a phospholipid bilayer. We therefore concentrated our attention on changes which take place around the putative binding pocket of 5-HT_{2A}, and the cluster analysis was therefore carried out by comparing a series of residues lining up the binding pocket. In details, we performed the cluster analysis by using the ptraj tool of Amber9²⁸⁰ and the average-linkage algorithm.²⁷⁵ The representative structure of each cluster, dumped by ptraj in the output file, represents the structure closest to the average structure, and it can be considered a sort of centroid of the

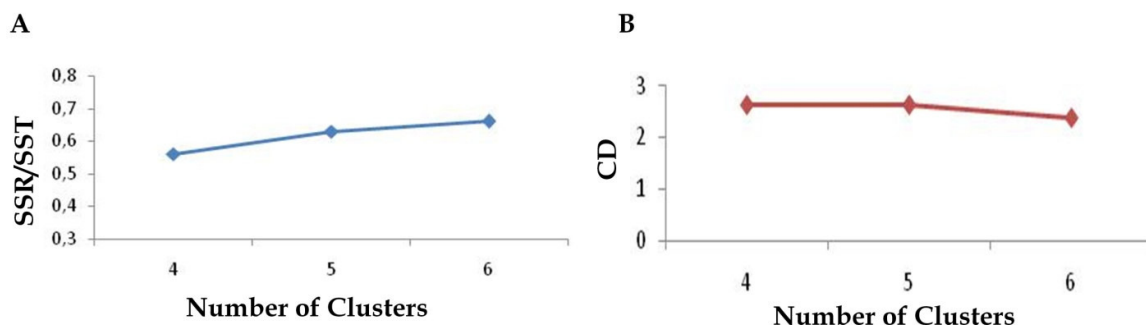
cluster, that retains the average properties of the cluster.^{275,280} For each 40ns simulation 2000 snapshots were collected and clustered according to RMSD of the backbone, CB and CG atoms of the residues lining up the serotonergic binding pocket (D^{3.32}, S^{3.36}, T^{3.37}, S^{5.43}, S^{5.46}, W^{6.48}, F^{6.51}, F^{6.52} and Y^{7.43}).²⁸¹⁻²⁸⁷

In order to assess the performance of a cluster analysis several indices or clustering metrics can be used, such as the Davies-Bouldin index (DBI), the pseudo F-static (pSF), the ratio SSR/SST (Sum of Squares Regression/Total Sum of Squares) explaining the percentage of variance of the data and the critical distance.^{275,280} In the paper of *Shao et al.*, the authors discussed the reliability of the clustering metrics, and they showed that using different metrics in conjunction with the examination of the results is a suitable way to assess the cluster quality.²⁷⁵ In our work we used the ratio SSR/SST and the critical distance as metrics in order to evaluate the quality of our tree of clusters (Table 11 and Figure 28a,b); furthermore, the obtained clusters were then analyzed by visual inspection. We performed several cluster analyses and, on the basis of the collected data, we selected the best parameters to cluster our simulations. For each MD simulations (5-HT_{2A}-mGluR2 heteromer complex, 5-HT_{2A} and 5-HT_{2A}-5-HT_{2A} homomer complex) we choose to cut our tree of clusters at six representative clusters.

Table 11. SSR/SST and Critical Distance Values for each cluster analysis performed with different number of cluster.

N° Cluster	SSR/SST	CD
4	0.63	3.62
5	0.66	2.37
6	0.56	2.63

Figure 28. (A) SSR/SST values against the number of clusters. (B) Critical Distance (CD) values against the number of clusters



3.4.6 Essential Dynamic Analysis

The Essential Dynamics (ED) analysis allows the identification of a new essential subspace of coordinates by the diagonalization of the covariance matrix of atomic fluctuations. For a $X(t)$ multidimensioned system, where X could be a system of spatial coordinates, frames of molecular dynamics simulations, etc., we could obtain the following covariance matrix:

$$C_{ij} = \left\langle \left(x_i - \langle x_i \rangle \right) \left(x_j - \langle x_j \rangle \right)^T \right\rangle$$

The symmetric matrix can be diagonalized by an orthonormal transformation matrix, which contains the eigenvectors or principal modes (columns of the matrix) and where the eigenvalues λ express the variance in the direction of the corresponding eigenvector. Every eigenvector is stored, in decreasing way, on the basis of the corresponding eigenvalue. Thus for a dynamic process the original data can be projected onto an eigenvector, and the eigenvectors with larger eigenvalues match the more important displacement.²⁸⁸⁻²⁹⁰

Amadei et al. in their work showed that the total positional fluctuation $\sum_i \langle (x_i - \langle x_i \rangle)^2 \rangle$ can be thought to be built from the contributions of the eigenvectors.²⁸⁸

The essential dynamics analysis allows us to identify a new essential subspace defined by new variables ($t_1; t_2; \dots; t_k$ or eigenvectors or principal mode), which are linked to the original $X(t)$ multidimensioned space by the loadings values (p). The $\sum_i \langle P_i^2 \rangle$ (or p square value) is an index of the importance of an atom on the definition of the principal mode, and it can be used in order to identify the residues most important in the definition of the considered principal mode.

In our case a Combined-Essential Dynamics (Comb-ED)²⁹¹ analysis was performed using the appropriate VMD plug-in in combination with the ptraj module of Amber9.^{280,292} In the Comb-ED the covariance matrix is calculated for two or more concatenated trajectories, the overall translational and rotational motion are eliminated fitting all the trajectories on the same reference structure. The reference structure on which we have been fitted the trajectories is represented by the initial structure of the monomer

embedded into the phospholipid bilayer before the equilibration and the production phases.

The resulting eigenvectors, extracted by the Comb-ED, do not represent the essential degree of motion of the systems, but they explain differences and similarities in the essential subspace of the compared simulated systems. In order to check differences between the 5-HT_{2A} monomer, the mGluR2/5-HT_{2A} heteromer and 5-HT_{2A}/5-HT_{2A} homomer simulations we extracted from each simulation the trajectories related to the only 5-HT_{2A} unit, thus excluding from the Comb-ED the mGluR2 trajectories. The trajectories of the homomer complex, including two 5-HT_{2A} protomers, were split in trajectories for the Protomer A (ProA) and trajectories for the Protomer B (ProB). After that, we concatenated the 40ns of the compared trajectories in the following manner: protomer 5-HT_{2A} from the heterocomplex (ProH), 5-HT_{2A} monomer, and the protomer 5-HT_{2A} from the homomer complex (ProA and ProB, respectively). After removing the roto-translational degree of freedom by aligning every frame of the simulations on a reference structure, the principal modes were computed for the C α atoms only.

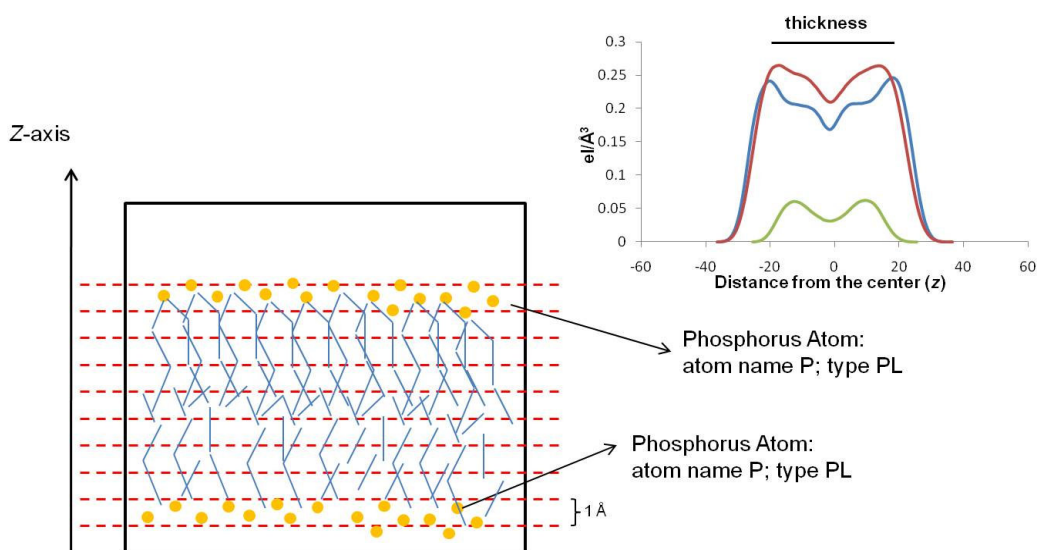
3.4.7 Electron Density Profile

It has been reported that the presence of cholesterol can modify the thickness of a lipid bilayer.^{293,294} To quantify the membrane thickness, we computed the local 1-D electron density profile of different species and functional groups (such as the entire SDPC and cholesterol molecules or the PO₄ groups of the SDPC molecules) projected along the bilayer normal. The density profile computations were performed with the VMD plugin *Density Profile Tool*²⁹⁵ as follows: first, the simulation box is partitioned into several parallel slabs, measuring $\Delta z = 1\text{\AA}$ along the z axis; the slabs extend up to the boundaries of the simulation box along x and y (Figure 29). The approximate number of electrons within each slab is then computed, for each simulation frame, summing the atomic number, Z, and the partial charge, δ , of the atoms whose centers are located inside each slab. The total is finally normalized by the slab volume, so that the local electron density at z, expressed in units of electrons/ \AA^3 , is as follows:

$$\rho(z) = \frac{1}{L_x L_y \Delta z} \sum_{i \in V} Z_i + \delta_i$$

where Δz is the slab thickness (profile resolution), L_x and L_y are the simulation box dimensions orthogonal to the z axis, V_z is the set of atoms whose centers lie inside the slab centered at z and Δz thick. We assumed the membrane thickness to be the peak-to-peak distance (in \AA) in the density profile plot.

Figure 29. At each simulation frame, the electron density profile is computed by summing the atomic number (Z) and the partial charges of the atoms falling into 1 \AA -thick slabs parallel to the z axis. The sum, normalized by volume, provides the local 1-D density value around z .



Average values: in order to compute the average values of the bilayer thickness and the location of the hydrophobic face of the H8, for each MD run we computed its own PO_4 and H8 (only the $\text{C}\alpha$ of the residue lining up the hydrophobic face) EDP profiles. The average values were computed as follows:

1. from each MD run we extrapolated the EDP values of each slab;
2. The EDP values at the corresponding slab (distance from the center along the z axes) were averaged along the ten MD runs; (For each slab we have ten values)
3. For each average value at that slab we computed the standard deviation parameter;
4. Finally, we plotted the average EDP profile for the membrane and the H8, with its cognate standard deviations.

The average thickness values were computed as follows:

1. For each MD run we computed the thickness

2. The average thickness and its cognate standard deviations values were computed using the ten MD runs of each system, with and without cholesterol
3. The H8 Hydrophobic face was computed using as reference the C α atoms of the H8 facing the membrane bilayer, the average plot was computed as described above.

Since the distance between the peak of the PO₄ groups and the hydrophobic face of the H8 represents an intriguing result of our study, we need to establish the exact amount of this value, with particular precision. So as to do this, the distance between the peak of the PO₄ groups and the hydrophobic face of the H8 was computed as follows:

1. In each MD run the maximum peak value showed certain degree of uncertainty, therefore in each MD run we identified the exact location (the exact slab where the peak is located) of the peak for both PO₄ and hydrophobic face of the H8
2. The average locations were computed using the exact slab values extrapolated from each MD run, we also computed the standard deviation of the average location.
3. The distance of the PO₄ and hydrophobic face of the H8 was computed using these values.

3.4.8 Kernel Density Function

The probability density function was estimated building a Bivariate Kernel Density Function.^{296,297} Kernel Density Estimation (KDE) is a non-parametric way of estimating the probability density function (PDF) of random variable. KDE is a fundamental data smoothing problem where inferences about the population are made, based on a finite data sample. To perform KDE we used the Free Statics and Forecasting Software Server, based on R language.²⁹⁸ KDE is strongly affected by the bandwidth selection, and the use of Free Statics and Forecasting Software Server allows us to appropriately choose the bandwidth matrix H, in this case to estimate H the simple covariance matrix was used.

Finally, to define the representative structures of each probable state found with the analysis of the Kernel Density function we clusterized the concatenated trajectories according to the RMSD and gyration radius of the backbone atoms of the residues forming the putative H8.

3.5 Ligand Docking

3.5.1 Analysis of the Dimer Interface Effects on the 5-HT_{2A} Binding Pocket.

A set of known 5-HT_{2A} ligands was selected from the GPCR-Ligand Database,^{299,300} and from data reported in the literature (Appendix A Table 1A).²⁸¹⁻²⁸⁷ The set of active 5-HT_{2A} ligands consists of nine HCs; nine NHCs and nine antagonists, and this dataset was enriched by 73 additional decoys obtained from a Schrödinger Library and from the International Union of Basic and Clinical Pharmacology database (Appendix A Table 2A).³⁰¹⁻³⁰³ The idea is to enrich the active set with chemotypes displaying common structural features with the selected 5-HT_{2A} ligands (similar molecular weight, number of nitrogens, number of oxygens and number of rings) but not reported to be active at the 5-HT_{2A} receptor subtype. The main aim of this part of the work was to verify whether considering several conformational states of the receptor would have an impact on the results of the docking studies. With regards to this aim, we selected, for each system, the representative structure of the first cluster as representative of the initial state of the system and the representative structure of the most populated cluster as representative of the most favored state for that simulation. Thus, eight different conformational states of the 5-HT_{2A} receptor were selected (two for the monomer, two for the 5-HT_{2A} complexed with the mGluR2 receptor, two for the ProA and two for the ProB) and employed in the docking studies with 100 ligands (23 known active compounds and 73 classified as inactive compounds). We decided to introduce flexibility by developing a protocol based on the induced fit docking (IFD) tool available in Maestro.^{301,302} Briefly, the protocol, summarized in Figure 30, is based on the IFD of selected ligands into representative structures of the receptor. This chosen protocol is intended to be a compromise between explicit treatment of flexibility and manageable computational time. Clearly, the use of the IFD protocol adds complexity to the study as the choice of a given ligand for a particular conformational state of the receptor in the IFD may well bias the subsequent rigid docking. Furthermore, there can be the possibility that the minimization procedure of the IFD will hide the differences resulting from the MD evolution. Also, by taking into account these possible drawbacks, the protocol described in Figure 30 is based on the choice of a representative chemotype of each class of the 5-HT_{2A} ligand for initial IFD. The

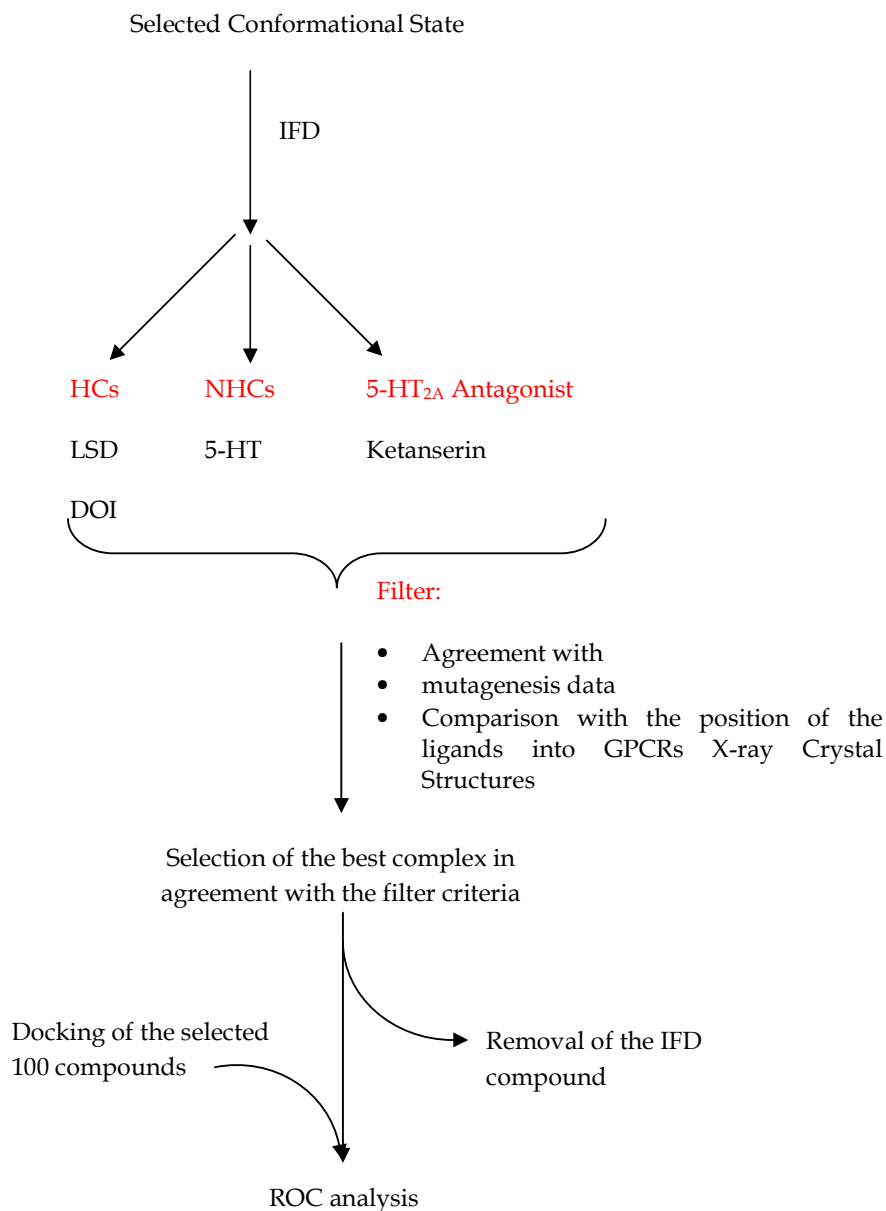
IFD results were evaluated, for each conformational states, on the basis of the adherence of the obtained poses to available mutagenesis data²⁸¹⁻²⁸⁷ and to the pose experimentally determined for other GPCR receptors.^{13,30,31,103} As a matter of fact, biogenic ammine subfamily seem to have a conserved orthosteric binding pocket for both agonists and antagonists (as already discussed in the Orthosteric Binding Site sections, and in the Activation Mechanism section). Thus, we carried out a total of 32 IFD runs (four ligands for two different conformational states, initial and most populated ones, for four different receptor states, monomer, heteromer, ProA and ProB). The 32 IFD complexes were evaluated for their agreement with experimental data and eight complexes were selected (Table 12). These complexes were used for the subsequent rigid docking runs. The obtained poses were ranked according to their G-score and the corresponding receiver operating characteristic (ROC) curves³⁰⁴ generated for each class of ligands, for the representative structures of the most populated clusters. In detail, the initial docking site was defined by a box of $18 \times 18 \times 18 \text{ \AA}$ centered on D^{3.32}; S^{3.36}, T^{3.37}, S^{5.43}, S^{5.46}, W^{6.48}, F^{6.51}, F^{6.52} and Y^{7.43}, and no interaction constraints were used, according to the protocol depicted in Figure 30. The van der Waals scaling factor was set to 0.8. Only the docking poses in agreement with filter criteria were retained. As filter criteria, we used the agreement with mutagenesis data and comparison of the obtained poses with the position of the ligand into available GPCRs x-ray crystal structures (Figure 30). In the second stage of the study, the whole set of 100 compounds (27 active and 73 inactive ones) was docked into the eight structures selected by the IFD protocol, keeping the same Glide grid of the selected IFD ligand-receptor complex. The ligands were ranked by their Glide Score and one pose per ligand was collected and a ROC analysis³⁰⁴ was performed using four different schemes of ligand classification:

- 5-HT_{2A} active ligands (27 compounds) versus the decoy set (73 compounds);
- 5-HT_{2A} agonists (18 compounds) versus decoy set enriched by the nine 5-HT_{2A} antagonists (82 compounds);
- 5-HT_{2A} antagonists (nine compounds) versus decoy set enriched by the 18 5-HT_{2A} agonists (91 compounds);

- HCs (nine compounds) versus decoy set enriched by the 5-HT_{2A} NHCs and antagonists (91 compounds).

In order to understand if particular conformational states discriminate among the different 5-HT_{2A} ligand classes, the area under the curve and the enrichment factors at 2, 5, 10 and 20% were computed for each ROC plot.

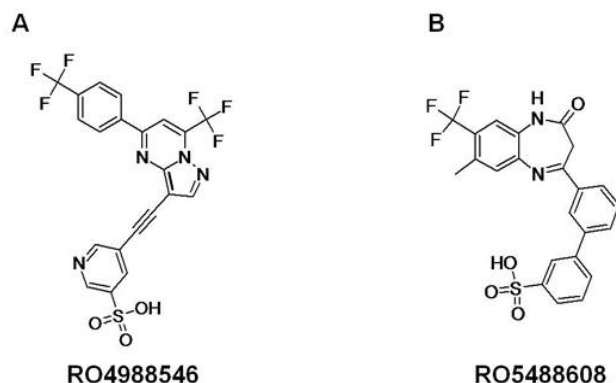
Figure 30. Protocol used for the docking studies.



3.5.2 mGluR2 Model Validation

To evaluate the structural architecture of the obtained mGluR2 model in more detail, two recently reported mGluR2 negative allosteric modulators, RO4988546 and RO5488608 (Figure 31), were docked into the model of TM-mGluR2. Recently, *Lundström et al.*²¹³ identified by site-directed mutagenesis eight residues involved in the binding of two negative allosteric modulators for the mGluR2 receptor. According to these data, compounds RO4988546 and RO5488608 (Figure 31) share a common binding pocket defined by the R^{3.28}, R^{3.29}, F^{3.36}, H^{EL2.52}, L^{5.43}, W^{6.48}, F^{6.55}, V^{7.43} residues. In order to validate our model based on the rhodopsin template we performed a preliminary docking study by using the same compounds (RO4988546 and RO5488608) and the information available in the work of *Lundström et al.*²¹³ Differently to the work of *Lundström et al.*²¹³ where compounds were manually docked, we performed docking studies by using the Glide induced fit docking (IFD) tool available in Maestro9.0.³⁰² The grid was centered on the residues shaping the putative allosteric binding pocket of the mGluR2 receptor (R^{3.28}, R^{3.29}, F^{3.36}, H^{EL2.52}, L^{5.43}, W^{6.48}, F^{6.55}, V^{7.43}), the flexible region was fixed until 5 Å around the center of the grid. Each docking run was carried out with the standard precision (SP) method, and the van der Waals scaling factor of non polar atoms was set to 0.8. For each compound we used the same IFD protocol that provided us with 15 docking poses per compound. Among these poses we selected the best pose in accordance with mutagenesis data. After that each complex ligand-receptor was subjected to minimization by using the MMFF94x available in MOE,³⁰⁵ until a gradient of 0.005 Kcal/mol*Å².

Figure 31. Compounds used for the docking studies on the mGluR2 receptor. RO4988546 (A) and RO5488608 (B).



Chapter 4

Results

4.1 Dimer Interface Effects Analysis

4.1.1 Analysis of the MD trajectories.

The molecular systems constituted by the dimeric assemblies (mGluR2-5-HT_{2A}, and 5-HT_{2a}-5-HT_{2A}) and by the 5HT_{2A} monomer, respectively, embedded in a rectangular box comprising a DMPC bilayer surrounded by explicit water were simulated for 40 ns each (see 3.4.4 section). The Root-Mean-Square Deviations (RMSD) of the C α of the protomers constituting the dimers (mGluR2, ProH, ProA, and ProB) were computed against the starting structures and are reported in Figure 32a,b. In the same figures, the RMSD of the C α atoms of the monomeric 5HT_{2A} simulation is also reported (purple line). It can be appreciated that: (i) the mGluR2 and ProH (5-HT_{2A}) protomers of the heterocomplex behave differently, as the mGluR2 unit (green line) has a lower deviation from the starting structure than the ProH protomer (black line); (ii) the 5-HT_{2A} protomers of the homomer complex (ProA, blue line and ProB, red line) display particularly different behavior, with the ProB (red line) endowed with higher fluctuations, from the starting structure; (iii) all the 5-HT_{2A} protomers (ProH, ProA, ProB) underlying specific dimer complexes show appreciable differences, with respect to the monomeric form of the same receptor (5-HT_{2A} as monomer, purple line). Interestingly, when simulated in a monomeric form (purple line), the 5HT_{2A} unit has a lower deviation from the same starting structure than the ProB and ProH protomers (red and black lines, respectively), whereas ProA (blue line) shows lower fluctuation than the monomeric form (purple line), with respect to the starting structure. The analysis of the RMSD plot, after that each system reaches the plateau

condition (Figure 32b), supports the observations described above, in which monomer and protomers show peculiar behavior, with respect to each other ones. However, the inspection of the plot of the average RMS fluctuation per residue, along the simulations, revealed a more complex picture. Indeed, when the 5HT_{2A} models (the monomer, purple line; the ProH, ProA, and ProB protomers, black, blue and red lines, respectively) are compared (Figure 33), it appears that residues belonging to TM1-TM3 have almost identical fluctuations, while modest differences are visible for residues belonging to TM4-TM7, with the monomer endowed with higher fluctuations. Most of the variance, however, is due to loop movements, and in particular of the C-terminus of the third intracellular loop, where the protomers of the dimeric complexes have the highest fluctuations. This is due to the mutual accommodation of the large third intracellular loops in the dimer, an effect which is not apparent in the monomer, where there are no interprotomer contacts to be relaxed (Figure 33). The comparison between the RMSD of the C α atoms of the four 5HT_{2A} models suggests the presence of clear effects of the dimerization interface (Figure 33, insets for the TM4-5). Indeed, the RMS fluctuations of C α belonging to TM1 and TM2, not involved in the interface, are almost identical in the two cases. Minor deviations are visible for residues belonging to TM3, while significant differences occurred in the case of residues belonging to TM4, TM5, TM6, and TM7, thus clearly indicating that the presence of the dimerization interface impacts the result of the MD simulations.

Figure 32. (A) RMSD of the C α atoms for ProH (black), ProA (blue), ProB (red), and mGluR2 (green) extracted from the dimeric complexes, and for the monomeric 5-HT_{2A} (purple). (B) RMSD of the C α of the same receptor models after that each system reaches the plateau condition.

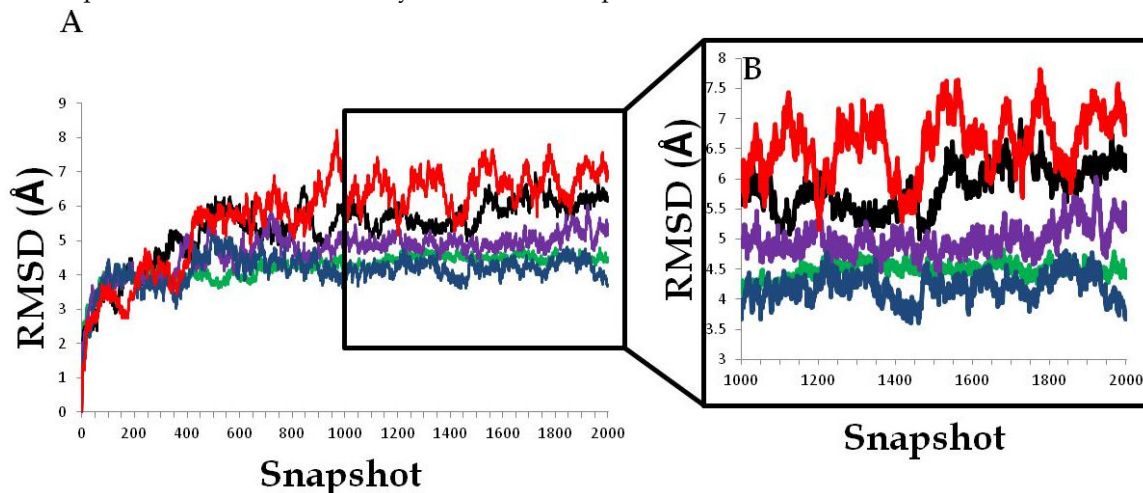
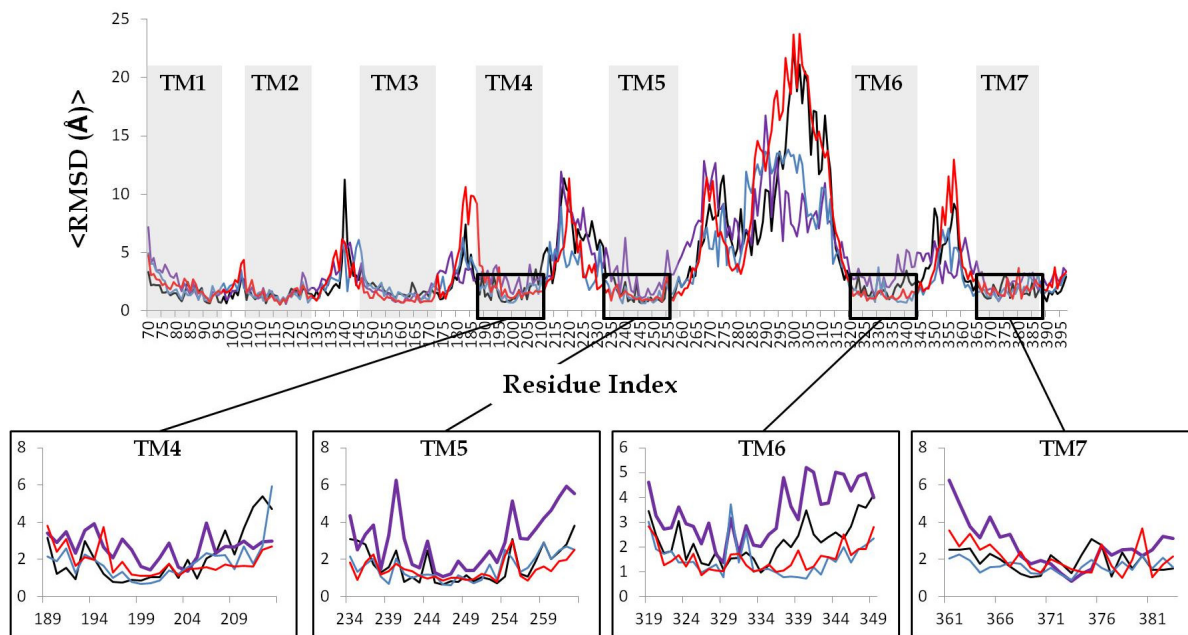


Figure 33. Average RMSD per residue of the C α atoms for ProH (black), ProA (blue), and ProB (red) extracted from the dimeric complexes, and for the monomeric 5-HT_{2A} (purple). Insets for the TM4-7 are highlighted in the black boxes.



4.1.2 Analysis of the Binding Pocket

A potentially very relevant outcome of the present study is the observation that the formation of the dimerization interface between the two protomers allosterically affects the shape of the binding pocket(s) of the individual protomers. In order to verify whether this allosteric cross-talk did actually occur, we analyzed the putative 5HT_{2A} binding pocket, which is quite well-defined from previous experimental results.²⁸¹⁻²⁸⁷ Thus, we analyzed nine residues known to be involved in 5-HT_{2A} ligand recognition, namely D^{3.32}, S^{3.36}, T^{3.37}, S^{5.43}, S^{5.46}, W^{6.48}, F^{6.51}, F^{6.52} and Y^{7.43}.²⁸¹⁻²⁸⁷ Figure 34 shows the RMSD of these residues for the protomers in the dimer simulations and for the monomer, respectively. Figure 35 shows the corresponding average RMSD fluctuation for the same residues. It can be appreciated that residues belonging to TM3 have an almost overlapping behavior, while significant deviations are detected between the simulations for the key residues S^{5.43}, S^{5.46}, W^{6.46}, F^{6.51}, F^{6.52}, and Y^{7.43}. The analysis of the average RMSD values per residue (Figure 35) clearly indicates the dependency of the binding pocket shape upon the simulation conditions. In particular, the key residues S^{5.43}, S^{5.46}, experimentally known to

be involved in HCs binding,²⁸³ and the residues F^{6.51} and F^{6.52} display significantly different displacement when 5-HT_{2A} is simulated as a monomer, or part of a homo- or heteromer complexes (Figure 35).

Figure 34. RMSD of C α atoms for selected residues lining up the binding pocket of 5HT_{2A}, for ProH (black), ProA (blue), and ProB (red) extracted from the dimeric complexes, and for the monomeric 5-HT_{2A} (purple).

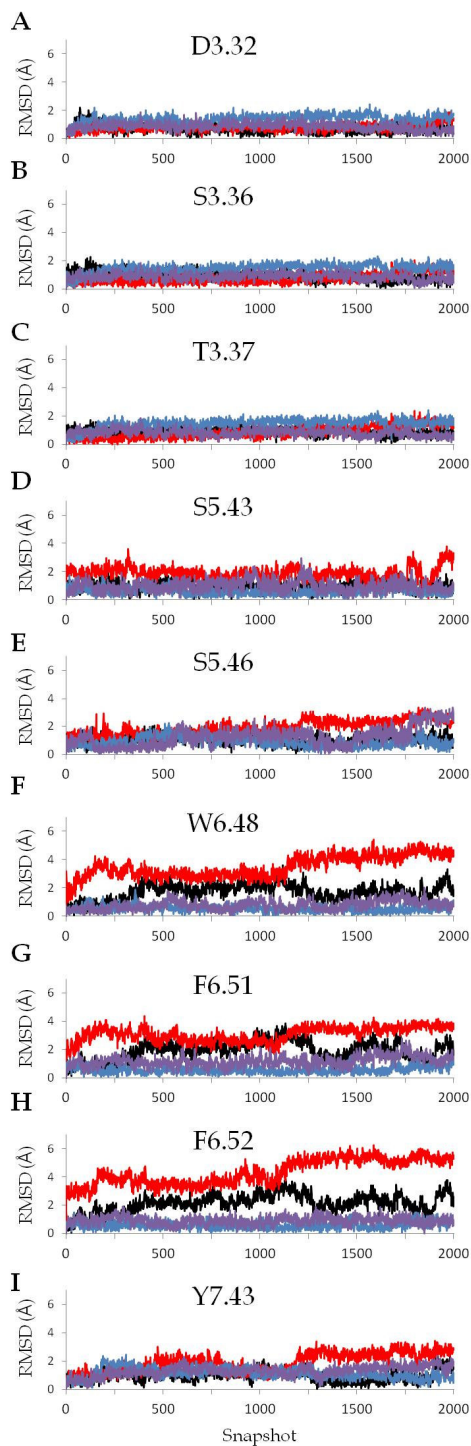
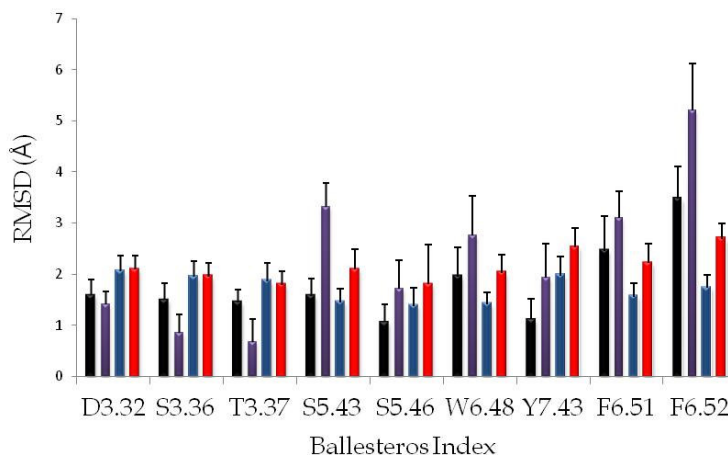
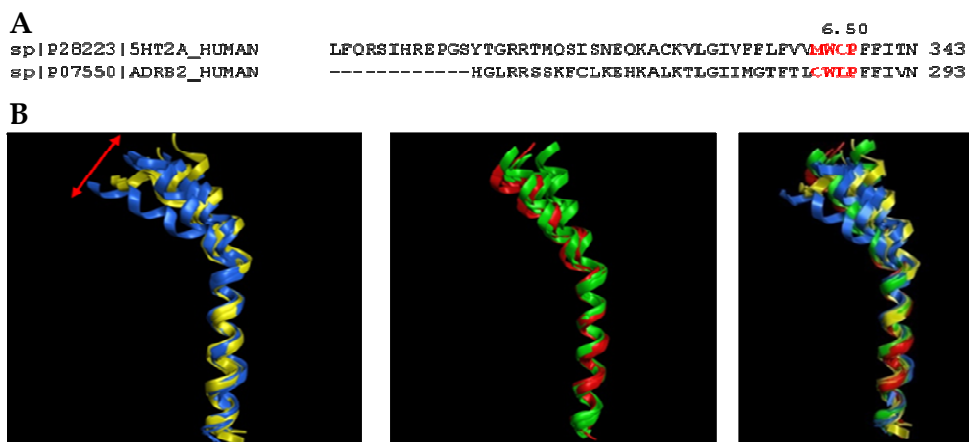


Figure 35. Average RMS fluctuations for the C α atoms for the selected residues lining up the binding pocket of 5HT_{2A}, for ProH (black), ProA (blue), and ProB (red) extracted from the dimeric complexes, and for the monomeric 5-HT_{2A} (purple). The vertical bars represent the standard deviations.



A particular comment deserves the high fluctuation (Figure 34 and 35) displayed by the W^{6.48}, F^{6.51} and F^{6.52} residues. These residues are located in a region of TM6 characterized by high flexibility.^{101,124,125,306} In particular, they are located one turn above the MWCP micro domain, which corresponds to the well known CWxP domain, conserved among several Class A GPCRs, (Figure 36a) and characterized by a high flexibility. In fact, the superimposition of TM6 of representative structures of each simulation (Figure 36b) indicates a wide oscillation of the terminal cap of TM6 induced by different movement of the micro domain.

Figure 36. (A) Alignment among the TM6 domains of human β_2 -adrenergic and 5-HT_{2A} receptors. (B) Superposition of the TM6 of representative structures for ProH (yellow), monomer (blue), ProA (green), ProB (red). The red arrow highlights the oscillatory motion of the TM6.



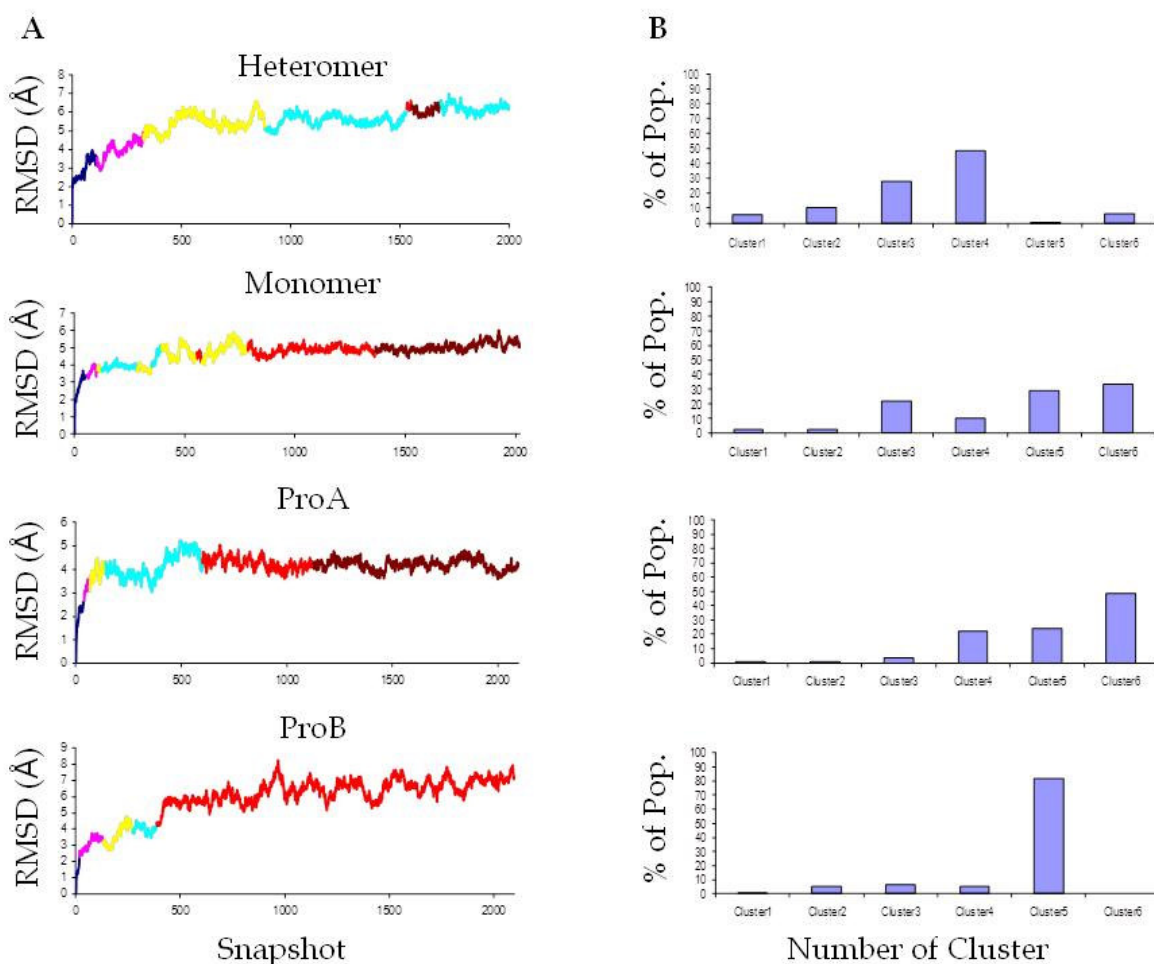
The oscillation is much larger in the case of the 5-HT_{2A} simulation as a monomer than in the case of the mGluR2-5-HT_{2A} and 5-HT_{2A}-5-HT_{2A} simulations. Therefore, it is clear that the presence and the type of dimerization interface visibly impact the flexibility of the TM6 helix. This is particularly relevant, since F^{6.51}, F^{6.52} and W^{6.48} form an hydrophobic pocket conserved among the class A of the GPCRs,^{101,124,125,306} especially for the subfamily of the biogenic amines. It has been hypothesized that these residues, together with the S^{5.43}, and S^{5.46} may play a crucial role in (i) the activation mechanism for a GPCR, by triggering the conformational changes required for receptor activation^{101,124,125,306} and (ii) ligand recognition.³⁰⁷ These observations are further supported by the resolution of the hypothetical active states for the opsin, turkey β_1 - and human β_2 -adrenergic, and A_{2A} receptors (see section 1.1.3),^{17,28-32,101-103} displaying that the residues located in the aforementioned conserved positions play a crucial role in ligand-binding recognition and activation mechanism (see section 1.2.1 and 1.3).

4.1.3 Cluster Analysis

Figure 37a shows the trajectories of the four systems under study, color-coded according to the six chosen clusters. Figure 37b shows the relative percentage of population of each cluster. It can be appreciated as the clusters are differently populated and in some cases the trajectories explore conformational states belonging to the same cluster during the simulation. This is the case of 5-HT_{2A} extracted from the heteromer simulation, or 5-HT_{2A} simulated as a monomer. Noteworthy is the case of the homomer simulation, in which the two protomers show very different behaviors. This is an interesting observation since the homomer represents a theoretical isotropic system, where each protomer is embedded in the same environment. Quite unexpectedly, when the trajectory extracted for ProB is clustered, we obtained only one large cluster that covers approximately 80% of the whole simulation. Conversely, in the case of ProA the population of the clusters is more evenly distributed around the last three ones (Figure 37a,b). The different results of the cluster analysis for the ProA and ProB are indicative that the homomer does not evolve, under our simulation conditions, in a symmetric way. The non-symmetric evolution of the homomer simulation suggests that the interactions at the homomer interface are thus

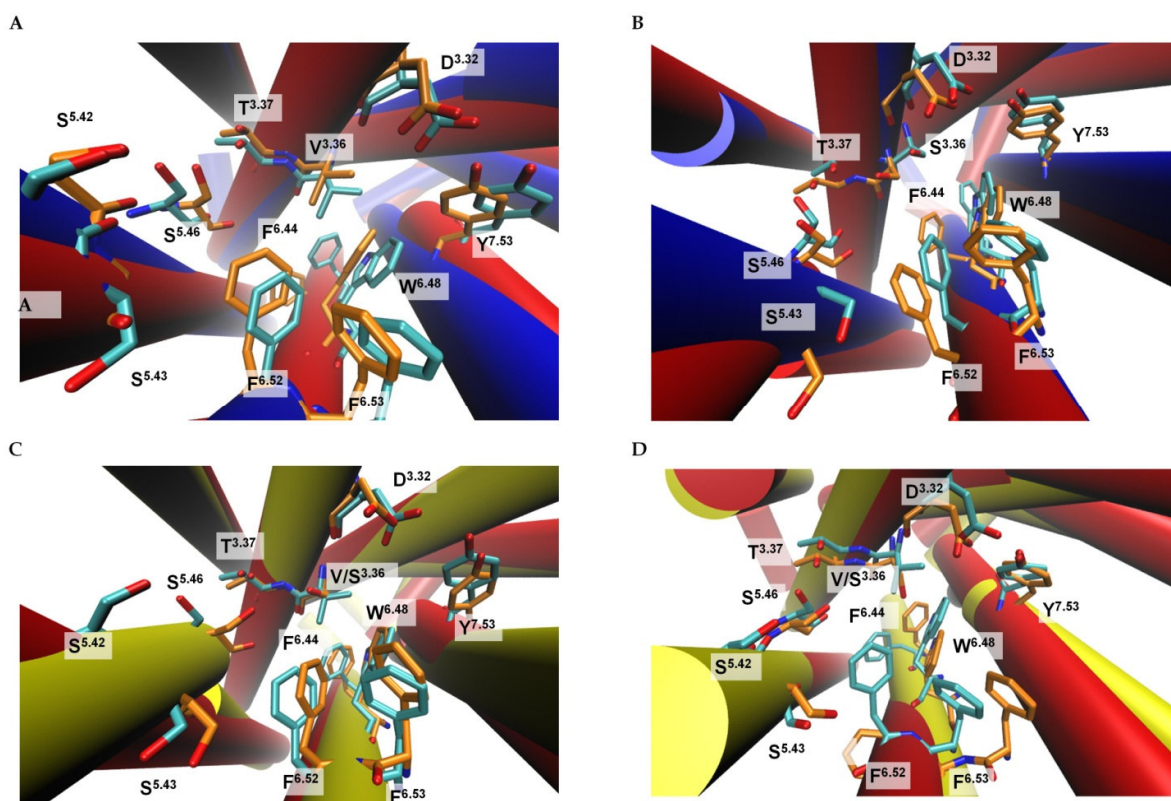
anisotropic and this is in agreement with the experimental evidence that one protomer is able to allosterically affect the behavior of each other protomer into the complex.¹⁶⁶

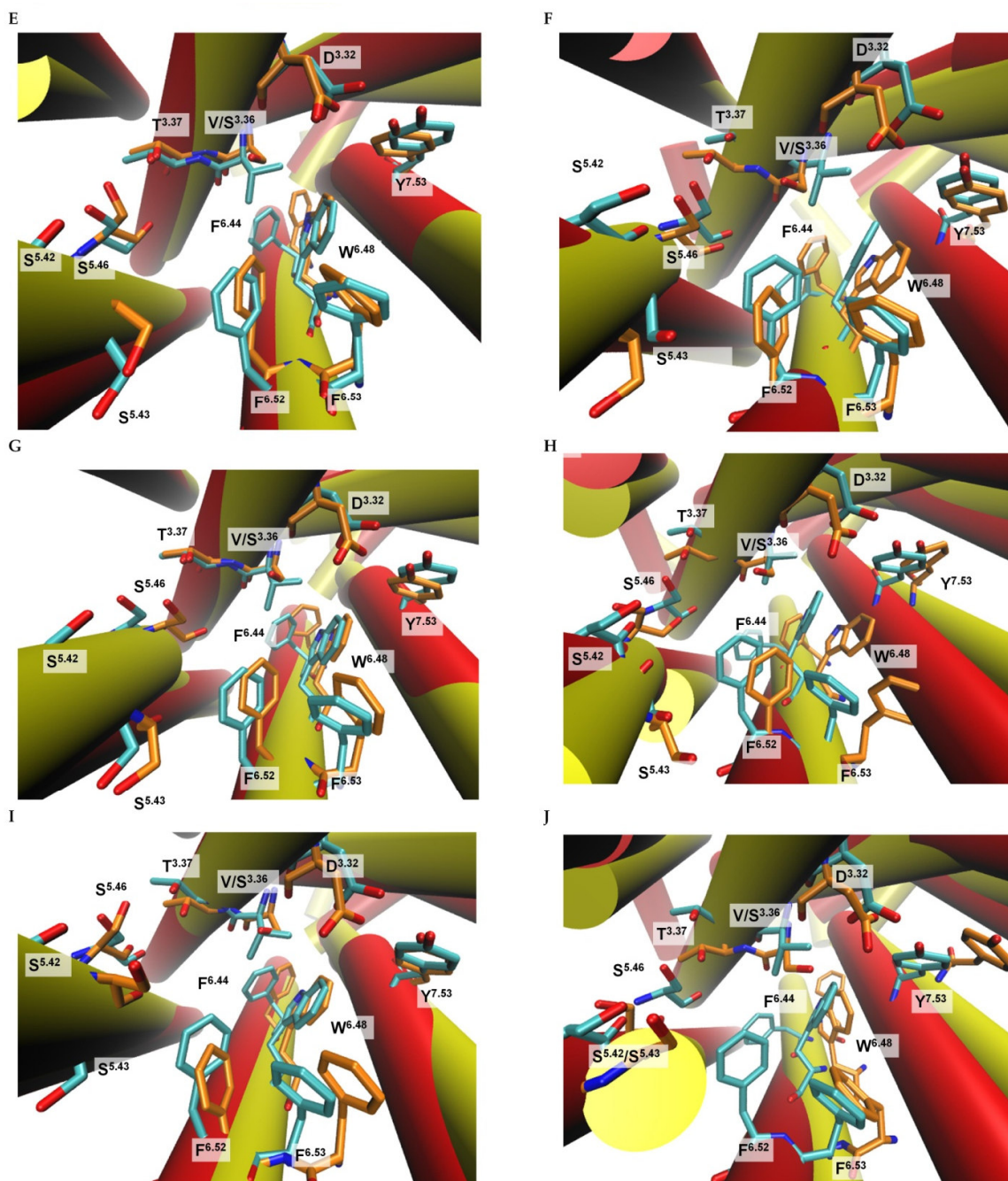
Figure 37. 2000 snapshots covering 40ns per simulation have been collected and clustered according to RMSD from the starting structure. (A) Snapshots belonging to individual clusters have been color-coded and projected on the RMSD plot of the trajectories. Blue: cluster 1; Pink: cluster 2; Yellow: cluster 3; Light Blue: cluster 4; Red: cluster 5; Brown: cluster 6. (B) Percentage of population of each cluster for each simulation



As described in section 3.4.5 during the cluster analysis we focused our attention on the residues lining up the putative 5-HT_{2A} binding pocket, and so as to assess how relevant are the displacement observed at the binding pocket level, we compare the starting structure and the structure of the most populated cluster of each system with respect to the X-ray crystal structures of the β_2 -adrenergic receptor in its inactive (2RH1), and the active (3SN6) states, respectively (Figure 38a-j).

Figure 38. Representation of the behavior of the residues lining up the putative 5-HT_{2A} binding pocket, the residues are reported in stick and color coded in orange and cyan depending on the structures considered, for each residues the amino acid name, and the Ballesteros index were reported; (A) Superposition of the human β_2 -adrenergic receptor in its inactive (red, stick and orange) and active (blue, stick and blue) states; (B) superposition of the most different structures of the 5-HT_{2A} receptor extracted from our trajectories, the initial structure of the monomeric form (red, stick and orange), and the ProB form (blue, stick and cyan) of the 5-HT_{2A} receptor; (C) superposition of the initial state of the ProH (yellow, stick and orange), and the inactive state of the human β_2 -adrenergic receptor (red, stick and cyan); (D) superposition of the representative structure of the most populated cluster of ProH (yellow, stick and orange), and the active state of the human β_2 -adrenergic receptor (red, stick and cyan); (E) superposition of the initial state of the ProA (yellow, stick and orange), and the inactive state of the human β_2 -adrenergic receptor (red, stick and cyan); (F) superposition of the representative structure of the most populated cluster of ProA (yellow, stick and orange), and the active state of the human β_2 -adrenergic receptor (red, stick and cyan); (G) superposition of the initial state of the ProB (yellow, stick and orange), and the inactive state of the human β_2 -adrenergic receptor (red, stick and cyan); (H) superposition of the representative structure of the most populated cluster of ProB (yellow, stick and orange), and the active state of the human β_2 -adrenergic receptor (red, stick and cyan); (I) superposition of the initial state of the monomeric form (yellow, stick and orange), and the inactive state of the human β_2 -adrenergic receptor (red, stick and cyan); (J) superposition of the representative structure of the most populated cluster of the monomeric form (yellow, stick and orange), and the active state of the human β_2 -adrenergic receptor (red, stick and cyan).





The analysis of the binding pockets of the selected structures (Figure 38 c-j), reveals a complex picture. Interesting is the case of the representative structure of the most populated cluster of ProH (Figure 38d), in which the S^{5.43}, and S^{5.46} residues display a spatial orientation quite similar, with respect to the S^{5.43}, and S^{5.46} residues of the human β_2 -adrenergic receptor in its active state. These residues are involved in the ligand-binding recognition, and activation mechanism of Class A GPCR (see section 1.2.1 and 1.3), and especially the S^{5.43}, and S^{5.46} residues are involved in the agonist-binding recognition for

the 5-HT_{2A} receptor. In the other cases the S^{5.43} residue of the 5-HT_{2A} receptor seems to occupy an intermediate position between the S^{5.42}, and S^{5.43} residues, when compared with the human β_2 -adrenergic receptor (Figure 38c-j). Finally, the selected structures of the monomeric form (Figure 38i,j) display residue locations that are not comparable neither with active or inactive states of the human β_2 -adrenergic receptor. The ensemble of structures selected by the cluster analysis highlights a peculiar behavior of each receptor form, depending on the presence and the nature of the dimer interface.

4.1.4 Ligand Docking experiments

As described in the 3.5.1 section a set of known 5-HT_{2A} ligands was selected from the GPCR-Ligand Database,^{299,300} and from data reported in the literature (Appendix A Table 1A).²⁸¹⁻²⁸⁷ The set of active 5-HT_{2A} ligands consists of nine HCs; nine NHCs and nine antagonists, and this dataset was enriched by 73 additional decoys obtained from a Schrödinger Library and from the International Union of Basic and Clinical Pharmacology database (Appendix A Table 2A).³⁰¹⁻³⁰³ The decoys were selected according to the criteria described in section 3.5.1. The Docking studies were carried out applying the protocol described in Figure 30. In Table 12 we report the selected complexes from the IFD docking analysis (see Figure 30 section 3.5.1). In Figure 39 we show, as an example, the obtained IFD complex for the LSD compared with the position of the co-crystallized ligands into available GPCR X-ray crystal structures of the β_2 -adrenergic receptor, displaying an overlapping binding cleft for the active and inactive states (see section 1.2.1). In Figure 40a,b we report the interaction maps for serotonin, LSD and the 5-HT_{2A} binding pocket.

Table 12. Selected complexes from the IFD docking analysis

Structures	Ligands
Representative Structure Cluster 1 Monomer	Serotonin
Representative Structure Most Populated Cluster Monomer	Ketanserin
Representative Structure Cluster 1 5-HT _{2A} -mGluR2	Serotonin
Representative Structure Most Populated Cluster 5-HT _{2A} -mGluR2	LSD
Representative Structure Cluster 1 5-HT _{2A} -ProA	Ketanserin
Representative Structure Most Populated Cluster 5-HT _{2A} -ProA	Ketanserin
Representative Structure Cluster 1 5-HT _{2A} -ProB	Serotonin
Representative Structure Most Populated Cluster 5-HT _{2A} -ProB	DOI

Figure 39. Superposition of the binding pose of the POG (3SN6, cyan), Carazolol (CAV, 2RH1, orange), and LSD (white, obtained docking pose using the IFD protocol on the representative structure of the ProH). In transparent and cartoon the HTM bundle of the 2RH1 (red), 3SN6 (blue), and 5-HT_{2A} model (yellow). It can be appreciate how the S^{5.43} of the serotonergic receptor (stick and white) overlaps the position of the S^{5.42} of the β_2 -adrenergic receptor (stick and cyan for the active state, orange for the inactive one). The S^{5.46} of the serotonergic receptor (stick and white), display a position quite similar to the S^{5.46} of the active state of the β_2 -adrenergic receptor (stick and cyan).

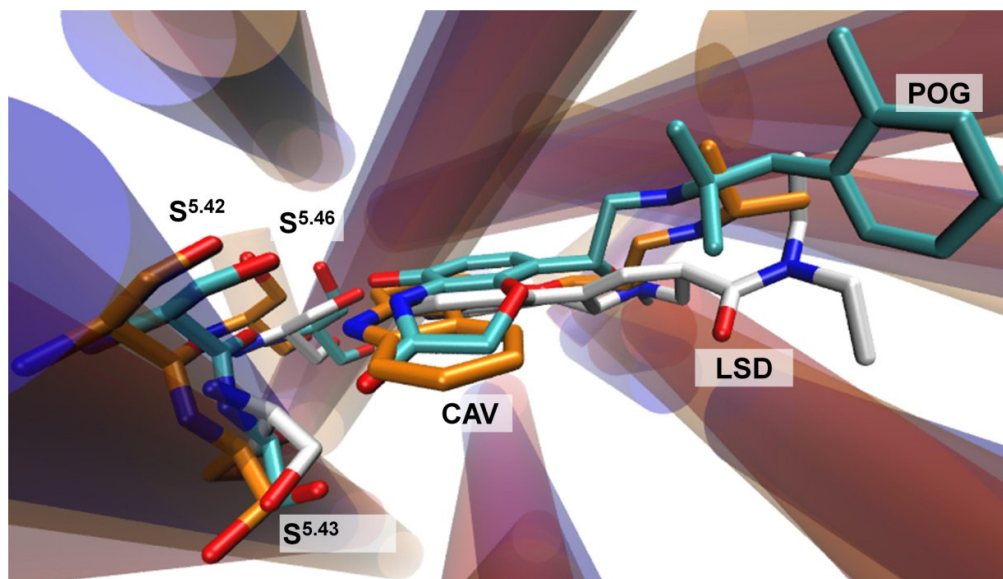
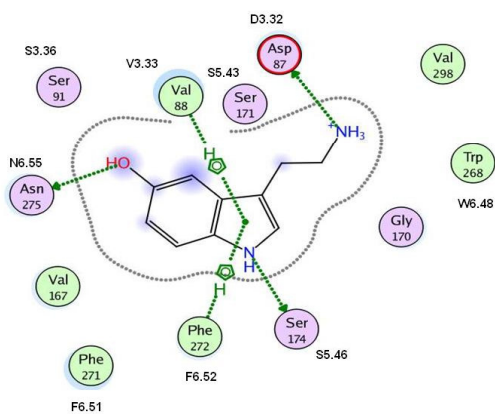
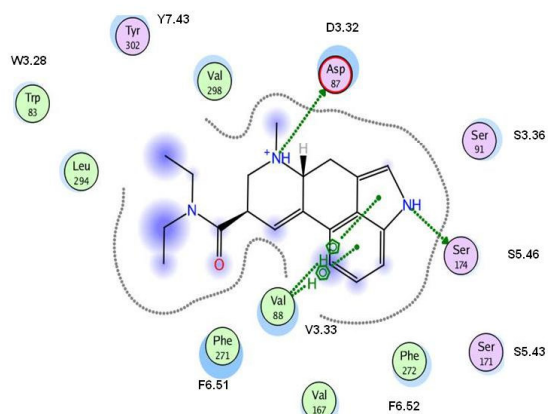


Figure 40. (A) Map of the interaction between serotonin and the 5-HT_{2A} receptor; (B) Map of the interaction between LSD and the 5-HT_{2A} receptor

A



B



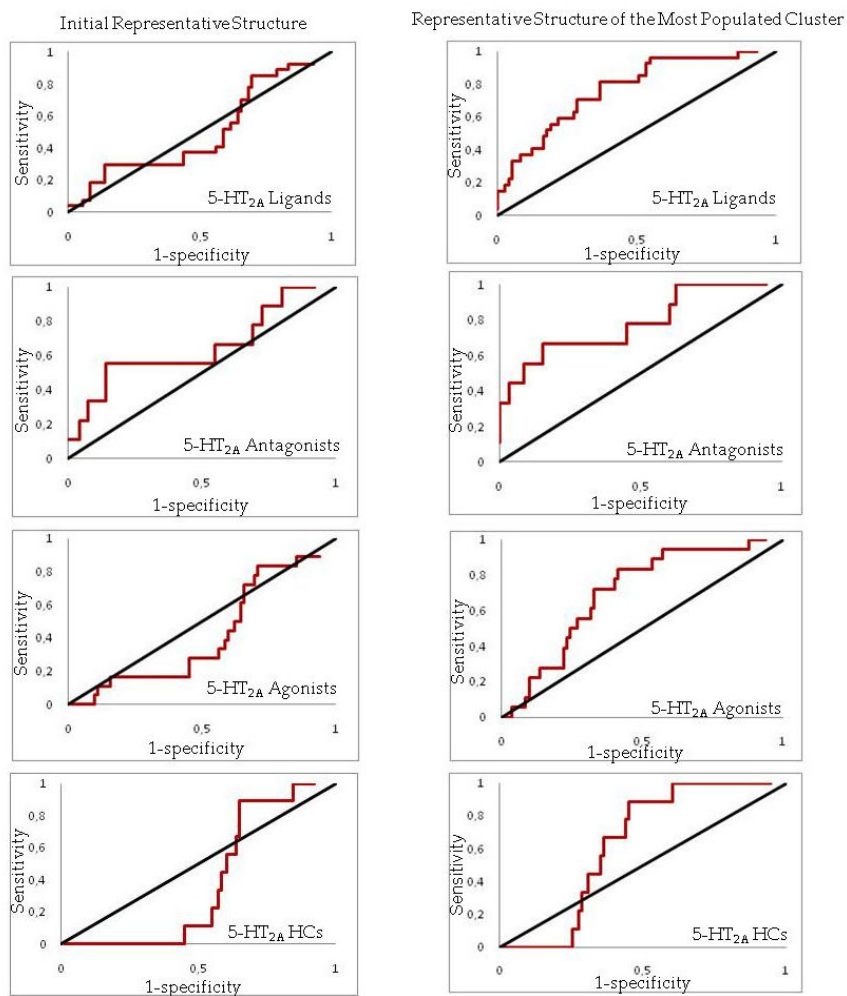
The results of the rigid docking runs carried out on the complexes selected by the IFD protocols (Table 12) were analyzed by generating ROC curves. Inspection of the curves (Figure 41a-d) revealed that in all cases the representative structure of the first clusters is not able to recognize a specific class of 5-HT_{2A} ligands. An exception is given by the representative structure of the first cluster of the monomeric and of the ProA forms which were able to poorly recognize 5-HT_{2A} antagonists (Figure 41a and 41c). The comparison of the ROC curves constructed for the first representative structures and for the representative structures of the most populated clusters allowed us to clearly appreciate how each form evolve in a time-dependent manner (Figure 37a and 41a-d). In fact, the monomeric and ProA forms start from a structure able to recognize 5-HT_{2A} antagonists (representative structure of the first cluster, Figure 41a and 41c) and along the simulations their ability to recognize the 5-HT_{2A} antagonists improved (representative structure of the most populated cluster Figure 41a and 41c). ProH starts from a structure not able to recognize any 5-HT_{2A} ligands (representative structure of the first cluster, Figure 41b), and evolves toward a structure able to better recognize the 5-HT_{2A} agonists (representative structure of the most populated cluster, Figure 41b). ProB starts from a structure not able to recognize any 5-HT_{2A} and it evolves toward a structure able to recognize different classes of 5-HT_{2A} ligands (Figure 41d), with a little preference for the 5-HT_{2A} antagonists.

The most interesting result is that the representative structures of the most populated cluster for each system were those best able to discriminate among the different classes of 5-HT_{2A} ligands (Figure 41), with the representative structure of the most populated cluster of ProB able to recognize different kind of 5-HT_{2A} ligands. Our results clearly indicate that the different molecular systems (heteromer, homomer, and monomer) evolve differentially during the MD simulations. This can be appreciated from ROC curves in Figure 41, where the initial structures of the molecular systems are compared with the respective most populated clusters. Furthermore, the most populated cluster of the trajectory of 5-HT_{2A} simulated as a monomer preferentially recognizes antagonist structures. This can be certainly related to the fact that the monomeric 5-HT_{2A} is modelled on the resting state of the human β_2 -adrenergic receptor. Conversely, the most populated clusters of 5-HT_{2A} extracted from the heteromeric simulation preferentially ranks 5-HT_{2A} agonist, and it is the

structure that best recognize the HCs (Figure 41b). These data must clearly be taken with caution and not overemphasized due to the short time of the MD simulation, nevertheless a clear effect of the dimerization interface is appreciable. From one side, the presence of the heteromeric interface induces a change in the binding pocket of 5-HT_{2A} switching the preference to 5-HT_{2A} agonists. From the other side, it seems that the homomeric interface transmits anisotropic changes, with the two protomers (ProA and ProB) behaving in a very different manner. This is a relevant outcome of our study, indicating a physical crosstalk between the protomers forming GPCR dimer complexes. Furthermore, our results support the notion that the simulation of the 5-HT_{2A} receptor in its dimeric forms lead to different results, with respect to the monomeric form of the same receptor, and simulated in the same experimental conditions.

Figure 41. (A) ROC curves and their statistical parameters for the monomeric form of the 5-HT_{2A}; (B) ROC curves and their statistical parameters for ProH, (C) ROC curves and their statistical parameters for ProA; (D) ROC curves and their statistical parameters for ProB.

A

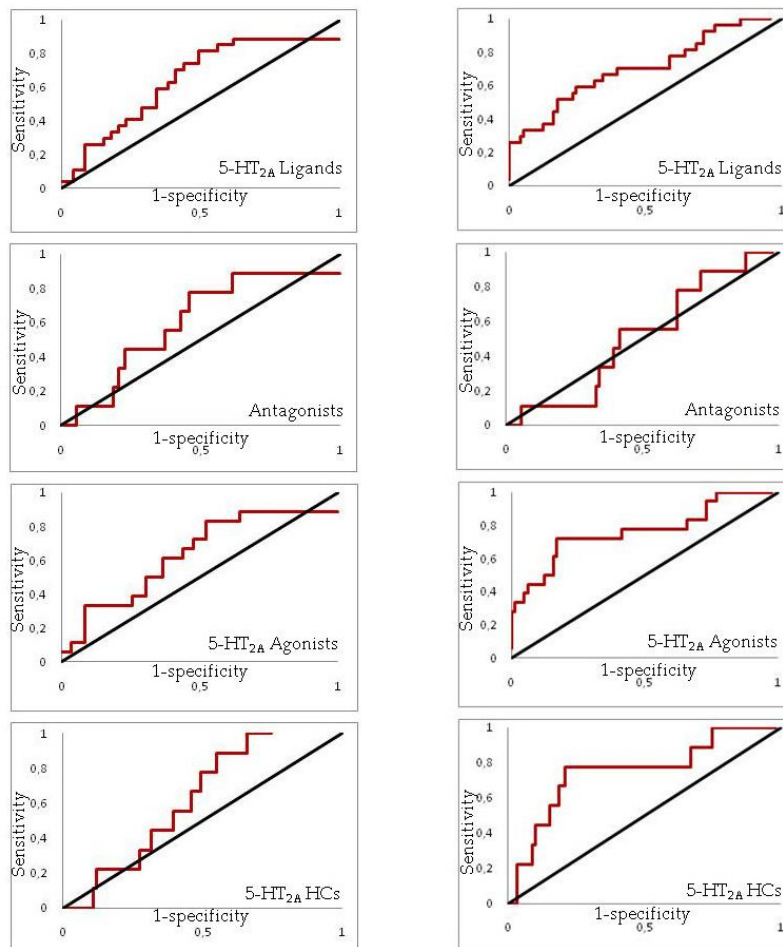


	Initial representative structure					Representative structure of most populated cluster				
	AUC	EF 2%	EF 5%	EF 10%	EF 20%	AUC	EF 2%	EF 5%	EF 10%	EF 20%
5-HT _{2A} Ligands	0.50	1.85	0.74	1.48	1.48	0.75	1.85	2.96	2.22	1.85
Antagonists	0.62	5.56	2.22	3.33	2.78	0.77	5.56	6.67	4.44	2.78
5-HT _{2A} Agonists	0.43	0.00	0.00	0.56	0.83	0.68	0.00	1.11	1.11	1.39
5-HT _{2A} HCs	0.33	0.00	0.00	0.00	0.00	0.61	0.00	0.00	0.00	0.00

B

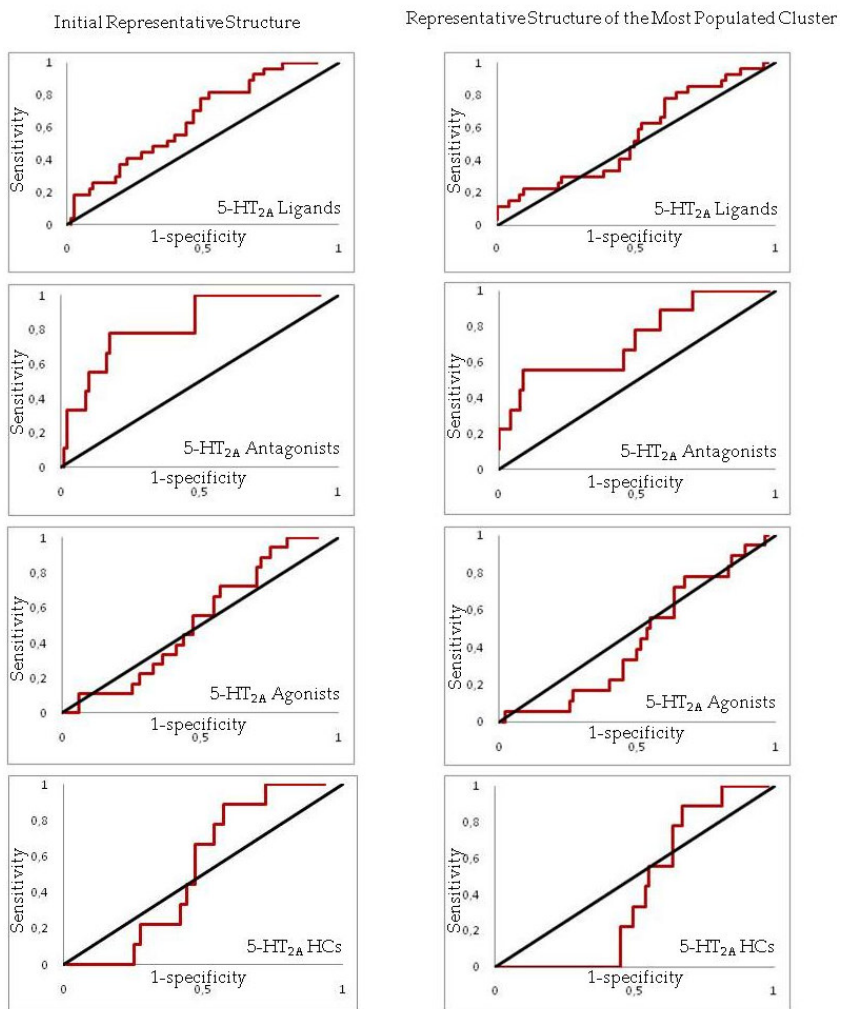
Initial Representative Structure

Representative Structure of the Most Populated Cluster



	Initial representative structure					Representative structure most populated cluster				
	AUC	EF 2%	EF 5%	EF 10%	EF 20%	AUC	EF 2%	EF 5%	EF 10%	EF 20%
5HT _{2A} Ligands	0,64	1,85	1,48	1,48	1,48	0,70	3,70	3,70	2,59	1,85
Antagonists	0,59	0,00	0,00	1,11	1,11	0,50	0,00	0,00	1,11	0,56
5HT _{2A} Agonists	0,63	2,78	2,22	1,67	1,67	0,76	5,56	5,56	3,33	2,50
5HT _{2A} HCs	0,51	0,00	0,00	0,00	1,11	0,75	0,00	4,44	2,22	2,78

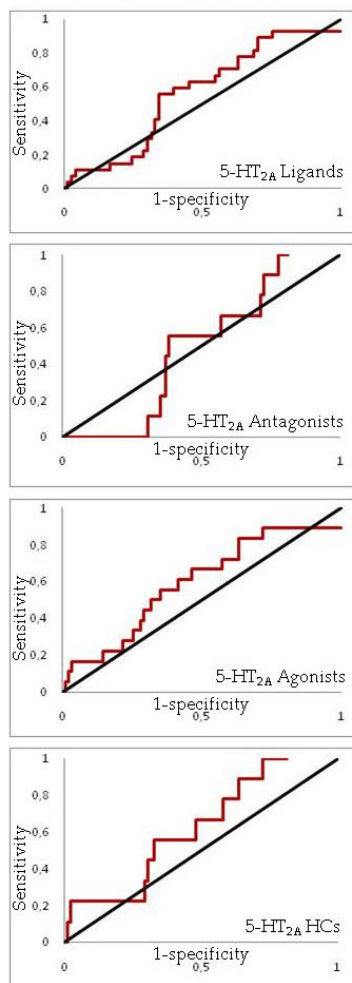
C



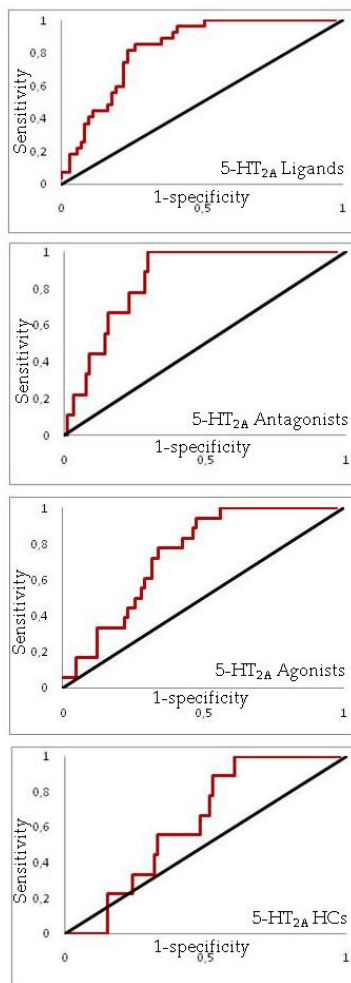
	Initial representative structure					Representative structure most populated cluster				
	AUC	EF 2%	EF 5%	EF 10%	EF 20%	AUC	EF 2%	EF 5%	EF 10%	EF 20%
5HT _{2A} Ligands	0,58	1,85	2,22	1,85	1,30	0,54	3,70	2,22	1,48	1,11
Antagonists	0,71	5,56	6,67	3,33	2,78	0,72	11,11	4,44	3,33	2,78
5HT _{2A} Agonists	0,52	0,00	0,00	1,11	0,56	0,43	0,00	1,11	0,56	0,28
5HT _{2A} HCs	0,51	0,00	0,00	0,00	0,00	0,40	0,00	0,00	0,00	0,00

D

Initial Representative Structure



Representative Structure of the Most Populated Cluster

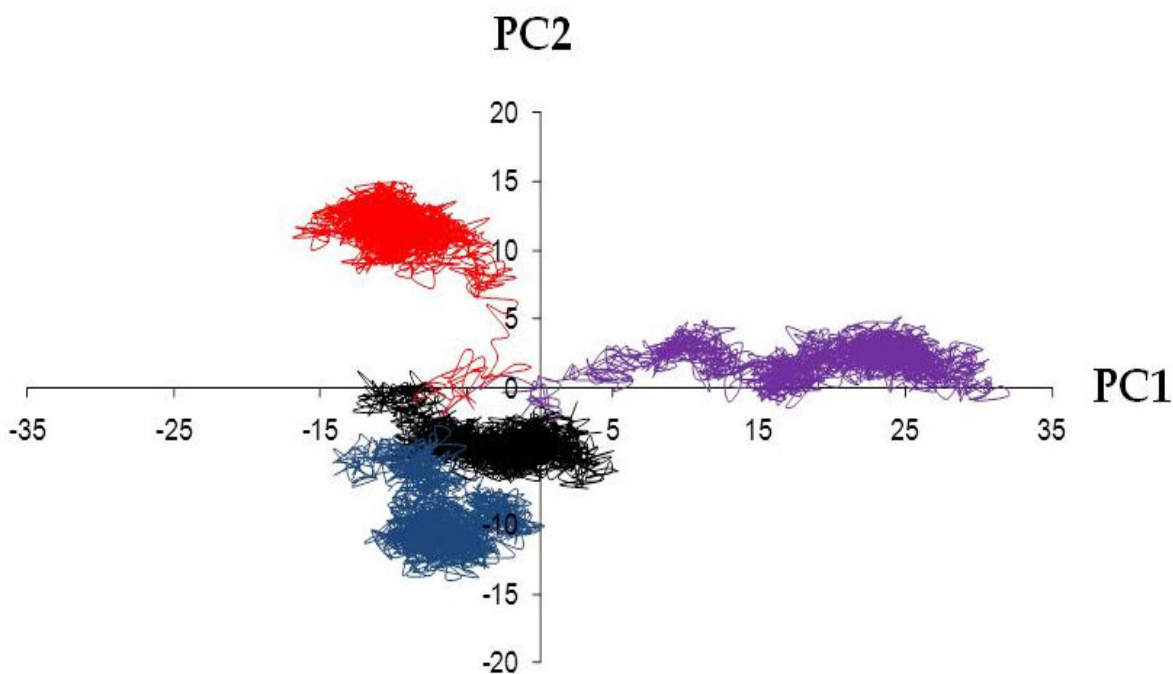


	Initial representative structure					Representative structure most populated cluster				
	AUC	EF 2%	EF 5%	EF 10%	EF 20%	AUC	EF 2%	EF 5%	EF 10%	EF 20%
5HT _{2A} Ligands	0,48	1,852	1,481	1,111	0,741	0,80	3,70	2,22	2,22	2,22
Antagonists	0,52	0,000	0,000	0,000	0,000	0,80	5,56	4,44	3,33	3,33
5HT _{2A} Agonists	0,57	2,778	2,222	1,667	1,111	0,70	2,78	1,11	1,67	1,67
5HT _{2A} HCs	0,54	5,556	4,444	2,222	1,111	0,62	0,00	0,00	0,00	1,11

4.1.5 Essential Dynamic Analysis

A crucial aspect of our studies is to identify the structural bases underlying the different behaviour of the systems, along the simulations. So as to grasp atomic details about the discriminating features among the systems, we performed a Comb-ED as described in section 3.4.6. This technique allows to catch differences and similarities in the essential subspace crossed by the trajectories of the compared systems. In Figure 42 the essential space explored by each system along the first two eigenvectors is reported.

Figure 42. Scoring plot computed only on the TM C α atoms of the 5-HT_{2A} receptor. Purple line: monomer simulation; Black line: ProH simulation; Blue line: ProA; Red line: ProB.



Analyzing the plot in Figure 42 it can be appreciate the separation along the first eigenvector among the monomeric simulations (purple), and the dimeric simulations (red, ProB; black, ProH; blue, ProA) of the 5-HT_{2A} receptor. So as to, the first principal component describes structural features discriminating among the monomeric and dimeric simulations of the 5-HT_{2A} receptor. Instead, the second principal component describes structural features discriminating the effects of the dimer interface on each protomer involved in a dimer complex. Indeed, in the upper-left region of the scoring plot the ProB simulations (red) is represented, while in the bottom left the ProH (black) and

ProA (blue) simulations are located. Since we became interested in the identification of the residues underlying the different effects caught by the eigenvectors, we analyzed the loadings matrix carried out from ptraj. Starting from the loading matrix we extracted the p square values (summation of the square values of the loadings for the x, y and z coordinates, for each residue), and then we plotted the p square values of the first eigenvector and the second eigenvector against the residue index (Figure 43a,b). Furthermore, for a better understanding we plotted the p square values of the first eigenvector against the p square values of the second eigenvector (Figure 44).

Figure 43. (A) p square values of the first eigenvector plotted against the residue index; (B) p square values of the second eigenvector plotted against the residue index

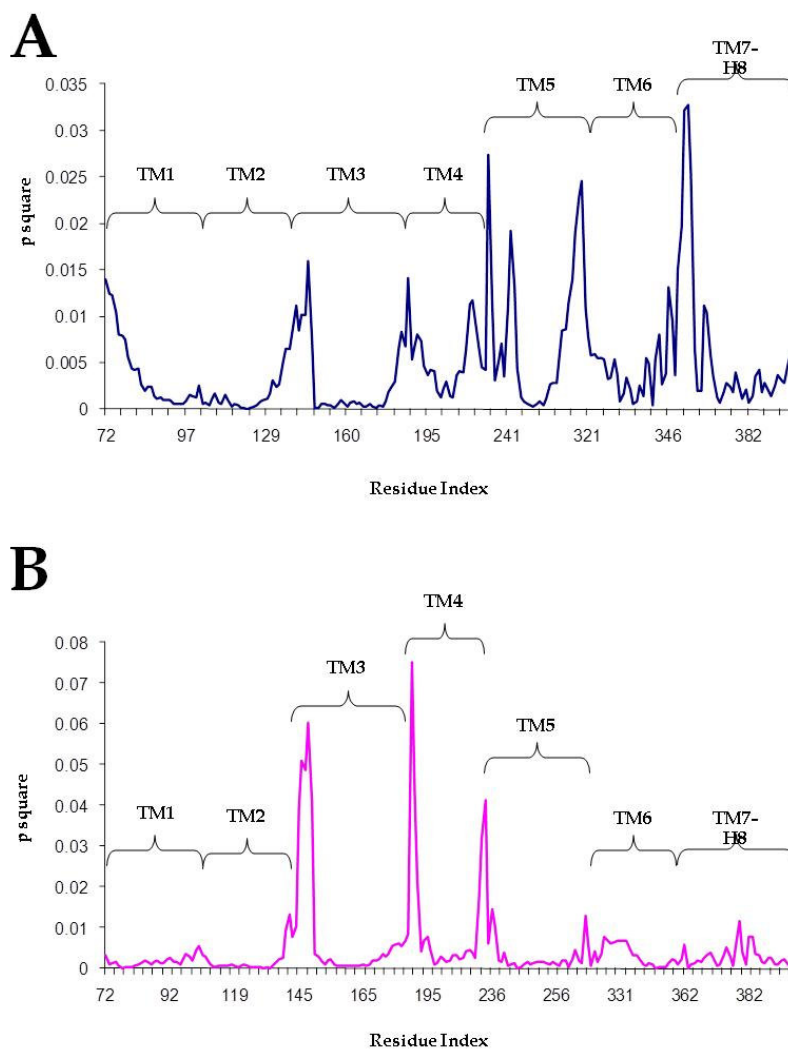
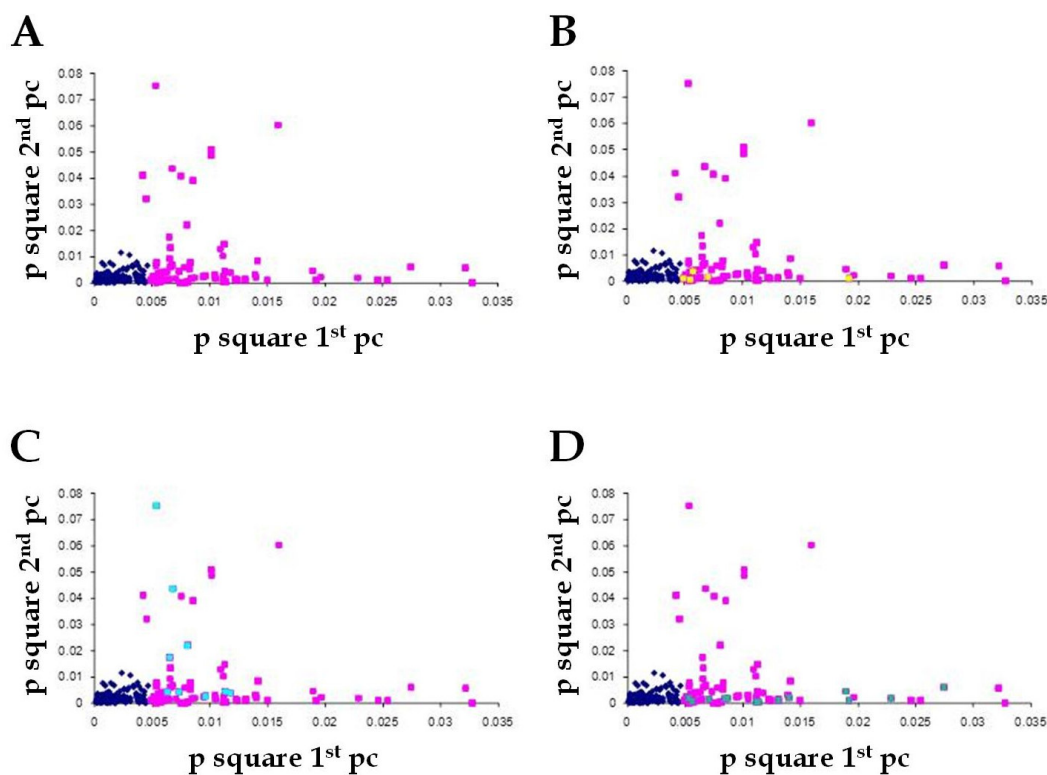


Figure 44. p square values of the first eigenvector plotted against the p square values of the second eigenvector. (A) Highlighted in pink the residues taken into account as relevant; (B) Highlighted in yellow box the residues lining up the binding pocket identified by the Comb-ED; (C) Highlighted in cyan the residues belonging to TM4 identified by Comb-ED; (D) Highlighted in dark blue the residues belonging to TM5 identified by Comb-ED.



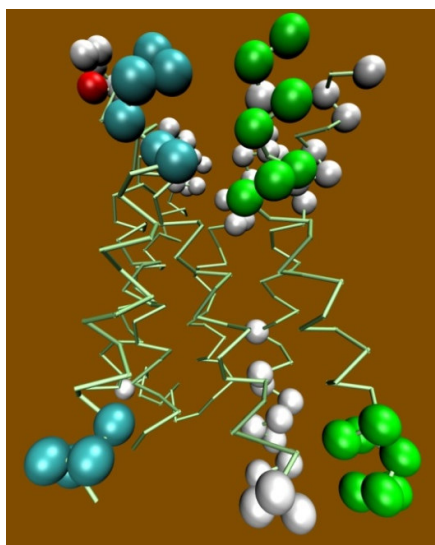
The plot reported in Figure 43 allows us to identify the behaviour of the TM5-7 and H8 domains as crucial for the differentiation of the behaviour of the system along the first principal mode (Figure 42), while the separation along the second principal mode (Figure 42) is linked to the behaviour of the TM3-5 domains, with the TM4 domain predominating the structural information carried in the second principal mode. Indeed, we identify the residues responsible for the differentiation of the simulations. Table 13 lists the residues identified during the Comb-ED analysis, and in Figure 45 are highlighted the C α atoms of the residues listed in Table 13. The residues are located on the intracellular and on extracellular side of TM domains (Figure 45). Interestingly, on TM1-3 and TM7 we identified only few residues (8, 3, 6 and 8 respectively), while on TM4-6 we identify more

residues (11, 11 and 16 respectively) than in TM1-3 domains. Furthermore, on TM3 we identified the residue of Cys148 (Figure 45 red sphere) as relevant for the differentiation of the simulations, this can suggest that also in the case of the GPCRs dimerization phenomena the communication among TM3 and EL2 by the disulphide bond is important. It is worth to mention that by this analysis it is possible to know which residues play a relevant role in the differentiation of the simulations, without saying anything about the nature of displacements.

Table 13. Residue identified by Comb-ED as indicate in Figure 17a. Highlighted in green the positions investigate in cross-linking experiment with other GPCRs belonging to family A.^{151,169,243,245,308,309}

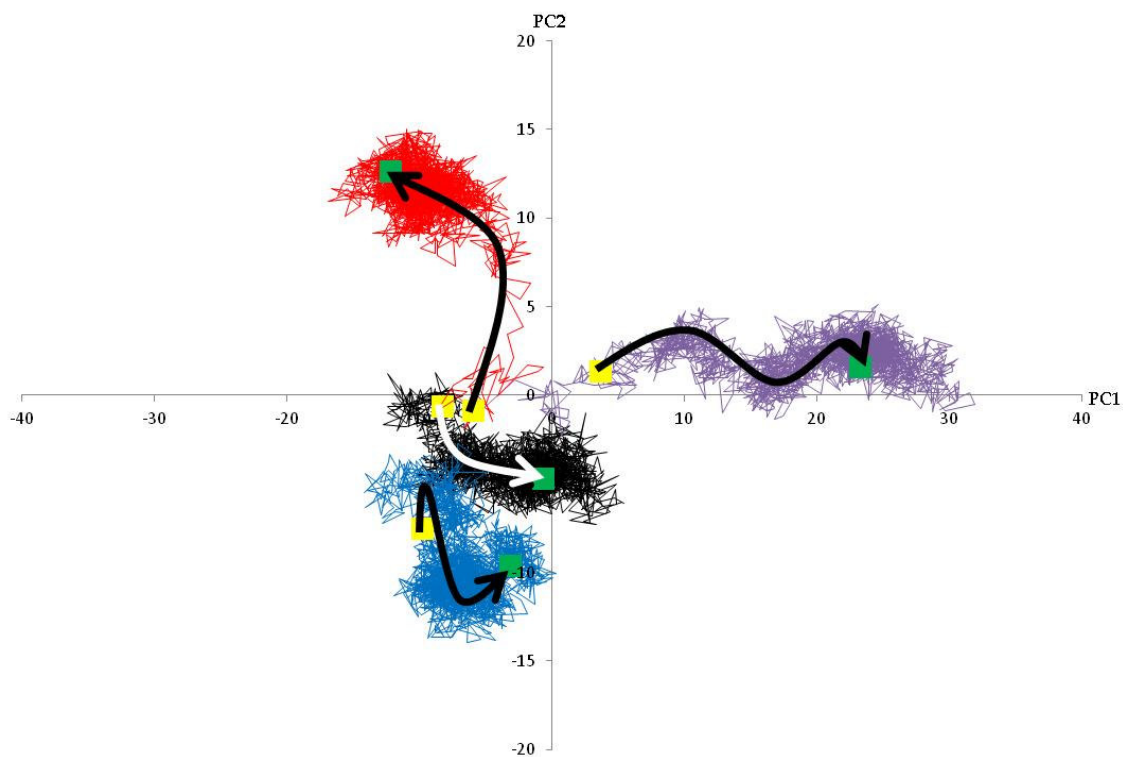
TM1	TM2	TM3	TM4	TM5	TM6	TM7
1.3	2.64	3.21	4.39	5.37	6.35	7.3
1.31	2.65	3.22	4.4	5.38	6.36	7.31
1.32	2.66	3.23	4.41	5.39	6.37	7.32
1.33	2.67	3.24	4.42	5.4	6.38	7.37
1.34		3.25	4.43	5.42	6.41	7.38
1.35		3.26	4.57	5.43	6.51	7.41
1.36		3.53	4.58	5.45	6.52	7.42
1.37		3.54	4.59	5.46	6.54	7.43
		3.55	4.6	5.47	6.55	7.67(H8)
			4.61	5.61	6.58	7.68(H8)
			4.62	5.62	6.59	
			4.63	5.63	6.61	
				5.64		
				5.65		
				5.66		

Figure 45. Representation of the residues identified by Comb-ED. The green spheres represents the C α atoms of the residue belonging to TM5, the cyan spheres the residues belonging to TM4, the white spheres the other residues identified and the red one is the C α atoms of the residue of Cys148 (C^{3.25}) involved in the disulphide bond connecting TM3 to EL2.



Analyzing the plots reported in Figure 43a and 43b we can conclude that the first principal mode brings information principally on TM5-7 and H8 domains, while the second principal mode brings information principally on TM3-5 domains. The results reported in Figure 44, along with the results of the cluster analysis (Figure 38), and the docking experiments (Figure 41) allow us to speculate about a direct connection among the behaviour of the dimer interface and the behaviour of residues lining up the binding pocket. In Figure 46 we compare the results of the cluster analysis with the Comb-ED analysis, showing that the sampled structures by the cluster analysis well describe the essential subspace crossed by each system, and supporting a direct connection among the effects of the dimer interface and the behaviour of the residues lining up the putative 5-HT_{2A} binding pocket (Figure 46 and Figure 41a-d).

Figure 46. Scoring plot computed only on the TM C α atoms of the 5-HT_{2A} receptor. Purple line: monomer simulation; Black line: ProH simulation; Blue line: ProA; Red line: ProB. The yellow boxes represent the initial representative structure of each system, while the green boxes the representative structure of the most populated cluster of that system, according to the Ligand Docking Protocol (Figure 42a-d). The white and black arrows represent a hypothetical pathway, describing how each system reaches its own representative structure of the most populated cluster.



Moreover the results achieved by the Comb-ED are in good accordance with what reported for the rhodopsin and D₂ homomers. Indeed, in these works the authors applying mutagenesis and cross-linking techniques identified residues involved in the dimer interface contacts, and most of those residues are located on the top or on the bottom sides of the TM4-5 domains, or they are directly exposed at the dimer interface level.^{151,169,243,245,308,309}

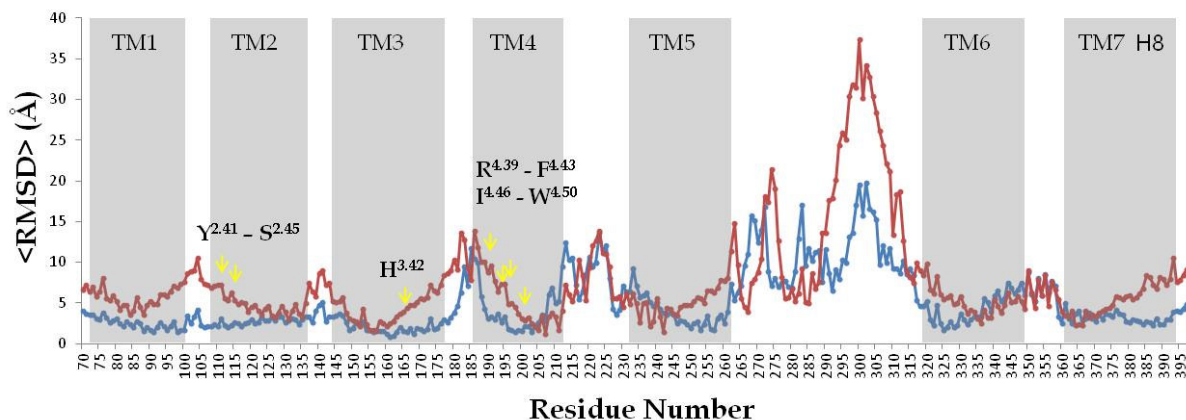
4.2 Cholesterol Effects Analysis

4.2.1 Cholesterol Effects on the Monomeric 5-HT_{2A}

The 5-HT_{2A} receptor belongs to the strict-CCM class (see section 1.5), and it is involved in several physiological and pathological processes (i.e. platelet aggregation, CNS disease etc...), representing one of the most interesting targets for the treatment of psychiatric disorders.³¹⁰ The 5-HT_{2A} receptors are highly expressed in different brain regions, where it is well known that cholesterol takes part in the formation of lipid rafts.^{311,312} With the aim to understand the effect of cholesterol on the stability and conformational properties of the monomeric 5-HT_{2A}, we carried out computational studies on the monomeric 5-HT_{2A} with different cholesterol concentrations (0-25%) (see section 3.4.4).

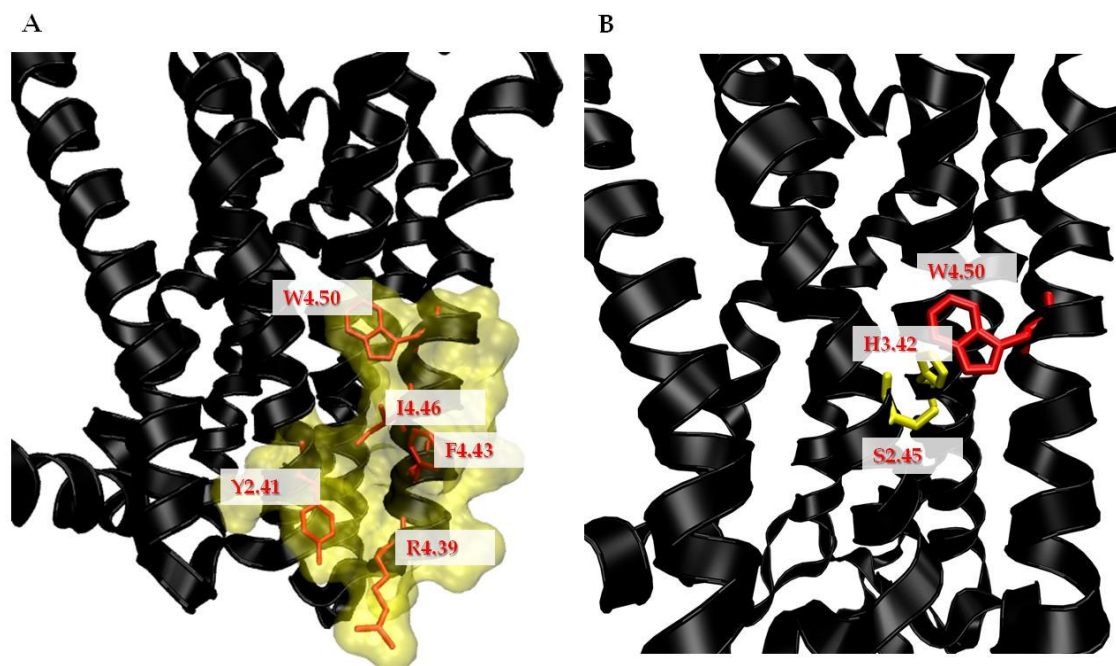
So as to evaluate the effect of the membrane composition on the conformational flexibility of the 5-HT_{2A} receptor, we measured the average RMS fluctuation per residue of the C α atoms of the 5-HT_{2A} receptor. The average RMS fluctuation were computed against the same reference structure (initial model carried out from the homology modeling protocol). In Figure 47, we report the plot of the average RMS fluctuation of both forms of the 5-HT_{2A} receptor (0% and 25% of cholesterol). It can be appreciated that the 5-HT_{2A} receptor in presence of cholesterol is more stable than the 5-HT_{2A} without cholesterol: the TM regions of the receptors simulated with cholesterol (Figure47, blue line) show a lower average RMS fluctuation than the simulation without cholesterol (Figure47, red line). This observation is constant for each TM excluding the extracellular end of the TM5, TM7 and TM3 and the intracellular end of the TM4 and TM6

Figure 47. average RMS fluctuation per residue of the C α atoms of the 5-HT_{2A} receptor. The blue line refers to the simulation with cholesterol (25%), the red one refers to the simulation without cholesterol (0%). The regions highlighted in gray represents the transmembrane regions (TM1-7) and the helix-8 (H8). The yellow arrows indicate the residues lining up the CCM.



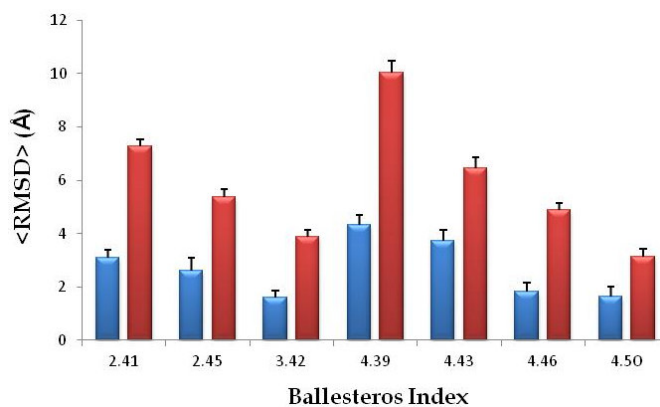
Noteworthy is the behavior of the residues forming the cholesterol consensus motif (CCM, Figure 47 yellow arrows). In the 5-HT_{2A} receptors this motif is constituted by Y^{2.41}; R^{4.29}; F^{4.43}; I^{4.46}; W^{4.50} bringing the 5-HT_{2A} receptors into the strict-CCM class (Figure 48a).⁹³ Also in this case the residues of the receptors simulated without cholesterol show a higher average RMS fluctuation from the reference structure than the simulation with cholesterol (CCM, Figure 47 yellow arrows). In order to understand the role of the cholesterol on the flexibility of the 5-HT_{2A}, we monitored the behavior of the residues forming the CCM along the whole trajectories of both systems (0%-25% cholesterol). Furthermore, we decided to monitor the behavior of other two residues: the S^{2.45} and H^{3.42} residues. This amino acid are in close contact with the W^{4.50}, and they are located on different TM domains and can form different types of interactions with the W^{4.50} (Figure 47b).

Figure 48. Representation of the 5-HT_{2A} strict-CCM, highlighted in red the residues forming the CCM and in yellow and transparent the surface of each residues forming the CCM. (A) The residues forming the strict-CCM; (B) the residues in close contact with the W^{4.50} (yellow and stick).



In Figure 49, we report the plot of the average RMS fluctuation per residue of the C α atoms of the CCM, it can be appreciated the differences in the average RMS fluctuation of each residue forming the CCM. In detail, the residues belonging to the 5-HT_{2A} embedded in the cholesterol-rich membrane (25%, Figure 49, blue) show lower average displacement than the residues belonging to the 5-HT_{2A} embedded in the cholesterol-free membrane (0%, Figure 49, red) from the reference structure.

Figure 49. average RMS fluctuation per residue of the C α atoms of the residues lining up the CCM with (blue) and without (red) cholesterol.



These differences in the average RMS fluctuation are due to the direct interaction of cholesterol molecules with the residues of the CCM, which results in a stabilization of the CCM region. In fact, after approximately 90 ns at least two cholesterol molecules form stable interaction with the residues of the CCM, and these interactions are retained until the end of the simulation (Figure 50). Interesting, the R^{4.29} residue seems to function as anchor point for the polar head (OH) of the cholesterol molecules. The effect of the direct interaction between cholesterol molecules and the residues of the CCM are highlighted by the different behavior of the TM4. In Figure 47, we report the average RMS fluctuation of the protein for both systems (0-25% cholesterol). It can be appreciated that TM4 accomplishes higher displacement in the absence of cholesterol than in the presence of cholesterol (Figure 47 TM4). Moreover, the direct interaction between the residues of the CCM and the cholesterol molecules alter the hydrogen-bonding network between the W^{4.50}, Y^{2.41} and the S^{2.45}, H^{3.42} residues. S^{2.45} and H^{3.42} residues are not involved in the interaction with the cholesterol molecules, while W^{4.50} and Y^{2.41} are directly involved in the interaction with the cholesterol molecules. Comparing the behavior of these residues in both simulations (with and without cholesterol) we observed a completely different pattern of interaction among the W^{4.50}, S^{2.45}, Y^{2.41} and H^{3.42} residues (Table 14).

Figure 50. Representative frames showing the direct interaction between the CCM and cholesterol molecules. The red arrow represent the time evolution of the MD simulation, the numbers in bolt represent the corresponding time (ns) of each frame. Cholesterol molecules are depicted in yellow-transparent surface while the CCM forming residues are shown in blue- transparent surface

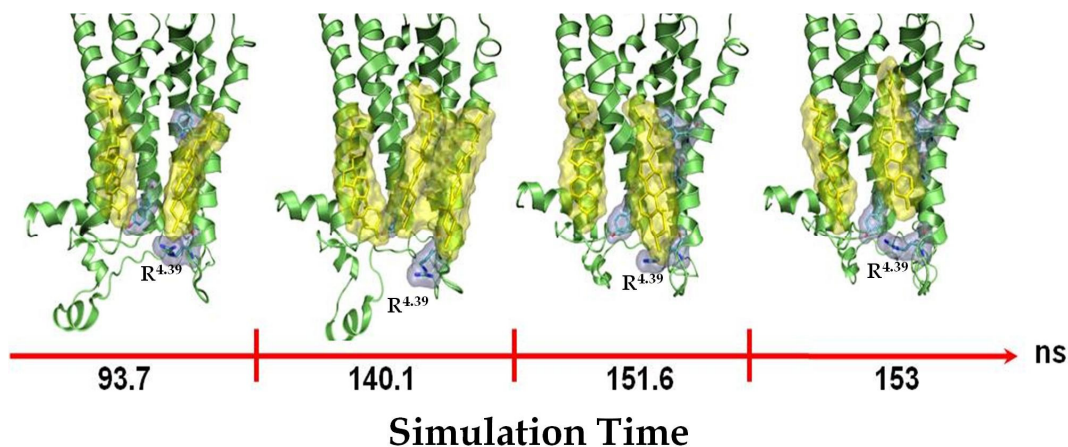


Table 14. Distribution (%) of each hydrogen bond among the W4.50, S2.45, Y2.41 and H3.42 residues.

	S ^{2.45} -Y ^{2.41}		S ^{2.45} -H ^{3.42}		S ^{2.45} -W ^{4.50}	
	Backbone	Sidechain	Backbone	Sidechain	Backbone	Sidechain
5-HT_{2A} 0% chol.	27.73%	16.05%	-	53.22%	-	12.18%
5-HT_{2A} 25% chol.	44.68%	67.70%	-	8.11%	-	4.33%

From the data reported in Table 14, it can be appreciated that in the simulation with cholesterol, the occurrence of the hydrogen bonds between the residues belonging to the same TM domains (S^{2.45}, Y^{2.41} on TM2) is increased, while the hydrogen bonds inter-helices are decreased. These data indicate a completely different behavior of the TM2-4 during the simulation of the 5-HT_{2A} in the presence of cholesterol molecules (Figure 47). Indeed, the analysis of the average RMS fluctuation of the TM2-4 (Figure 47 TM2; TM3 and TM4) reveals that TM2-4 in the absence of cholesterol are more flexible than in the presence of cholesterol. Furthermore, the analysis of the electron density profile plot shows a different behavior of the membrane environment depending on the cholesterol concentration (Figure 51). It has been reported that the cholesterol has a different effect on the membrane behavior depending on the amount of cholesterol and the nature of the phospholipids constituting the membrane.³¹³⁻³²⁰ From the plot reported in Figure 51 it can be appreciated an increase of the thickness in the simulation of the 5-HT_{2A} receptor with cholesterol. The system with cholesterol shows a distance peak-to-peak of 37 Å, while the system without cholesterol shows a distance peak-to-peak of 31 Å. The thickness values of 37 Å are in good agreement with those available in literature.³²¹⁻³²⁵ Interestingly, the plot of the electron density profile of the SDPC bilayer (Figure 51) reveals a slight asymmetrical behavior of the bilayer. This phenomenon is due to a different amount of SDPC and cholesterol in each layer. Indeed, the number of SDPC and cholesterol molecules in the extracellular monolayer is different from the number of SDPC and cholesterol molecules in the intracellular monolayer, in Table 15 we report the exact composition of each layer for each 5-HT_{2A} system.

Figure 51. Electron Density Profile of the SDPC bilayer with cholesterol (blue), without cholesterol (red) and of the cholesterol molecules (green) for the simulation of the 5-HT_{2A} receptor embedded into the cholesterol-rich membrane (25%).

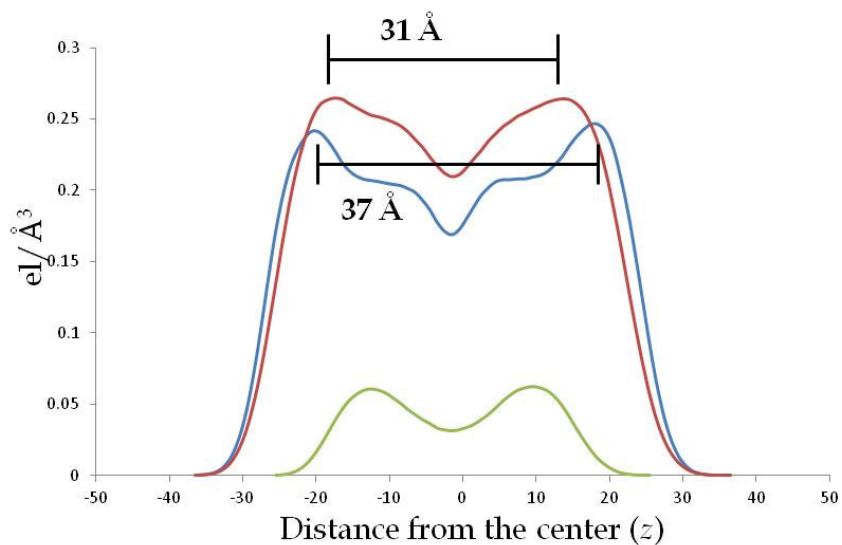


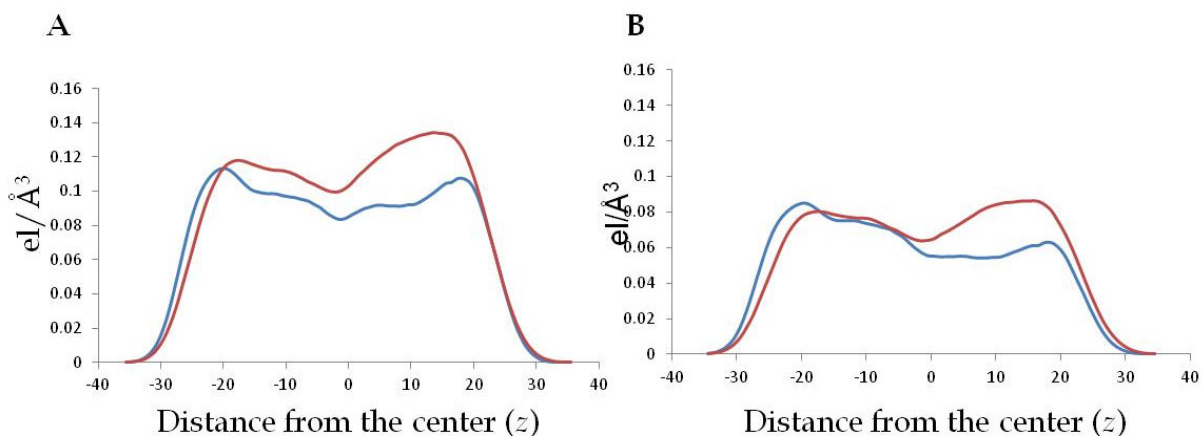
Table 15. Monolayer composition of each 5-HT_{2A} system.

	Extracellular layer		Intracellular layer	
	SDPC molecules	Chol. molecules	SDPC molecules	Chol. Molecules
5-HT_{2A} 0% Chol.	97	-	98	-
5-HT_{2A} 25% Chol.	85	28	89	30

Furthermore, the presence of the amphipatic helix-8 and the irregular shape of the receptor increase the asymmetric behavior of the bilayer, this observation is confirmed by the analysis of the Electron Density Profile of lipids shell (10 and 5 Å) around the protein (Figure 52a,b). Noteworthy is the observation that the asymmetric behavior is different depending on the presence of the cholesterol. This indicates a different hydrophobic

mismatch between the TM regions of the 5-HT_{2A} receptor and the hydrophobic environment of the membrane.

Figure 52. Electron Density Profile of a SDPC shell of 10 Å (A) and 5 Å (B) around the protein, for the 5-HT_{2A} simulation with (blue) and without (red) cholesterol.

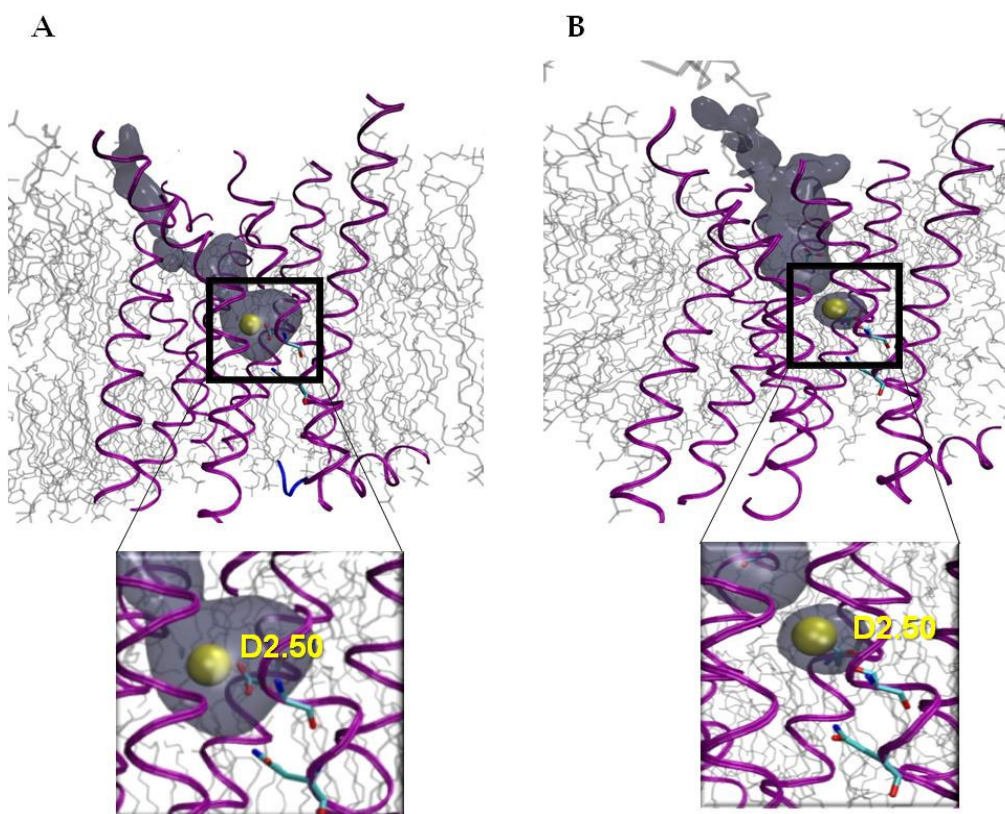


4.2.2 A Sodium Binding Pathway in the 5-HT_{2A} receptor

Quite unexpectedly during the 160 ns MD simulations we observed that at least one sodium ion enters the 5-HT_{2A} binding pocket in both systems (0-25% cholesterol). The presence of the sodium ions alters the behavior of relevant residues on TM2 and TM7, in detail the L^{2.46}; D^{2.50} and N^{7.49} residues, for which it has been reported that they play a crucial role in the active-inactive states transition for the 5-HT_{2A} receptor.¹⁰⁰ Furthermore, it has been reported that some Class A GPCRs are ion sensitive (see section 1.2.2).^{75,94,96-100,326,327} Noteworthy is the case of the D₂ dopaminergic receptor^{75,96,97,326,327} with which 5-HT_{2A} has a sequence identity of 39.53%. Comparing the behavior of the L^{2.46}; D^{2.50} and N^{7.49} residues, with respect to the behavior of the same residues in our previous simulations, where we simulated the monomeric form of the 5-HT_{2A} receptor in DMPC bilayer in presence of KCl (see section 3.3), we found that the K⁺ ions were not able to enter the 5-HT_{2A} binding site causing a completely different behavior of the L^{2.46}; D^{2.50} and N^{7.49} residues, with respect to the simulations carried out with Na⁺ ions.

The sodium pathway reported in Figure 53 was computed using the VolMap Tool of VMD1.8.7.^{233,252} It is worth to mention that no biological data about the effect of the sodium ions on the 5-HT_{2A} receptors functions have been reported to date. However, in literature, a huge number of papers discussing about the role of the conserved D^{2.50} residue and the effects of the ions on the GPCRs functioning have been reported (see section 1.2.2).^{94,95,97-100,327} For instance, biological^{75,96,326} and computational³²⁷ data about the allosteric effects of the sodium ion have been reported for the dopaminergic D₂ receptor.

Figure 53. Sodium Pathway (transparent-gray) for the simulation with (25%, A) and without (0%, B) cholesterol. In tube and purple the 5-HT_{2A} receptor, the yellow sphere (vdW radii) is the sodium ions. Highlighted in the black boxes the regions corresponding to the position of the D^{2.50}.



The human D₂ and the human 5-HT_{2A} receptors belong to the same GPCR subfamily, the biogenic amine subfamily, and comparing the amino acidic sequences of both receptors we found a high sequence identity among the residues 4.5 Å around the D^{2.50} residues (Figure 55). Twelve residues form this sort of ion binding pocket, and only three are not

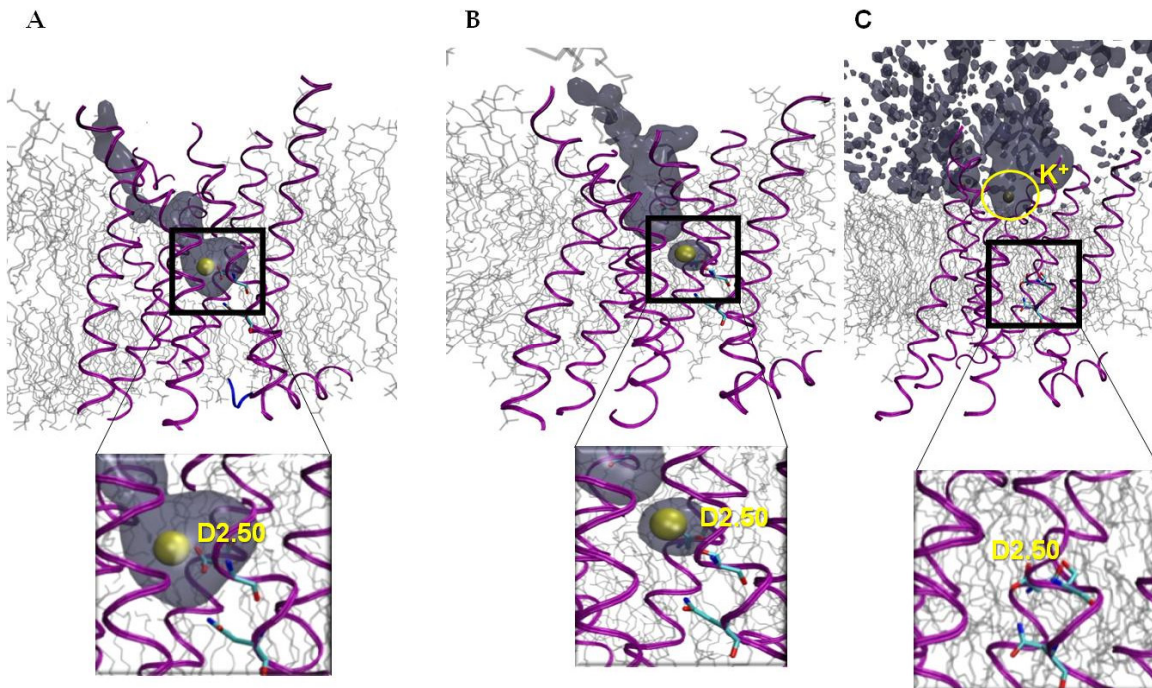
conserved between the D₂ and 5-HT_{2A} sequences, specifically the T^{1.46}; L^{2.53} and G^{2.54} (Figure 54).

Figure 54. Sequence alignment between the D₂ and 5-HT_{2A} receptors. Highlighted in red, the residues in a 4.5 Å shell around the 5-HT_{2A} D^{2.50} residue, and the corresponding residues of the D₂ receptor. In this case we took into account only the residues facing towards the inner part of the 5-HT_{2A} receptor. Highlighted in gray the TM domains in which we found these residues.

	TM1		
sp P14416 DRD2_HUMAN	HYNYYATLLTLLIAVIVFGNVLVCM	60	
sp P28223 5HT2A_HUMAN	EKNWSALLTAVVIILTIAGNILVIM	100	
	TM2	TM3	
sp P14416 DRD2_HUMAN	TTNYLIVSLAVADLLVATLVMPWVYLEVVG-EWKF	SRIHC	109
sp P28223 5HT2A_HUMAN	ATNYFLMSLAIADMLLGFVMPVSMLTILYGYRWPL	PSKLC	150
	TM3		
sp P14416 DRD2_HUMAN	FVTLDVMMCTASILNLC	CAISIDRYTAVA	
sp P28223 5HT2A_HUMAN	WIYLDVLFSTASIMHLC	CAISLDRYVAIQ	
	TM6		
sp P14416 DRD2_HUMAN	EKKATQMLAIVLGVFIICWLPFFITHILNIH	398	
sp P28223 5HT2A_HUMAN	EQKACKVLGIVFFLEFVVMWCPFFITNIMAVI	348	
	TM7		
sp P14416 DRD2_HUMAN	LYSAFTWLG YVNSAVNPIIYTTFNIEFRKAFLKIL	440	
sp P28223 5HT2A_HUMAN	LLNVFVWIGYLSAVNPLVYTLFNKTYRSAFSRYI	395	

Finally, we compared the new results with our previous works, where we simulated the 5-HT_{2A} receptor in DMPC phospholipids bilayer and with an ionic strength of 0.15M KCl. Comparing these simulations we found that the K⁺ ions are not able to enter deeply into the 5-HT_{2A} receptor. In detail, during the MD simulation, two K⁺ ions enter from the extracellular side of the serotonergic receptor moving towards the orthosteric binding site D^{3.32}. Importantly, potassium ions never reach the allosteric ion binding site D^{2.50} as it was observed in this study for Na⁺ ions (Figure 55)

Figure 55. Sodium pathway (gray and transparent) for the simulation with (25%, A) and without (0%, B) cholesterol, and potassium pathway (gray and transparent, C). In tube and purple the 5-HT_{2A} receptor, in VDW sphere and yellow the sodium ions. Highlighted in the black square the regions corresponding to the position of the D^{2.50}.

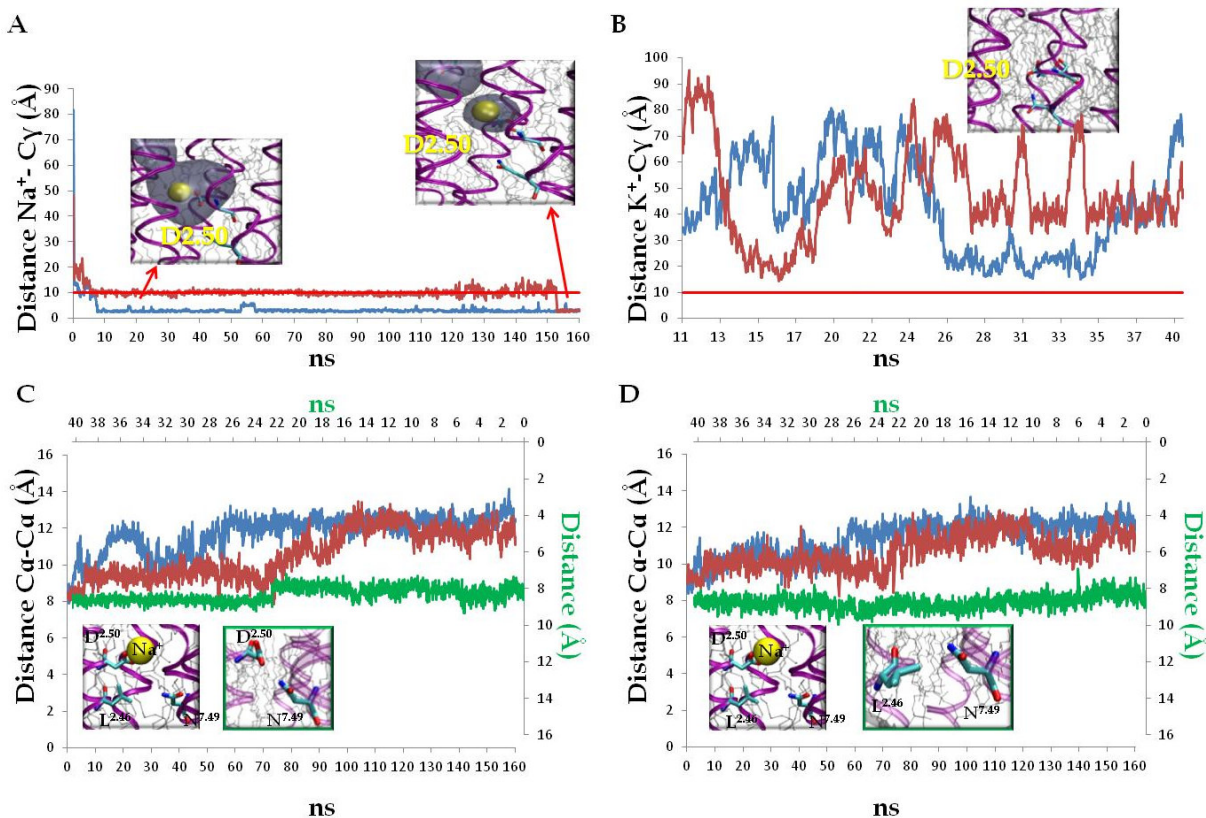


In Figure 56a,b, we report the distance between the ions (Na^+/K^+) and the C γ atom of the D^{2.50} residues only for the production phases, compared with the distances of the initial state of each system (values of the frame 0 = minimized structure). It can be appreciated that, (i) the Na^+ ion which is already present in the binding pocket moves towards the putative allosteric binding site D^{2.50} in the 5-HT_{2A} receptor after about 10 ns during the production phase (Figure 56a); (ii) the K^+ -C γ distance is always greater than the Na^+ -C γ distance (Figure 56a,b); (iii) in the simulation of the 5-HT_{2A} receptor in the cholesterol-free membrane, the Na^+ ion interact with the D^{2.50} later than in the simulation of the 5-HT_{2A} receptor in the cholesterol-rich membrane (Figure 56a). In the former case the Na^+ ion spend time in the interaction with the conserved residue of aspartate on TM3 (D^{3.32}), after that the ion enter deepest in the serotonergic binding pocket and interact with D^{2.50}.

Comparing both simulations, we also observed that the Na^+ ions mediate interactions between the D^{2.50} and the N^{7.49} forming a sort of bridge, while in the simulation with the K^+

ions these two residues are in direct contact. The different behavior of the two ion species leads to an increased distance between the C α atoms of the D^{2.50} and N^{7.49} residues in the simulation of the Na⁺ ions with/without cholesterol (Figure 56c, blue/red) compared to the K⁺ simulation (Figure 56c, green).

Figure 56. (A) Distance Na⁺-C γ D^{2.50} in the simulations of the 5-HT_{2A} receptor in the cholesterol-free (red line) and cholesterol-rich (blue line) membranes; (B) Distance K⁺-C γ D^{2.50} in our previous simulations, the red and blue line indicate the two different pathways of the two different K⁺ ion. The continues red line at 10 Å highlights the different behavior of the different ion species; (C) Distance C α -C α between the D^{2.50} and N^{7.49} residues in the simulation with (blue) and without (red) cholesterol, the green one indicates the distance C α -C α between the D^{2.50} and N^{7.49} in the simulation with K⁺; (D) Distance C α -C α between the L^{2.46} and N^{7.49} residues in the simulation with (blue) and without (red) cholesterol, the green one indicates the distance C α -C α between the L^{2.46} and N^{7.49} in the simulation with K⁺.



It has been reported that the mutation of these two residues in the 5-HT_{2A} receptor has important consequences in the receptor activation mechanism by agonist.¹⁰⁰ Furthermore, L^{2.46} is one of the most conserved residues in the GPCRs family, the mutation of this residue with an alanine leads to constitutively active receptor in rhodopsin³²⁸ and

thyrotropin³²⁹ receptors. Recently, it has been also reported that the mutation L^{2.46}-A^{2.46} thermostabilizes the active conformation of the A_{2A} receptor.³³ The authors explain the effect of this mutation by the fact that L^{2.46} faces towards the relevant conserved motif NPxxY in TM7, and the L^{2.46} could be involved in hydrophobic interaction with N^{7.49} stabilizing the receptor in its inactive state.^{33,328,329} In our case the presence of a ion between the residues of D^{2.50} and N^{7.49} increases the distance between L^{2.46}, D^{2.50} and N^{7.49} (Figure 56c,d) reducing the interaction between the L^{2.46} and N^{7.49}.

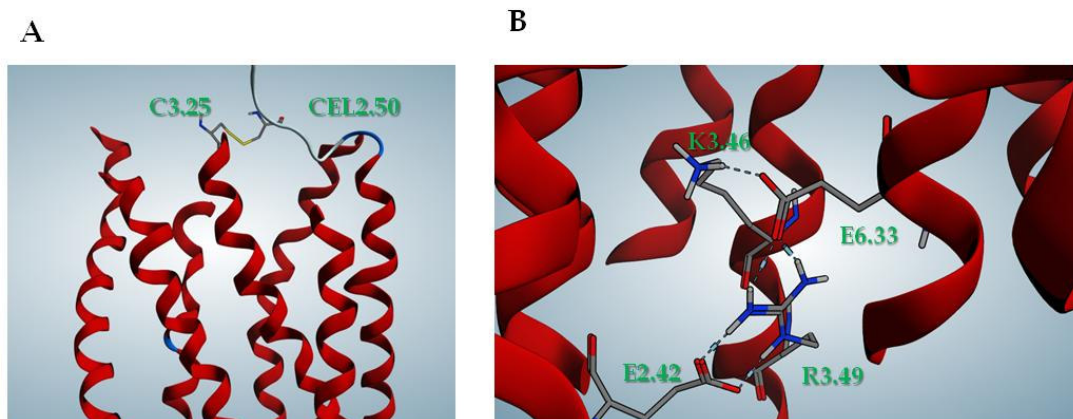
4.2.3 Cholesterol Effects on the Monomeric mGluR2

The mGluR2 receptor belongs to Class C GPCRs (see section 1.1.1), and is expressed in several human brain regions, where it is well known that cholesterol takes part in the formation of lipid rafts.^{311,312} Differently from 5-HT_{2A} receptor, and other Class A GPCRs, mGluR2 does not show the characteristic CCM. Nevertheless, it has been reported that mGluR2 functioning is strongly affected by the membrane composition.¹⁸⁴ As a matter of fact, mGluR2 exists in two different affinity states, for the glutamate, the low- and high-affinity states.¹⁸⁴ The enrichment of the membrane environment with cholesterol molecules shifts the receptor in its high-affinity state for the glutamate.¹⁸⁴ It is worth to mention that glutamate binds the orthosteric binding site, at the VFT level, which is exposed to the solvent in the extracellular environment (see section 1.2.1). On the contrary, the HTM domain is embedded in the membrane environment, where the increased cholesterol concentration modulates the functional state of the receptor.¹⁸⁴ With the aim to shed light on the structural bases underlying the cholesterol effects on the signaling status of the mGluR2 receptor, we set up computational studies on the monomeric form of the mGluR2, with different cholesterol concentrations (0-25%) (see section 3.4.4).

Model Generation and Validation: the 3D structure of the mGluR2 receptor was built by using the structure of the bovine rodhopsin (1GZM) as template and the sequence of the human mGluR2 receptor (Q14416) (see section 3.1.2). With respect to our previous model of the mGluR2 receptor, we used a new alignment (see section 3.1.2). Comparing the new alignment with the old one, the main change refers to the TM5, where we shifted the

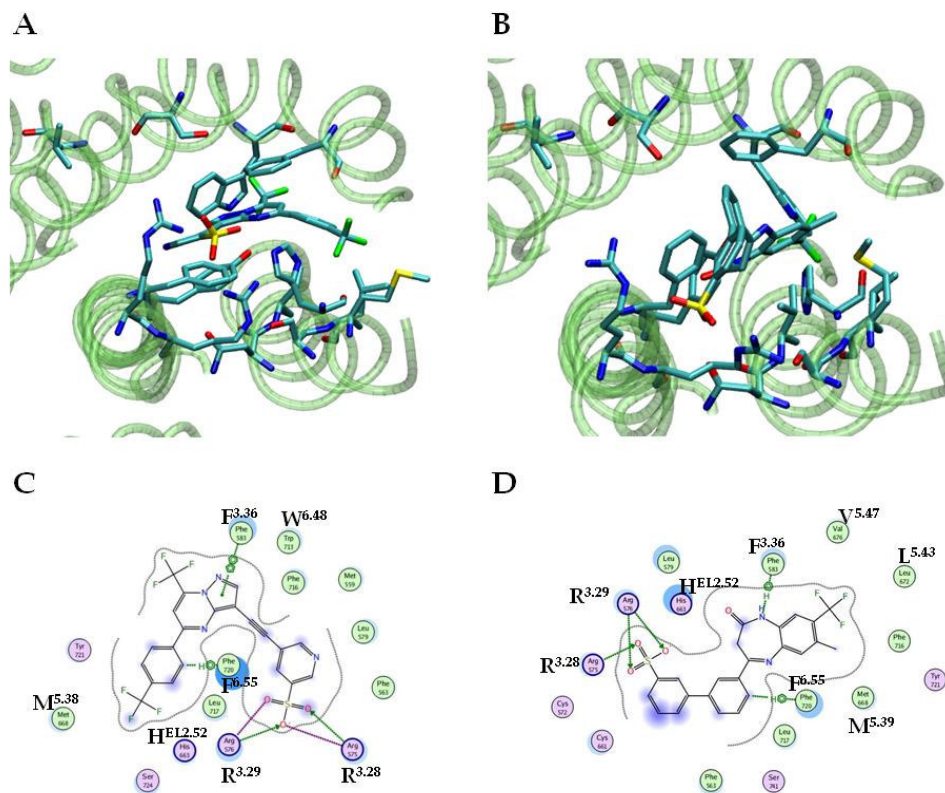
alignment of four residues (see section 3.1.2, Figure 27a,b). Finally, the new alignment was compared with the information available in literature.^{20,213} We evaluated the quality of the model on the basis of structural properties such as the presence of the conserved ionic lock and the presence of the disulphide bond between C^{3.25} and C^{EL2.50}. In Figure 57a and b, we report the selected model of the mGluR2 receptor. It can be appreciated the presence of the disulphide bond (Figure 57a) and a tight network of interaction, in the bottom part of the receptor, involving the E^{2.42}; K^{3.46}; R^{3.49} and E^{6.33} (Figure 57b).

Figure 57. Representation of the structural features of the mGluR2. (A) Disulphide bond between the residues of C^{3.25} and C^{EL2.50}; (B) Ionic interactions at the bottom part (intracellular end of the TM domains) of the mGluR2 receptor.



To evaluate the structural architecture of the obtained mGluR2 model in more detail, two recently reported mGluR2 negative allosteric modulators, RO4988546 and RO5488608 (see section 3.5.2, Figure 31),²¹³ were docked into the model of TM-mGluR2 (Figure 58). Importantly, the ligand-receptor interactions are in good agreement with mutagenesis data Lundström et al.²¹³ (Figure 58) stressing the biological relevance of mGluR2 model.

Figure 58. Representation of the docking poses for the RO4988546 (A) and RO5488608 (B) compounds and the ligand-receptor interaction C and D respectively.

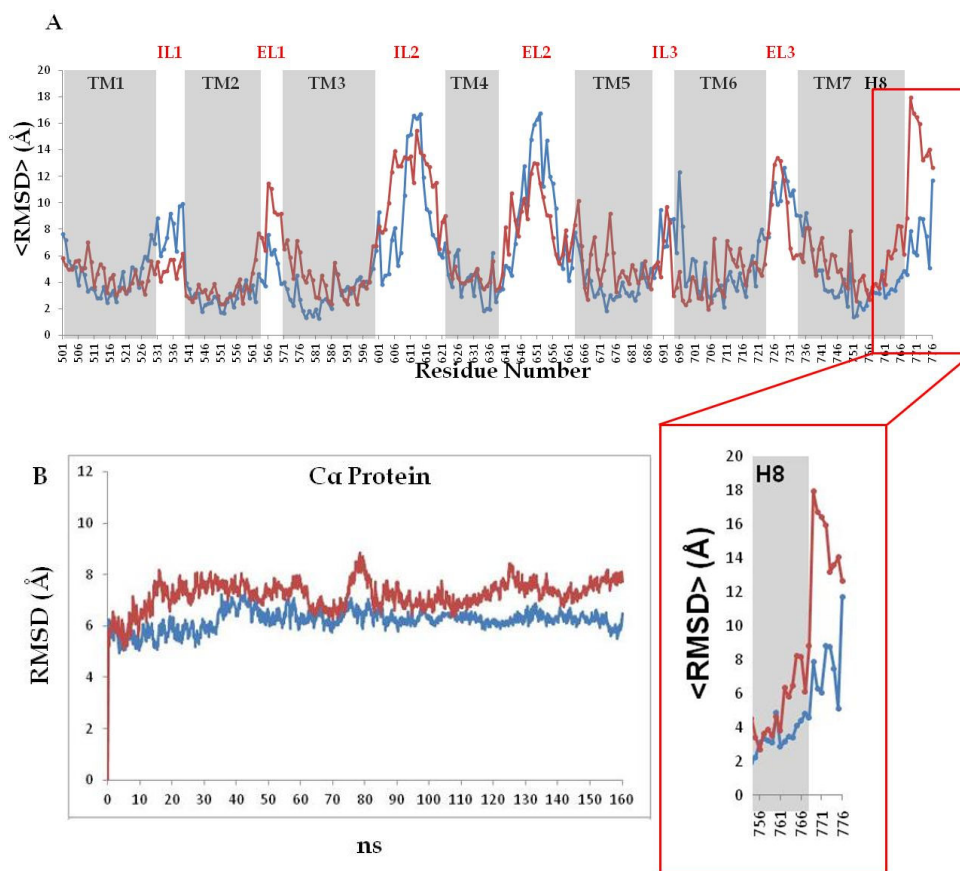


Dynamic receptor properties in cholesterol-depleted and -rich membranes: in order to evaluate the effect of the membrane composition on the receptor conformational flexibility, we carried out a 160ns MD simulation and monitored the mGluR2 receptor stability as the average RMS fluctuation per residue of the C α atoms of the TM-mGluR2 receptor (Figure 59a).

The TM-mGluR2 is simulated in the presence (Figure 59a, blue line) and in the absence (Figure 59a, red line) of cholesterol. As expected, in general, transmembrane regions (Figure 59a, highlighted in grey) are more stable than intra- and extracellular loop regions (IL1-3 and EL1-3). Interestingly, cholesterol affects the stability of the receptor on TM3, 5, 7, and in particular H8 comparing the simulation with (Figure 59a, blue line) and without cholesterol (Figure 59, red line). Intriguing is the observation that H8 shows increased flexible features, when evolving in a cholesterol-depleted membrane environment

undergoing (Figure 59a). In Figure 60b we report the RMSD of the C α atoms of the whole protein in the cholesterol-rich (blue line), and cholesterol-depleted (red line) environment.

Figure 59. (A) Average RMSD per residue of the C α atoms of the mGluR2 receptor. The blue line refers to the simulation with cholesterol (25%), the red one refers to the simulation without cholesterol (0%). The regions highlighted in gray represents the transmembrane regions (TM1-7) and the helix-8 (H8). (B) RMSD of C α atoms of mGluR2 with (blue) and without (brown) cholesterol for a single re-run MD run.



Statistical Analysis: In order to rule out that this effect of the membrane composition on H8 stability is due to a random effect in our simulations, we performed a statistical analysis based on 10 MD runs for both systems (total simulation time 3.2 μs). A visual inspection of the 10 MD runs of the mGluR2 receptor in cholesterol-rich membranes reveals in all cases an integer α -helical H8 structure (100 % folded) (Table 16). Importantly, the 10 MD runs in the cholesterol-depleted membrane show a destabilization of H8 in 60% of the runs, whereas the H8 maintains folded in 40% of the runs (Table 16).

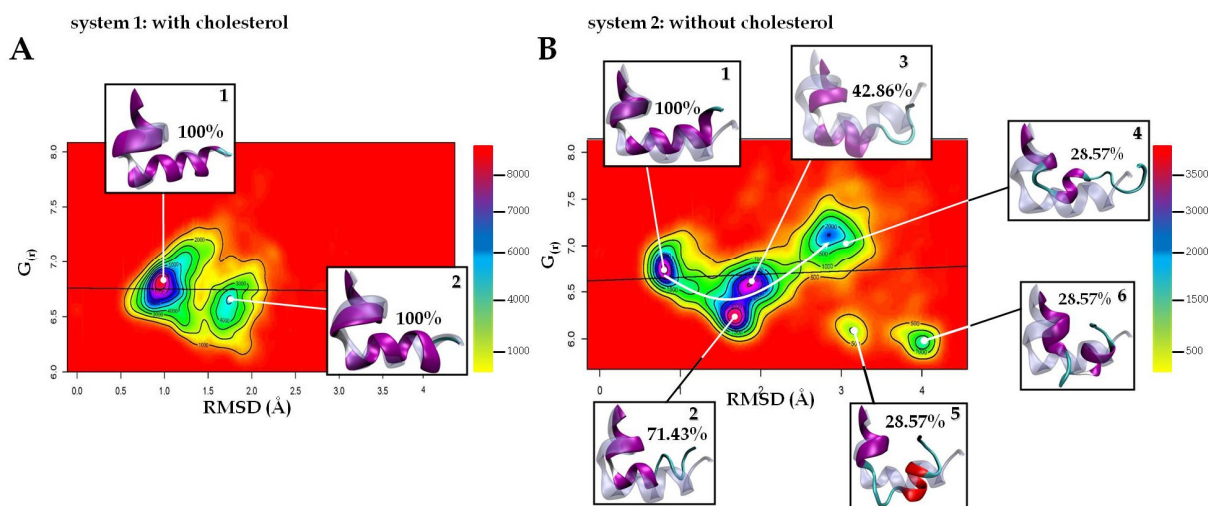
Table 16. Conservation of the H8 structure in the last frame of each simulation expressed as % of H-bonds formed by backbone atoms which stabilize the α -helical structures

Runs	α -helical H8 structure [%]	
	cholesterol-depleted	cholesterol-rich
run 1	30	100
run 2	0	100
run 3	20	100
run 4	100	100
run 5	100	100
run 6	100	100
run 7	100	100
run 8	20	100
run 9	30	100
run 10	40	100
stability	60% unstable	0% unstable

With the aim to shed light on the structural bases of the different conformational H8 behavior in the presence (system 1) and absence (system 2) of cholesterol, we concatenated the 10 MD runs for each system and estimated a probability density function (PDF) using a two dimensional space defined by the values of the radius of gyration ($G_{(r)}$) and the RMSD of the H8 from the starting structure (see section 3.4.7). Such PDF plots allow distinguishing between different probable H8 states which occur in cholesterol-rich (Figure 60a) and cholesterol-depleted (Figure 60b) systems during the accumulated simulation time of 1.6 μ s each. The PDF plots highlight significant differences in conformational states of mGluR2-H8 and their probabilities between the cholesterol-rich (Figure 60a) and cholesterol-depleted (Figure 60b) receptor-membrane system. In the cholesterol-rich system, the mGluR2-H8 is characterized by two states (Figure 60a). State 1 has a higher probability than state 2; both contain an intact 100% folded α -helical structure as indicated by the average structure of each cluster (Figure 60a, insets). In contrast, in the cholesterol-depleted system (Figure 60b), the mGluR2-H8 adopts multiple conformational states with following probability: states 1-3 (high), state 4 (medium), state 5 and 6 (low). Among them, state 1 is 100% folded as reflected by the average structure (Figure 60b, inset) and similar to the one found in state 1 of the cholesterol-rich simulation (Figure 60a, inset). A partial destabilization of the α -helical H8 structure is seen for state 2 and 3 of the

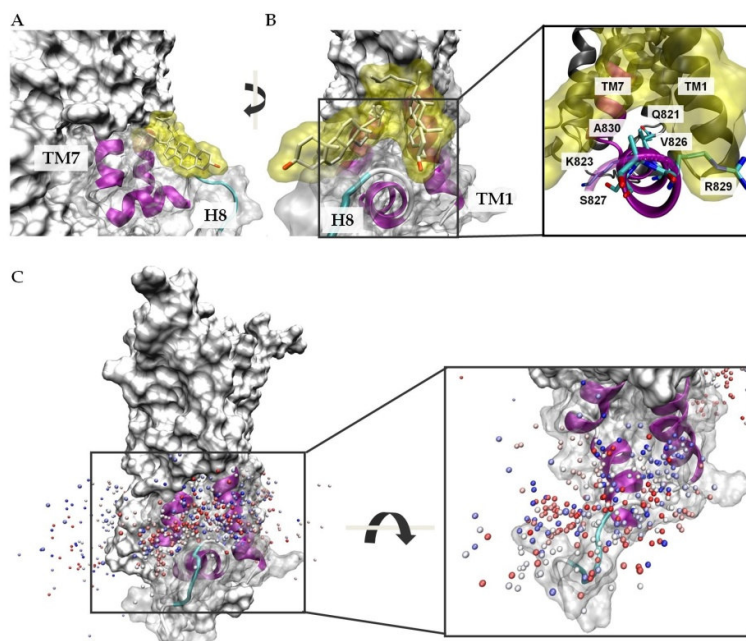
cholesterol-depleted systems (Figure 60b, inset, state 2: 71.43% folded and state 3: 42.86 % folded). Finally, a strongly disturbed H8 containing only 28.57% of the original α -helical starting structure is found in state 4 (Figure 60b, inset). According to the PDF plot of the cholesterol-depleted system (Figure 60b), the highly probable states 2 and 3 could represent transition states between the completely folded state 1 and the strongly disturbed H8 in state 4. The slightly separated and less probable states 5 and 6 show also a strongly destabilized H8 (28.57% folded) and may originate from state 4 (Figure 60b and insets). Rationalizing the results of the conformational analysis of mGluR2-H8 using PDF plots for 3.2 μ s accumulated simulation time, strongly suggests that the presence/absence of cholesterol drives the conformational state of H8: thereby, cholesterol presence stabilizes the canonical amphipatic mGluR2-H8 whereas its absence has a destabilizing effect. This interesting finding raises the question about the underlying mechanism of the cholesterol-mediated stabilization of the α -helical H8 structure.

Figure 60. (A) PDF plot of the MD runs with cholesterol, and without cholesterol (B). The plots show the location of each frame, the corresponding density and the standard kernel density estimate. The contour plots represent the standard kernel density estimate and its bandwidth. The colored bar beside the counter plot described the density estimation for that state (yellow, green, cyan, blue, purple and red color scale). Higher is the number, greater is the probability to find that state. This analysis provides a relative estimation of the probability density function to find some states in our simulation, because of it is based on the finite data sample described by our MD runs. It can be appreciate how (A) and (B) display a different distribution of the frame, and interestingly the probability to find states is quite different depending on the cholesterol presence.



The analysis of the individual 160 ns production runs of the mGluR2 embedded in a cholesterol-rich membrane reveals direct and indirect cholesterol effects as crucial determinant for H8 stabilization. Direct cholesterol contacts is mediated by at least two cholesterol molecules which occupy a pocket formed by TM1, TM7 and H8 (Figure 61) interacting steadily with hydrophobic and polar residues of the α -helical structure of H8 during the 160 ns (Figure 61). These firm cholesterol contacts most likely promote a proper H8 location with respect to the polar head groups of the SDPC molecules, promoting stable interaction among the H8 and the membrane layer (Figure 61), and thus contribute to a stable H8 domain. This finding is consistent with the fact that direct cholesterol-GPCR contacts have been reported to play crucial role in the stabilization of the secondary structure of different GPCRs.^{330,331}

Figure 61. Representation of the direct cholesterol contacts with the mGluR2 receptor. **(A-B)** Different view of the cholesterol cleft described by TM1-TM7-H8 (new cartoon and purple, and transparent and white) the whole receptor is represented by vdW surface (white). Cholesterol is represented by white stick (red stick for the O atoms) and the vdW surface (yellow and transparent), inset: Residues lining up the hydrophobic face of the H8 (Q821, K823, V824, V825, S826, R829, and A830). **(C)** the distribution of the O atoms of the OH group of the cholesterol in a shell of 2 Å around the mGluR2 receptor (TM1-TM7-H8 new cartoon and purple). In this case we concatenated all the MD runs of the simulations with cholesterol and we sampled the O location every 10ns. The O atom are represented by dot colored according to the time scale evolution using a red-white-blue time scale, in which red represent the early location of the O atoms while blue the final one. Highlighted in the black box a membrane view of the O location.



However, the most interesting finding is an indirect cholesterol effect on the mGluR2-H8 stability which is mediated by the thickness of the membrane bilayer. Plotting the average electron density profile (see section 3.4.7) of the membrane bilayer for all runs with and without cholesterol shows a cholesterol-depended increase in membrane thickness (Figure 62a and d). The systems with cholesterol adopt an average peak-to-peak distance (equal to bilayer thickness) of $43.8 \pm 0.42 \text{ \AA}$ (brown line, Figure 62a) in which each EDP peak refers to the PO_4 group of the SDPC membrane ($D_{\text{PO}_4\text{-PO}_4}$). The system without cholesterol (brown line, Figure 63d) shows an approx. 2 \AA smaller $D_{\text{PO}_4\text{-PO}_4}$ distance (41.36 ± 0.92) than the simulation with cholesterol (Figure 62a), which are in good agreement with experimental and computational values available in literature.³²¹⁻³²⁵ The physical correctness of the observed cholesterol-mediated increase in membrane thickness is also supported by measuring the peak-to-peak distance for carbonyl group of the lipid tails: with cholesterol: $35.00 \pm 0.63 \text{ \AA}$, without cholesterol: $30.00 \pm 1.15 \text{ \AA}$ (Figure 63) which are once more in good agreement with experimental data³²¹⁻³²⁵.

Important insight into the role of the bilayer thickness in the definition of the H8 conformational state is obtained by plotting the average location of the hydrophobic face (C_α atoms of the following residues Q821, K822, V824, V825, S826, R828, and A829, Figure 61) of the amphipatic H8 (H8-EDP $_{\text{C}_\alpha}$) as EDP of the C_α atoms (blue line, Figure 62a,d) over the average membrane thickness as EDP of the PO_4 group ($\text{PO}_4\text{-EDP}$) of the SDPC membrane (brown line, Figure 62a,d). Thereby, the H8-EDP $_{\text{C}_\alpha}$ and the $\text{PO}_4\text{-EDP}$ are averaged over $1.6 \mu\text{s}$ for each system (see section 3.4.7). An interesting finding is that in the simulation with cholesterol the peak of the hydrophobic H8 face is located 1.60 \AA left from the peak of the PO_4 groups (blue line, Figure 62a) whereas in the simulation without cholesterol the hydrophobic face of H8 (blue line, Figure 62d) is shifted to 1.73 \AA right from the PO_4 groups (blue line, Figure 62d). Importantly, structural visualization (Figure 62c and F) of this observed cholesterol-dependent H8 shift with a total difference of 3.33 \AA gives insight into a possible mechanism how cholesterol indirectly drives H8 stabilization via membrane thickness. In the cholesterol rich system, the H8 is nicely embedded in the membrane, exposing the hydrophobic H8 face to the hydrophobic acyl chains and

cholesterol molecules while the polar H8 face is contacting the polar PO₄ groups (Figure 62c), and is partially solvent-exposed. In contrast, in the cholesterol-depleted system, H8 drops out of the membrane bilayer into a completely polar environment due to the smaller membrane thickness (Figure 62f). As a result, H8 loses important hydrophobic contacts of its hydrophobic face with the membrane acyl chain which leads to a destabilized and more flexible H8 with various conformational states as found in the cluster 2, 3, 4 and 5 (Figure 60b) for the cholesterol-depleted system.

Figure 62. (A) Average EDP of the PO4 groups (brown line and dots) and H8 (blue line and dots) for the simulation with cholesterol, the red bars refer to the standard deviation of the $\text{el}/\text{\AA}^3$ values of the PO4 for each slab, while the black bars refer to the standard deviation of the $\text{el}/\text{\AA}^3$ of the H8 values for each slab. (B) Average location of the peaks for the PO4 (brown) and H8 (blue) location, respectively. The black bars refer to the standard deviation of the location of the peaks. (C) Location of H8 in cholesterol-rich system relative to the PO4 groups corresponding to the main state 1 (see Figure 61a) showing each 10th frame of a total 981 frames. (D) Average EDP of the PO4 groups (brown line and dots) and H8 (blue line and dots) for the simulation without cholesterol, the red bars refer to the standard deviation of the $\text{el}/\text{\AA}^3$ values of the PO4 for each slab, while the black bars refer to the uncertainty (standard deviation) of the $\text{el}/\text{\AA}^3$ of the H8 values for each slab. (E) Average location of the peaks for the PO4 (brown) and H8 (blue) location, respectively. The black bars refer to the standard deviation of the location of the peaks. (F) Location of H8 in cholesterol-depleted system relative to the PO4 groups corresponding to state 4 (see Figure 61) showing each frame of a total 51 frames. The structural representations (C) and (D) are generated using VMD 1.8.7, drawing mode: NewCartoon and coloring method: Secondary Structure.

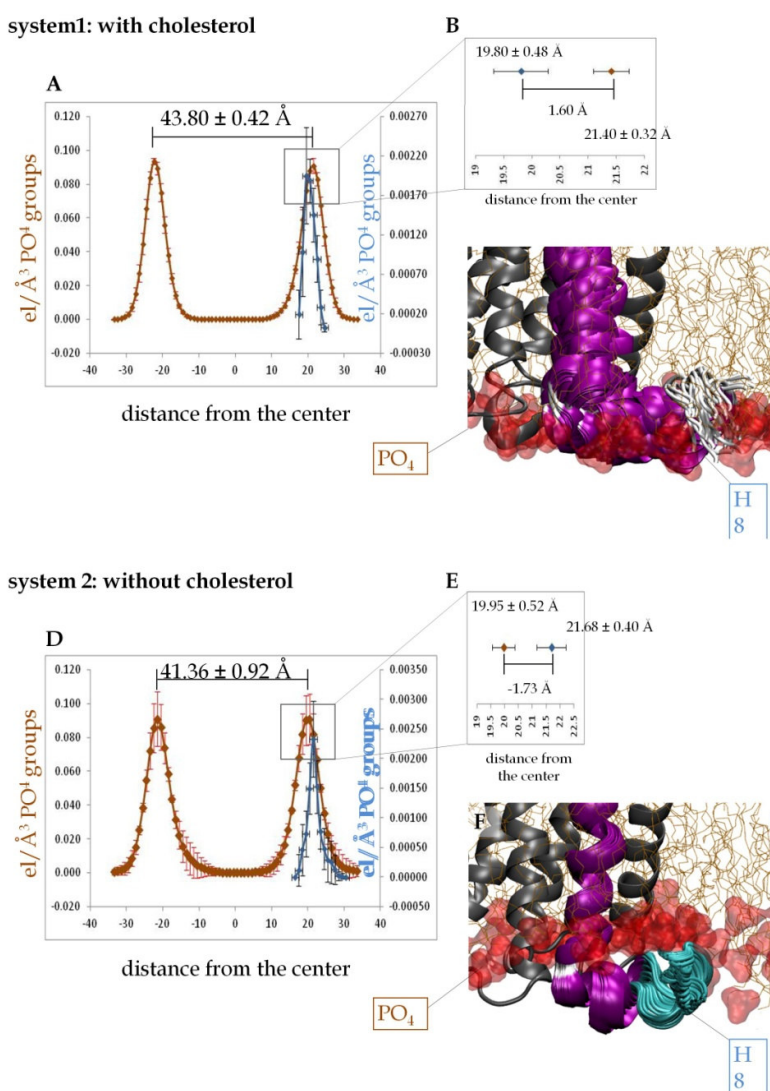
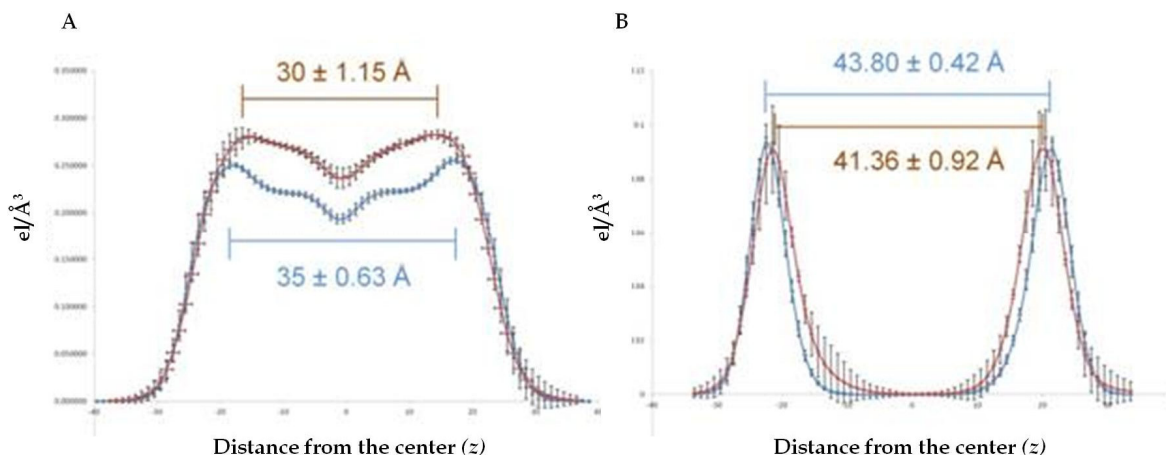


Figure 63. Average EDP of the whole bilayer (A) and EDP of the PO₄ groups (B). In blue the average EDP for the simulation with cholesterol, while the simulation without cholesterol is the brown one.



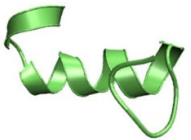


To sum up, on one hand we find that a H8-EDP_{C α} location of 1.6 Å above the PO₄ peak of the intracellular layer in a hydrophobic environment (Figure 62a-c) is correlated with a stable H8 domain. On the other hand, a H8-EDP_{C α} location at the same level or below the PO₄ peak of the intracellular layer in a polar environment (Figure 62d-f) results in a destabilization of H8. From this we can conclude that a correct orientation of the mGluR2-H8 hydrophobic face in the membrane environment is crucial for the definition of the H8 conformational state. These findings suggest for the first time the existence of different membrane-sensitive conformational states for the mGluR2-H8 which could serve as a sort of sensor for cholesterol concentration. Accordingly, mGluR2-H8 could behave as a membrane environment modulator as reported for the CB₁ receptor³³² or could play a crucial role in the mGluR2 membrane trafficking, and signaling.

To further assess the existence of α -helical H8 structure in the mGluR2, we carried out a structural prediction analysis (Table 17). The analysis revealed three protein structures (PDB ID 3EFO.pdb, 1IC8.pdb, 2I5D.pdb, Table 17) with homologue sequence fragments adopting a α -helical conformation. This finding corroborates once more that the mGluR2 could possess an amphipatic H8 with a α -helical conformation which however depends on the membrane environment as indicated by our extended MD simulation runs. Such an environment-dependent H8 conformation has been also suggested for the CXCR4 receptor

by Chien *et al.*¹⁵ Their recently solved X-ray crystal structure for this class A receptor lacks surprisingly an earlier assumed α -helical H8 structure, which could be a consequence of the crystallization conditions.¹⁵

Table 17. Prediction of the secondary structure of the H8 for bovine rhodopsin and the chemokine CXCR4 receptor (protocol validation) and test set for the mGluR2-H8. Numbering from the full length sequences of each protein. Highlighted in red the region corresponding to α -helix structures.

Bovine Rhodopsin receptor							
	Related Protein			Related Sequences		Secondary Structure	Score (bits)
A  Bovine Rhodopsin 307 IMMNKQFRNCMVTTLCCGK 325	3QGB.pdb	Rhod.	Bov.	307 IMMNKQFRN----CMVTTLCC 323		α -helix	25.7
		3QGB		330 IMMFHQFGNYVVQCML-TICC 349			
	3K5Q.pdb	Rhod.	Bov.	307 IMMNKQFRN----CMVTTLCC 323		α -helix	25.7
		3K5Q		329 IMMFHQFGNYVVQCML-TICC 348			
	1LKX.pdb	Rhod.	Bov.	312 QFRNCM---VTTL 321		α -helix	24.0
		1LKX		565 QFRNAMNALITTL 577			
CXCR4 receptor							
	Related Protein			Related Sequences		Secondary Structure	Score (bits)
B  CXCR4 303 AFLGAKFKTSAQHAlTSV 320	1SJ8.pdb	CXCR4		311 TSAQHALT 318		α -helix	23.5
		1SJ8		8 TSAQQALT 15			
	2JRC.pdb	CXCR4		305 LGAKFK 310		random coil	21
		2JRC		36 LGAKFK 41			
	2BEK.pdb	CXCR4		310 KTSAQHAlTS 319		α -helix	21
		2BEK		220 KTIAQHAlTS 229			
mGluR2 receptor							
	Related Protein			Related Sequences		Secondary Structure	Score
C  mGluR2 receptor 817 ILFQPQKNVSHR 829	3EFO.pdb	mGluR2		817 ILFQPQKNV 825		Partial α -helix	28.6
		3EFO		347 ILFQPQTNV 355			
	2I5D.pdb	mGluR2		819 FQP-----QKNVSHR 829		α -helix	23.1
		2I5D		158 FQPDGYEQTYAEMPKA EKNVSHR 181			
	1IC8.pdb	mGluR2		817 ILFQP---QKN 824		α -helix	20.6
		1IC8		129 ILFQAYERQKN 139			

Chapter 5

Conclusions

5.1 General Overview

In Chapter 1 I introduced some concepts highlighting the extraordinary pharmacological and dynamical versatility of GPCRs. These membrane-bound proteins revealed a complex pharmacological behavior, supported by extraordinary flexible structure properties. For many years this dynamic flexibility was elusive, representing one of the greatest challenges for medicinal and computational chemists. Now, in the light of experimental evidences, it is becoming apparent that computational approaches must be integral to any effort aimed at understanding GPCR functioning. Taking into account the breakthroughs made in the computational chemistry field, it is possible, nowadays, to address at an atomic level more complicated computational experiments. As a matter of fact, it is possible to set up more complex MD experiments (i.e. dimer simulations in explicit membrane environment), with simulation time longer than previously reported works. Nonetheless, before to set up complex MD experiments it is necessary to assess the sensitivity of such methods to different experimental simulation conditions, and which is the real impact of the conditions used on the results carried out. For instance, one can ask whether explicit MD experiments can better address issues related to GPCR pharmacology, such as dimerization aspects, cholesterol effects, as well as ion species effects.

With our studies we clearly show that the MD experimental conditions strongly impact the MD results carried out. For instance, the presence of a dimerization interface does affect the outcome of the MD simulation on the topology of the individual protomers (see

section 4.1.1-4.1.3), and this must be taken into account when using these models for in silico screening or docking purposes (see section 4.1.4). Moreover, it is worth to mention that most of the so far reported MD simulations of GPCRs in an explicit membrane environment did not take cholesterol as membrane component into account (see section 4.2.1 and 4.2.3). Finally, also the choice of an appropriate ions species has an impact on the results of MD experiments, as clearly showed by the different behavior of the K^+ , and Na^+ species for the 5-HT_{2A} receptor (see section 4.2.2). As we show by our study that cholesterol, as well as ions, and GPCR aggregation phenomenon play crucial roles in GPCR flexibility and conformational behavior, the methodologies investigated may be applicable also to other GPCRs families for which effects of the aforementioned aspects are reported, unraveling tools of general interest in biomedical and pharmaceutical research.

5.2 Dimer Interface Effects

A growing body of evidence indicates that GPCR may aggregate into homo- and heteromers or oligomers. It was recently reported that two unrelated GPCRs, namely mGluR2 (belonging to class C GPCR) and 5HT_{2A} (belonging to class A GPCR), can form functional dimers and that the formation of the heterocomplex influences the hallucinogen signaling mediated by classes of serotonergic agonists.¹⁴⁸⁻¹⁵⁰ We constructed and simulated by MD in an explicit DMPC bilayer a model of the heterocomplex between 5HT_{2A} and the transmembrane region of mGluR2, as well as the homomeric 5-HT_{2A}-5-HT_{2A} complex. For comparison purposes, an identical MD simulation was carried out on the 5HT_{2A} monomer, embedded in the same DMPC bilayer. According to experimental evidence, the dimer complexes were constructed by coupling the two protomers through a TM4/TM5 interface (see section 1.3). The interface were initially assembled by rigid backbone docking, by using Rosetta++, starting from models of the protomers generated by homology modeling. As a kind of prevalidation, we have used the same protocol to reproduce the theoretical model of the rhodopsin homomer, and it turned out that the scoring function was unable to correctly sort the interface disposition. We thus decided to visually sort the Rosetta++ output, and the selected interfaces were the ones visually

characterized as the most similar to the rhodopsin homomer (see section 3.2.1). The interfaces significantly changed during the MD simulation (see section 4.1.1, and Figure 33; and section 4.1.5, and Figure 43). This brings support to the notion that rigid backbone docking is likely to yield a number of quasi-isoenergetic dispositions of the protein-protein interfaces, which cannot be sorted out by scoring functions. This should be carefully taken into account when performing simulations of homo- or heteromers of GPCR, since the choice of the initial structure may introduce a strong bias in the final results. In our present case, the choice was driven by the experimental evidence that the interface is made up of TM4/TM5, but among the several possible TM4/TM5 arrangements, the starting complex was selected based on visual inspection and coherence with the structure of a theoretical model of the rhodopsin homodimer,^{151,243,244} and not based on quantitative scoring. The energy minimization and the subsequent MD simulation demonstrated that the chosen interface is stable under the simulation conditions, but it cannot be ruled out that alternative disposition could have led to equally stable results. The dimer complexes were highly stable during the simulation, and both protomers maintained all the secondary structures elements. Nevertheless, when the 5HT_{2A} protomer was simulated as a monomer under the same conditions of the dimers, some perceptible differences were noticed (see section 4.1.1-4.1.5). While these differences can by no means be used, in our opinion, to speculate about the functional role of the dimers, they clearly indicate that the presence of a dimerization interface does affect the outcome of the MD simulation on the topology of the individual protomers, and this has to be taken into account when using these models for in silico screening or docking purposes (see section 4.1.4). This is particularly relevant in view of the observation that the mGluR2 component of the heteromer affects the hallucinogen signaling operated by serotonergic agonists (see section 1.8.2). It can be speculated that the dimerization interface allosterically induces perceptible modifications on the shape of the 5HT_{2A} binding pocket (see section 4.1.3 and Figure 38), thus resulting in a modified affinity. From MD simulations studies we were able to extract a set of receptor conformations by using cluster analysis (see section 4.1.3 Figure 37). A clear result that turns out is that the shape of the binding pocket is tightly linked to the presence and to the type of a dimerization interface (see section 4.1.3, and Figure 38; and section 4.1.5). In particular, the interface seems to significantly impact the flexibility of the CWxP micro-

domain-associated region on TM6, which is in turn responsible for shaping up a hydrophobic pocket conserved among members of class A GPCRs (Figure 35).^{101,124,125,306} Our data suggests that this hydrophobic pocket is affected by the presence of the dimerization interface and by the nature of the dimer partner. These changes in topology reflect a different ability of the heteromer, homomer, and monomer to rank a set of 5-HT_{2A} ligands in docking studies (see section 4.1.4). In particular, heteromerization seems to allosterically induce a modification in the binding pocket of 5-HT_{2A} which promote binding of 5-HT agonist and its ability to recognize HCs improves along the simulation, while homomerization anisotropically affects the two identical 5-HT_{2A} protomers constituting the dimer. Moreover, new X-ray crystal structures of the human β 2-adrenergic receptors were disclosed, showing that an agonist produces at least three main effects: (i) conformational changes of S^{5.43} and S^{5.46}; (ii) conformational changes in TM5 and (iii) contraction of the binding pocket (see section 1.3). Furthermore, the comparison of the new and the previously published X-ray crystal structures of members of the aminergic GPCRs subfamily (see section 1.2.1, and Figure 5; and sections 4.1.3 and 4.1.4 and Figures 38 and 39) shows that the binding pocket of agonists, antagonists, partial inverse agonists and inverse agonists is highly overlapped, with appreciable differences related to the interaction with the residues of S^{5.43} and S^{5.46}. With our studies we detect conformational differences only at the S^{5.43} and S^{5.46} level, according to the experimental evidences showing that the presence of mGluR2/5-HT_{2A} as dimer partner alters the ability of the 5-HT_{2A} receptor to interact with 5-HT_{2A} ligands. Nonetheless, relevant conformational changes at TM5 level, and the contraction of the 5-HT_{2A} binding pocket are not detected. This is likely due to the fact that the simulation time of our studies is too short to detect conformational changes at the helix level, and to the fact that our simulations were carried out in the apo form of the receptor. Our studies clearly indicate that some flexible regions of the 5-HT_{2A} are affected by the presence of the dimerization interface and this impact the results of the docking studies.

5.3 Cholesterol Effects

5.3.1 Cholesterol Effects on 5-HT_{2A} Flexibility

The disclosure of the human β_2 adrenergic receptors^{12,93} highlighted the importance of the cholesterol interaction with GPCRs, confirming the evidences indicating that membrane composition (i.e. cholesterol concentration) is able to affect the functions of some GPCRs by direct and indirect effects.³³³⁻³³⁹ Cholesterol plays a crucial role in the definition of the GPCRs functioning, such as protein compartmentalization into membrane environment,^{320,336-339} in the GPCRs signaling pathway,^{333,334} in the stabilization of different GPCRs conformation states,³⁴⁰ and it has been reported that cholesterol facilitates the crystallization of GPCRs receptors.^{12,93} To understand the molecular bases of the interaction occurring among cholesterol molecules and several Class A GPCRs represents a new challenge for medicinal and computational chemists. The serotonergic receptor 5-HT_{2A} belongs to the strict-CCM class³ and it is involved in several physiological and pathological processes (i.e. platelet aggregation, CNS disease etc...) and represents one of the most interesting targets for the treatment of psychiatric disorders.³¹⁰ Thus, we carried out computational studies on the monomeric form of the 5-HT_{2A} receptor, with different cholesterol concentrations (0-25%). Our results clearly indicate direct interaction between cholesterol molecules and the 5-HT_{2A} receptor. In particular, our results corroborate cholesterol binding at the CCM motif of the 5-HT_{2A} receptor (see section 4.2.1). Direct interactions between cholesterol molecules and CCM residues result in a stabilized TM4 domain, while the same domain shows higher flexibility in a cholesterol-free membrane (see Figure 47). The direct cholesterol-5-HT_{2A} interactions impact the behavior of the whole receptor (Figure 47). The cholesterol interaction with the residues lining up the CCM are transmitted to the rest of the receptor, by a hinge region (Figure 48b) constituted by the W^{4.50}, Y^{2.41} and the S^{2.45}, H^{3.42} residues, as it is shown by the different pattern of hydrogen bonding network among the TM2-4 domains (Table 14). In details, the occurrence of the hydrogen bonds between the residues belonging to the same TM domains (S^{2.45}, Y^{2.41} on TM2 Table 14) is increased, while interhelical hydrogen bonds are decreased (Table 14). These data indicate a completely different behavior of TM2-4 of the 5-HT_{2A} receptor in the presence of cholesterol molecules.

Moreover, also indirect cholesterol effects on the 5HT_{2A} receptor were detected, which are mediated through a different membrane structural organization and membrane thickness (Figure 51). Obviously, membrane thickness is important for an adequate match of the membrane-protein interface or can also causes a hydrophobic mismatch (Figure 52) of the membrane-protein interface, thus impacting GPCR conformation.³⁴¹

Finally, our results support the ion-sensitive nature of the 5-HT_{2A} receptor. As a matter of fact, during the simulations one sodium ions enter the serotonergic binding pocket. In both simulations (with/without cholesterol) the sodium ion enters from the extracellular side and binds the conserved aspartate residue on TM2 (D^{2.50}) (see section 4.2.2, and Figure 53). It is worth to mention that no biological data about the effects of the sodium ions on the 5-HT_{2A} receptors functionality have been reported, to date. However, in literature, a huge number of papers discussing the role of the conserved D^{2.50} residue, and the effects of ions on the GPCRs functions have been reported.^{94,95,97-100,327} Comparing the sequence of the human 5-HT_{2A} receptor, with respect to the D₂ receptor, which is known to bind sodium at D^{2.50}, we found a high sequence identity among the residues 4.5 Å around the D^{2.50} residues (Figure 54), corroborating a putative sodium binding site D^{2.50} in the 5HT_{2A} receptor. we also compared this Na⁺-related results with our previous simulations where we simulated the 5-HT_{2A} receptor with an ionic strength of 0.15M KCl in DMPC phospholipids bilayer. Interestingly, we found that the K⁺ ions are not able to enter deeply into the 5-HT_{2A} receptor. Although, two K⁺ ions enter from the extracellular side of the serotonergic receptor, interacting with the orthosteric D^{3.32} site, they never reach the putative allosteric D^{2.50} binding site as we observed for Na⁺ ions (Figure 55, and 56). The different behavior of the two ion species leads to a different conformational properties of relevant residues, such as the D^{2.50}, N^{7.49} and L^{2.46} residues (Figure 56). It has been reported that these residues play a crucial role in the active-inactive state transition and in the stabilization of the active state for different Class A GPCRs.^{100,328-33} Our results suggest (i) a direct interaction between cholesterol molecules and the 5-HT_{2A} receptors, the cholesterol-protein interactions alter the conformational behavior of the 5-HT_{2A} suggesting a direct role of the cholesterol in the modulation of the 5-HT_{2A} functionality; (ii) 5-HT_{2A} could be an ion sensitive receptor, in details Na⁺ ions could allosterically alter the ligand

binding or the coupling with G protein. Our results suggest several experiments to verify the structural hypothesis of the cholesterol and ion effects on the 5-HT_{2A} receptor.

5.3.2 Cholesterol Effects on the mGluR2 Flexibility

The mGluR2 receptor belongs to Class C GPCRs (see section 1.1.1), and is expressed in several human brain regions, where it is well known that cholesterol takes part in the formation of lipid rafts.^{311,312} Differently from 5-HT_{2A} receptor, and other Class A GPCRs, mGluR2 does not show the characteristic CCM. Nevertheless, it has been reported that mGluR2 functioning is strongly affected by the membrane composition.¹⁸⁴ With the aim to shed light on the structural bases underlying the cholesterol effects on the signaling status of the mGluR2 receptor, we set up computational studies on the monomeric form of the mGluR2, with different cholesterol concentrations (0-25%) (see section 3.4.4). To evaluate the structural architecture of the obtained mGluR2 model in more detail, two recently reported mGluR2 negative allosteric modulators, RO4988546 and RO5488608 (see section 3.5.2, Figure 31),²¹³ were docked into the model of TM-mGluR2 (Figure 58). Importantly, the ligand-receptor interactions are in good agreement with mutagenesis data reported by *Lundström et al.*²¹³ (Figure 58), stressing the biological relevance of mGluR2 model.

As well as in the case of the 5-HT_{2A} receptor model, also the conformational behavior of the mGluR2 receptor model is strongly affected by the membrane composition (Figure 59). The most intriguing result is represented by the fact that mGluR2 shows a stable H8 only under certain condition, and that cholesterol influences H8 stability through direct, and indirect effects.

The obtained results strongly support the existence of a α -helical structured H8 in mGluR2 but only under certain conditions. In this respect, we found that the membrane composition impacts the conformational behavior of the H8 in our simulations (Figure 60). This study reveals that cholesterol, an important component in cell membranes, drives H8 stabilization by direct and indirect effects (Figure 60-62). In the absence of membrane cholesterol, H8 loses its defined α -helical structure adopting an ensemble of different destabilized conformational states. Importantly, these results indicate that mGluR2-H8 can adopt membrane-sensitive conformational states, thus behaving as a “sensor of cholesterol

concentration". In summary we propose the existence of an amphipatic H8 with a α -helical conformation in class C mGluR2, a structural feature so far observed only in class A GPCRs. Importantly, extended molecular dynamics simulations reveal that α -helical H8 structure is not a general structural feature but depends on the environment. In particular, cholesterol influences the H8 conformational state through direct and indirect effects. The former are mediated by an unprecedented cholesterol binding cleft (Figure 61), while the latter take place by altering the membrane thickness (Figure 62). Interestingly, the observed link between membrane cholesterol and H8 stability suggests that, in mGluR2, H8 behaves as a sensor of cholesterol concentration, adopting different membrane-sensitive conformational states (Figure 60, and 62). This would conciliate with the evidences that cholesterol is a factor released by glia to modulate membrane properties,³⁴²⁻³⁴⁶ and that mGluR2 expression, functioning, and trafficking is tightly linked to the membrane composition.^{184,185,347} Importantly, taking into account that the C-terminus of mGluRs is likely involved in direct G-protein coupling,^{20,59,348} membrane-sensitive conformational H8 states could be part of a dynamic mechanism to regulate mGluR2 signaling transduction, as already reported for the PAR1,³⁴⁹ and the rhodopsin receptors.³⁵⁰ This intriguing result also conciliates with the GPCR ensemble theory.¹³⁶ This theory postulates that membrane-bound receptors adopt different micro-conformational states at the cytoplasmic side, which can activate different downstream signaling pathways, such as G protein-dependent pathway³⁴⁹ or G protein-independent pathway.³⁵⁰

Chapter 6

Future Perspectives/Outlook

6.1 Future Computational Work

As evidences on the role of hetero- or homomerization in GPCR functioning increase, the need of computational procedures for simulating the effect of this process in ligand recognition will become more urgent. Long scale molecular dynamics simulations are likely to become a privileged tool to analyze the effect of the dimerization process, and the ability to extract information from these simulations will become central to the use of such approaches in an integrated drug design effort in the GPCR field.

The data collected along this project will allow us to set up further computational work, such as the simulation of the heteromer complex 5-HT_{2A}-mGluR2, and the homomer complex 5-HT_{2A}-5-HT_{2A}, in an explicit membrane environment taking into account cholesterol concentration issue.

Moreover, recently it has been reported that the 5-HT_{2A} receptor can be involved in the formation of other relevant heteromers, such as the 5-HT_{2A}-D₂ heteromer.¹⁷⁰⁻¹⁷³ Thus, it would be of great interest to compare the behaviour of the 5-HT_{2A} receptor in different heteromer complex.

Finally, so as to understand how relevant are the differences observed in the simulation with different cholesterol concentration, it would be interesting to perform docking studies on selected conformation from the trajectories of the simulation with and without cholesterol of the mGluR2 and 5-HT_{2A} receptors. Moreover, to simulate the active form of

each receptor considered, so as to establish which is the effect of the cholesterol concentration on the inactive and active states of those receptors.

6.2 Biological assays

The computational results suggest that cholesterol has an impact on the monomeric 5HT_{2A} receptor structure/function, due to direct and indirect cholesterol effects. In order to confirm our hypothesis we propose to test:

- A) Effect of cholesterol on the monomeric 5HT_{2A} receptor
- B) Effect of cholesterol on 5HT_{2A}-5HT_{2A} dimer formation
- C) Identification of residues forming the cholesterol binding site

As reference for the planned experimental studies can be used the methodology of already published studies, as recently performed on 5HT_{1A}, rhodopsin and the β_1 and β_2 receptors.^{93,183,351-354}

These experimental assays will be performed in the context of a collaboration between the CADD group at the GRIB center, and the Universidad de Santiago de Compostela. In particular we are going to test:

1. the 5-HT_{2A} functioning using different cholesterol concentrations, as reported for the study of *Hanson et al.* for the human β_2 -adrenergic receptor;⁹³
2. determination of the competition binding curves for different 5HT_{2A} ligand classes in the presence of different cholesterol membrane concentrations;
3. identification of the residues forming the 5-HT_{2A} CCM by mutagenesis studies of the residues involved in cholesterol interaction, along our MD simulations.

References

- (1) Congreve, M.; Langmead, C. J.; Mason, J. S.; Marshall, F. H. Progress in Structure Based Drug Design for G Protein-Coupled Receptors. *Journal of Medicinal Chemistry* **2011**, *54*, 4283-4311.
- (2) Lagerstrom, M. C.; Schiöth, H. B. Structural diversity of G protein-coupled receptors and significance for drug discovery. *Nat Rev Drug Discov* **2008**, *7*, 339-357.
- (3) IUPHAR DATABASE | G PROTEIN-COUPLED RECEPTOR LIST <http://www.iuphar-db.org/DATABASE/GPCRListForward> (accessed 19 May, 2011).
- (4) Rosenbaum, D. M.; Rasmussen, S. G. F.; Kobilka, B. K. The structure and function of G-protein-coupled receptors. *Nature* **2009**, *459*, 356-363.
- (5) Bockaert, J.; Pin, J. P. Molecular tinkering of G protein-coupled receptors: an evolutionary success. *EMBO J* **1999**, *18*, 1723-1729.
- (6) Pin, J.-P.; Galvez, T.; Prézeau, L. Evolution, structure, and activation mechanism of family 3/C G-protein-coupled receptors. *Pharmacol. Ther* **2003**, *98*, 325-354.
- (7) Magalhaes, A. C.; Dunn, H.; Ferguson, S. S. G. Regulation of G-protein Coupled receptor activity, Trafficking and Localization by GPCR-interacting proteins. *Br J Pharmacol* **2011**.
- (8) GLIDA: GPCR-Ligand Database <http://pharminfo.pharm.kyoto-u.ac.jp/services/glida/> (accessed 01 Sep 2011).
- (9) Fredriksson, R.; Lagerström, M. C.; Lundin, L.-G.; Schiöth, H. B. The G-protein-coupled receptors in the human genome form five main families. Phylogenetic analysis, paralogon groups, and fingerprints. *Mol. Pharmacol* **2003**, *63*, 1256-1272.
- (10) Lundstrom, K. Latest development in drug discovery on G protein-coupled receptors. *Curr. Protein Pept. Sci* **2006**, *7*, 465-470.
- (11) Russ, A. P.; Lampel, S. The druggable genome: an update. *Drug Discovery Today* **2005**, *10*, 1607-1610.
- (12) Cherezov, V.; Rosenbaum, D. M.; Hanson, M. A.; Rasmussen, S. G. F.; Thian, F. S.; Kobilka, T. S.; Choi, H.-J.; Kuhn, P.; Weis, W. I.; Kobilka, B. K.; Stevens, R. C. High-Resolution Crystal Structure of an Engineered Human β 2-Adrenergic G Protein-Coupled Receptor. *Science*

2007, 318, 1258 -1265.

(13) Chien, E. Y. T.; Liu, W.; Zhao, Q.; Katritch, V.; Won Han, G.; Hanson, M. A.; Shi, L.; Newman, A. H.; Javitch, J. A.; Cherezov, V.; Stevens, R. C. Structure of the Human Dopamine D3 Receptor in Complex with a D2/D3 Selective Antagonist. *Science* **2010**, 330, 1091 -1095.

(14) Shimamura, T.; Shiroishi, M.; Weyand, S.; Tsujimoto, H.; Winter, G.; Katritch, V.; Abagyan, R.; Cherezov, V.; Liu, W.; Han, G. W.; Kobayashi, T.; Stevens, R. C.; Iwata, S. Structure of the human histamine H1 receptor complex with doxepin. *Nature* **2011**, 475, 65-70.

(15) Wu, B.; Chien, E. Y. T.; Mol, C. D.; Fenalti, G.; Liu, W.; Katritch, V.; Abagyan, R.; Brooun, A.; Wells, P.; Bi, F. C.; Hamel, D. J.; Kuhn, P.; Handel, T. M.; Cherezov, V.; Stevens, R. C. Structures of the CXCR4 Chemokine GPCR with Small-Molecule and Cyclic Peptide Antagonists. *Science* **2010**, 330, 1066 -1071.

(16) Jaakola, V.-P.; Griffith, M. T.; Hanson, M. A.; Cherezov, V.; Chien, E. Y. T.; Lane, J. R.; IJzerman, A. P.; Stevens, R. C. The 2.6 Angstrom Crystal Structure of a Human A2A Adenosine Receptor Bound to an Antagonist. *Science* **2008**, 322, 1211-1217.

(17) Rasmussen, S. G. F.; DeVree, B. T.; Zou, Y.; Kruse, A. C.; Chung, K. Y.; Kobilka, T. S.; Thian, F. S.; Chae, P. S.; Pardon, E.; Calinski, D.; Mathiesen, J. M.; Shah, S. T. A.; Lyons, J. A.; Caffrey, M.; Gellman, S. H.; Steyaert, J.; Skiniotis, G.; Weis, W. I.; Sunahara, R. K.; Kobilka, B. K. Crystal structure of the [bgr]2 adrenergic receptor-Gs protein complex. *Nature* **2011**, 477, 549-555.

(18) Palczewski, K.; Kumasaka, T.; Hori, T.; Behnke, C. A.; Motoshima, H.; Fox, B. A.; Le Trong, I.; Teller, D. C.; Okada, T.; Stenkamp, R. E.; Yamamoto, M.; Miyano, M. Crystal structure of rhodopsin: A G protein-coupled receptor. *Science* **2000**, 289, 739-745.

(19) Lebon, G.; Warne, T.; Edwards, P. C.; Bennett, K.; Langmead, C. J.; Leslie, A. G. W.; Tate, C. G. Agonist-bound adenosine A2A receptor structures reveal common features of GPCR activation. *Nature* **2011**, 474, 521-525.

(20) Binet, V.; Duthey, B.; Lecaillon, J.; Vol, C.; Quoyer, J.; Labesse, G.; Pin, J.-P.; Prézeau, L. Common Structural Requirements for Heptahelical Domain Function in Class A and Class C G Protein-coupled Receptors. *Journal of Biological Chemistry* **2007**, 282, 12154 -12163.

(21) Warne, T.; Serrano-Vega, M. J.; Baker, J. G.; Moukhametzianov, R.; Edwards, P. C.; Henderson, R.; Leslie, A. G. W.; Tate, C. G.; Schertler, G. F. X. Structure of a [bgr]1-adrenergic G-protein-coupled receptor. *Nature* **2008**, 454, 486-491.

(22) Kobilka, B. K.; Deupi, X. Conformational complexity of G-protein-coupled receptors. *Trends in Pharmacological Sciences* **2007**, 28, 397-406.

(23) Deupi, X.; Kobilka, B. K. Energy landscapes as a tool to integrate GPCR structure, dynamics and function. *Physiology (Bethesda)* **2010**, 25, 293-303.

(24) Perez, D. M.; Karnik, S. S. Multiple Signaling States of G-Protein-Coupled Receptors. *Pharmacological Reviews* **2005**, 57, 147 -161.

(25) Vaidehi, N.; Kenakin, T. The role of conformational ensembles of seven transmembrane

receptors in functional selectivity. *Current Opinion in Pharmacology* **2010**, *10*, 775-781.

(26) Pardo, L.; Ballesteros, J. A.; Osman, R.; Weinstein, H. On the use of the transmembrane domain of bacteriorhodopsin as a template for modeling the three-dimensional structure of guanine nucleotide-binding regulatory protein-coupled receptors. *Proc. Natl. Acad. Sci. U.S.A.* **1992**, *89*, 4009-4012.

(27) Carpenter, E. P.; Beis, K.; Cameron, A. D.; Iwata, S. Overcoming the challenges of membrane protein crystallography. *Current Opinion in Structural Biology* **2008**, *18*, 581-586.

(28) Scheerer, P.; Park, J. H.; Hildebrand, P. W.; Kim, Y. J.; Krauss, N.; Choe, H.-W.; Hofmann, K. P.; Ernst, O. P. Crystal structure of opsin in its G-protein-interacting conformation. *Nature* **2008**, *455*, 497-502.

(29) Park, J. H.; Scheerer, P.; Hofmann, K. P.; Choe, H.-W.; Ernst, O. P. Crystal structure of the ligand-free G-protein-coupled receptor opsin. *Nature* **2008**, *454*, 183-187.

(30) Rasmussen, S. G. F.; Choi, H.-J.; Fung, J. J.; Pardon, E.; Casarosa, P.; Chae, P. S.; DeVree, B. T.; Rosenbaum, D. M.; Thian, F. S.; Kobilka, T. S.; Schnapp, A.; Konetzki, I.; Sunahara, R. K.; Gellman, S. H.; Pautsch, A.; Steyaert, J.; Weis, W. I.; Kobilka, B. K. Structure of a nanobody-stabilized active state of the [bgr]₂ adrenoceptor. *Nature* **2011**, *469*, 175-180.

(31) Rosenbaum, D. M.; Zhang, C.; Lyons, J. A.; Holl, R.; Aragao, D.; Arlow, D. H.; Rasmussen, S. G. F.; Choi, H.-J.; DeVree, B. T.; Sunahara, R. K.; Chae, P. S.; Gellman, S. H.; Dror, R. O.; Shaw, D. E.; Weis, W. I.; Caffrey, M.; Gmeiner, P.; Kobilka, B. K. Structure and function of an irreversible agonist-[bgr]₂ adrenoceptor complex. *Nature* **2011**, *469*, 236-240.

(32) Xu, F.; Wu, H.; Katritch, V.; Han, G. W.; Jacobson, K. A.; Gao, Z.-G.; Cherezov, V.; Stevens, R. C. Structure of an Agonist-Bound Human A_{2A} Adenosine Receptor. *Science* **2011**.

(33) Lebon, G.; Bennett, K.; Jazayeri, A.; Tate, C. G. Thermostabilisation of an Agonist-Bound Conformation of the Human Adenosine A_{2A} Receptor. *Journal of Molecular Biology* **2011**, *409*, 298-310.

(34) Nakamichi, H.; Okada, T. Crystallographic analysis of primary visual photochemistry. *Angew. Chem. Int. Ed. Engl.* **2006**, *45*, 4270-4273.

(35) Nakamichi, H.; Okada, T. Local peptide movement in the photoreaction intermediate of rhodopsin. *Proc. Natl. Acad. Sci. U.S.A.* **2006**, *103*, 12729-12734.

(36) Ruprecht, J. J.; Mielke, T.; Vogel, R.; Villa, C.; Schertler, G. F. X. Electron crystallography reveals the structure of metarhodopsin I. *EMBO J.* **2004**, *23*, 3609-3620.

(37) Park, P. S.-H.; Lodowski, D. T.; Palczewski, K. Activation of G protein-coupled receptors: beyond two-state models and tertiary conformational changes. *Annu. Rev. Pharmacol. Toxicol.* **2008**, *48*, 107-141.

(38) Hubbell, W. L.; Altenbach, C.; Hubbell, C. M.; Khorana, H. G. Rhodopsin structure, dynamics, and activation: a perspective from crystallography, site-directed spin labeling, sulfhydryl reactivity, and disulfide cross-linking. *Adv. Protein Chem.* **2003**, *63*, 243-290.

- (39) Ye, S.; Zaitseva, E.; Caltabiano, G.; Schertler, G. F. X.; Sakmar, T. P.; Deupi, X.; Vogel, R. Tracking G-protein-coupled receptor activation using genetically encoded infrared probes. *Nature* **2010**, *464*, 1386-1389.
- (40) Bockaert, J.; Fagni, L.; Dumuis, A.; Marin, P. GPCR interacting proteins (GIP). *Pharmacology & Therapeutics* **2004**, *103*, 203-221.
- (41) Tate, C. G.; Stevens, R. C. Growth and excitement in membrane protein structural biology. *Current Opinion in Structural Biology* **2010**, *20*, 399-400.
- (42) Cherezov, V.; Abola, E.; Stevens, R. C. Recent progress in the structure determination of GPCRs, a membrane protein family with high potential as pharmaceutical targets. *Methods Mol. Biol.* **2010**, *654*, 141-168.
- (43) Steyaert, J.; Kobilka, B. K. Nanobody stabilization of G protein-coupled receptor conformational states. *Curr. Opin. Struct. Biol.* **2011**, *21*, 567-572.
- (44) Bill, R. M.; Henderson, P. J. F.; Iwata, S.; Kunji, E. R. S.; Michel, H.; Neutze, R.; Newstead, S.; Poolman, B.; Tate, C. G.; Vogel, H. Overcoming barriers to membrane protein structure determination. *Nat. Biotechnol.* **2011**, *29*, 335-340.
- (45) Zheng, H.; Loh, H. H.; Law, P. Agonist-selective signaling of G protein-coupled receptor: Mechanisms and implications. *IUBMB Life* **2010**, *62*, 112-119.
- (46) Kenakin, T. Functional Selectivity and Biased Receptor Signaling. *Journal of Pharmacology and Experimental Therapeutics* **2011**, *336*, 296 -302.
- (47) Kenakin, T. Functional Selectivity through Protean and Biased Agonism: Who Steers the Ship? *Molecular Pharmacology* **2007**, *72*, 1393 -1401.
- (48) Kenakin, T. Ligand-selective receptor conformations revisited: the promise and the problem. *Trends in Pharmacological Sciences* **2003**, *24*, 346-354.
- (49) Yao, X. J.; Vélez Ruiz, G.; Whorton, M. R.; Rasmussen, S. G. F.; DeVree, B. T.; Deupi, X.; Sunahara, R. K.; Kobilka, B. The effect of ligand efficacy on the formation and stability of a GPCR-G protein complex. *Proc. Natl. Acad. Sci. U.S.A.* **2009**, *106*, 9501-9506.
- (50) Kobilka Lab, Stanford University <http://med.stanford.edu/kobilkalab/>.
- (51) Warne, T.; Serrano-Vega, M. J.; Tate, C. G.; Schertler, G. F. X. Development and crystallization of a minimal thermostabilised G protein-coupled receptor. *Protein Expression and Purification* **2009**, *65*, 204-213.
- (52) Tate, C. G.; Schertler, G. F. X. Engineering G protein-coupled receptors to facilitate their structure determination. *Curr. Opin. Struct. Biol.* **2009**, *19*, 386-395.
- (53) Katritch, V.; Cherezov, V.; Stevens, R. C. Diversity and modularity of G protein-coupled receptor structures. *Trends in Pharmacological Sciences* **2011**.
- (54) Congreve, M.; Langmead, C. J.; Mason, J. S.; Marshall, F. H. Progress in structure based

drug design for G protein-coupled receptors. *J. Med. Chem.* **2011**, *54*, 4283-4311.

(55) Sugimoto, Y.; Fujisawa, R.; Tanimura, R.; Lattion, A. L.; Cotecchia, S.; Tsujimoto, G.; Nagao, T.; Kurose, H. Beta(1)-selective agonist (-)-1-(3,4-dimethoxyphenethylamino)-3-(3,4-dihydroxy)-2-propanol [(-)-RO363] differentially interacts with key amino acids responsible for beta(1)-selective binding in resting and active states. *J. Pharmacol. Exp. Ther.* **2002**, *301*, 51-58.

(56) Baker, J. G. The selectivity of beta-adrenoceptor antagonists at the human beta1, beta2 and beta3 adrenoceptors. *Br. J. Pharmacol.* **2005**, *144*, 317-322.

(57) Houamed, K. M.; Kuijper, J. L.; Gilbert, T. L.; Haldeman, B. A.; O'Hara, P. J.; Mulvihill, E. R.; Almers, W.; Hagen, F. S. Cloning, expression, and gene structure of a G protein-coupled glutamate receptor from rat brain. *Science* **1991**, *252*, 1318-1321.

(58) Masu, M.; Tanabe, Y.; Tsuchida, K.; Shigemoto, R.; Nakanishi, S. Sequence and expression of a metabotropic glutamate receptor. *Nature* **1991**, *349*, 760-765.

(59) Rondard, P.; Goudet, C.; Kniazeff, J.; Pin, J.-P.; Prézeau, L. The complexity of their activation mechanism opens new possibilities for the modulation of mGlu and GABAB class C G protein-coupled receptors. *Neuropharmacology* **2011**, *60*, 82-92.

(60) Nicoletti, F.; Bockaert, J.; Collingridge, G. L.; Conn, P. J.; Ferraguti, F.; Schoepp, D. D.; Wroblewski, J. T.; Pin, J. P. Metabotropic glutamate receptors: from the workbench to the bedside. *Neuropharmacology* **2011**, *60*, 1017-1041.

(61) Goudet, C.; Magnaghi, V.; Landry, M.; Nagy, F.; Gereau, R. W., 4th; Pin, J.-P. Metabotropic receptors for glutamate and GABA in pain. *Brain Res Rev* **2009**, *60*, 43-56.

(62) Ossowska, K.; Konieczny, J.; Wardas, J.; Pietraszek, M.; Kuter, K.; Wolfarth, S.; Pilc, A. An influence of ligands of metabotropic glutamate receptor subtypes on parkinsonian-like symptoms and the striatopallidal pathway in rats. *Amino Acids* **2007**, *32*, 179-188.

(63) Costantino, G.; Marinozzi, M.; Camaioni, E.; Natalini, B.; Sarichelou, I.; Micheli, F.; Cavanni, P.; Faedo, S.; Noe, C.; Moroni, F.; Pellicciari, R. Stereoselective synthesis and preliminary evaluation of (+)- and (-)-3-methyl-5-carboxy-thien-2-yl-glycine (3-MATIDA): identification of (+)-3-MATIDA as a novel mGluR1 competitive antagonist. *Farmaco* **2004**, *59*, 93-99.

(64) Bräuner-Osborne, H.; Wellendorph, P.; Jensen, A. A. Structure, pharmacology and therapeutic prospects of family C G-protein coupled receptors. *Curr Drug Targets* **2007**, *8*, 169-184.

(65) Filosa, R.; Marinozzi, M.; Costantino, G.; Hermit, M. B.; Thomsen, C.; Pellicciari, R. Synthesis and biological evaluation of (2S)- and (2R)-2-(3'-phosphonobicyclo[1.1.1]pentyl)glycines as novel group III selective metabotropic glutamate receptor ligands. *Bioorg. Med. Chem.* **2006**, *14*, 3811-3817.

(66) Kunishima, N.; Shimada, Y.; Tsuji, Y.; Sato, T.; Yamamoto, M.; Kumasaka, T.; Nakanishi, S.; Jingami, H.; Morikawa, K. Structural basis of glutamate recognition by a dimeric metabotropic glutamate receptor. *Nature* **2000**, *407*, 971-977.

- (67) Tsuchiya, D.; Kunishima, N.; Kamiya, N.; Jingami, H.; Morikawa, K. Structural views of the ligand-binding cores of a metabotropic glutamate receptor complexed with an antagonist and both glutamate and Gd³⁺. *Proceedings of the National Academy of Sciences* **2002**, *99*, 2660-2665.
- (68) Muto, T.; Tsuchiya, D.; Morikawa, K.; Jingami, H. Structures of the extracellular regions of the group II/III metabotropic glutamate receptors. *Proceedings of the National Academy of Sciences* **2007**, *104*, 3759-3764.
- (69) Pin, J.-P.; Kniazeff, J.; Goudet, C.; Bessis, A.-S.; Liu, J.; Galvez, T.; Acher, F.; Rondard, P.; Prézeau, L. The activation mechanism of class-C G-protein coupled receptors. *Biology of the Cell* **2004**, *96*, 335-342.
- (70) Rovira, X.; Pin, J.-P.; Giraldo, J. The asymmetric/symmetric activation of GPCR dimers as a possible mechanistic rationale for multiple signalling pathways. *Trends Pharmacol. Sci.* **2010**, *31*, 15-21.
- (71) Keov, P.; Sexton, P. M.; Christopoulos, A. Allosteric modulation of G protein-coupled receptors: A pharmacological perspective. *Neuropharmacology* **2011**, *60*, 24-35.
- (72) Ritter, S. L.; Hall, R. A. Fine-tuning of GPCR activity by receptor-interacting proteins. *Nat Rev Mol Cell Biol* **2009**, *10*, 819-830.
- (73) Chini, B.; Parenti, M. G-protein-coupled receptors, cholesterol and palmitoylation: facts about fats. *J Mol Endocrinol* **2009**, *42*, 371-379.
- (74) Escribá, P. V.; Wedegaertner, P. B.; Goñi, F. M.; Vögler, O. Lipid-protein interactions in GPCR-associated signaling. *Biochimica et Biophysica Acta (BBA) - Biomembranes* **2007**, *1768*, 836-852.
- (75) Ericksen, S. S.; Cummings, D. F.; Weinstein, H.; Schetz, J. A. Ligand selectivity of D2 dopamine receptors is modulated by changes in local dynamics produced by sodium binding. *J. Pharmacol. Exp. Ther* **2009**, *328*, 40-54.
- (76) Milligan, G.; Canals, M.; Pediani, J. D.; Ellis, J.; Lopez-Gimenez, J. F. The role of GPCR dimerisation/oligomerisation in receptor signalling. *Ernst Schering Found Symp Proc* **2006**, 145-161.
- (77) La Motta, C.; Sartini, S.; Morelli, M.; Taliani, S.; Da Settimo, F. Allosteric modulators for adenosine receptors: an alternative to the orthosteric ligands. *Curr Top Med Chem* **2010**, *10*, 976-992.
- (78) Conn, P. J.; Jones, C. K.; Lindsley, C. W. Subtype-selective allosteric modulators of muscarinic receptors for the treatment of CNS disorders. *Trends Pharmacol. Sci.* **2009**, *30*, 148-155.
- (79) Schetz, J. A. Allosteric modulation of dopamine receptors. *Mini Rev Med Chem* **2005**, *5*, 555-561.
- (80) Nemeth, E. F.; Heaton, W. H.; Miller, M.; Fox, J.; Balandrin, M. F.; Van Wagenen, B. C.; Colloton, M.; Karbon, W.; Scherrer, J.; Shatzen, E.; Rishton, G.; Scully, S.; Qi, M.; Harris, R.;

- Lacey, D.; Martin, D. Pharmacodynamics of the type II calcimimetic compound cinacalcet HCl. *J. Pharmacol. Exp. Ther.* **2004**, *308*, 627-635.
- (81) Urwyler, S. Allosteric modulation of family C G-protein-coupled receptors: from molecular insights to therapeutic perspectives. *Pharmacol. Rev* **2011**, *63*, 59-126.
- (82) Bridges, T. M.; Lindsley, C. W. G-protein-coupled receptors: from classical modes of modulation to allosteric mechanisms. *ACS Chem. Biol.* **2008**, *3*, 530-541.
- (83) Conn, P. J.; Christopoulos, A.; Lindsley, C. W. Allosteric modulators of GPCRs: a novel approach for the treatment of CNS disorders. *Nat Rev Drug Discov* **2009**, *8*, 41-54.
- (84) Valant, C.; Gregory, K. J.; Hall, N. E.; Scammells, P. J.; Lew, M. J.; Sexton, P. M.; Christopoulos, A. A novel mechanism of G protein-coupled receptor functional selectivity. Muscarinic partial agonist McN-A-343 as a bitopic orthosteric/allosteric ligand. *J. Biol. Chem.* **2008**, *283*, 29312-29321.
- (85) Covic, L.; Gresser, A. L.; Talavera, J.; Swift, S.; Kuliopulos, A. Activation and inhibition of G protein-coupled receptors by cell-penetrating membrane-tethered peptides. *Proc. Natl. Acad. Sci. U.S.A.* **2002**, *99*, 643-648.
- (86) Changeux, J.-P.; Edelstein, S. J. Allosteric mechanisms of signal transduction. *Science* **2005**, *308*, 1424-1428.
- (87) Göblyös, A.; Ijzerman, A. P. Allosteric modulation of adenosine receptors. *Biochim. Biophys. Acta* **2011**, *1808*, 1309-1318.
- (88) May, L. T.; Leach, K.; Sexton, P. M.; Christopoulos, A. Allosteric modulation of G protein-coupled receptors. *Annu. Rev. Pharmacol. Toxicol.* **2007**, *47*, 1-51.
- (89) Nicholls, D. J.; Tomkinson, N. P.; Wiley, K. E.; Brammall, A.; Bowers, L.; Grahames, C.; Gaw, A.; Meghani, P.; Shelton, P.; Wright, T. J.; Mallinder, P. R. Identification of a putative intracellular allosteric antagonist binding-site in the CXC chemokine receptors 1 and 2. *Mol. Pharmacol.* **2008**, *74*, 1193-1202.
- (90) Dowal, L.; Sim, D. S.; Dilks, J. R.; Blair, P.; Beaudry, S.; Denker, B. M.; Koukos, G.; Kuliopulos, A.; Flaumenhaft, R. Identification of an antithrombotic allosteric modulator that acts through helix 8 of PAR1. *Proc. Natl. Acad. Sci. U.S.A.* **2011**, *108*, 2951-2956.
- (91) Gimpl, G.; Reitz, J.; Brauer, S.; Trossen, C. Oxytocin receptors: ligand binding, signalling and cholesterol dependence. *Prog. Brain Res.* **2008**, *170*, 193-204.
- (92) Smith, N. J.; Bennett, K. A.; Milligan, G. When simple agonism is not enough: Emerging modalities of GPCR ligands. *Molecular and Cellular Endocrinology* **2011**, *331*, 241-247.
- (93) Hanson, M. A.; Cherezov, V.; Griffith, M. T.; Roth, C. B.; Jaakola, V.-P.; Chien, E. Y. T.; Velasquez, J.; Kuhn, P.; Stevens, R. C. A Specific Cholesterol Binding Site Is Established by the 2.8 Å Structure of the Human [beta]2-Adrenergic Receptor. *Structure* **2008**, *16*, 897-905.
- (94) Parker, M. S.; Wong, Y. Y.; Parker, S. L. An ion-responsive motif in the second

transmembrane segment of rhodopsin-like receptors. *Amino Acids* **2008**, *35*, 1-15.

(95) Ananthanarayanan, V. S.; Kerman, A. Role of metal ions in ligand-receptor interaction: insights from structural studies. *Mol. Cell. Endocrinol* **2006**, *246*, 53-59.

(96) Neve, K. A.; Cox, B. A.; Henningsen, R. A.; Spanoyannis, A.; Neve, R. L. Pivotal role for aspartate-80 in the regulation of dopamine D2 receptor affinity for drugs and inhibition of adenylyl cyclase. *Mol. Pharmacol* **1991**, *39*, 733-739.

(97) Neve, K. A.; Cumbay, M. G.; Thompson, K. R.; Yang, R.; Buck, D. C.; Watts, V. J.; DuRand, C. J.; Teeter, M. M. Modeling and mutational analysis of a putative sodium-binding pocket on the dopamine D2 receptor. *Mol. Pharmacol* **2001**, *60*, 373-381.

(98) Parkel, S.; Näsman, J.; Rincken, A. Enhancement of agonist binding to 5-HT1A receptors in rat brain membranes by millimolar Mn²⁺. *Neuroscience Letters* **2009**, *457*, 32-35.

(99) Parkel, S.; Töntson, L.; Rincken, A. Millimolar Mn²⁺ influences agonist binding to 5-HT1A receptors by inhibiting guanosine nucleotide binding to receptor-coupled G-proteins. *NeuroToxicology* **2011**, *32*, 25-30.

(100) Sealfon, S. C.; Chi, L.; Ebersole, B. J.; Rodic, V.; Zhang, D.; Ballesteros, J. A.; Weinstein, H. Related Contribution of Specific Helix 2 and 7 Residues to Conformational Activation of the Serotonin 5-HT_{2A} Receptor. *Journal of Biological Chemistry* **1995**, *270*, 16683 -16688.

(101) Standfuss, J.; Edwards, P. C.; D'Antona, A.; Fransen, M.; Xie, G.; Oprian, D. D.; Schertler, G. F. X. The structural basis of agonist-induced activation in constitutively active rhodopsin. *Nature* **2011**, *471*, 656-660.

(102) Lebon, G.; Warne, T.; Edwards, P. C.; Bennett, K.; Langmead, C. J.; Leslie, A. G. W.; Tate, C. G. Agonist-bound adenosine A(2A) receptor structures reveal common features of GPCR activation. *Nature* **2011**.

(103) Warne, T.; Moukhametzianov, R.; Baker, J. G.; Nehmé, R.; Edwards, P. C.; Leslie, A. G. W.; Schertler, G. F. X.; Tate, C. G. The structural basis for agonist and partial agonist action on a $\beta(1)$ -adrenergic receptor. *Nature* **2011**, *469*, 241-244.

(104) Fahmy, K.; Jäger, F.; Beck, M.; Zvyaga, T. A.; Sakmar, T. P.; Siebert, F. Protonation states of membrane-embedded carboxylic acid groups in rhodopsin and metarhodopsin II: a Fourier-transform infrared spectroscopy study of site-directed mutants. *Proc. Natl. Acad. Sci. U.S.A.* **1993**, *90*, 10206-10210.

(105) Rath, P.; DeCaluwé, L. L.; Bovee-Geurts, P. H.; DeGrip, W. J.; Rothschild, K. J. Fourier transform infrared difference spectroscopy of rhodopsin mutants: light activation of rhodopsin causes hydrogen-bonding change in residue aspartic acid-83 during meta II formation. *Biochemistry* **1993**, *32*, 10277-10282.

(106) Barbhaiya, H.; McClain, R.; Ijzerman, A.; Rivkees, S. A. Site-directed mutagenesis of the human A1 adenosine receptor: influences of acidic and hydroxy residues in the first four transmembrane domains on ligand binding. *Mol. Pharmacol.* **1996**, *50*, 1635-1642.

- (107) Ghanouni, P.; Schambye, H.; Seifert, R.; Lee, T. W.; Rasmussen, S. G.; Gether, U.; Kobilka, B. K. The effect of pH on beta(2) adrenoceptor function. Evidence for protonation-dependent activation. *J. Biol. Chem.* **2000**, *275*, 3121-3127.
- (108) Tashiro, M.; Kato, M.; Miyake, M.; Watanuki, S.; Funaki, Y.; Ishikawa, Y.; Iwata, R.; Yanai, K. Dose dependency of brain histamine H(1) receptor occupancy following oral administration of cetirizine hydrochloride measured using PET with [¹¹C]doxepin. *Hum Psychopharmacol* **2009**, *24*, 540-548.
- (109) Gillard, M.; Chatelain, P. Changes in pH differently affect the binding properties of histamine H1 receptor antagonists. *European Journal of Pharmacology* **2006**, *530*, 205-214.
- (110) Gibson, W. J.; Roques, T. W.; Young, J. M. Modulation of antagonist binding to histamine H1-receptors by sodium ions and by 2-amino-2-hydroxymethyl-propan-1,3-diol HCl. *Br. J. Pharmacol.* **1994**, *111*, 1262-1268.
- (111) Kenakin, T.; Miller, L. J. Seven transmembrane receptors as shapeshifting proteins: the impact of allosteric modulation and functional selectivity on new drug discovery. *Pharmacol. Rev.* **2010**, *62*, 265-304.
- (112) Valant, C.; Sexton, P. M.; Christopoulos, A. Orthosteric/allosteric bitopic ligands: going hybrid at GPCRs. *Mol. Interv.* **2009**, *9*, 125-135.
- (113) Ong, J.; Kerr, D. I. B. Clinical potential of GABAB receptor modulators. *CNS Drug Rev* **2005**, *11*, 317-334.
- (114) Froestl, W. Novel GABA(B) receptor positive modulators: a patent survey. *Expert Opin Ther Pat* **2010**, *20*, 1007-1017.
- (115) Kew, J. N. C. Positive and negative allosteric modulation of metabotropic glutamate receptors: emerging therapeutic potential. *Pharmacol. Ther.* **2004**, *104*, 233-244.
- (116) Ritzén, A.; Mathiesen, J. M.; Thomsen, C. Molecular pharmacology and therapeutic prospects of metabotropic glutamate receptor allosteric modulators. *Basic Clin. Pharmacol. Toxicol.* **2005**, *97*, 202-213.
- (117) Wood, M. R.; Hopkins, C. R.; Brogan, J. T.; Conn, P. J.; Lindsley, C. W. "Molecular Switches" on mGluR Allosteric Ligands That Modulate Modes of Pharmacology. *Biochemistry* **2011**, *50*, 2403-2410.
- (118) Harrington, P. E.; Fotsch, C. Calcium sensing receptor activators: calcimimetics. *Curr. Med. Chem.* **2007**, *14*, 3027-3034.
- (119) Kenakin, T. Collateral efficacy in drug discovery: taking advantage of the good (allosteric) nature of 7TM receptors. *Trends in Pharmacological Sciences* **2007**, *28*, 407-415.
- (120) Bokoch, M. P.; Zou, Y.; Rasmussen, S. G. F.; Liu, C. W.; Nygaard, R.; Rosenbaum, D. M.; Fung, J. J.; Choi, H.-J.; Thian, F. S.; Kobilka, T. S.; Puglisi, J. D.; Weis, W. I.; Pardo, L.; Prosser, R. S.; Mueller, L.; Kobilka, B. K. Ligand-specific regulation of the extracellular surface of a G-protein-coupled receptor. *Nature* **2010**, *463*, 108-112.

- (121) Ruprecht, J. J.; Mielke, T.; Vogel, R.; Villa, C.; Schertler, G. F. X. Electron crystallography reveals the structure of metarhodopsin I. *EMBO J.* **2004**, *23*, 3609-3620.
- (122) Ye, S.; Zaitseva, E.; Caltabiano, G.; Schertler, G. F. X.; Sakmar, T. P.; Deupi, X.; Vogel, R. Tracking G-protein-coupled receptor activation using genetically encoded infrared probes. *Nature* **2010**, *464*, 1386-1389.
- (123) Deupi, X.; Standfuss, J. Structural insights into agonist-induced activation of G-protein-coupled receptors. *Curr. Opin. Struct. Biol.* **2011**, *21*, 541-551.
- (124) Schwartz, T. W.; Frimurer, T. M.; Holst, B.; Rosenkilde, M. M.; Elling, C. E. Molecular Mechanism of 7TM Receptor Activation-a global Toggle Switch Model. *Annual Review of Pharmacology and Toxicology* **2006**, *46*, 481-519.
- (125) Holst, B.; Nygaard, R.; Valentin-Hansen, L.; Bach, A.; Engelstoft, M. S.; Petersen, P. S.; Frimurer, T. M.; Schwartz, T. W. A conserved aromatic lock for the tryptophan rotameric switch in TM-VI of seven-transmembrane receptors. *J. Biol. Chem.* **2010**, *285*, 3973-3985.
- (126) Ballesteros, J. A.; Jensen, A. D.; Liapakis, G.; Rasmussen, S. G.; Shi, L.; Gether, U.; Javitch, J. A. Activation of the beta 2-adrenergic receptor involves disruption of an ionic lock between the cytoplasmic ends of transmembrane segments 3 and 6. *J. Biol. Chem.* **2001**, *276*, 29171-29177.
- (127) Deupi, X.; Standfuss, J. Structural insights into agonist-induced activation of G-protein-coupled receptors. *Current Opinion in Structural Biology* **2011**, *21*, 541-551.
- (128) Angel, T. E.; Chance, M. R.; Palczewski, K. Conserved waters mediate structural and functional activation of family A (rhodopsin-like) G protein-coupled receptors. *Proc. Natl. Acad. Sci. U.S.A.* **2009**, *106*, 8555-8560.
- (129) Angel, T. E.; Gupta, S.; Jastrzebska, B.; Palczewski, K.; Chance, M. R. Structural waters define a functional channel mediating activation of the GPCR, rhodopsin. *Proc. Natl. Acad. Sci. U.S.A.* **2009**, *106*, 14367-14372.
- (130) Deupi, X.; Kobilka, B. Activation of G protein-coupled receptors. *Adv. Protein Chem.* **2007**, *74*, 137-166.
- (131) Doré, A. S.; Robertson, N.; Errey, J. C.; Ng, I.; Hollenstein, K.; Tehan, B.; Hurrell, E.; Bennett, K.; Congreve, M.; Magnani, F.; Tate, C. G.; Weir, M.; Marshall, F. H. Structure of the Adenosine A2A Receptor in Complex with ZM241385 and the Xanthines XAC and Caffeine. *Structure* **2011**, *19*, 1283-1293.
- (132) Rasmussen, S. G. F.; Choi, H.-J.; Rosenbaum, D. M.; Kobilka, T. S.; Thian, F. S.; Edwards, P. C.; Burghammer, M.; Ratnala, V. R. P.; Sanishvili, R.; Fischetti, R. F.; Schertler, G. F. X.; Weis, W. I.; Kobilka, B. K. Crystal structure of the human beta2 adrenergic G-protein-coupled receptor. *Nature* **2007**, *450*, 383-387.
- (133) Kenakin, T. Principles: receptor theory in pharmacology. *Trends Pharmacol. Sci.* **2004**, *25*, 186-192.

- (134) Weiss, J. M.; Morgan, P. H.; Lutz, M. W.; Kenakin, T. P. The cubic ternary complex receptor-occupancy model. III. resurrecting efficacy. *J. Theor. Biol.* **1996**, *181*, 381-397.
- (135) Onaran, H. O.; Costa, T. Agonist efficacy and allosteric models of receptor action. *Ann. N. Y. Acad. Sci.* **1997**, *812*, 98-115.
- (136) Kenakin, T. Efficacy at G-protein-coupled receptors. *Nat Rev Drug Discov* **2002**, *1*, 103-110.
- (137) Ghanouni, P.; Gryczynski, Z.; Steenhuis, J. J.; Lee, T. W.; Farrens, D. L.; Lakowicz, J. R.; Kobilka, B. K. Functionally different agonists induce distinct conformations in the G protein coupling domain of the beta 2 adrenergic receptor. *J. Biol. Chem.* **2001**, *276*, 24433-24436.
- (138) Kenakin, T. Protean agonists. Keys to receptor active states? *Ann. N. Y. Acad. Sci.* **1997**, *812*, 116-125.
- (139) Kenakin, T. Agonist-receptor efficacy. I: Mechanisms of efficacy and receptor promiscuity. *Trends Pharmacol. Sci.* **1995**, *16*, 188-192.
- (140) Kenakin, T. Agonist-receptor efficacy. II. Agonist trafficking of receptor signals. *Trends Pharmacol. Sci.* **1995**, *16*, 232-238.
- (141) Milligan, G. G protein-coupled receptor hetero-dimerization: contribution to pharmacology and function. *Br. J. Pharmacol.* **2009**, *158*, 5-14.
- (142) González-Maeso, J. GPCR oligomers in pharmacology and signaling. *Mol Brain* **2011**, *4*, 20.
- (143) Pin, J.-P.; Neubig, R.; Bouvier, M.; Devi, L.; Filizola, M.; Javitch, J. A.; Lohse, M. J.; Milligan, G.; Palczewski, K.; Parmentier, M.; Spedding, M. International Union of Basic and Clinical Pharmacology. LXVII. Recommendations for the recognition and nomenclature of G protein-coupled receptor heteromultimers. *Pharmacol. Rev.* **2007**, *59*, 5-13.
- (144) Skrabanek, L.; Murcia, M.; Bouvier, M.; Devi, L.; George, S. R.; Lohse, M. J.; Milligan, G.; Neubig, R.; Palczewski, K.; Parmentier, M.; Pin, J.-P.; Vriend, G.; Javitch, J. A.; Campagne, F.; Filizola, M. Requirements and ontology for a G protein-coupled receptor oligomerization knowledge base. *BMC Bioinformatics* **2007**, *8*, 177.
- (145) Salahpour, A.; Angers, S.; Bouvier, M. Functional Significance of Oligomerization of G-protein-coupled Receptors. *Trends in Endocrinology & Metabolism* **2000**, *11*, 163-168.
- (146) Chabre, M.; le Maire, M. Monomeric G-protein-coupled receptor as a functional unit. *Biochemistry* **2005**, *44*, 9395-9403.
- (147) Marshall, F. H.; Jones, K. A.; Kaupmann, K.; Bettler, B. GABAB receptors - the first 7TM heterodimers. *Trends Pharmacol. Sci.* **1999**, *20*, 396-399.
- (148) Fribourg, M.; Moreno, J. L.; Holloway, T.; Provasi, D.; Baki, L.; Mahajan, R.; Park, G.; Adney, S. K.; Hatcher, C.; Eltit, J. M.; Ruta, J. D.; Albizu, L.; Li, Z.; Umali, A.; Shim, J.; Fabiato, A.; MacKerell Jr., A. D.; Brezina, V.; Sealfon, S. C.; Filizola, M.; González-Maeso, J.; Logothetis,

D. E. Decoding the Signaling of a GPCR Heteromeric Complex Reveals a Unifying Mechanism of Action of Antipsychotic Drugs. *Cell* **2011**, *147*, 1011-1023.

(149) Gonzalez-Maeso, J.; Ang, R. L.; Yuen, T.; Chan, P.; Weisstaub, N. V.; Lopez-Gimenez, J. F.; Zhou, M.; Okawa, Y.; Callado, L. F.; Milligan, G.; Gingrich, J. A.; Filizola, M.; Meana, J. J.; Sealfon, S. C. Identification of a serotonin/glutamate receptor complex implicated in psychosis. *Nature* **2008**, *452*, 93-97.

(150) Moreno, J. L.; Holloway, T.; Albizu, L.; Sealfon, S. C.; González-Maeso, J. Metabotropic glutamate mGlu2 receptor is necessary for the pharmacological and behavioral effects induced by hallucinogenic 5-HT_{2A} receptor agonists. *Neuroscience Letters* **2011**, *493*, 76-79.

(151) Kota, P.; Reeves, P. J.; Rajbhandary, U. L.; Khorana, H. G. Opsin is present as dimers in COS1 cells: identification of amino acids at the dimeric interface. *Proc. Natl. Acad. Sci. U.S.A.* **2006**, *103*, 3054-3059.

(152) Neri, M.; Vanni, S.; Tavernelli, I.; Rothlisberger, U. Role of aggregation in rhodopsin signal transduction. *Biochemistry* **2010**, *49*, 4827-4832.

(153) Rondard, P.; Goudet, C.; Kniazeff, J.; Pin, J.-P.; Prézeau, L. The complexity of their activation mechanism opens new possibilities for the modulation of mGlu and GABAB class C G protein-coupled receptors. *Neuropharmacology* **2011**, *60*, 82-92.

(154) Liang, Y.; Fotiadis, D.; Filipek, S.; Saperstein, D. A.; Palczewski, K.; Engel, A. Organization of the G protein-coupled receptors rhodopsin and opsin in native membranes. *J. Biol. Chem.* **2003**, *278*, 21655-21662.

(155) Smith, N. J.; Milligan, G. Allosteric at G Protein-Coupled Receptor Homo- and Heteromers: Uncharted Pharmacological Landscapes. *Pharmacological Reviews* **2010**, *62*, 701 -725.

(156) Maurice, P.; Kamal, M.; Jockers, R. Asymmetry of GPCR oligomers supports their functional relevance. *Trends in Pharmacological Sciences In Press, Corrected Proof*.

(157) Ayoub, M. A.; Levoye, A.; Delagrangé, P.; Jockers, R. Preferential formation of MT₁/MT₂ melatonin receptor heterodimers with distinct ligand interaction properties compared with MT₂ homodimers. *Mol. Pharmacol.* **2004**, *66*, 312-321.

(158) Levoye, A.; Dam, J.; Ayoub, M. A.; Guillaume, J.-L.; Couturier, C.; Delagrangé, P.; Jockers, R. The orphan GPR50 receptor specifically inhibits MT₁ melatonin receptor function through heterodimerization. *EMBO J.* **2006**, *25*, 3012-3023.

(159) Levac, B. A. R.; O'Dowd, B. F.; George, S. R. Oligomerization of opioid receptors: generation of novel signaling units. *Curr Opin Pharmacol* **2002**, *2*, 76-81.

(160) Park, P. S.-H.; Palczewski, K. Diversifying the repertoire of G protein-coupled receptors through oligomerization. *Proc. Natl. Acad. Sci. U.S.A.* **2005**, *102*, 8793-8794.

(161) Mercier, J.-F.; Salahpour, A.; Angers, S.; Breit, A.; Bouvier, M. Quantitative assessment of beta 1- and beta 2-adrenergic receptor homo- and heterodimerization by bioluminescence resonance energy transfer. *J. Biol. Chem.* **2002**, *277*, 44925-44931.

- (162) Lavoie, C.; Mercier, J.-F.; Salahpour, A.; Umapathy, D.; Breit, A.; Villeneuve, L.-R.; Zhu, W.-Z.; Xiao, R.-P.; Lakatta, E. G.; Bouvier, M.; Hébert, T. E. Beta 1/beta 2-adrenergic receptor heterodimerization regulates beta 2-adrenergic receptor internalization and ERK signaling efficacy. *J. Biol. Chem.* **2002**, *277*, 35402-35410.
- (163) Ianoul, A.; Grant, D. D.; Rouleau, Y.; Bani-Yaghoub, M.; Johnston, L. J.; Pezacki, J. P. Imaging nanometer domains of beta-adrenergic receptor complexes on the surface of cardiac myocytes. *Nat. Chem. Biol.* **2005**, *1*, 196-202.
- (164) Sartania, N.; Appelbe, S.; Padiani, J. D.; Milligan, G. Agonist occupancy of a single monomeric element is sufficient to cause internalization of the dimeric beta2-adrenoceptor. *Cell. Signal.* **2007**, *19*, 1928-1938.
- (165) Kobayashi, H.; Ogawa, K.; Yao, R.; Lichtarge, O.; Bouvier, M. Functional Rescue of β 1-Adrenoceptor Dimerization and Trafficking by Pharmacological Chaperones. *Traffic* **2009**, *10*, 1019-1033.
- (166) Brea, J.; Castro, M.; Giraldo, J.; López-Giménez, J. F.; Padín, J. F.; Quintián, F.; Cadavid, M. I.; Vilaró, M. T.; Mengod, G.; Berg, K. A.; Clarke, W. P.; Vilardaga, J.-P.; Milligan, G.; Loza, M. I. Evidence for Distinct Antagonist-Revealed Functional States of 5-Hydroxytryptamine_{2A} Receptor Homodimers. *Molecular Pharmacology* **2009**, *75*, 1380 -1391.
- (167) Shashack, M. J.; Cunningham, K. A.; Seitz, P. K.; McGinnis, A.; Smith, T. D.; Watson, C. S.; Gilbertson, S. R. Synthesis and Evaluation of Dimeric Derivatives of 5-HT_{2A} Receptor (5-HT_{2AR}) Antagonist M-100907. *ACS Chem. Neurosci.* **2011**, *2*, 640-644.
- (168) Urizar, E.; Yano, H.; Kolster, R.; Galés, C.; Lambert, N.; Javitch, J. A. CODA-RET reveals functional selectivity as a result of GPCR heteromerization. *Nat. Chem. Biol.* **2011**, *7*, 624-630.
- (169) Guo, W.; Shi, L.; Filizola, M.; Weinstein, H.; Javitch, J. A. Crosstalk in G protein-coupled receptors: changes at the transmembrane homodimer interface determine activation. *Proc. Natl. Acad. Sci. U.S.A.* **2005**, *102*, 17495-17500.
- (170) Albizu, L.; Holloway, T.; González-Maeso, J.; Sealfon, S. C. Functional crosstalk and heteromerization of serotonin 5-HT_{2A} and dopamine D₂ receptors. *Neuropharmacology* **2011**, *61*, 770-777.
- (171) Borroto-Escuela, D. O.; Romero-Fernandez, W.; Tarakanov, A. O.; Marcellino, D.; Ciruela, F.; Agnati, L. F.; Fuxe, K. Dopamine D₂ and 5-hydroxytryptamine 5-HT_(2A) receptors assemble into functionally interacting heteromers. *Biochem. Biophys. Res. Commun.* **2010**, *401*, 605-610.
- (172) Łukasiewicz, S.; Faron-Górecka, A.; Kędracka-Krok, S.; Dziedzicka-Wasylewska, M. Effect of clozapine on the dimerization of serotonin 5-HT_(2A) receptor and its genetic variant 5-HT_(2A)H425Y with dopamine D₍₂₎ receptor. *Eur. J. Pharmacol.* **2011**, *659*, 114-123.
- (173) Łukasiewicz, S.; Polit, A.; Kędracka-Krok, S.; Wędzony, K.; Maćkowiak, M.; Dziedzicka-Wasylewska, M. Hetero-dimerization of serotonin 5-HT_(2A) and dopamine D₍₂₎ receptors. *Biochim. Biophys. Acta* **2010**, *1803*, 1347-1358.
- (174) Rodríguez-Frade, J. M.; Vila-Coro, A. J.; Martín, A.; Nieto, M.; Sánchez-Madrid, F.;

Proudfoot, A. E.; Wells, T. N.; Martínez-A, C.; Mellado, M. Similarities and differences in RANTES- and (AOP)-RANTES-triggered signals: implications for chemotaxis. *J. Cell Biol.* **1999**, *144*, 755-765.

(175) Smith, N. J.; Milligan, G. Allostery at G protein-coupled receptor homo- and heteromers: uncharted pharmacological landscapes. *Pharmacol. Rev.* **2010**, *62*, 701-725.

(176) Panetta, R.; Greenwood, M. T. Physiological relevance of GPCR oligomerization and its impact on drug discovery. *Drug Discov. Today* **2008**, *13*, 1059-1066.

(177) Simons, K.; Gerl, M. J. Revitalizing membrane rafts: new tools and insights. *Nat. Rev. Mol. Cell Biol.* **2010**, *11*, 688-699.

(178) Ostrom, R. S.; Insel, P. A. The evolving role of lipid rafts and caveolae in G protein-coupled receptor signaling: implications for molecular pharmacology. *Br. J. Pharmacol.* **2004**, *143*, 235-245.

(179) Mitchell, D. C.; Niu, S. L.; Litman, B. J. Optimization of receptor-G protein coupling by bilayer lipid composition I: kinetics of rhodopsin-transducin binding. *J. Biol. Chem.* **2001**, *276*, 42801-42806.

(180) Niu, S. L.; Mitchell, D. C.; Litman, B. J. Optimization of receptor-G protein coupling by bilayer lipid composition II: formation of metarhodopsin II-transducin complex. *J. Biol. Chem.* **2001**, *276*, 42807-42811.

(181) Pucadyil, T. J.; Chattopadhyay, A. Role of cholesterol in the function and organization of G-protein coupled receptors. *Prog. Lipid Res.* **2006**, *45*, 295-333.

(182) The Department of Molecular Biology and Chemistry, The Stevens Lab
<http://stevens.scripps.edu/>.

(183) Pontier, S. M.; Percherancier, Y.; Galandrin, S.; Breit, A.; Galés, C.; Bouvier, M. Cholesterol-dependent Separation of the β 2-Adrenergic Receptor from Its Partners Determines Signaling Efficacy. *Journal of Biological Chemistry* **2008**, *283*, 24659 -24672.

(184) Eroglu, Ç.; Brügger, B.; Wieland, F.; Sinning, I. Glutamate-binding affinity of Drosophila metabotropic glutamate receptor is modulated by association with lipid rafts. *Proceedings of the National Academy of Sciences* **2003**, *100*, 10219 -10224.

(185) Francesconi, A.; Kumari, R.; Zukin, R. S. Regulation of Group I Metabotropic Glutamate Receptor Trafficking and Signaling by the Caveolar/Lipid Raft Pathway. *The Journal of Neuroscience* **2009**, *29*, 3590 -3602.

(186) Stern, C. M.; Mermelstein, P. G. Caveolin regulation of neuronal intracellular signaling. *Cell. Mol. Life Sci.* **2010**, *67*, 3785-3795.

(187) Barnes, N. M.; Sharp, T. A review of central 5-HT receptors and their function. *Neuropharmacology* **1999**, *38*, 1083-1152.

(188) Jones, B. J.; Blackburn, T. P. The medical benefit of 5-HT research. *Pharmacol. Biochem.*

Behav. **2002**, *71*, 555-568.

(189) Jensen, N. H.; Cremers, T. I.; Sotty, F. Therapeutic potential of 5-HT_{2C} receptor ligands. *ScientificWorldJournal* **2010**, *10*, 1870-1885.

(190) Brea, J.; Castro-Palomino, J.; Yeste, S.; Cubero, E.; Párraga, A.; Domínguez, E.; Loza, M. I. Emerging opportunities and concerns for drug discovery at serotonin 5-HT_{2B} receptors. *Curr Top Med Chem* **2010**, *10*, 493-503.

(191) Emsley, R. Drugs in development for the treatment of schizophrenia. *Expert Opin Investig Drugs* **2009**, *18*, 1103-1118.

(192) Blaazer, A. R.; Smid, P.; Kruse, C. G. Structure-activity relationships of phenylalkylamines as agonist ligands for 5-HT(2A) receptors. *ChemMedChem* **2008**, *3*, 1299-1309.

(193) Nagatomo, T.; Rashid, M.; Abul Muntasir, H.; Komiyama, T. Functions of 5-HT_{2A} receptor and its antagonists in the cardiovascular system. *Pharmacol. Ther.* **2004**, *104*, 59-81.

(194) Berg, K. A.; Harvey, J. A.; Spampinato, U.; Clarke, W. P. Physiological and therapeutic relevance of constitutive activity of 5-HT_{2A} and 5-HT_{2C} receptors for the treatment of depression. *Prog. Brain Res.* **2008**, *172*, 287-305.

(195) González-Maeso, J.; Weisstaub, N. V.; Zhou, M.; Chan, P.; Ivic, L.; Ang, R.; Lira, A.; Bradley-Moore, M.; Ge, Y.; Zhou, Q.; Sealfon, S. C.; Gingrich, J. A. Hallucinogens Recruit Specific Cortical 5-HT_{2A} Receptor-Mediated Signaling Pathways to Affect Behavior. *Neuron* **2007**, *53*, 439-452.

(196) González-Maeso, J.; Yuen, T.; Ebersole, B. J.; Wurmbach, E.; Lira, A.; Zhou, M.; Weisstaub, N.; Hen, R.; Gingrich, J. A.; Sealfon, S. C. Transcriptome Fingerprints Distinguish Hallucinogenic and Nonhallucinogenic 5-Hydroxytryptamine 2A Receptor Agonist Effects in Mouse Somatosensory Cortex. *The Journal of Neuroscience* **2003**, *23*, 8836 -8843.

(197) Ross, C. A.; Margolis, R. L.; Reading, S. A. J.; Pletnikov, M.; Coyle, J. T. Neurobiology of schizophrenia. *Neuron* **2006**, *52*, 139-153.

(198) Sawa, A.; Snyder, S. H. Schizophrenia: diverse approaches to a complex disease. *Science* **2002**, *296*, 692-695.

(199) Howes, O. D.; Kapur, S. The dopamine hypothesis of schizophrenia: version III--the final common pathway. *Schizophr Bull* **2009**, *35*, 549-562.

(200) Miyamoto, S.; Duncan, G. E.; Marx, C. E.; Lieberman, J. A. Treatments for schizophrenia: a critical review of pharmacology and mechanisms of action of antipsychotic drugs. *Mol. Psychiatry* **2005**, *10*, 79-104.

(201) Marek, G. J. Metabotropic glutamate_{2/3} (mGlu_{2/3}) receptors, schizophrenia and cognition. *Eur. J. Pharmacol.* **2010**, *639*, 81-90.

(202) Marek, G. J. Metabotropic glutamate _{2/3} receptors as drug targets. *Curr Opin Pharmacol* **2004**, *4*, 18-22.

- (203) Patil, S. T.; Zhang, L.; Martenyi, F.; Lowe, S. L.; Jackson, K. A.; Andreev, B. V.; Avedisova, A. S.; Bardenstein, L. M.; Gurovich, I. Y.; Morozova, M. A.; Mosolov, S. N.; Neznanov, N. G.; Reznik, A. M.; Smulevich, A. B.; Tochilov, V. A.; Johnson, B. G.; Monn, J. A.; Schoepp, D. D. Activation of mGlu2/3 receptors as a new approach to treat schizophrenia: a randomized Phase 2 clinical trial. *Nat. Med.* **2007**, *13*, 1102-1107.
- (204) Halberstadt, A. L.; Geyer, M. A. LSD but not lisuride disrupts prepulse inhibition in rats by activating the 5-HT(2A) receptor. *Psychopharmacology (Berl.)* **2010**, *208*, 179-189.
- (205) González-Maeso, J.; Sealfon, S. C. Agonist-trafficking and hallucinogens. *Curr. Med. Chem* **2009**, *16*, 1017-1027.
- (206) Krakowski, M.; Czobor, P. Cholesterol and cognition in schizophrenia: A double-blind study of patients randomized to clozapine, olanzapine and haloperidol. *Schizophrenia Research* **2011**, *130*, 27-33.
- (207) Lehto, S. M.; Hintikka, J.; Niskanen, L.; Tolmunen, T.; Koivumaa-Honkanen, H.; Honkalampi, K.; Viinamäki, H. Low HDL cholesterol associates with major depression in a sample with a 7-year history of depressive symptoms. *Prog. Neuropsychopharmacol. Biol. Psychiatry* **2008**, *32*, 1557-1561.
- (208) Nakanishi, S.; Masu, M. Molecular diversity and functions of glutamate receptors. *Annu Rev Biophys Biomol Struct* **1994**, *23*, 319-348.
- (209) Nakanishi, S. Molecular diversity of glutamate receptors and implications for brain function. *Science* **1992**, *258*, 597-603.
- (210) Conn, P. J.; Pin, J. P. Pharmacology and functions of metabotropic glutamate receptors. *Annu. Rev. Pharmacol. Toxicol.* **1997**, *37*, 205-237.
- (211) Fraley, M. E. Positive allosteric modulators of the metabotropic glutamate receptor 2 for the treatment of schizophrenia. *Expert Opin Ther Pat* **2009**, *19*, 1259-1275.
- (212) Trabanco, A. A.; Cid, J. M.; Lavreysen, H.; Macdonald, G. J.; Tresadern, G. Progress in the development of positive allosteric modulators of the metabotropic glutamate receptor 2. *Curr. Med. Chem.* **2011**, *18*, 47-68.
- (213) Lundström, L.; Bissantz, C.; Beck, J.; Wettstein, J. G.; Woltering, T. J.; Wichmann, J.; Gatti, S. Structural determinants of allosteric antagonism at metabotropic glutamate receptor 2: mechanistic studies with new potent negative allosteric modulators. *Br J Pharmacol* **2011**.
- (214) Monn, J. A.; Valli, M. J.; Massey, S. M.; Wright, R. A.; Salhoff, C. R.; Johnson, B. G.; Howe, T.; Alt, C. A.; Rhodes, G. A.; Robey, R. L.; Griffey, K. R.; Tizzano, J. P.; Kallman, M. J.; Helton, D. R.; Schoepp, D. D. Design, synthesis, and pharmacological characterization of (+)-2-aminobicyclo[3.1.0]hexane-2,6-dicarboxylic acid (LY354740): a potent, selective, and orally active group 2 metabotropic glutamate receptor agonist possessing anticonvulsant and anxiolytic properties. *J. Med. Chem.* **1997**, *40*, 528-537.
- (215) Monn, J. A.; Valli, M. J.; Massey, S. M.; Hansen, M. M.; Kress, T. J.; Wepsiec, J. P.; Harkness, A. R.; Grutsch, J. L., Jr; Wright, R. A.; Johnson, B. G.; Andis, S. L.; Kingston, A.;

Tomlinson, R.; Lewis, R.; Griffey, K. R.; Tizzano, J. P.; Schoepp, D. D. Synthesis, pharmacological characterization, and molecular modeling of heterobicyclic amino acids related to (+)-2-aminobicyclo[3.1.0] hexane-2,6-dicarboxylic acid (LY354740): identification of two new potent, selective, and systemically active agonists for group II metabotropic glutamate receptors. *J. Med. Chem.* **1999**, *42*, 1027-1040.

(216) Woolley, M. L.; Pemberton, D. J.; Bate, S.; Corti, C.; Jones, D. N. C. The mGlu2 but not the mGlu3 receptor mediates the actions of the mGluR2/3 agonist, LY379268, in mouse models predictive of antipsychotic activity. *Psychopharmacology (Berl.)* **2008**, *196*, 431-440.

(217) Fell, M. J.; Svensson, K. A.; Johnson, B. G.; Schoepp, D. D. Evidence for the role of metabotropic glutamate (mGlu)2 not mGlu3 receptors in the preclinical antipsychotic pharmacology of the mGlu2/3 receptor agonist (-)-(1R,4S,5S,6S)-4-amino-2-sulfonylbicyclo[3.1.0]hexane-4,6-dicarboxylic acid (LY404039). *J. Pharmacol. Exp. Ther.* **2008**, *326*, 209-217.

(218) Albizu, L.; Moreno, J. L.; González-Maeso, J.; Sealfon, S. C. Heteromerization of G protein-coupled receptors: relevance to neurological disorders and neurotherapeutics. *CNS Neurol Disord Drug Targets* **2010**, *9*, 636-650.

(219) González-Maeso, J.; Sealfon, S. C. Psychedelics and schizophrenia. *Trends in Neurosciences* **2009**, *32*, 225-232.

(220) Gray, J. A.; Roth, B. L. Paradoxical trafficking and regulation of 5-HT_{2A} receptors by agonists and antagonists. *Brain Research Bulletin* **2001**, *56*, 441-451.

(221) Berg, K. A.; Maayani, S.; Goldfarb, J.; Scaramellini, C.; Leff, P.; Clarke, W. P. Effector pathway-dependent relative efficacy at serotonin type 2A and 2C receptors: evidence for agonist-directed trafficking of receptor stimulus. *Mol. Pharmacol.* **1998**, *54*, 94-104.

(222) Molinaro, G.; Traficante, A.; Riozzi, B.; Di Menna, L.; Curto, M.; Pallottino, S.; Nicoletti, F.; Bruno, V.; Battaglia, G. Activation of mGlu2/3 metabotropic glutamate receptors negatively regulates the stimulation of inositol phospholipid hydrolysis mediated by 5-hydroxytryptamine_{2A} serotonin receptors in the frontal cortex of living mice. *Mol. Pharmacol.* **2009**, *76*, 379-387.

(223) Marek, G. J.; Wright, R. A.; Schoepp, D. D. 5-Hydroxytryptamine_{2A} (5-HT_{2A}) receptor regulation in rat prefrontal cortex: interaction of a phenethylamine hallucinogen and the metabotropic glutamate_{2/3} receptor agonist LY354740. *Neurosci. Lett.* **2006**, *403*, 256-260.

(224) Marek, G. J.; Wright, R. A.; Schoepp, D. D.; Monn, J. A.; Aghajanian, G. K. Physiological antagonism between 5-hydroxytryptamine_{2A} and group II metabotropic glutamate receptors in prefrontal cortex. *J. Pharmacol. Exp. Ther.* **2000**, *292*, 76-87.

(225) Kondo, M.; Sawa, A. Anti-/Pro-psychotic Drug Signaling via Heteromeric GPCRs-A Balancing Act? *Cell* **2011**, *147*, 964-965.

(226) Zhang, S. In *Drug Design and Discovery - Computer-Aided Drug Discovery and Development*; Humana Press: Totowa, NJ, 2011; Vol. 716, pagg. 23-38.

(227) Mobarec, J. C.; Sanchez, R.; Filizola, M. Modern Homology Modeling of G-Protein Coupled Receptors: Which Structural Template to Use? *Journal of Medicinal Chemistry* **2009**, *52*,

5207-5216.

- (228) Blois, T. M.; Bowie, J. U. G protein coupled receptor structures were not built in a day. *Protein Science* **2009**, *18*, 1335-1342.
- (229) Cavasotto, C. N.; Phatak, S. S. Homology modeling in drug discovery: current trends and applications. *Drug Discov. Today* **2009**, *14*, 676-683.
- (230) Patny, A.; Desai, P. V.; Avery, M. A. Homology modeling of G-protein-coupled receptors and implications in drug design. *Curr. Med. Chem* **2006**, *13*, 1667-1691.
- (231) Yarnitzky, T.; Levit, A.; Niv, M. Y. Homology modeling of G-protein-coupled receptors with X-ray structures on the rise. *Curr Opin Drug Discov Devel* **2010**, *13*, 317-325.
- (232) Martí-Renom, M. A.; Stuart, A. C.; Fiser, A.; Sánchez, R.; Melo, F.; Šali, A. Comparative Protein Structure Modeling of Genes and Genomes. *Annu. Rev. Biophys. Biomol. Struct.* **2000**, *29*, 291-325.
- (233) Theoretical and Computational Biophysics Group <http://www.ks.uiuc.edu/Research/vmd/> (accessed May 5 2011).
- (234) ClustalW2 - Multiple Sequence Alignment <http://www.ebi.ac.uk/Tools/msa/clustalw2/>.
- (235) Vanejvs, M.; Jatzke, C.; Renner, S.; Müller, S.; Hechenberger, M.; Bauer, T.; Klochkova, A.; Pyatkin, I.; Kazyulkin, D.; Aksenova, E.; Shulepin, S.; Timonina, O.; Haasis, A.; Gutcaits, A.; Parsons, C. G.; Kauss, V.; Weil, T. Positive and Negative Modulation of Group I Metabotropic Glutamate Receptors. *Journal of Medicinal Chemistry* **2008**, *51*, 634-647.
- (236) ExPASy: SIB Bioinformatics Resource Portal - Home expasy.org.
- (237) MODELLER, salilab.org/modeller (accessed 11 Nov 2011).
- (238) Khan, S. H.; Ahmad, F.; Ahmad, N.; Flynn, D. C.; Kumar, R. Protein-protein interactions: principles, techniques, and their potential role in new drug development. *J. Biomol. Struct. Dyn.* **2011**, *28*, 929-938.
- (239) James, J. R.; Oliveira, M. I.; Carmo, A. M.; Iaboni, A.; Davis, S. J. A rigorous experimental framework for detecting protein oligomerization using bioluminescence resonance energy transfer. *Nat. Methods* **2006**, *3*, 1001-1006.
- (240) Moreira, I. S.; Fernandes, P. A.; Ramos, M. J. Protein-protein docking dealing with the unknown. *J Comput Chem* **2010**, *31*, 317-342.
- (241) Gray, J. J.; Moughon, S.; Wang, C.; Schueler-Furman, O.; Kuhlman, B.; Rohl, C. A.; Baker, D. Protein-Protein Docking with Simultaneous Optimization of Rigid-body Displacement and Side-chain Conformations. *Journal of Molecular Biology* **2003**, *331*, 281-299.
- (242) Kaufmann, K. W.; Lemmon, G. H.; Deluca, S. L.; Sheehan, J. H.; Meiler, J. Practically useful: what the Rosetta protein modeling suite can do for you. *Biochemistry* **2010**, *49*, 2987-2998.

- (243) Fotiadis, D.; Liang, Y.; Filipek, S.; Saperstein, D. A.; Engel, A.; Palczewski, K. The G protein-coupled receptor rhodopsin in the native membrane. *FEBS Lett.* **2004**, *564*, 281-288.
- (244) Liang, Y.; Fotiadis, D.; Filipek, S.; Saperstein, D. A.; Palczewski, K.; Engel, A. Organization of the G protein-coupled receptors rhodopsin and opsin in native membranes. *J. Biol. Chem.* **2003**, *278*, 21655-21662.
- (245) Mancina, F.; Assur, Z.; Herman, A. G.; Siegel, R.; Hendrickson, W. A. Ligand sensitivity in dimeric associations of the serotonin 5HT_{2c} receptor. *EMBO Rep.* **2008**, *9*, 363-369.
- (246) Berthouze, M.; Rivail, L.; Lucas, A.; Ayoub, M. A.; Russo, O.; Sicsic, S.; Fischmeister, R.; Berque-Bestel, I.; Jockers, R.; Lezoualc'h, F. Two transmembrane Cys residues are involved in 5-HT₄ receptor dimerization. *Biochem. Biophys. Res. Commun.* **2007**, *356*, 642-647.
- (247) RosettaCON2011 Tutorials Collection | RosettaCommons <http://www.rosettacommons.org/>.
- (248) CHARMM-GUI, www.charmm-gui.org.
- (249) Jo, S.; Kim, T.; Iyer, V. G.; Im, W. CHARMM-GUI: a web-based graphical user interface for CHARMM. *J Comput Chem* **2008**, *29*, 1859-1865.
- (250) Jo, S.; Kim, T.; Im, W. Automated builder and database of protein/membrane complexes for molecular dynamics simulations. *PLoS ONE* **2007**, *2*, e880.
- (251) Lomize, A. L.; Pogozheva, I. D.; Lomize, M. A.; Mosberg, H. I. Positioning of proteins in membranes: a computational approach. *Protein Sci.* **2006**, *15*, 1318-1333.
- (252) Humphrey, W.; Dalke, A.; Schulten, K. VMD: visual molecular dynamics. *J Mol Graph* **1996**, *14*, 33-38, 27-28.
- (253) CHARMM ff params, http://mackerell.umaryland.edu/CHARMM_ff_params.html (accessed 05 May, 2011).
- (254) Adcock, S. A.; McCammon, J. A. Molecular dynamics: survey of methods for simulating the activity of proteins. *Chem. Rev.* **2006**, *106*, 1589-1615.
- (255) Klepeis, J. L.; Lindorff-Larsen, K.; Dror, R. O.; Shaw, D. E. Long-timescale molecular dynamics simulations of protein structure and function. *Curr. Opin. Struct. Biol.* **2009**, *19*, 120-127.
- (256) Dror, R. O.; Jensen, M. Ø.; Borhani, D. W.; Shaw, D. E. Exploring atomic resolution physiology on a femtosecond to millisecond timescale using molecular dynamics simulations. *J Gen Physiol* **2010**, *135*, 555-562.
- (257) Torrie, G. M.; Valleau, J. P. Nonphysical sampling distributions in Monte Carlo free-energy estimation: Umbrella sampling. *Journal of Computational Physics* **1977**, *23*, 187-199.
- (258) Barducci, A.; Bussi, G.; Parrinello, M. Well-tempered metadynamics: a smoothly converging and tunable free-energy method. *Phys. Rev. Lett.* **2008**, *100*, 020603.
- (259) Bond, P. J.; Holyoake, J.; Ivetac, A.; Khalid, S.; Sansom, M. S. P. Coarse-grained molecular

- dynamics simulations of membrane proteins and peptides. *J. Struct. Biol.* **2007**, *157*, 593-605.
- (260) Grossfield, A. Recent progress in the study of G protein-coupled receptors with molecular dynamics computer simulations. *Biochim. Biophys. Acta* **2011**, *1808*, 1868-1878.
- (261) Johnston, J. M.; Filizola, M. Showcasing modern molecular dynamics simulations of membrane proteins through G protein-coupled receptors. *Current Opinion in Structural Biology* **2011**, *21*, 552-558.
- (262) Jin, H.; Jespersen, D.; Mehrotra, P.; Biswas, R.; Huang, L.; Chapman, B. High performance computing using MPI and OpenMP on multi-core parallel systems. *Parallel Computing* **2011**, *37*, 562-575.
- (263) Karimi, K.; Dickson, N.; Hamze, F. High-performance Physics Simulations Using Multi-core CPUs and GPGPUs in a Volunteer Computing Context. *International Journal of High Performance Computing Applications* **2011**, *25*, 61 -69.
- (264) Papadrakakis, M.; Stavroulakis, G.; Karatarakis, A. A new era in scientific computing: Domain decomposition methods in hybrid CPU-GPU architectures. *Computer Methods in Applied Mechanics and Engineering* **2011**, *200*, 1490-1508.
- (265) Stone, J. E.; Hardy, D. J.; Ufimtsev, I. S.; Schulten, K. GPU-accelerated molecular modeling coming of age. *J. Mol. Graph. Model.* **2010**, *29*, 116-125.
- (266) NAMD - Scalable Molecular Dynamics <http://www.ks.uiuc.edu/Research/namd/>.
- (267) Phillips, J. C.; Braun, R.; Wang, W.; Gumbart, J.; Tajkhorshid, E.; Villa, E.; Chipot, C.; Skeel, R. D.; Kalé, L.; Schulten, K. Scalable molecular dynamics with NAMD. *Journal of Computational Chemistry* **2005**, *26*, 1781-1802.
- (268) ACEMD - Multiscale Laboratory <http://multiscalelab.org/acemd>.
- (269) Harvey, M. J.; Giupponi, G.; Fabritiis, G. D. ACEMD: Accelerating Biomolecular Dynamics in the Microsecond Time Scale. *J. Chem. Theory Comput.* **2009**, *5*, 1632-1639.
- (270) Harvey, M. J.; De Fabritiis, G. An Implementation of the Smooth Particle Mesh Ewald Method on GPU Hardware. *J. Chem. Theory Comput.* **2009**, *5*, 2371-2377.
- (271) VMD - Visual Molecular Dynamics <http://www.ks.uiuc.edu/Research/vmd/>.
- (272) Humphrey, W.; Dalke, A.; Schulten, K. VMD: visual molecular dynamics. *J Mol Graph* **1996**, *14*, 33-38, 27-28.
- (273) Parallel Programming Laboratory <http://charm.cs.uiuc.edu/>.
- (274) Darden, T.; York, D.; Pedersen, L. Particle mesh Ewald: An $N \cdot \log(N)$ method for Ewald sums in large systems. *J. Chem. Phys.* **1993**, *98*, 10089.
- (275) Shao, J.; Tanner, S. W.; Thompson, N.; Cheatham, T. E. Clustering Molecular Dynamics Trajectories: 1. Characterizing the Performance of Different Clustering Algorithms. *J. Chem.*

Theory Comput. **2007**, 3, 2312-2334.

(276) Vaidehi, N. Dynamics and flexibility of G-protein-coupled receptor conformations and their relevance to drug design. *Drug Discov. Today* **2010**, 15, 951-957.

(277) Amaro, R. E.; Baron, R.; McCammon, J. A. An improved relaxed complex scheme for receptor flexibility in computer-aided drug design. *J. Comput. Aided Mol. Des.* **2008**, 22, 693-705.

(278) Mobarec, J. C.; Filizola, M. Advances in the Development and Application of Computational Methodologies for Structural Modeling of G-Protein Coupled Receptors. *Expert Opin Drug Discov* **2008**, 3, 343-355.

(279) Totrov, M.; Abagyan, R. Flexible ligand docking to multiple receptor conformations: a practical alternative. *Curr. Opin. Struct. Biol.* **2008**, 18, 178-184.

(280) The Amber Molecular Dynamics Package ambermd.org.

(281) Roth, B. L.; Willins, D. L.; Kristiansen, K.; Kroeze, W. K. 5-Hydroxytryptamine₂-family receptors (5-hydroxytryptamine_{2A}, 5-hydroxytryptamine_{2B}, 5-hydroxytryptamine_{2C}): where structure meets function. *Pharmacol. Ther* **1998**, 79, 231-257.

(282) Kristiansen, K.; Kroeze, W. K.; Willins, D. L.; Gelber, E. I.; Savage, J. E.; Glennon, R. A.; Roth, B. L. A highly conserved aspartic acid (Asp-155) anchors the terminal amine moiety of tryptamines and is involved in membrane targeting of the 5-HT_{2A} serotonin receptor but does not participate in activation via a «salt-bridge disruption» mechanism. *J. Pharmacol. Exp. Ther* **2000**, 293, 735-746.

(283) Braden, M. R.; Nichols, D. E. Assessment of the roles of serines 5.43(239) and 5.46(242) for binding and potency of agonist ligands at the human serotonin 5-HT_{2A} receptor. *Mol. Pharmacol* **2007**, 72, 1200-1209.

(284) Shapiro, D. A.; Kristiansen, K.; Kroeze, W. K.; Roth, B. L. Differential modes of agonist binding to 5-hydroxytryptamine(2A) serotonin receptors revealed by mutation and molecular modeling of conserved residues in transmembrane region 5. *Mol. Pharmacol* **2000**, 58, 877-886.

(285) Roth, B. L.; Shoham, M.; Choudhary, M. S.; Khan, N. Identification of conserved aromatic residues essential for agonist binding and second messenger production at 5-hydroxytryptamine_{2A} receptors. *Mol. Pharmacol* **1997**, 52, 259-266.

(286) Ebersole, B. J.; Visiers, I.; Weinstein, H.; Sealfon, S. C. Molecular basis of partial agonism: orientation of indoleamine ligands in the binding pocket of the human serotonin 5-HT_{2A} receptor determines relative efficacy. *Mol. Pharmacol* **2003**, 63, 36-43.

(287) Kao, H. T.; Adham, N.; Olsen, M. A.; Weinshank, R. L.; Branchek, T. A.; Hartig, P. R. Site-directed mutagenesis of a single residue changes the binding properties of the serotonin 5-HT₂ receptor from a human to a rat pharmacology. *FEBS Lett* **1992**, 307, 324-328.

(288) Amadei, A.; Linssen, A. B.; Berendsen, H. J. Essential dynamics of proteins. *Proteins* **1993**, 17, 412-425.

- (289) Hess Similarities between principal components of protein dynamics and random diffusion. *Phys Rev E Stat Phys Plasmas Fluids Relat Interdiscip Topics* **2000**, *62*, 8438-8448.
- (290) Mongan, J. Interactive essential dynamics. *J. Comput. Aided Mol. Des.* **2004**, *18*, 433-436.
- (291) Filizola, M.; Wang, S. X.; Weinstein, H. Dynamic models of G-protein coupled receptor dimers: indications of asymmetry in the rhodopsin dimer from molecular dynamics simulations in a POPC bilayer. *J Comput Aided Mol Des* **2006**, *20*, 405-416.
- (292) Interactive Essential Dynamics <http://mccammon.ucsd.edu/ied/>.
- (293) Olsen, B. N.; Schlesinger, P. H.; Baker, N. A. Perturbations of Membrane Structure by Cholesterol and Cholesterol Derivatives Are Determined by Sterol Orientation. *Journal of the American Chemical Society* **2009**, *131*, 4854-4865.
- (294) Eriksson, E. S. E.; Eriksson, L. A. The Influence of Cholesterol on the Properties and Permeability of Hypericin Derivatives in Lipid Membranes. *Journal of Chemical Theory and Computation* **2011**, *7*, 560-574.
- (295) Toni Giorgino, Computing 1D atomic densities in macromolecular simulations: the Density Profile Tool for VMD, manuscript in preparation
<http://multiscalelab.org/utilities/DensityProfileTool> (accessed April 5, 2011).
- (296) Sheather, S. J.; Jones, M. C. A Reliable Data-Based Bandwidth Selection Method for Kernel Density Estimation. *Journal of the Royal Statistical Society. Series B (Methodological)* **1991**, *53*, 683-690.
- (297) Yeung, K. Y.; Fraley, C.; Murua, A.; Raftery, A. E.; Ruzo, W. L. Model-based clustering and data transformations for gene expression data. *Bioinformatics* **2001**, *17*, 977-987.
- (298) Bivariate Kernel Density Estimation - Free Statistics and Forecasting Software (Calculators) v.1.1.23-r7, http://www.wessa.net/rwasp_bidensity.wasp (accessed 10 Nov 2011).
- (299) Okuno, Y.; Tamon, A.; Yabuuchi, H.; Nijijima, S.; Minowa, Y.; Tonomura, K.; Kunimoto, R.; Feng, C. GLIDA: GPCR ligand database for chemical genomics drug discovery database and tools update. *Nucleic Acids Research* **2007**, *36*, D907-D912.
- (300) GLIDA:GPCR-Ligand Database <http://pharminfo.pharm.kyoto-u.ac.jp/services/glida/>.
- (301) Friesner, R. A.; Banks, J. L.; Murphy, R. B.; Halgren, T. A.; Klicic, J. J.; Mainz, D. T.; Repasky, M. P.; Knoll, E. H.; Shelley, M.; Perry, J. K.; Shaw, D. E.; Francis, P.; Shenkin, P. S. Glide: a new approach for rapid, accurate docking and scoring. 1. Method and assessment of docking accuracy. *J. Med. Chem.* **2004**, *47*, 1739-1749.
- (302) Schrödinger <http://www.schrodinger.com/>.
- (303) IUPHAR DATABASE <http://www.iuphar-db.org/DATABASE/ReceptorFamiliesForward?type=GPCR>.
- (304) Sonogo, P.; Kocsor, A.; Pongor, S. ROC analysis: applications to the classification of

biological sequences and 3D structures. *Brief. Bioinformatics* **2008**, *9*, 198-209.

(305) Chemical Computing Group. Scalable Software Scalable Science <http://www.chemcomp.com/> (accessed May 5, 2011).

(306) Hofmann, K. P.; Scheerer, P.; Hildebrand, P. W.; Choe, H.-W.; Park, J. H.; Heck, M.; Ernst, O. P. A G protein-coupled receptor at work: the rhodopsin model. *Trends in Biochemical Sciences* **2009**, *34*, 540-552.

(307) Parrish, J. C.; Braden, M. R.; Gundy, E.; Nichols, D. E. Differential phospholipase C activation by phenylalkylamine serotonin 5-HT 2A receptor agonists. *J. Neurochem.* **2005**, *95*, 1575-1584.

(308) Filipek, S.; Krzysko, K. A.; Fotiadis, D.; Liang, Y.; Saperstein, D. A.; Engel, A.; Palczewski, K. A concept for G protein activation by G protein-coupled receptor dimers: the transducin/rhodopsin interface. *Photochem. Photobiol. Sci.* **2004**, *3*, 628-638.

(309) Fotiadis, D.; Liang, Y.; Filipek, S.; Saperstein, D. A.; Engel, A.; Palczewski, K. Atomic-force microscopy: Rhodopsin dimers in native disc membranes. *Nature* **2003**, *421*, 127-128.

(310) González-Maeso, J.; Sealfon, S. C. Psychedelics and schizophrenia. *Trends in Neurosciences* **2009**, *32*, 225-232.

(311) Björk, K.; Svenningsson, P. Modulation of Monoamine Receptors by Adaptor Proteins and Lipid Rafts: Role in Some Effects of Centrally Acting Drugs and Therapeutic Agents. *Annu. Rev. Pharmacol. Toxicol.* **2011**, *51*, 211-242.

(312) Simons, K.; Gerl, M. J. Revitalizing membrane rafts: new tools and insights. *Nat. Rev. Mol. Cell Biol* **2010**, *11*, 688-699.

(313) Kučerka, N.; Nieh, M.-P.; Katsaras, J. Asymmetric Distribution of Cholesterol in Unilamellar Vesicles of Monounsaturated Phospholipids. *Langmuir* **2009**, *25*, 13522-13527.

(314) Rukmini, R.; Rawat, S. S.; Biswas, S. C.; Chattopadhyay, A. Cholesterol organization in membranes at low concentrations: effects of curvature stress and membrane thickness. *Biophys. J* **2001**, *81*, 2122-2134.

(315) Pandit, S. A.; Chiu, S.-W.; Jakobsson, E.; Grama, A.; Scott, H. L. Cholesterol Packing around Lipids with Saturated and Unsaturated Chains: A Simulation Study. *Langmuir* **2008**, *24*, 6858-6865.

(316) Saiz, L.; Klein, M. L. Influence of highly polyunsaturated lipid acyl chains of biomembranes on the NMR order parameters. *J. Am. Chem. Soc* **2001**, *123*, 7381-7387.

(317) Pitman, M. C.; Suits, F.; Mackerell, A. D., Jr; Feller, S. E. Molecular-level organization of saturated and polyunsaturated fatty acids in a phosphatidylcholine bilayer containing cholesterol. *Biochemistry* **2004**, *43*, 15318-15328.

(318) Feller, S. E.; Gawrisch, K.; MacKerell, A. D., Jr Polyunsaturated fatty acids in lipid bilayers: intrinsic and environmental contributions to their unique physical properties. *J. Am. Chem. Soc*

2002, *124*, 318-326.

- (319) Mannoock, D. A.; Lewis, R. N. A. H.; McMullen, T. P. W.; McElhaney, R. N. The effect of variations in phospholipid and sterol structure on the nature of lipid-sterol interactions in lipid bilayer model membranes. *Chem. Phys. Lipids* **2010**, *163*, 403-448.
- (320) Paila, Y. D.; Chattopadhyay, A. The function of G-protein coupled receptors and membrane cholesterol: specific or general interaction? *Glycoconj. J* **2009**, *26*, 711-720.
- (321) Binder, H.; Gawrisch, K. Effect of Unsaturated Lipid Chains on Dimensions, Molecular Order and Hydration of Membranes. *The Journal of Physical Chemistry B* **2001**, *105*, 12378-12390.
- (322) Gamba, Z. Effective potentials and electrostatic interactions in self-assembled molecular bilayers II: The case of biological membranes. *J. Chem. Phys.* **2008**, *129*, 215104.
- (323) Koenig, B. W.; Strey, H. H.; Gawrisch, K. Membrane lateral compressibility determined by NMR and x-ray diffraction: effect of acyl chain polyunsaturation. *Biophysical Journal* **1997**, *73*, 1954-1966.
- (324) Saiz, L.; Klein, M. L. Structural Properties of a Highly Polyunsaturated Lipid Bilayer from Molecular Dynamics Simulations. *Biophysical Journal* **2001**, *81*, 204-216.
- (325) Mihailescu, M.; Soubias, O.; Worcester, D.; White, S. H.; Gawrisch, K. Structure and Dynamics of Cholesterol-Containing Polyunsaturated Lipid Membranes Studied by Neutron Diffraction and NMR. *J Membrane Biol* **2010**, *239*, 63-71.
- (326) Schetz, J. A. Allosteric modulation of dopamine receptors. *Mini Rev Med Chem* **2005**, *5*, 555-561.
- (327) Selent, J.; Sanz, F.; Pastor, M.; De Fabritiis, G. Induced Effects of Sodium Ions on Dopaminergic G-Protein Coupled Receptors. *PLoS Comput Biol* **2010**, *6*, e1000884.
- (328) Madabushi, S.; Gross, A. K.; Philippi, A.; Meng, E. C.; Wensel, T. G.; Lichtarge, O. Evolutionary trace of G protein-coupled receptors reveals clusters of residues that determine global and class-specific functions. *J. Biol. Chem* **2004**, *279*, 8126-8132.
- (329) Urizar, E.; Claeyens, S.; Deupí, X.; Govaerts, C.; Costagliola, S.; Vassart, G.; Pardo, L. An activation switch in the rhodopsin family of G protein-coupled receptors: the thyrotropin receptor. *J. Biol. Chem* **2005**, *280*, 17135-17141.
- (330) Khelashvili, G.; Grossfield, A.; Feller, S. E.; Pitman, M. C.; Weinstein, H. Structural and dynamic effects of cholesterol at preferred sites of interaction with rhodopsin identified from microsecond length molecular dynamics simulations. *Proteins: Structure, Function, and Bioinformatics* **2009**, *76*, 403-417.
- (331) Lyman, E.; Higgs, C.; Kim, B.; Lupyan, D.; Shelley, J. C.; Farid, R.; Voth, G. A. A Role for a Specific Cholesterol Interaction in Stabilizing the Apo Configuration of the Human A2A Adenosine Receptor. *Structure* **2009**, *17*, 1660-1668.
- (332) Tiburu, E. K.; Gulla, S. V.; Tiburu, M.; Janero, D. R.; Budil, D. E.; Makriyannis, A.

Dynamic Conformational Responses of a Human Cannabinoid Receptor-1 Helix Domain to Its Membrane Environment. *Biochemistry* **2009**, *48*, 4895-4904.

(333) Whorton, M. R.; Bokoch, M. P.; Rasmussen, S. G. F.; Huang, B.; Zare, R. N.; Kobilka, B.; Sunahara, R. K. A monomeric G protein-coupled receptor isolated in a high-density lipoprotein particle efficiently activates its G protein. *Proc. Natl. Acad. Sci. U.S.A* **2007**, *104*, 7682-7687.

(334) Xiang, Y.; Rybin, V. O.; Steinberg, S. F.; Kobilka, B. Caveolar localization dictates physiologic signaling of beta 2-adrenoceptors in neonatal cardiac myocytes. *J. Biol. Chem* **2002**, *277*, 34280-34286.

(335) Paila, Y. D.; Chattopadhyay, A. Membrane cholesterol in the function and organization of G-protein coupled receptors. *Subcell. Biochem* **2010**, *51*, 439-466.

(336) Saxena, R.; Chattopadhyay, A. Membrane organization and dynamics of the serotonin1A receptor in live cells. *Journal of Neurochemistry* **2011**, *116*, 726-733.

(337) Kalipatnapu, S.; Chattopadhyay, A. Membrane organization and function of the serotonin(1A) receptor. *Cell. Mol. Neurobiol* **2007**, *27*, 1097-1116.

(338) Jean-Alphonse, F.; Hanyaloglu, A. C. Regulation of GPCR signal networks via membrane trafficking. *Molecular and Cellular Endocrinology* **2011**, *331*, 205-214.

(339) Pucadyil, T. J.; Chattopadhyay, A. Role of cholesterol in the function and organization of G-protein coupled receptors. *Prog. Lipid Res* **2006**, *45*, 295-333.

(340) Bennett, M. P.; Mitchell, D. C. Regulation of membrane proteins by dietary lipids: effects of cholesterol and docosahexaenoic acid acyl chain-containing phospholipids on rhodopsin stability and function. *Biophys. J* **2008**, *95*, 1206-1216.

(341) Mondal, S.; Khelashvili, G.; Shan, J.; Andersen, O. S.; Weinstein, H. Quantitative modeling of membrane deformations by multihelical membrane proteins: application to G-protein coupled receptors. *Biophys. J.* **2011**, *101*, 2092-2101.

(342) Ikonen, E. Cellular cholesterol trafficking and compartmentalization. *Nat Rev Mol Cell Biol* **2008**, *9*, 125-138.

(343) Simons, K.; Ikonen, E. How cells handle cholesterol. *Science* **2000**, *290*, 1721-1726.

(344) Horváth, I.; Multhoff, G.; Sonnleitner, A.; Vigh, L. Membrane-associated stress proteins: More than simply chaperones. *Biochimica et Biophysica Acta (BBA) - Biomembranes* **2008**, *1778*, 1653-1664.

(345) Eroglu, C.; Barres, B. A. Regulation of synaptic connectivity by glia. *Nature* **2010**, *468*, 223-231.

(346) Göritz, C.; Mauch, D. H.; Nägler, K.; Pfrieder, F. W. Role of glia-derived cholesterol in synaptogenesis: new revelations in the synapse-glia affair. *J. Physiol. Paris* **2002**, *96*, 257-263.

(347) Stern, C. M.; Mermelstein, P. G. Caveolin regulation of neuronal intracellular signaling.

Cell. Mol. Life Sci. **2010**, *67*, 3785-3795.

(348) Pin, J. P.; Joly, C.; Heinemann, S. F.; Bockaert, J. Domains involved in the specificity of G protein activation in phospholipase C-coupled metabotropic glutamate receptors. *EMBO J* **1994**, *13*, 342-348.

(349) Dowal, L.; Sim, D. S.; Dilks, J. R.; Blair, P.; Beaudry, S.; Denker, B. M.; Koukos, G.; Kuliopulos, A.; Flaumenhaft, R. Identification of an antithrombotic allosteric modulator that acts through helix 8 of PAR1. *Proceedings of the National Academy of Sciences* **2011**, *108*, 2951 -2956.

(350) Kirchberg, K.; Kim, T.-Y.; Möller, M.; Skegro, D.; Dasara Raju, G.; Granzin, J.; Büldt, G.; Schlesinger, R.; Alexiev, U. Conformational dynamics of helix 8 in the GPCR rhodopsin controls arrestin activation in the desensitization process. *Proceedings of the National Academy of Sciences* **2011**, *108*, 18690 -18695.

(351) Pucadyil, T. J.; Chattopadhyay, A. Cholesterol depletion induces dynamic confinement of the G-protein coupled serotonin(1A) receptor in the plasma membrane of living cells. *Biochim. Biophys. Acta* **2007**, *1768*, 655-668.

(352) Niu, S.-L.; Mitchell, D. C.; Litman, B. J. Manipulation of cholesterol levels in rod disk membranes by methyl-beta-cyclodextrin: effects on receptor activation. *J. Biol. Chem.* **2002**, *277*, 20139-20145.

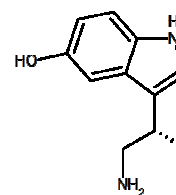
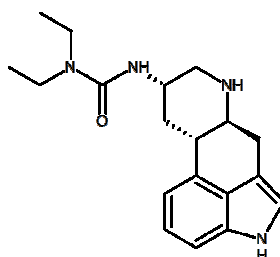
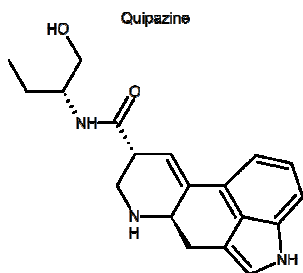
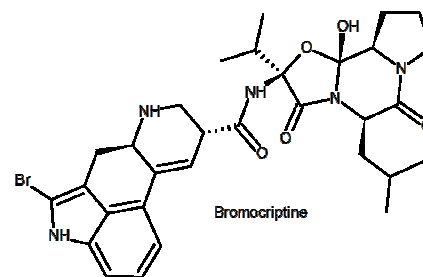
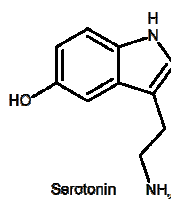
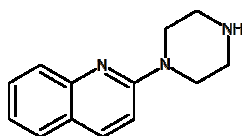
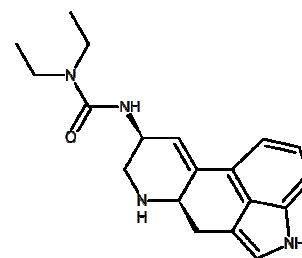
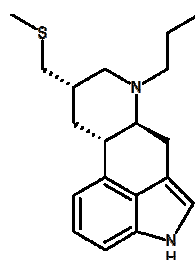
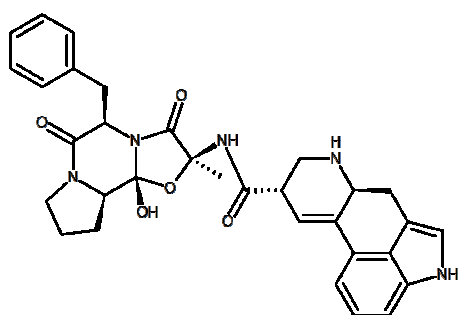
(353) Prasad, R.; Paila, Y. D.; Chattopadhyay, A. Membrane cholesterol depletion enhances ligand binding function of human serotonin1A receptors in neuronal cells. *Biochem. Biophys. Res. Commun.* **2009**, *390*, 93-96.

(354) Prasad, R.; Paila, Y. D.; Jafurulla, M.; Chattopadhyay, A. Membrane cholesterol depletion from live cells enhances the function of human serotonin(1A) receptors. *Biochem. Biophys. Res. Commun.* **2009**, *389*, 333-337.

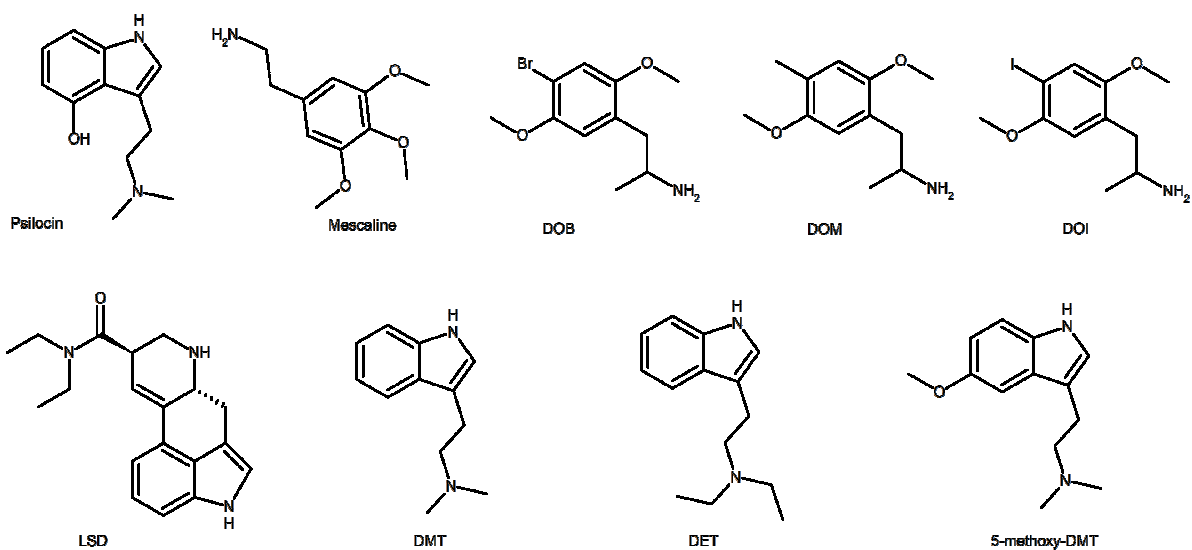
Appendix A

Table 1A. Set of known 5-HT_{2A} ligands.

A. 5-HT_{2A} non hallucinogenic agonists



B. 5-HT_{2A} hallucinogenic agonists



C. 5-HT_{2A} antagonists

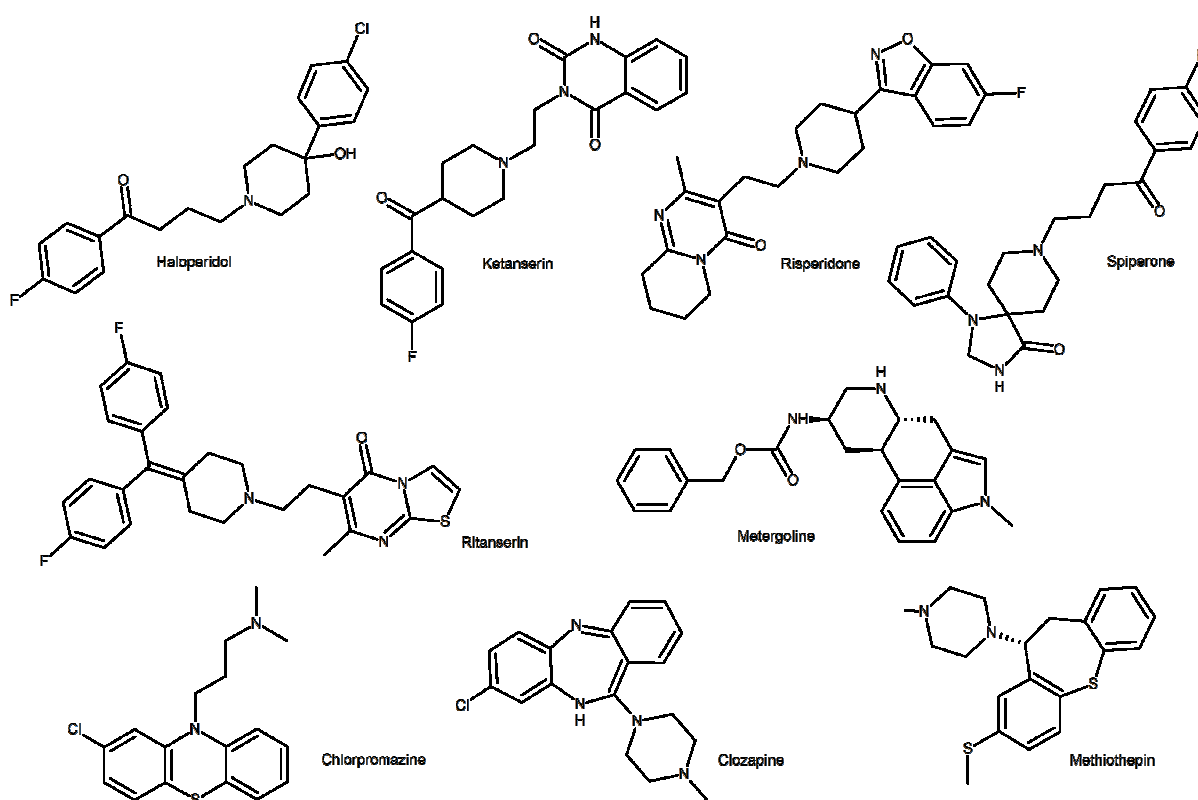


Table 2A. Decoy compounds.

